UNIVERSIDAD POLITECNICA DE VALENCIA

DEPARTAMENTO DE COMUNICACIONES

Thesis for the degree of Doctor of Philosophy

Photonic Techniques for Next-Generation Integrated Optical Networks Based on Ultra-Wideband Radio

Técnicas Fotónicas para Redes Ópticas Integradas de Próxima Generación Basadas en Radio de Banda Ultraancha

Marta Beltrán Ramírez

Supervisor: Dr. Roberto Llorente Sáez

March 2012

Acknowledgement

This Ph.D. thesis has been developed in the framework of the Optical Networks and Systems Area of the Valencia Nanophotonics Technology Centre (NTC), Universidad Politécnica de Valencia (UPV), Spain, to meet the requirements of the Ph.D. degree in telecommunication in the Department of Communications of the UPV.

This work has been funded by the Ministry of Science and Innovation, Spain, by a predoctoral research fellowship Formación de Personal Investigador BES-2006-12066. The European Commission has also indirectly funded this work by the European projects FP6-IST-026592 ISIS, FP7-ICT-216785 UCELLS, FP7-ICT-216863 BONE, FP7-ICT-249142 FIVER, and FP7-ICT-224402 EURO-FOS. Furthermore, this thesis has been indirectly financially supported by the national projects FREDIT “Desarrollo de un Demostrador Tecnológico de Procesador Fotónico para Receptores Electrónicos Digitales”, ULTRADEF “Distribución Fotónica de Vídeo en Ultraalta Definición mediante la Multiplexación de Longitudes de Onda con Modulación en Banda Ultraancha”, and IT-HOGAR “Infraestructura de Telecomunicaciones del Hogar del Futuro“.

This work would not have been possible without the help of a number of people. First of all, I would like to give special thanks to the supervisor of this work, Prof. Roberto Llorente, for his help and support; for everything what I have learned from him as a researcher. Special thanks also to José Caraquitena, who offered me the opportunity to work with him. I also thank Prof. Javier Martí, who gave me the opportunity to join the NTC.

I would like to express my sincere gratitude to the NTC people who have disinterestedly helped me on this work: Karsten Schulze, José M. Martínez, Javier Herrera, Javier Carrascosa, and Teresa Mengual. Thank you also to Maria Morant, Joaquín Pérez, and Rakesh Sambaraju for their collaborative work. I am also grateful to all the NTC people for the nice moments and for contributing to a good atmosphere.

I would also give special thanks to Prof. Idelfonso Tafur Monroy for hosting me for a research stay at DTU Fotonik, Department of Photonics Engineering of the Technical University of Denmark in Kongens Lyngby, Denmark. Thank you to Neil Guerrero, Timothy B. Gibbon, Jesper B. Jensen, Xianbin Yu, Roberto Rodes, and Jing Xu, who helped me on many things. I will not forget either the nice moments shared with Maisara, Xu, Kamau, Thang, Alex, Darko, and also with the people of the High-Speed Optical Communications group.

Finally, I would like to dedicate this Ph.D. thesis to my parents and my sister. Furthermore, I dedicate to the memory of my grandparents. I also appreciate the encouragement and support of the rest of my family.

Abstract

The herein presented Ph.D. thesis finds its application in fibre-to-the-home (FTTH) optical access networks. FTTH networks have been widely deployed worldwide and are expected to evolve toward wavelength-division multiplexing (WDM) architectures.

As the capacity and bandwidth per user requirements for broadband communication services continuously increase, technologies such as hybrid wireless-optical, ultra-wideband (UWB) radio, and millimetre-wave radio are being investigated as viable solutions to provide data rates exceeding Gigabit per second per user. Hybrid wireless-optical networks can provide simpler backhaul and are foreseen to play an important role in next-generation access networks which will require flexible deployment, high capacity, upgradeability, scalable to user number and demand, and economically feasible. Radio-over-fibre techniques combined with multigigabit wireless systems that provide capacities comparable to optical fibre communication systems is seen as a fast deployable and cost-effective solution for providing seamless integrated wired/wireless access to broadband services for the end-user.

UWB and millimetre-wave wireless systems are capable of multigigabit communications. UWB permits an efficient use of the 3.1–10.6 GHz spectrum due to its unique coexistence characteristics and has market maturity. However, UWB is constrained by regulation worldwide. This regulation constraint makes millimetre-wave 60 GHz radio of great interest due to 7 GHz bandwidth consistently regulated worldwide, without coexistence restrictions.

Two are the main technical objectives of this Ph.D. thesis: First, the proposal, analysis, and experimental demonstration of enabling techniques for flexible and cost-effective UWB radio-over-fibre systems. The work herein presented targets to extend the operation of conventional UWB radio-over-fibre systems in the 3.1−10.6 GHz band to the next-generation 60 GHz band. 60 GHz operation would reuse and extend UWB technology in terms of range and flexibility, and is the focus of this work. Second, the implementation of reconfigurable multiwavelength sources for flexible bandwidth aggregation in future WDM networks as an interesting solution for hybrid wireless-optical networks as herein developed. These two objectives are fulfilled by means of optical signal processing techniques.

This Ph.D. thesis proposes and demonstrates experimentally several novel photonic techniques for UWB radio-over-fibre generation to remotely provide multigigabit wireless communications in different frequency bands, ranging from baseband to millimetre-wave, for a wide variety of applications. The operational limits of the proposed UWB-over-fibre systems are also analysed by simulation (VPItransmissionMaker™).

The major achievements of the work herein presented can be summarized as follows:

a) Proposal and proof-of-concept experimental demonstration of two techniques for remote UWB pulse shaping: (1) based on optical delay and balanced photodetection, and (2) based on differential photoreceiver and electrical delay. These techniques permit to adapt UWB spectrum to optical access transmission with varying fibre dispersion by adjusting delay.

b) Proof-of-concept experimental demonstration of a 60 GHz UWB radio-over-fibre system at 1.25 Gb/s with 100 m of standard single-mode fibre (SSMF) transmission. The application of this system to interference-sensitive in-aircraft scenarios with a high number of users is proposed and analysed by simulation. A techno-economic comparison with a potential competitor solution based on baseband data over fibre and remote UWB generation and frequency up-conversion is also performed.

c) Millimetre-wave UWB generation based on frequency shifting in the fibre of optical access networks is proposed and experimentally demonstrated. The technique employs optical carrier suppression in a Mach-Zehnder modulator combined with matched fibre chromatic dispersion targeting to overcome the bandwidth limitation of optical up-conversion, with the advantage of being easily reconfigurable generating simultaneously different RF bands. A comprehensive simulation analysis is performed with special focus on capabilities for dual 24 GHz/60 GHz operation paired with experimental demonstration at 1.25 Gb/s. Such an approach is suitable for integrating 60 GHz FTTH and 24 GHz UWB vehicular applications served from the same central unit. Practical implementation is addressed and competitive approaches are discussed.

d) UWB operation in the 60 GHz band is proposed and experimentally demonstrated to extend UWB capabilities in FTTH networks. 60 GHz UWB generation with combined 40 km of SSMF and 5 m of wireless transmission is experimentally demonstrated at 1.44 Gb/s. Transmission performance is evaluated for two major UWB implementations –dual-carrier modulation orthogonal frequency-division multiplexing (OFDM) reusing market-available devices, and binary phase-shift keying (BPSK) impulse radio- which directly modulate a cost-effective vertical-cavity surface-emitting laser (VCSEL). The results permit, from an application point-of-view, to select a given UWB implementation depending on network reach and system complexity desired.

e) 60 GHz UWB generation, combined transmission over 6.5 km SSMF or 1 km of indoor bend-insensitive single-mode fibre and 2 m of wireless transmission, and RF power detection of on-off keying (OOK) impulse-radio UWB is proposed and experimentally demonstrated at 3.125 Gb/s. VCSEL is proposed for frequency up-conversion based on optical heterodyning and compared with conventional low-linewidth external-cavity laser (ECL). The results permit, from an application point-of-view, to select a given laser technology depending on network reach and system complexity desired.

f) Finally, reconfigurable multiwavelength sources based on the spectral Talbot effect is proposed, numerically analysed, and experimentally demonstrated in this thesis. Twofold and fourfold multiplication of the number of wavelengths and wavelength shifting of a pulsed laser are demonstrated employing an electrooptic phase modulator. Potential applications of the reconfiguration technique are discussed.

Resumen

La presente Tesis Doctoral encuentra su ámbito de aplicación en redes de acceso ópticas de fibra hasta el hogar o FTTH (del inglés *fibre-to-the-home*). Las redes FTTH han sido ampliamente desplegadas en todo el mundo y se prevé que evolucionen hacia arquitecturas de multiplexación por división en longitud de onda o WDM (del inglés *wavelength-division multiplexing*).

Conforme los requerimientos de capacidad y ancho de banda por usuario para servicios de comunicación de banda ancha se incrementan continuamente, tecnologías tales como tecnologías híbridas radio-fibra óptica, radio de banda ultraancha o UWB (del inglés *ultra-wideband*), y radio de onda milimétrica se están investigando como soluciones viables para proporcionar tasas de datos excediendo Gigabits por segundo por usuario. Las redes híbridas radio-fibra óptica pueden proporcionar *backhaul* más simple y se prevé que desempeñen un papel importante en redes de acceso de próxima generación que requerirán despliegue flexible, alta capacidad, habilidad de ampliación, escalable en número de usuarios y demanda, y factible económicamente. Las técnicas radio sobre fibra combinadas con sistemas inalámbricos multigigabit que proporcionen capacidades comparables a sistemas de comunicaciones de fibra óptica se ve como una solución rápidamente desplegable y efectiva en coste para proporcionar acceso transparente cableado/inalámbrico integrado a servicios de banda ancha para el usuario final.

Los sistemas inalámbricos UWB y de onda milimétrica son capaces de proporcionar comunicaciones multigigabit. UWB permite un uso eficiente del espectro 3.1–10.6 GHz debido a sus características únicas de coexistencia y tiene madurez de mercado. Sin embargo, la tecnología UWB está restringida por regulación en todo el mundo. Esta restricción de regulación hace de gran interés a la radio de onda milimétrica en 60 GHz debido a los 7 GHz de ancho de banda regulado consistentemente en todo el mundo, sin restricciones de coexistencia.

Esta Tesis Doctoral tiene dos principales objetivos técnicos: Primero, la propuesta, análisis y demostración experimental de técnicas para sistemas UWB radio sobre fibra flexibles y efectivos en coste. El trabajo realizado persigue extender el funcionamiento de sistemas convencionales UWB radio sobre fibra en la banda 3.1–10.6 GHz a la banda de 60 GHz de próxima generación. El funcionamiento en 60 GHz reutilizaría y extendería tecnología UWB en términos de rango y flexibilidad, y es el foco de este trabajo. Segundo, la implementación de fuentes multilongitud de onda reconfigurables para agregación flexible de ancho de banda en redes WDM futuras como una solución interesante para redes híbridas radio-fibra óptica como se desarrolla en este trabajo. Estos dos objetivos son abordados mediante técnicas de procesamiento de señal en el dominio óptico.

Esta Tesis Doctoral propone y demuestra experimentalmente varias técnicas fotónicas novedosas para generación UWB radio sobre fibra para proporcionar remotamente comunicaciones inalámbricas multigigabit en diferentes bandas de frecuencia, que van desde banda base hasta onda milimétrica, para una amplia variedad de aplicaciones. Asimismo se

analizan en simulación (VPItransmissionMaker™) los límites de funcionamiento de los sistemas UWB sobre fibra propuestos.

Los principales logros del trabajo realizado se pueden resumir como sigue:

a) Propuesta y demostración experimental prueba de concepto de dos técnicas para conformación remota de pulsos UWB: (1) basada en retardo óptico y fotodetección balanceada, y (2) basada en fotoreceptor diferencial y retardo eléctrico. Estas técnicas permiten adaptar el espectro UWB a transmisión de acceso óptico con dispersión de fibra variante mediante ajuste de retardo.
b) Demostración experimental prueba de concepto de un sistema UWB radio sobre fibra en 60 GHz a 1.25 Gb/s con transmisión en 100 m de fibra monomodo estándar. Se propone y analiza mediante simulación la aplicación de este sistema a escenarios de interior sensibles a interferencias tales como aviones con un número alto de usuarios. Asimismo se realiza una comparación tecno-económica con una solución potencialmente competidora basada en distribución de datos en banda base sobre fibra y generación UWB y subida en frecuencia remotas.
c) La generación UWB en frecuencias de onda milimétrica basada en desplazamiento en frecuencia en la fibra de redes de acceso ópticas se propone y demuestra experimentalmente. La técnica emplea modulación de supresión de portadora óptica en un modulador Mach-Zehnder combinada con dispersión adaptada cromática de fibra a fin de superar la limitación de ancho de banda de la subida óptica en frecuencia, con la ventaja de ser fácilmente reconfigurable generando simultáneamente diferentes bandas de radiofrecuencia. Se realiza un análisis de simulación exhaustivo con especial foco en capacidades para funcionamiento dual 24 GHz/60 GHz pareado con demostración experimental a 1.25 Gb/s. Tal técnica es adecuada para integrar aplicaciones UWB 60 GHz FTTH y 24 GHz vehicular servidas por la misma unidad central. Se trata la implementación práctica y se discuten técnicas competitivas.
d) El funcionamiento de UWB en la banda de 60 GHz se propone y demuestra experimentalmente para extender capacidades UWB en redes FTTH. La generación UWB en 60 GHz con transmisión combinada sobre 40 km de fibra monomodo estándar y 5 m de distancia inalámbrica se demuestra experimentalmente a 1.44 Gb/s. Se evalúan las prestaciones de transmisión para dos implementaciones UWB importantes –*dual-carrier modulation* OFDM (del inglés *orthogonal frequency-division multiplexing*) reutilizando dispositivos disponibles en el mercado y BPSK *impulse radio* (del inglés *binary phase-shift keying*)- que modulan directamente a un diodo láser de cavidad vertical y emisión por superficie o VCSEL (del inglés *vertical-cavity surface-emitting laser*). Los resultados permiten, desde el punto de vista de aplicación, seleccionar una implementación UWB dada dependiendo del alcance de red y complejidad del sistema deseados.
e) La generación UWB en 60 GHz, transmisión combinada sobre 6.5 km de fibra monomodo estándar o 1 km de fibra monomodo insensible a curvaturas para instalaciones de interiores y 2 m de distancia inalámbrica, y detección de envolvente de OOK *impulse radio* (del inglés *on-off keying*) UWB se propone y demuestra experimentalmente a 3.125 Gb/s. Se propone el uso de un VCSEL para subida en

frecuencia basada en batido óptico y se compara con el uso de un láser convencional de cavidad externa o ECL (del inglés *external-cavity laser*) con ancho de línea bajo. Los resultados permiten, desde el punto de vista de la aplicación, seleccionar una tecnología láser dada dependiendo del alcance de red y complejidad del sistema deseados.

f) Fuentes multilongitud de onda reconfigurables basadas en el efecto Talbot espectral se propone, analiza numéricamente y demuestra experimentalmente en esta Tesis Doctoral. Se demuestra duplicación y cuadruplicación del número de longitudes de onda y desplazamiento de longitud de onda de un láser pulsado utilizando un modulador de fase electro-óptico. Se habla de potenciales aplicaciones de la técnica de reconfiguración.

Resum

La present Tesi Doctoral troba el seu àmbit d'aplicació en xarxes d'accés òptiques de fibra fins a la llar o FTTH (de l'anglès *fibre-to-the-home*). Les xarxes FTTH han sigut àmpliament desplegades a tot el món i es preveu que evolucionen cap a arquitectures de multiplexació per divisió en longitud d'ona o WDM (de l'anglès *wavelength-division multiplexing*).

Conforme els requeriments de capacitat i ample de banda per usuari per a serveis de comunicació de banda ampla s'incrementen contínuament, tecnologies tals com tecnologies híbrides ràdio-fibra òptica, ràdio de banda ultraampla o UWB (de l'anglès *ultra-wideband*), i ràdio d'ona mil·limètrica s'estan investigant com a solucions viables per a proporcionar taxes de dades excedint gigabits per segon per usuari. Les xarxes híbrides ràdio-fibra òptica poden proporcionar *backhaul* més simple i es preveu que exercisquen un paper important en xarxes d'accés de pròxima generació que requeriran desplegament flexible, alta capacitat, habilitat d'ampliació, escalabilitat en nombre d'usuaris i demanda, i factible econòmicament. Les tècniques ràdio sobre fibra combinades amb sistemes sense fils multigigabit que proporcionen capacitats comparables a sistemes de comunicacions de fibra òptica es veu com una solució ràpidament desplegable i efectiva en cost per a proporcionar accés transparent cablejat/sense fil integrat a serveis de banda ampla per a l'usuari final.

Els sistemes sense fils UWB i d'ona mil·limètrica són capaços de proporcionar comunicacions multigigabit. UWB permet un ús eficient de l'espectre 3.1–10.6 GHz a causa de les seues característiques úniques de coexistència i té maduresa de mercat. No obstant açò, la tecnologia UWB està restringida per regulació a tot el món. Aquesta restricció de regulació fa de gran interès a la ràdio d'ona mil·limètrica en 60 GHz a causa de 7 GHz d'ample de banda regulat consistentment a tot el món, sense restriccions de coexistència.

Aquesta Tesi Doctoral té dos principals objectius tècnics: Primer, la proposta, anàlisi i demostració experimental de tècniques per a sistemes UWB ràdio sobre fibra flexibles i efectius en cost. El treball realitzat persegueix estendre el funcionament de sistemes convencionals UWB ràdio sobre fibra en la banda 3.1–10.6 GHz a la banda de 60 GHz de pròxima generació. El funcionament en 60 GHz reutilitzaria i estendria tecnologia UWB en termes de rang i flexibilitat, i és el focus d'aquest treball. Segon, la implementació de fonts multilongitud d'ona reconfigurables per a agregació flexible d'ample de banda en xarxes WDM futures com una solució interessant per a xarxes híbrides ràdio-fibra òptica com es desenvolupa en aquest treball. Aquests dos objectius són abordats mitjançant tècniques de processament de senyal en el domini òptic.

Aquesta Tesi Doctoral proposa i demostra experimentalment diverses tècniques fotòniques noves per a generació UWB ràdio sobre fibra per a proporcionar remotament comunicacions sense fils multigigabit en diferents bandes de freqüència, que van des de banda base fins a ona mil·limètrica, per a una àmplia varietat d'aplicacions. Així mateix s'analitzen en simulació (VPItransmissionMaker™) els límits de funcionament dels sistemes UWB sobre fibra proposats.

Els principals assoliments del treball realitzat es poden resumir com segueix:

a) Proposta i demostració experimental prova de concepte de dues tècniques per a conformació remota de polsos UWB: (1) basada en retard òptic i fotodetecció balancejada, i (2) basada en fotoreceptor diferencial i retard elèctric. Aquestes tècniques permeten adaptar l'espectre UWB a transmissió d'accés òptic amb dispersió de fibra variant mitjançant ajust de retard.
b) Demostració experimental prova de concepte d'un sistema UWB ràdio sobre fibra en 60 GHz a 1.25 Gb/s amb transmissió en 100 m de fibra monomode estàndard. Es proposa i analitza mitjançant simulació l'aplicació d'aquest sistema a escenaris d'interior sensibles a interferències com a avions amb un alt nombre d'usuaris. Així mateix es realitza una comparació tecno-econòmica amb una solució potencialment competidora basada en distribució de dades en banda base sobre fibra i generació UWB i pujada en freqüència remotes.
c) La generació UWB en freqüències d'ona mil·limètrica basada en desplaçament en freqüència en la fibra de xarxes d'accés òptiques es proposa i demostra experimentalment. La tècnica empra modulació de supressió de portadora òptica en un modulador Mach-Zehnder combinada amb dispersió adaptada cromàtica de fibra a fi de superar la limitació d'ample de banda de la pujada òptica en freqüència, amb l'avantatge de ser fàcilment reconfigurable generant simultàniament diferents bandes de radiofreqüència. Es realitza una anàlisi de simulació exhaustiu amb especial focus en capacitats per a funcionament dual 24 GHz/60 GHz apariat amb demostració experimental a 1.25 Gb/s. Tal tècnica és adequada per a integrar aplicacions UWB 60 GHz FTTH i 24 GHz vehicular servides per la mateixa unitat central. Es tracta la implementació pràctica i es discuteixen tècniques competitives.
d) El funcionament d'UWB en la banda de 60 GHz es proposa i demostra experimentalment per a estendre capacitats UWB en xarxes FTTH. La generació UWB en 60 GHz amb transmissió combinada sobre 40 km de fibra monomode estàndard i 5 m de distància sense fil es demostra experimentalment a 1.44 Gb/s. S'avaluen les prestacions de transmissió per a dues implementacions UWB importants –*dual-carrier modulation* OFDM (de l'anglès *orthogonal frequency-division multiplexing*) reutilitzant dispositius disponibles en el mercat i BPSK *impulse radio* (de l'anglès *binary phase-shift keying*)- que modulen directament a un díode làser de cavitat vertical i emissió per superfície o VCSEL (de l'anglès *vertical-cavity surface-emitting laser*). Els resultats permeten, des del punt de vista d'aplicació, seleccionar una implementació UWB donada depenent de l'abast de xarxa i complexitat del sistema desitjats.
e) La generació UWB en 60 GHz, transmissió combinada sobre 6.5 km de fibra monomode estàndard o 1 km de fibra monomode insensible a curvatures per a instal·lacions d'interiors i 2 m de distància sense fil, i detecció d'envolupant d'OOK *impulse radio* (de l' anglès *on-off keying*) UWB es proposa i demostra experimentalment a 3.125 Gb/s. Es proposa l'ús d'un VCSEL per a pujada en freqüència basada en batut òptic i es compara amb l'ús d'un làser convencional de cavitat externa o ECL (de l'anglès *external-cavity laser*) amb ample de línia baix. Els resultats permeten, des del punt de vista de l'aplicació, seleccionar una tecnologia làser donada depenent de l'abast de xarxa i complexitat del sistema desitjats.

f) Fonts multilongitud d'ona reconfigurables basades en l'efecte Talbot espectral es proposa, analitza numèricament i demostra experimentalment en aquesta Tesi Doctoral. Es demostra duplicació i quadruplicació del nombre de longituds d'ona i desplaçament de longitud d'ona d'un làser polsat utilitzant un modulador de fase electro-òptic. Es parla de potencials aplicacions de la tècnica de reconfiguració.

Contents

List of Acronyms

Amp	Amplification
ADC	Analogue-to-Digital Converter
AON	Active Optical Network
ASE	Amplified Spontaneous Emission
ASK	Amplitude Shift Keying
AWG	Arbitrary Waveform Generator
BER(T)	Bit Error Rate (Tester)
BPG	Bit Pattern Generator
BPSK	Binary Phase-Shift Keying
BI-MMF	Bend-Insensitive Multimode Fibre
BI-SMF	Bend-Insensitive Single-Mode Fibre
BPF	Band-Pass Filter
BT	Bias Tee
B2B	Back-to-Back
CMOS	Complementary Metal-Oxide Semiconductor
CW	Continuous Wave
DAA	Detect-and-Avoid
DAC	Digital-to-Analogue Converter
DAS	Distributed Antenna System
DCA	Digital Communications Analyser
DCF	Dispersion Compensating Fibre
DCM	Dual-Carrier Modulation
DeMux	Demultiplexer
DET	Power Detector
DFB	Distributed Feedback
DMT	Discrete Multitone
DSB	Double Sideband
DSO	Digital Sampling Oscilloscope
DSP	Digital Signal Processing
EAM	Electro-Absorption Modulator
ECC	Electronic Communications Committee
ECL	External-Cavity Laser
EDFA	Erbium-Doped Fibre Amplifier
EIRP	Equivalent Isotropic Radiated Power
ETSI	European Telecommunications Standards Institute
EVM	Error Vector Magnitude
FBG	Fibre Bragg Grating
FEC	Forward Error Correction
FFT	Fast Fourier Transform
FSO	Free Space Optics
FTTH	Fibre-to-the-Home
FWHM	Full Width at Half Maximum
GbE	Gigabit Ethernet
HD	High-Definition
HDMI	High-Definition Multimedia Interface
HEU	Head-End Unit
HNLF	Highly Nonlinear Fibre
HPA	High-Power Amplifier

IDF	Inverse Dispersion Fibre
IF	Intermediate Frequency
IFFT	Inverse Fast Fourier Transform
IP	Intellectual Property
LAN	Local Area Network
LED	Light-Emitting Diode
LO	Local Oscillator
LOS	Line-of-Sight
LPF	Low-Pass Filter
LNA	Low-Noise Amplifier
MAN	Metropolitan Area Network
MIMO	Multiple-Input Multiple-Output
MLL	Mode-Locked Laser
MMF	Multimode Fibre
MMIC	Monolithic Microwave Integrated Circuit
MZM	Mach-Zehnder Modulator
Mux	Multiplexer
NLOS	Non-Line-of-Sight
NRZ	Non-Return-to-Zero
NZ-DSF	Non-Zero Dispersion-Shifted Fibre
OBPF	Optical Band-Pass Filter
ODL	Optical Delay Line
OFDM	Orthogonal Frequency-Division Multiplexing
OFM	Optical Frequency Multiplication
OLT	Optical Line Terminal
ONT	Optical Network Terminal
OOK	On-Off Keying
OSA	Optical Spectrum Analyser
PAM	Pulse Amplitude Modulation
PAPR	Peak-to-Average Power Ratio
PC	Polarization Controller
PD	Photodetector
PDM	Polarization Division Multiplexing
PM	Phase Modulator
PMD	Polarization Mode Dispersion
POF	Plastic (or Polymer) Optical Fibre
PON	Passive Optical Network
PPG	Pulse Pattern Generator
PPM	Pulse-Position Modulation
PS	Phase Shifter
PSK	Phase Shift Keying
PSM	Pulse Shape Modulation
P2P	Point-to-Point
P2MP	Point-to-Multipoint
QAM	Quadrature Amplitude Modulation
QPSK	Quadrature Phase-Shift Keying
RAU	Remote Antenna Unit
RF	Radio Frequency
RG	Residential Gateway
RIN	Relative Intensity Noise
RMS	Root Mean Square
RZ	Return-to-Zero

Rx	Receiver
SNR	Signal-to-Noise Ratio
SCM	Sub-Carrier Multiplexing
SOA	Semiconductor Optical Amplifier
SSB	Single Sideband
SSMF	Standard Single-Mode Fibre
TIA	Transimpedance Amplifier
TFC	Time-Frequency Code
Tx	Transmitter
USB	Universal Serial Bus
UWB	Ultra-Wideband
VCSEL	Vertical-Cavity Surface-Emitting Laser
VA	Variable Attenuator
VOA	Variable Optical Attenuator
WDM	Wavelength Division Multiplexing
WLAN	Wireless Local Area Network
WMAN	Wireless Metropolitan Area Network
WPAN	Wireless Personal Area Network
WWAN	Wireless Wide Area Network

1

Introduction

1.1 Motivation

As the capacity per user requirements for broadband communication services continuously increase, technologies such as ultra-wideband (UWB) radio, millimetre-wave radio around 60 GHz and beyond, free space optics (FSO), and indoor optical wireless technologies such as infrared light and visible light communications are being investigated as viable solutions to provide data rates exceeding Gigabit per second per user, as reviewed in Section 2.1.

UWB is a radio technology supporting high bandwidth broadcast of bidirectional services to multiple televisions and computers distributed throughout a dwelling/office thus replacing pervasive, high-definition (HD) audio/video and high-speed Internet cabling. UWB uses regulated spectrum from 3.1 to 10.6 GHz with a minimum signal bandwidth of 500 MHz or 20% fractional bandwidth [1]. The 24 GHz band has also been regulated for UWB vehicular radar applications [1], [2] and can be simultaneously used for communications [3], [4]. UWB presents the unique characteristic of being designed for coexistence in the same frequency range with other licensed or unlicensed services complementary in terms of bit rate and range such as WiMAX and Wi-Fi. This is achieved by limiting the mean equivalent isotropic radiated power (EIRP)[1] spectral density to −41.3 dBm/MHz and introducing detect-and-avoid (DAA) mechanisms [5]. The maximum EIRP spectral density limits the effective transmission range to a few meters. This limit range constrains UWB to wireless personal area networks (WPAN).

[1] EIRP is given as

$$EIRP = P_T(f) + G_T(f),$$

where $EIRP$ and P_T (transmitter power spectral density) are in dBm, and G_T is the gain response of the transmitting antenna in dBi. Note that $P_{out} = \int_{-\infty}^{\infty} P_T(f)\,df$ is the total average transmitter power applied to the antenna.

The radio-over-fibre transport of UWB signals (UWB-over-fibre) is a rapid and cost-effective solution to extend the UWB radio range to in-home, in-building or even wide area applications. UWB-over-fibre takes advantage of the high bandwidth of the optical media to centralize modulation and other functionalities thus simplifying the remote antenna units and enabling network infrastructures transparent to the specific UWB implementation employed. This flexibility is of special interest for operators as UWB regulation is still evolving. UWB-over-fibre systems have been considered for two main applications which are described and illustrated in Section 2.5.4. First, indoor distributed antenna systems (DAS) in which UWB signals are distributed over optical fibre links from a central unit to remote antenna units. The fibre length in the indoor DAS application is in the range of a few hundred meters [6]. In the second application, UWB signals are distributed from a central office through fibre-to-the-home (FTTH) networks with further UWB wireless transmission in home [Llo08a], [Llo08c]. Cost-effective standard single-mode fibre (SSMF) is widely used for UWB over FTTH with distances up to 20 km or more. FTTH networks are being deployed at very fast pace with significant deployments in Asia, Europe and North America [7].

There are two major UWB implementations: (1) based on impulse radio, and (2) based on multiband orthogonal frequency-division multiplexing (OFDM), as specified by the WiMedia Alliance [8] and adopted in the ECMA-368 standard [9]. OFDM UWB provides high spectral efficiency (up to 480 Mb/s per 528 MHz band) and single-chip solutions are available in consumer electronics devices targeting video streaming and wireless universal serial bus (wireless-USB) applications [10], [11]. Furthermore, OFDM-based devices employ efficient software to facilitate coexistence with a simplified system design [12]. On the other hand, impulse-radio UWB is capable of providing high-resolution radar ranging and localization applications [13] providing simultaneously high-speed communications with much simpler implementation [3].

UWB technology is capable of providing multi-Gb/s wireless communications. Maximum capacity in actual UWB devices is 480 Mb/s per band (WiMedia specification v1.2 [8], [9]). This gives an overall capacity of 6.72 Gb/s per user when the fourteen OFDM bands are combined. This capacity is supported in single-chip UWB implementations [10]. The maximum theoretical UWB capacity would be achieved when the fourteen UWB bands are used bearing 1024 Mb/s each (WiMedia specification v1.5 [8]) giving 14.336 Gb/s aggregated data rate per user. Nevertheless, no commercial equipment to date supports this configuration. However, UWB capacity is further limited outside the U.S. The spectrum useable for unlicensed UWB operation in the 3.1−10.6 GHz band is differently regulated worldwide due to coexistence issues. UWB operation in the 60 GHz band is an open opportunity to provide potential data rates of >3 Gb/s worldwide [14].

60 GHz radio is about to become easily available for consumer applications and permits secure multi-Gb/s wireless communications potentially for short-distance use. Several technologies in the 60 GHz band have been proposed in the recent years. Some of them are WirelessHD, ECMA-387, IEEE 802.15.3c, and WiGig. WirelessHD-based single-chip solutions have been integrated into consumer electronics products targeting uncompressed HD video applications up to 7 Gb/s [15]. An interesting characteristic of ECMA-387 is that single-chip solutions are

available targeting file transfer and HD streaming [16], giving the advantage of reduced board space requirements and lower manufacturing cost.

The introduction of UWB operation in the 60 GHz band is interesting for several reasons:

1) The unlicensed frequency range regulated for generic 60 GHz radio worldwide (57−66 GHz in Europe and Australia, 57–64 GHz in the U.S. and Canada, 59–66 GHz in Japan) can allocate very well the UWB bandwidth in current regulation (up to 7.5 GHz).
2) UWB is a mature technology with efficient software and single-chip solutions are also available. This permits UWB to be introduced in devices with specific space and power requirements, like mobile phones.
3) UWB is, in origin, a coexistence technology. Translating UWB technology from the 3.1−10.6 GHz band to the 60 GHz band opens the opportunity of coexistence with other wireless transmissions in the band.
4) UWB operation in the 60 GHz band permits to increase the mean EIRP from −41.3 dBm/MHz as in current UWB regulation worldwide to 13 dBm/MHz as permitted in regulation in force in the band [17]. This permits extending transmission reach provided the approximately 20 dB higher free-space path loss is compensated. Nevertheless, the atmospheric attenuation in the 60 GHz band of up to approximately 30 dB/km further limits outdoor reach [18].

This thesis proposes and experimentally demonstrates a number of techniques enabling UWB-over-fibre systems to provide multi-Gb/s WPAN communications in different frequency bands ranging from baseband to millimetre-wave (>55 GHz). The proposed systems also have potential ranging capabilities taking advantage of the excellent accuracy of impulse-radio UWB when extremely short impulses are employed. The operational limits of the proposed UWB-over-fibre systems are also investigated by simulation.

The first technical objective of this thesis is to propose, investigate, and experimentally demonstrate UWB operation in the next-generation 60 GHz band. The 60 GHz UWB systems proposed could operate in a dual 3.1−10.6 GHz/60 GHz configuration if desired, but dual operation is out of the scope of this thesis. 60 GHz operation would reuse and extend UWB technology in terms of range and flexibility, and is the focus of this work. The herein presented 60 GHz UWB techniques have potential application for FTTH access networks as well as indoor scenarios where interference is a critical issue such as aircrafts, telecommunication operators, and government premises.

Additionally, (second target) a technique to bring spectral reconfiguration capabilities to pulsed lasers is proposed, analysed, and experimentally demonstrated in this thesis. The technique has potential application for wavelength division multiplexing (WDM) networks. Current FTTH networks are expected to evolve toward WDM passive optical networks (WDM-PON) to keep up with the requirements of future broadband optical access networks [19], [20].

The technical advances investigated include:

- Generation techniques for bandwidth- and band-flexible impulse-radio UWB-over-fibre systems

- Generation and integrated optical and wireless transmission performance of 60 GHz UWB signals. The use of vertical-cavity surface-emitting lasers (VCSEL) is investigated to perform electrooptic conversion and optical frequency up-conversion. In recent years, VCSEL have gained a lot of interest due to the relative low cost.
- Reconfiguration of multiwavelength sources in terms of wavelength spacing and wavelength allocation

The techniques developed are implemented in the optical domain and fall in the field usually known as “optical signal processing”. Optical techniques are critical for future-proof, versatile and high-capacity service provisioning in optical networks. Optical techniques can also benefit from the well-known advantages offered by microwave photonics devices, such as light weight, small size, and immunity to electromagnetic interference [21].

1.2 State-of-the-art

UWB-over-fibre technology has been actively investigated during the time of realization of this thesis. In this Section, the state-of-the-art of the generation, optical and wireless transmission, and detection of UWB signals for UWB-over-fibre systems is reviewed.

1.2.1 Impulse-radio UWB generation in the 3.1−10.6 GHz band

In impulse-radio UWB systems, the selection of the pulse shape by taking into account the frequency response of the transmitting antenna is critical for system performance [22]. The Gaussian monocycle and doublet pulses are typically employed due to better performance compared with other pulse shapes [23]. A Gaussian monocycle can be generated by performing the first-order derivative of a Gaussian pulse, and a Gaussian doublet can be generated by performing the second-order derivative of a Gaussian pulse. However, these pulse shapes are not compliant with the UWB EIRP spectral mask in current regulation [1] without reducing power. Gaussian monocycle and doublet pulses can also meet regulation after adequate filtering e.g. by the frequency response of a commercially-available UWB antenna [24] or custom antenna [25], or by a high-pass filter [26]. Other higher-frequency pulse shapes such as higher-order derivative Gaussian pulses [27] and linear combination of low-order derivatives [28], [29], have been proposed to comply with the UWB mask with high power efficiency, however they are generally more complicated to implement.

Electrical impulse-radio UWB generation

There are different approaches to implement UWB-over-fibre systems. Typically, a UWB RF signal modulates the intensity of a laser diode directly or externally followed by optical fibre transmission [30]. Electrical impulse-radio UWB generation techniques can be divided into four categories [31], [32]:

1) A baseband pulse is up-converted to the target frequency band by mixing with a local oscillator (LO).

2) Shaping a very short baseband pulse to the desired UWB pulses employing band-pass filtering. Filtering a Gaussian pulse is equivalent to the implementation of different orders of differentiation of a Gaussian pulse.
3) UWB pulse design based on combining pulses. For instance, combining baseband Gaussian pulses with different delays and amplitudes.
4) High-speed arbitrary waveform generation (AWG) with sampling rate over 20 GS/s based on digital-to-analogue converters (DAC).

A Gaussian monocycle generator consisting of an impulse generator followed by an impulse forming network is a commercially available solution [33]. This impulse generator requires a clock input to generate impulses, which can be gated by external data up to 2.5 Gb/s. Single-chip prototypes with modulation capabilities have also been demonstrated in the literature with potential cost advantage [31], [34]. State-of-the-art single-chip solutions enable generation of UWB pulses with not only low power consumption, but also reconfigurable shape, signal bandwidth of 6 GHz, and data rate up to 2.5 Gb/s [31].

Optical impulse-radio UWB generation

Impulse-radio UWB generation in the optical domain can overcome the difficulty of electrical techniques in generating high-quality high-bandwidth EIRP-efficient pulses reconfigurable in terms of bandwidth, shape, and pulse encoding. Furthermore, optical techniques remove the impact of nonlinearity using electrooptic conversion due to high peak-to-average power ratio (PAPR) of impulse-radio UWB signals. Data are typically encoded on impulse-radio UWB signals employing on-off keying (OOK) modulation, pulse polarity modulation (or bi-phase modulation or binary phase-shift keying (BPSK), pulse position modulation (PPM), and pulse shape modulation (PSM).

Photonic generation of impulse-radio UWB signals has been widely investigated in recent years [22], [24]–[26], [35]–[57]. Most techniques can be classified into four categories according to the operation principle:

1) Gaussian monocycle or doublet pulse generation based on first- or second-order differentiation of a Gaussian pulse. This can be accomplished by direct modulation of a laser and chirp-to-intensity conversion employing an optical linear filter [36]. Another simple technique is to perform phase-modulation-to-intensity-modulation (PM-IM) conversion employing an optical frequency discriminator. A method to avoid using a fixed-long-length dispersive fibre is to use a frequency discriminator based on an optical filter, such as a fibre Bragg grating (FBG) [37], [38]. The optical phase modulation can be implemented employing electrooptic phase modulation [37] or cross-phase modulation (XPM) in nonlinear fibre for all-optical generation [38]. A simple UWB pulse generator which is capable of performing BPSK or PSM at high speed (up to 40 Gb/s) has also been demonstrated by adjusting the voltages applied to two arbitrary wave plates [39].
2) Combined delayed optical Gaussian pulses with opposite polarities. A simple technique employs an integrated dual-parallel Mach-Zehnder modulator (MZM) to generate Gaussian monocycle or doublet pulses [40]. Another possible implementation is to

employ a microwave photonic filter. Gaussian monocycle or doublet pulses can be generated employing two-coefficient or three-coefficient filters, respectively. The polarity inversion can be performed based on cross-polarization modulation [41], [42], and employing two MZM biased at opposite slopes [43]. Polarization-dependent delay is introduced by birefringent fibre [41], [42], or wavelength-dependent delay by a dispersive device such as a dispersive fibre distributing the UWB pulse to a remote site [43]. The microwave photonic filter proposed in [43] can overcome the difficulty of other approaches to add and control more than two coefficients. High-frequency pulses can be generated from four coefficients however each additional coefficient requires an extra laser. The technique in [43] also permits reconfiguration in terms of pulse shape and encoding up to 100 Mb/s. In addition, a monocycle generation technique employing an electrooptic phase modulator, a delay interferometer, and an optical delay line has been demonstrated [44]. This technique employs a low-speed electrical non-return-to-zero (NRZ) signal and BPSK modulation can be realized by adjusting the delay or by electrically switching the bias voltage of the delay interferometer.

3) Dynamic behaviour of a semiconductor optical amplifier (SOA) [45] and of a directly-modulated [46], [47] or optically-injected distributed feedback laser (DFB) [47]–[49]. These methods are simple, requiring one laser. A specific regulation-compliant high-frequency pulse has been generated based on the relaxation oscillations of DFB [47]–[49]. BPSK modulation has been demonstrated employing an adequate electrical data pattern [49], however multi-Gb/s data rates would require a high-speed pulse pattern generator (>20 Gb/s).
4) Optical spectrum shaping and frequency-to-time conversion. Usually, the spectrum of an ultra-short pulse is shaped by a spatial light modulator (SLM) [50] or optical filtering [22], [51], [52]. The shaped spectrum is converted to the time domain employing a dispersive element with a minimum required total dispersion, such as a dispersive fibre, which at the same time distributes the UWB pulse to a remote site [52], or a linearly-chirped FBG to simplify the system [51]. These techniques have more flexibility in generating UWB pulses with arbitrary shapes however they are based on complicated implementations requiring costly mode-locked laser sources [22], [51], and either bulky free-space optics [50] or custom environment-sensitive FBG-based devices [22], [51], [52].

In addition to the techniques discussed above, other techniques have been proposed for high-frequency UWB generation such as those based on nonlinear propagation in optical fibres [53] and combination of delayed monocycles with opposite polarity [54]. In addition, UWB generation with PPM encoding [55], [56], and simple UWB generation reconfigurable for multiple modulation formats have been demonstrated [57].

1.2.2 Millimetre-wave impulse-radio UWB generation

There are different approaches for implementing millimetre-wave UWB-over-fibre systems. Optical frequency up-conversion is an attractive solution to reduce overall complexity and cost by centralised broadband up-conversion and network management. However, this approach

may require high-speed electrooptic devices and suffer from RF power fading induced by fibre chromatic dispersion, which may limit performance [58]. On the other hand, the centralised approach may find a competitor in a distributed single-chip solution based on UWB over fibre and millimetre-wave up-conversion using complementary metal-oxide semiconductor (CMOS) at RF front-end. A few research groups have already demonstrated CMOS radios at 60 GHz. However, there are limitations such as device design and integration, making high-performance communication extremely difficult.

A number of techniques have been demonstrated for millimetre-wave impulse-radio UWB-over-fibre generation based on centralised optical frequency up-conversion [3], [40], [59]–[62]. The use of RF pulse shapes, such as Gaussian monocycles and higher-frequency pulses, offers two advantages as compared to pulse shapes having DC component in the spectrum, such as Gaussian and rectangular pulses: (1) easy filtering of the up-converted UWB spectrum to remove residual RF carrier which can limit maximum EIRP density to meet regulation in force, thus limiting UWB range [60]; (2) the baseband signal which is also available after photodetection could be radiated in the 3.1−10.6 GHz band provided an adequate spectrum and UWB antenna are combined. Several millimetre-wave techniques have been demonstrated in the 24 GHz band in proof-of-concept experiments [3], [40], [60]–[62] and are summarized as follows:

- Kuri *et al.* (Oct. 2006) [3]: Frequency up-conversion is based on optical carrier suppression in a MZM, an arrayed waveguide grating, and a special MZM with high extinction ratio to suppress the residual RF carrier when rectangular pulses are employed. This complex technique has been proposed to overcome dispersion-induced RF power fading. The technique would require 30 GHz electrooptic devices to be upgraded to the 60 GHz band. 3 m of wireless transmission of the 24 GHz UWB signal is demonstrated at 250 Mb/s.
- Le Guennec *et al.* (Jul. 2007) [60]: Frequency up-conversion of electrical monocycles at 200 Mb/s is performed based on optical carrier suppression in a MZM. This technique is simple and the same architecture can be reused for coherent down-conversion. However, the technique requires high-cost high-frequency electrooptic devices, which make it difficult to be upgraded to millimetre-wave frequency bands, e.g. 60 GHz devices for the 60 GHz band.
- Fu *et al*. (Jun. 2008) [61]: Frequency up-conversion of optical monocycles at 750 Mb/s is performed based on optical carrier suppression in a MZM and nonlinear polarization rotation in a SOA. The technique operates in the whole *C*-band however it employs a complex architecture and the slow carrier recovery speed of the SOA limits high-frequency operation in the millimetre-wave bands.
- Chang *et al*. (Oct. 2008) [40]: Optical monocycle or doublet pulses at 625 Mb/s are up-converted based on optical carrier suppression in a MZM. The technique would require 30 GHz electrooptic devices to be upgraded to the 60 GHz band.
- Li *et al*. (Sept. 2009) [62]: Frequency up-conversion of optical monocycle or doublet pulses at 470 Mb/s is performed based on optical carrier suppression in a MZM and a fibre optical parametric amplifier (OPA) employing 1 km of highly nonlinear fibre (HNLF). This technique employs a complex architecture however it could be upgraded

to the 60 GHz band by filtering the second-order optical sidebands with a relaxed frequency requirement for electrooptic devices as low as 7.5 GHz. In addition, the technique exhibits large mixing bandwidth capability due to the ultrafast response of the HNLF.

The techniques [61], [62] can be deployed in the remote local oscillator delivery scheme to mitigate dispersion-induced RF power fading in the long-reach access networks where the SOA and HNLF serve as both frequency up-converter and signal amplifier in a local exchange [63]. Furthermore, Zhang *et al*. have demonstrated simultaneous generation of two wavelength channels of UWB monocycles in the 3.1–10.6 GHz band and two wavelength channels in the 24 GHz band based on a similar scheme employing 60 m of a highly nonlinear photonic crystal fibre [64].

Additionally, several photonic schemes have been demonstrated for shaping of high-frequency impulse-radio UWB signals [53], [65].

Gigabit impulse-radio UWB transmitters have also been developed in the 60 GHz band in CMOS technology targeting low cost and low power consumption [66]. In hybrid wireless-optical systems, such transmitters could be used at remote antenna units after photodetection of digital baseband-over-fibre signals.

Finally, a photonic impulse-radio UWB transmitter in the *W*-band (75–110 GHz) employing a near-ballistic uni-traveling-carrier photodiode and a 10 GHz mode-locked laser has been demonstrated for high density user UWB-over-fibre in-building applications [59].

1.2.3 Detection and transmission performance of impulse-radio UWB signals

Many reports focused on the optical generation of impulse-radio UWB signals in recent years. However, a few reports detected the UWB signals and further evaluated the performance of the whole UWB-over-fibre system including fibre and wireless transmission. Radio-over-fibre distribution of impulse-radio and OFDM UWB signals in FTTH networks was proposed and compared in [Llo08a], [Llo08c]. Optical transmission up to 50 km of SSMF was experimentally demonstrated for both UWB implementations at 1.25 Gb/s. Other optimized impulse-radio UWB generation and detection schemes have been demonstrated employing optical signal processing. Table I summarizes the state-of-the-art of the integrated optical fibre and wireless transmission performance of impulse-radio UWB-over-fibre communication systems in different frequency bands.

The performance of impulse-radio UWB signals is usually evaluated in terms of bit error rate (BER) which is the ratio between the number of bits with errors and the total number of bits.

Table I. State-of-the-art of transmission performance of impulse-radio UWB-over-fibre systems

Reference	Encoding	Data rate	Fibre transmission	Wireless distance	Considerations
3.1–10.6 GHz band					
Abtahi *et al*. [22]	OOK	500 Mb/s	B2B	65 cm	• Photonic envelope detection+*Q*-factor
Hanawa *et al*. [25]	OOK	1.025 Gb/s	5 km DCF+10 km SSMF	20 cm	• Pre-amplified receiver • Custom antennas • Detection directly by BERT (>10^{-5})
Yu *et al*. [49]	BPSK	781.25 Mb/s	30 km SSMF+5 km DCF	B2B	• DSO+DSP detection (BER >10^{-4})
Shams *et al*. [55]	PPM	1.625 Gb/s	200 m SSMF	~20 cm	• UWB shaping by electrical BPF • Detection by electrical mixing+BERT (>10^{-9})
Pan & Yao [24]	OOK	1.6875 Gb/s	24 km SSMF	5 cm	• Chirp-free UWB signal • Detection by electrical mixing+BERT (>10^{-9})
Gibbon *et al*. [48]	OOK	3.125 Gb/s	25 km SMF+25 km IDF	2.9 m	• EIRP= −31.3 dBm/MHz • DSO+DSP detection (BER >10^{-5})
Shams *et al*. [56]	PPM	1.625 Gb/s	37 km SSMF (or 10 km with a simpler scheme)	B2B	• Pre-amplified receiver • UWB shaping by electrical BPF • Detection by electrical mixing+BERT (>10^{-9})
Pan & Yao [57]	OOK, BPSK, PSM, PAM	625 Mb/s	20 km SSMF	10 cm	• Detection by electrical mixing+BERT (>10^{-9})
Chang *et al.* [67]	OOK	1.25 Gb/s	25 km SSMF	30 cm	• Pre-amplified receiver • Custom antennas • Detection directly by BERT (>10^{-5})
Zhou *et al*. [54]	OOK	3.125 Gb/s	22.5 km SMF+4.4 km DCF	B2B	• Photonic envelope detection+BERT (>10^{-9})
60 GHz band					
This work (Section 4.1) [Bel10c], [Bel11a]	BPSK	1.44 Gb/s	40 km SSMF; 25 km SSMF+500 m BI-SMF	5 m	• DSO+DSP detection (BER >10^{-5})
This work (Section 4.2) [Bel11b]	OOK	3.125 Gb/s	20 km NZ-DSF (≡ 6.5 km SSMF); 1 km BI-SMF	2 m	• RF power detection+BERT (>10^{-9})
75–110 GHz band					
Chow *et al*. [59]	OOK	2.5 Gb/s	250 m SSMF+50 m DCF	1.6 m	• Optical power budget< 30 dB • RF power detection+BERT (>10^{-6})

Impulse-radio UWB signals have been detected by several techniques:

1) The UWB signal in the 3.1–10.6 GHz band has been down-converted by electrical mixing with a LO signal. However, this technique introduces a power penalty due to a broad UWB spectrum and is constrained to data rates of less than 3–4 Gb/s [56]. The resulting baseband signal is measured by an oscilloscope providing performance in terms of *Q*-factor [Llo08a], [Llo08c]. BER is calculated from *Q*-factor measurements however under the assumption of Gaussian noise. Alternatively, the down-converted baseband signal can be measured by a BER tester (BERT) [24], [55].
2) BER has been evaluated offline by digital signal processing (DSP) based on bit-per-bit comparison [68]. This technique gives high sensitivity and permits to implement in the digital domain functions such as matched filtering to increase signal-to-noise ratio (SNR) thus improving performance. However, a broadband high-speed digital sampling oscilloscope (DSO) is required. The minimum BER evaluated (or maximum number of bits evaluated) is also limited by the DSO performance to 10^{-6} typically. This BER limit is above the limit of 10^{-9} typical for error-free communication systems without employing forward error correction (FEC) [69].
3) Envelope detection (or power detection) can be employed for OOK-modulated UWB signals avoiding the need for a phase-locked LO signal and broadband RF mixer. Photonic envelope detection of RF UWB pulses has been demonstrated based on a MZM biased at the quadrature point, high-speed photodetection, and low-pass filtering [3]. High-speed photodetection permits to regenerate the RF UWB signal. Another possibility is to employ an electro-absorption modulator (EAM) or a MZM biased at the minimum transmission point [22], [54]. MZM leads to full rectification of the RF UWB signal resulting in higher detected power. However, MZM are sensitive to polarization. On the other hand, EAM leads to half wave rectification, can operate on lower driving voltage, and are compatible with photonic integration [22]. RF power detection has also been employed to detect impulse-radio UWB signals in the 75−110 GHz band [59]. An advantage of the photonic envelope detection is the broadband operation providing transparency to the RF frequency and capability of detecting broad intermediate frequency (IF) bandwidths.

1.2.4 Multiband OFDM UWB radio-over-fibre

OFDM UWB radio-over-fibre systems have been considered as a solution for high-capacity wireless access networks. OFDM UWB signals are usually generated employing commercially-available UWB devices or AWG signal generation, which then modulate a laser diode directly or externally followed by optical fibre transmission. OFDM detection is performed employing a DSO, and custom DSP or commercially-available software. The maximum number of OFDM symbols to be evaluated is limited by the DSO performance and software employed. The quality of OFDM UWB communication is usually assessed in terms of error vector magnitude (EVM) which is a measure of errors between the measured symbols and the expected symbols. SNR and BER performance metrics can be estimated from EVM assuming a Gaussian noise distribution when OFDM UWB employs quadrature phase-shift keying (QPSK) modulation [70].

Combined radio-over-fibre and wireless transmission of OFDM UWB signals has been experimentally analysed employing external modulation [Mor08c], [71]. Commercially-available UWB devices are employed to generate a dual-band OFDM signal at 400 Mb/s. The OFDM signal is successfully distributed up to 10 km of SSMF and 1.5 m of wireless range or up to 50 km of SSMF with optical amplification in the field and 1 m wireless distance. Optical transmission performance of OFDM UWB up to 200 Mb/s has also been experimentally investigated and theoretically analysed in [72]. In addition, bidirectional OFDM UWB transmission over 1 km of SSMF has been demonstrated at 480 Mb/s employing VCSELs [73]. Finally, the potential of glass multimode fibres (MMF) and multimode plastic optical fibres (POF) to extend the in-building coverage of OFDM UWB has been demonstrated at 200 Mb/s and 480 Mb/s [74].

Millimetre-wave OFDM UWB systems have also been investigated. Performance of 30 GHz three-band OFDM UWB at 600 Mb/s when transmitted over 20 km of SSMF has been experimentally demonstrated employing an optically pre-amplified receiver [75]. Optical frequency quadrupling up-conversion based on two cascaded dual-drive MZM is proposed in this technique. 60 GHz OFDM UWB generation have also been investigated at 200 Mb/s without transmission based on external modulation of OFDM UWB combined with up-conversion by optical carrier suppression in a MZM [76].

1.2.5 UWB optical and wireless coexistence

UWB-over-fibre systems supporting simultaneous multiservice delivery are attracting great interest for converged access networking. Simultaneous transmission over up to 25 km SSMF of OFDM UWB and WiMAX signals has been demonstrated employing polarization multiplexing [77]. Optical coexistence of impulse-radio UWB and WiMAX over a 50 km dispersion-managed optical link has been demonstrated employing a directly-modulated VCSEL [26]. Bidirectional radio-over-fibre transmission of simultaneous wireless standards UWB, WiMAX, and LTE has been experimentally demonstrated to deliver triple-play services (HD audio/video, data, and cellular phone, respectively) in next-generation optical access networks [Llo11b]. Optical transmission over 50.6 km of SSMF [78] and combined transmission over 20.2 km of SSMF and 3 m of wireless distance [79] have been demonstrated. In-building optical extension after 20.2 km of SSMF has also been demonstrated up to 200 m of bend-insensitive single-mode fibre (BI-SMF) and up to 50 m of POF [80]. In addition, optical-wireless transmission of converged wired and UWB radio services over MMF [Jen10] and over POF [81] has been demonstrated for in-building networks. Multi-standard OFDM-based transmission of UWB and 802.11 has also been demonstrated over POF [82]. Finally, wireless coexistence of UWB and WiMAX up to 10 m has been evaluated by on-field experiments [Per09a], [Per09b], [Per09c].

1.3 Improvement over the state-of-the-art

This thesis proposes several innovative approaches –in the optical domain- to enable flexible and cost-effective multi-Gb/s UWB-over-fibre systems for next-generation hybrid wireless-optical networks. UWB operation in the next-generation 60 GHz band is proposed to extend

UWB capabilities to a wider variety of scenarios including FTTH networks overcoming coexistence issues and in-aircraft environments with interference limitations.

The main improvements over the state-of-the-art in this thesis can be summarized in:

1) Two simple techniques are proposed and experimentally demonstrated for Gaussian-monocycle shaping, which are based on: (1) optical delay and balanced photodetection [Bel08c], and (2) differential photoreceiver and electrical delay [Bel09a], [Bel10a]. The effects of the chromatic dispersion of optical access fibre over the generated UWB pulse can be compensated by adjusting delay. The techniques exhibit the advantage of being implemented at the remote antenna units permitting to flexibly adapt UWB spectrum to different fibre dispersion. The implementation trade-offs for UWB-over-fibre generation in the 3.1−10.6 GHz band are also addressed.
2) The combination of both radio technologies impulse-radio UWB and 60 GHz is proposed in this thesis to wirelessly provide in-flight entertainment services minimizing interference [Bel09a], [Bel10a]. The use of an impulse-radio UWB implementation is of special interest for in-flight environments to simultaneously provide for instance localization of interfering users. A 60 GHz UWB-over-fibre system with 100 m of SSMF in-cabin transmission is demonstrated at 1.25 Gb/s in a laboratory proof-of-concept experiment. A techno-economic analysis is also performed suggesting that the system which is based on UWB-over-fibre with optical frequency up-conversion could compete with an approach based on baseband data over fibre and remote UWB generation and frequency up-conversion in the electrical domain.
3) UWB impulse radio optical generation by frequency shifting in dispersive optical fibre providing remote connectivity is proposed and experimentally demonstrated in this thesis [Bel10b], [Bel11d]. The technique combines optical carrier suppression in a MZM with matched fibre chromatic dispersion targeting to overcome the bandwidth limitation of optical frequency up-conversion, with the advantage of being easily reconfigurable generating simultaneously different RF bands. The technical aspects and possible configurations of multiband generation tailored for UWB-over-fibre transmission in optical access networks is investigated with special focus on dual 24 GHz/60 GHz operation. The impulse-radio UWB implementation can simultaneously serve different applications including 24 GHz vehicular radar and infrastructure-to-car communications and 60 GHz FTTH through simple optical access infrastructure. 60 GHz signal generation by 12.5 km of SSMF and 1 m of wireless transmission, and dual 24 GHz/60 GHz operation have been experimentally demonstrated at 1.25 Gb/s. Enabling technologies for reliable, simple, and cost-effective real implementation are also discussed.
4) UWB operation in the 60 GHz band is proposed in this thesis to deliver high-bandwidth services in FTTH networks [Bel10c], [Bel11a]. UWB generation with combined optical and wireless transmission performance is experimentally evaluated when operating in the 60 GHz band. VCSEL direct modulation combined with optical carrier suppression in a MZM is investigated for generation of two major UWB implementations –three-band dual-carrier modulation (DCM) OFDM reusing commercially-available chips, and BPSK impulse radio. 60 GHz UWB generation with combined 40 km of SSMF and 5 m of

wireless transmission is experimentally demonstrated at 1.44 Gb/s, as shown in Table I. The results permit, from an application point-of-view, to select a given UWB implementation depending on network reach and system complexity desired.

5) The use of a VCSEL for flexible UWB frequency up-conversion is investigated and compared with conventional low-linewidth external-cavity laser (ECL) [Bel11b]. Extension to the 60 GHz band, combined transmission over 6.5 km SSMF or 1 km of in-building BI-SMF and 2 m of wireless transmission, and RF power detection of OOK impulse-radio UWB [48], is experimentally demonstrated at 3.125 Gb/s, as shown in Table I. The results permit, from an application point-of-view, to select a given laser technology depending on network reach and system complexity desired.
6) Novel multiwavelength sources with great reconfiguration capabilities based on the spectral self-imaging effect (or Talbot effect) by time-domain multiphase modulation of a periodic pulse train [Car11] are proposed in this thesis [Bel11c]. The reconfiguration technique offers the advantage of being able to multiply the number of optical carriers without influencing bandwidth and time-domain pulses. Reconfiguration of a pulsed laser in terms of wavelength spacing and wavelength allocation is experimentally demonstrated employing external electrooptic bi-phase modulation. The technique is of special interest to provide stable and flexible channel spacing in WDM and OFDM optical transmission systems [83].

1.4 Outline of this work

The contents of this thesis are organized in six chapters:

In Chapter 2, the fundamentals of hybrid wireless-optical systems, and the associated transmission impairments are drawn. Emphasis is made in enabling technologies required to provide multigigabit wireless communications including UWB and 60 GHz radios. Radio-over-fibre technology is reviewed focusing on state-of-the-art transmission systems and the enabling techniques used in generation and demodulation of wireless signals. As a major application of this work, the integration of UWB radio-over-fibre in FTTH optical access networks is also discussed.

In Chapter 3, the work performed in this thesis related to generation of impulse-radio UWB signals in the optical domain is described. First, two techniques for simple and flexible UWB pulse shaping are proposed and experimentally demonstrated. Second, pulses generated by one of these techniques are employed in a proof-of-concept experiment of a UWB-over-fibre system in the 60 GHz band. The combination of UWB and 60 GHz radio technologies for interference-sensitive in-aircraft scenarios is discussed. A techno-economic comparison of the system with a potential competitor solution is also presented. The key parameters and expected performance of the scheme is further identified by simulation analysis (VPItransmissionMaker™). Finally, flexible photonic generation of impulse-radio UWB up to millimetre-wave bands based on frequency shifting in optical access fibre is proposed. Feasibility of the technique in FTTH networks operating in the 60 GHz band is experimentally demonstrated. Practical multiband capabilities and limitations of this system are also addressed by comprehensive simulation analysis (VPItransmissionMaker™). Dual

24 GHz/60 GHz operation is also experimentally demonstrated. Practical implementation is addressed and competitive approaches are discussed.

In Chapter 4, performance of UWB signals when operating in the 60 GHz band is evaluated combining optical and wireless transmission. Two experimental demonstrations are performed investigating the use of VCSEL for direct modulation and up-conversion, respectively. In the first experiment, two major UWB implementations –DCM OFDM and BPSK impulse radio- are compared. A simulation analysis (VPItransmissionMaker™) is performed to investigate the operational limits. VCSEL is compared with conventional ECL in the second experiment. Limitations of this system are also analysed by simulation (VPItransmissionMaker™).

In Chapter 5, reconfigurable multiwavelength sources are proposed and experimentally demonstrated. Twofold and fourfold multiplication of the number of wavelengths and wavelength shifting of a pulsed laser are demonstrated. The impact of laser chirp and noise is numerically analysed (MATLAB®). Potential applications of the technique are also discussed.

Finally, the conclusion of this Ph.D. thesis and the ongoing and future work are addressed in Chapter 6.

2

Hybrid wireless-optical systems based on ultra-wideband (UWB) radio

Next-generation access networks will require flexible deployment, high capacity, upgradeability, scalable to user number and demand, and be economically feasible. Hybrid wireless-optical systems that combine high-capacity optical fibre transmission and the flexibility of wireless technologies are foreseen to play an important role in next-generation access networks. The wireless part provides a multiple access solution to eliminate the need for optical fibre to every end-user thus saving on network deployment cost [84]. Integrated wired/wireless access can also extend the reach of existing optical access infrastructure to those users that cannot be connected directly to the fibre for economic, environmental or other reasons [85]. Multigigabit wireless systems that provide capacities comparable to optical fibre communication systems will pave the way for providing seamless integrated wired/wireless access to broadband services for the end-user. Radio-over-fibre technology combined with multigigabit wireless systems is seen as a fast deployable and cost-effective solution for providing seamless integrated wired/wireless access [Llo08a], [85].

2.1 Multigigabit wireless communications

Popular wireless standards, which operate at frequencies below 10 GHz (e.g. cellular, Wi-Fi, WiMAX, etc.), can support data rates up to several tens of megabit per second. In addition, fixed wireless radios operating in the microwave frequency bands from 6 to 40 GHz are widely used for connecting buildings and other point-to-point (P2P) data connectivity. P2P microwave is limited in providing speeds higher than few hundreds of megabit per second [86]. With the advent of popular bandwidth services such as HD video or on-line gaming, wireless systems are required to offer data rates higher than these provided by conventional wireless standards and P2P microwave links.

UWB is a radio technology capable of providing a wide variety of applications including multigigabit communications. UWB features low EIRP density which limits wireless range to a few meters. This technology offers significant benefits, making it a suitable candidate to complement other wireless technologies to achieve ubiquitous communications. UWB has

been designed to be able to coexist with other wireless technologies operating in the same frequency range thus enabling efficient use of the RF spectrum. However, in order to ensure a robust communication link, the issue of coexistence and interference of UWB systems with current and future wireless systems must be considered, as discussed in Section 2.1.1. Furthermore, one of the main constraints to widen the deployment of this technology is the lack of harmonization of worldwide regulations due to coexistence issues.

Millimetre-wave radio systems are also considered as a promising solution to provide multigigabit communications [86]. These systems are reviewed in Section 2.1.2. Millimetre-wave bands at around 60 GHz and higher can provide bandwidth enough to easily support multi-Gb/s capacities. Of great interest, the 60 GHz band is about to become easily available for consumer electronics applications led by the bandwidth availability of 7 GHz worldwide with high EIRP allowed.

Additionally, FSO technologies are able to support multi-Gb/s data rates. FSO technologies operate in optical frequency regions, where very large bandwidths are available that enables very high data rate transmission. However, range is significantly shortened by fog and complex systems are required to compensate for other physical effects [86]. FSO links are commercially available, offering 1, 10, and even 40 Gb/s for outdoor communications over distances of several kilometres [87].

Finally, optical wireless transmission systems have been demonstrated for broadband indoor applications based on infrared radiation (mostly around 850 nm or 1550 nm) as well as visible light (400–780 nm) [88], [89]. These systems are of interest as a huge unregulated bandwidth is available and these signals do not penetrate walls, thus enabling high-capacity wireless networks with potential application for interference-sensitive scenarios. Infrared multi-Gb/s communications have been demonstrated up to 12.5 Gb/s (error-free) [90]. However, a lot of technological advances are required to achieve low-cost systems with wide coverage area. In addition, visible light systems have been demonstrated to support high data rates exceeding 500 Mb/s or 800 Mb/s with WDM, employing discrete multitone (DMT) modulation [91]. Adaptive modulation techniques could theoretically produce >1 Gb/s. Relatively low cost light emitting diode (LED) sources are employed however their low bandwidth mostly limit system performance. Few-meter distances could be achieved employing several LEDs in parallel.

2.1.1 Coexistence and interference with regulated narrowband services

Fig. 1 compares high data rate wireless technologies in terms of data rate and distance.

Wireless fidelity (Wi-Fi: 802.11) is a short-distance technology, popular for local area network (LAN) or hotspot connectivity. The most recent variation of the standard, 802.11n, offers theoretical data rates up to 600 Mb/s. However, practical data rates are typically 1−2 Mb/s.

Worldwide interoperability for microwave access (WiMAX: 802.16) targets short- to medium-range wireless communications providing theoretical data rates of tens of megabit per second, although real implementations provide data rates of approximately 2−4 Mb/s. Future extension 802.16m is expected to offer up to 1 Gb/s fixed access speeds or 100 Mb/s in mobility.

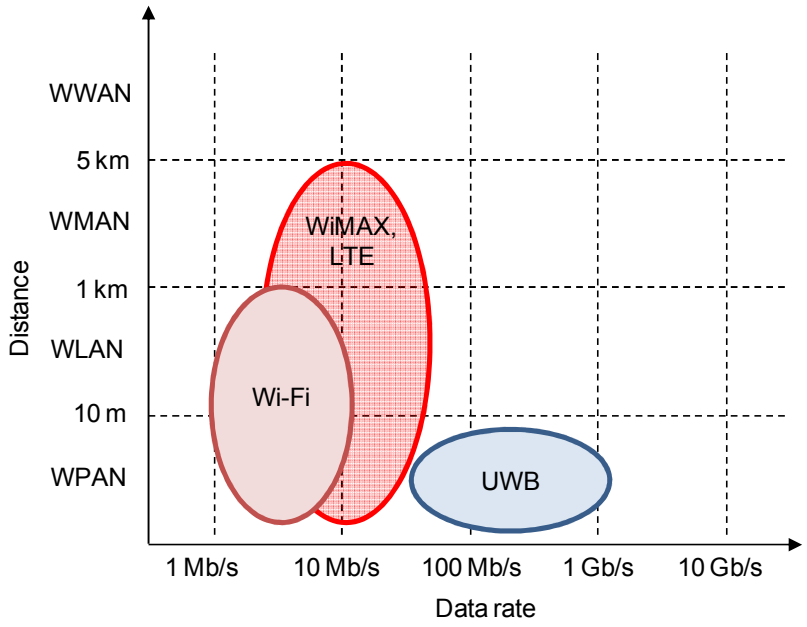

Fig. 1. Comparison of the major high data rate wireless standards operating up to 10.6 GHz in terms of coverage area and data rate, showing the complementarity of UWB.

Long-term evolution (LTE: 3GPP) is expected to become an important part of next-generation cellular networks. LTE-Advanced update offers data rates up to 1 Gb/s fixed speeds and 100 Mb/s to mobile users. The most common frequency band is 2.6 GHz, but LTE also operates at 800 MHz, 1.5 GHz, 1.8 GHz and 3.5 GHz.

UWB is a radio technology capable of providing short-range multigigabit communications using regulated spectrum from 3.1 to 10.6 GHz. UWB signals are defined as any radio signals with a minimum 10 dB bandwidth of 500 MHz or 20% fractional bandwidth [1], as summarized in Table II in Section 2.3.2. The maximum mean EIRP spectral density is −41.3 dBm/MHz, which limits the communication range to a few meters (WPAN). The range of UWB radio has been reported to exceed 10 m at 100 Mb/s data rate [27], or up to 1.1 m at 1067 Mb/s [92].

Maximum capacity in actual UWB devices is 480 Mb/s per band following WiMedia specification v1.2 [8], [9]. This gives 6.72 Gb/s aggregated data rate per user when the fourteen OFDM bands are combined covering the whole 3.1–10.6 GHz band. This capacity is supported in single-chip UWB implementations [10]. The maximum theoretical aggregated data rate per user is 14.336 Gb/s by combining the fourteen OFDM bands bearing 1024 Mb/s each (WiMedia specification v1.5 [8]). Nevertheless, no commercial equipment to date supports this configuration.

UWB operates at a much wider bandwidth and much lower EIRP density than conventional narrowband wireless data technologies in order to enable operation along the same time interval without causing any harmful interference, even if narrowband wireless signals operate within the UWB frequency band. Fig. 2 shows several existing narrowband wireless data standards that could be potentially interfered by UWB operation. UWB must guarantee the interoperability with other radio communication systems deployed in the same WPAN environment.

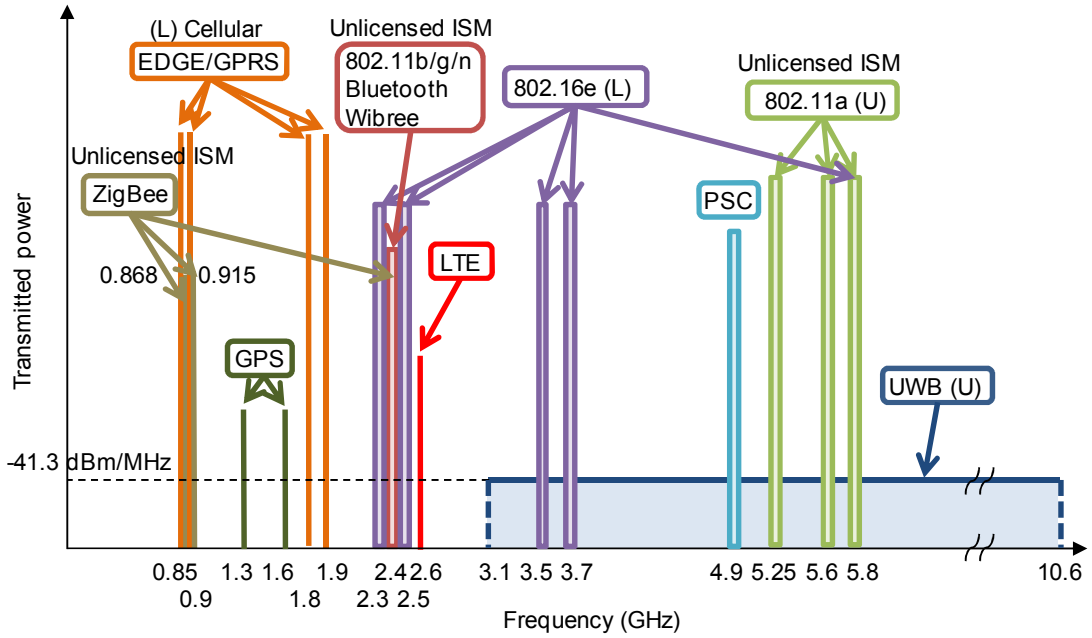

Fig. 2. Frequency allocation of licensed (L)/unlicensed (U) wireless communication standards up to 10.6 GHz, showing narrowband technologies which could be potentially interfered by UWB. ISM: Industrial, Scientifical and Medical. PSC: Public Safety Communications. (Note: power and bandwidths not to scale)

Furthermore, UWB protection from interference caused by other wireless systems must not be requested. For instance, there are deployed WPAN systems such as Bluetooth 802.15.1 and ZigBee 802.15.4 and also there are other systems present in WPAN environments, such as Wi-Fi 802.11, WiMAX 802.16, and LTE. Complementary to narrowband wireless standards such as Wi-Fi, WiMAX, and LTE, UWB is capable of providing data speeds higher than 1 Gb/s at a few meters range, as shown in Fig. 1. Hence, coexistence of UWB with other narrowband communication systems enables an efficient use of the RF spectrum and simultaneous multiservice provision of desired information on any devices anywhere and at any time.

Although EIRP spectral density masks have been defined in current UWB regulation in several countries, as discussed in Section 2.3.2, the potential UWB interference has to be further evaluated for the successful interoperation with the existing and coming systems. There are many parameters that can influence the way a UWB system would interfere to a narrowband system, or vice versa, such as the number and distribution of the interferers, the relative power of the interferers, UWB modulation, data rate, the centre frequency of the narrowband system, and the type and structure of the receivers. As an example, coexistence between standard UWB in the 3.168–4.752 GHz band up to 200 Mb/s and WiMAX 802.16e at 3.5 GHz up to 12.68 Mb/s (20 MHz bandwidth) has been evaluated by field trials in a real meeting room scenario at different WPAN distances up to 10 m [Per09a], [Per09b], [Per09c]. In this scenario, UWB is intended to provide short-range services such as file sharing and printing (UWB-enabled laptops and portable printers) and HD video streaming (UWB-enabled projectors), whereas WiMAX is intended for wireless LAN (WLAN) connectivity and Internet access.

Interference mitigation techniques have been proposed so as to further facilitate radio coexistence, such as DAA techniques as required in current UWB regulation in the EU, Japan and Korea, as discussed in Section 2.3.2. UWB devices implementing DAA techniques are capable of dynamically detecting the presence of radio services operating in the vicinity which could be potentially interfered and controlling the emitted power in order to not interfere.

2.1.2 Millimetre-wave radio technology

Millimetre-wave bands at around 60 GHz and higher can provide bandwidth enough to easily support multi-Gb/s capacities even when high spectral efficiency modulation formats such as OFDM are not used. The 60 GHz band has been widely studied as 7 GHz bandwidth has been allocated by regulation worldwide, which can be used for unlicensed communications, as discussed in Section 2.4.2. A number of technologies in the 60 GHz band providing data rates up to 7 Gb/s have recently been proposed for short-distance WPAN use, particularly in a home environment, as discussed in Section 2.4.3. In addition, the 71−76/81−86 GHz paired band has been allocated for commercial use in the United States, Europe, and other countries, and permits outdoor communications over distances of several kilometres [86]. Commercial equipment is easily available in the 60 and 71−76/81−86 GHz bands supporting 1.25 Gb/s Gigabit Ethernet (GbE) P2P communications. Dyadyuk *et al*. have also reported a 6 Gb/s wireless link in the 81−86 GHz band over a distance of 250 m [93]. Furthermore, bands around 100 GHz and higher show larger bandwidths which have not been allocated to specific applications yet and possibly can be used to support envisioned capacities ranging from 10 Gb/s to 100 Gb/s for optical access network applications and close proximity bulk data transfer [94]. 10 Gb/s data rate is an urgent need for the wireless transmission of 10-GbE signals, for ultrafast LAN connectivity similar to the wired GbE standards, and multiplexed uncompressed HD television (HDTV) signals. In the future, higher data rates will be required for the wireless technologies to transmit Super Hi-Vision (SHV)/Ultra High Definition (UHD) TV data, having 16 times the resolution of HDTV (at least 24 Gb/s), OC-768/STM-256 data (43 Gb/s), and 100-GbE (100 Gb/s). A 10 Gb/s wireless link at 120 GHz for fixed wireless access over 800 m wireless distance has been demonstrated [95].

Millimetre-wave wireless systems are not only a potential solution for mobile backhauling but also for future seamless integrated optical/wireless access [85]. As for the technology, radio-over-fibre techniques have been widely exploited for millimetre-wave wireless systems which could potentially offer capacities of 10 Gb/s or even higher in the 60 GHz band and for frequencies up to 300 GHz, as reviewed in Section 2.5.1.

2.2 OFDM technology

OFDM is a modulation technique which employs multiple orthogonal subcarriers to multiplex low-rate data signals into a single channel for transmission. OFDM is currently used in most new broadband optical wireless communication systems and is also a promising technology for optical communications [96]. OFDM is the basis of many current telecommunication standards such as digital video broadcasting (DVB), WiMAX, Wi-Fi, UWB, and LTE. In this Section the fundamentals of OFDM are briefly described.

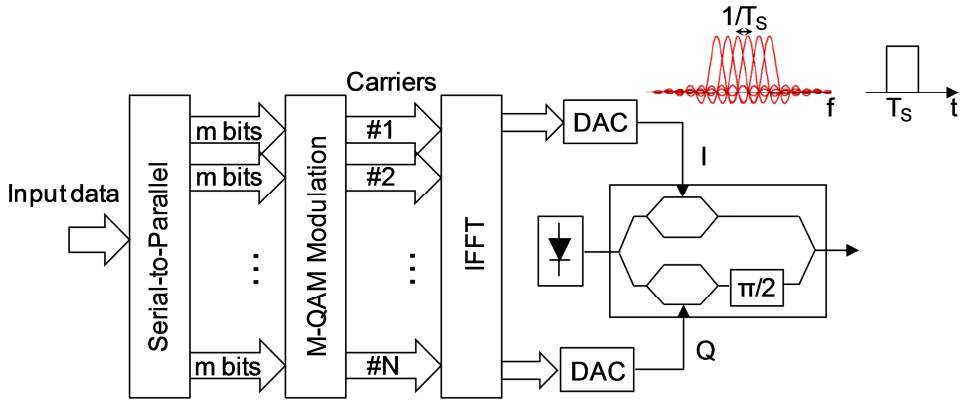

Fig. 3. Block diagram of a typical OFDM transmitter. OFDM spectrum and time pulse are shown as inset.

In OFDM, modulation process takes place in the frequency domain. A channel of bandwidth B is divided into N subcarriers and each subcarrier is modulated with a data sequence. The data sequence comprises data modulated with a modulation format, M-level quadrature amplitude modulation (M-QAM) typically. Carrier spacing is then given by $\Delta f = B/N$. The block diagram of a generic multicarrier transmitter is shown in Fig. 3. The input serial data sequence is converted into N sequences in parallel which are modulated by the N subcarriers after filtering. The difference between OFDM and conventional frequency division multiplexing (FDM) is that OFDM employs a subcarrier spacing Δf given by $\Delta f = 1/T_S$, where T_S is the OFDM symbol duration. As a result, the spectra of neighbouring subcarriers overlap significantly thus maximizing spectral efficiency. OFDM employs filtering with rectangular response in the time domain so that the spectrum of an individual OFDM subcarrier has a "sinc" form. This is illustrated as an inset in Fig. 3 where the orthogonality of the subcarriers is observed where at the central frequency of a given subcarrier the rest of subcarriers have a value of zero. In this way, the influence of neighbouring subcarriers can be eliminated without the need for analogue filtering to separate the subcarriers at the receiver. However, the challenge is to compensate channel impairments. On the other hand, the sinc-like spectrum of each OFDM subcarrier has significant sidelobes over a frequency range which includes many other subcarriers. This is the cause of one of the major disadvantages of OFDM: high sensitivity to frequency offset and phase noise [96]. Differences in the frequency and phase of the receiver LO and the carrier of the received signal can degrade system performance. This will set stringent requirements on the linewidth of lasers. However, it is possible to compensate for these effects to a certain extent by DSP. Another major disadvantage of OFDM is its sensitivity to non-linearity due to a high peak-to-average power ratio (PAPR) [96]. Pre-distortion of the OFDM signal before transmission may reduce the effect of non-linearity.

For wireless transmission, the baseband OFDM signal is up-converted in frequency by a carrier signal at the desired RF frequency. Fig. 3 shows the block diagram of a typical OFDM transmitter, where the inverse fast Fourier transform (IFFT) translates the signal to the time domain making possible that OFDM technology can be implemented in a chip. Digital-to-analogue conversion (DAC) is required previous to signal up-conversion when the IFFT approach is employed, as also shown in Fig. 3.

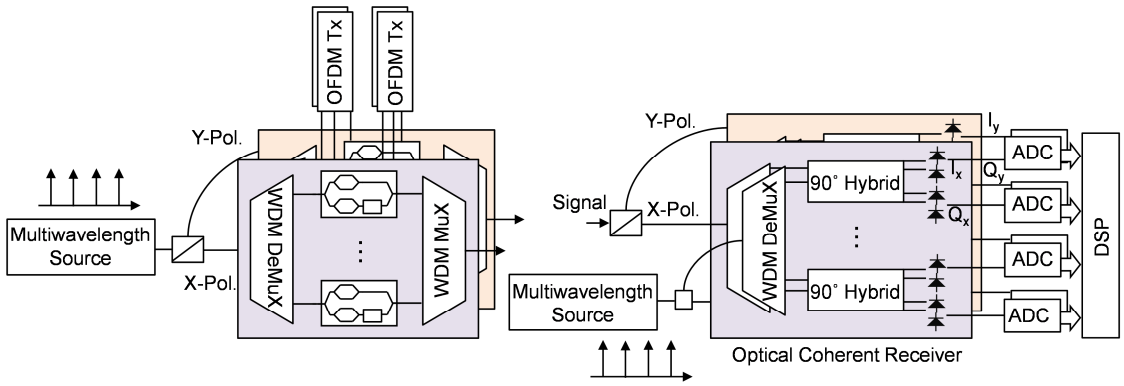

Fig. 4. Basic setup of a WDM system combined with PDM based on electrical OFDM. Adapted from [83].

The OFDM signal is transmitted over the optical and/or wireless communications channel. At receiver, the signal is down-converted in frequency and the transmitted data symbols are demodulated after analogue-to-digital conversion (ADC) by DSP. Receiver DSP comprises FFT, time synchronization, frequency estimation, channel estimation to compensate channel impairments such as chromatic dispersion and polarization mode dispersion (PMD) of optical fibre transmission, data recovery, signal quality assessment e.g. BER analysis.

The addition of a form of guard interval called a cyclic prefix makes OFDM resilient to intersymbol interference induced by a linear dispersive channel [96]. Multipath fading in wireless channels and fibre chromatic dispersion can be compensated by simple DSP. The cyclic prefix is a portion of the data which is appended at the beginning of each OFDM symbol before the data thus reducing symbol rate slightly below the subcarrier spacing. In addition, training symbols may be added at the beginning of a group of OFDM symbols to facilitate synchronization and channel estimation. Pilot subcarriers may also be added for phase noise estimation. However, the use of cyclic prefix, training symbols, and pilot subcarriers reduces spectral efficiency.

There are different approaches for optical transmission of OFDM signals. One approach is depicted in Fig. 3 where the in-phase (I) and quadrature (Q) components of the complex baseband OFDM signal are converted to the optical domain employing an IQ electrooptic modulator. I and Q signals require half of the signal bandwidth thus relaxing the bandwidth requirement of DAC and electrooptic modulation, although as the IQ modulator is biased at the minimum transmission point, it introduces high transmission loss. This approach can be combined with WDM architectures to increase the aggregated bandwidth/data rate, which is herein referred to as WDM-electrical OFDM. A basic system setup of a WDM-electrical OFDM approach is shown in Fig. 4. In the transmitter, a number of optical lines are produced by a frequency comb generator (or multiwavelength source) for stable channel spacing or by a continuous-wave (CW) laser array, and then the lines are separated, individually modulated, and recombined. The difference with an alternative all-optical OFDM approach is that the optical lines are here modulated with electrical baseband OFDM signals. On the other hand, all-optical OFDM implementations modulate a number of orthogonal optical lines with a baseband single-carrier signal such as QAM. Some baseband single-carrier signals can be optically generated modulating electrooptic modulators with bit patterns with adequate amplitude [97], [98]. At the receiver, all-optical OFDM signals are detected employing all-

optical FFT implementations and an optical modulation analyser whereas WDM-electrical OFDM channels are separated by an optical filter and individually detected by coherent detection, as shown in Fig. 4 [83].

Higher order modulation formats, such as 16-QAM, in combination with polarization division multiplexing (PDM) and coherent detection can achieve higher spectral efficiencies, but due to the cost of higher required optical SNR to reach certain system performance.

2.3 UWB radio technology

2.3.1 Features and current standardization status

UWB has attracted a great deal of interest from academia, industry, and global standardization bodies. Several UWB implementations have been proposed for wireless communications. An UWB implementation based on multiband OFDM with high spectral efficiency (up to 480 Mb/s per 528 MHz band) has been proposed in the ECMA-368 international standard [9]. This OFDM UWB implementation supports fourteen bands in the frequency range from 3.1 to 10.6 GHz. The ECMA-368 standard has led to commercial devices which are actively used in computer peripheral interconnection, namely wireless-USB, and HD audio/video streaming e.g. from the computer to the TV set. On the other hand, the IEEE 802.15.4a standard has specified an UWB implementation based on impulse-radio technology for low data rate (< 26.95 Mb/s) applications such as sensor networks. This impulse-radio UWB implementation is designated frequencies in three ranges: below 1 GHz, 3−5 GHz, and 6−10 GHz. UWB single-chip solutions compliant with IEEE 802.15.4a have been developed by the Belgium IMEC Research Centre [99] and DecaWave (ScenSor). Finally, vendor-specific implementations have been developed, such as Pulse~LINK CWave® based on impulse-radio UWB technology operating in 3.3–4.7 GHz up to 675 Mb/s with commercially-available chipset solutions targeting wireless high-definition multimedia interface (Wireless-HDMI) applications [100].

UWB technology has been around since 1960, when it was mainly used for radar and military applications. Since the 1990's, interest has increased due to several advantages UWB systems offer that make them attractive for wireless communications and many other applications. UWB advantages include:

1) Ultrahigh data rate communications: Current UWB systems are capable of providing up to 6.72 Gb/s per user when fourteen OFDM bands are combined (bearing 480 Mb/s each) employing market-available standard devices [10]. The multi-Gb/s capability allows UWB to address ultrahigh-speed computer peripheral interconnection and HD audio/video streaming functionalities that conventional technologies cannot provide.
2) Low EIRP spectral density (< −41.3 dBm/MHz in current regulation): UWB systems have low EIRP density that allows them to coexist with other services such as cellular systems, GPS, etc. [101] and to be inherently covert and extremely difficult to be intercepted since they may be near or below the noise floor of hostile detection devices [102]. At the same time, low EIRP density limits the UWB transmission range to WPAN distances up to 10 m typically.

3) UWB is a mature technology and a large number of standard OFDM-based single-chip devices with small-size, low-cost, and low power consumption are available in the market (Alereon AL5100, Wisair WSR601, Realtek RTU7012, Staccato Communications Ripcord®2, etc.) Such implementations permit UWB to be available in handheld devices with specific space and power requirements like mobile phones, etc. Furthermore, such devices can use efficient software to control de spectrum thus facilitating coexistence.
4) High accuracy ranging: Impulse-radio UWB signals have fine time resolution due to the narrowness of the pulses, being capable of providing sub-centimetre resolution for localization and tracking applications [13].
5) Fading robustness: UWB systems are highly tolerant to multipath fading due to OFDM format, and impulse-radio short pulses at expense of spectral efficiency. Impulse-radio UWB systems are capable of resolving multipath components even in dense multipath environments. Resolvable paths can be combined to reduce the fading margin and enhance system performance [13], [103].
6) Low loss penetration: UWB systems can penetrate obstacles and thus operate under both line-of-sight (LOS) and non-LOS (NLOS) conditions [104].
7) Low latency: UWB offers low protocol overhead, which is important for reaching a short transmission latency time [105].

2.3.2 Worldwide regulatory status

UWB has been approved for commercial use in the 3.1−10.6 GHz band for a wide variety of applications including communications and in the 24 GHz band for vehicular short-range radar.

The usable UWB frequency range has been differently regulated in several countries due to coexistence issues. In addition, according to current regulation, UWB systems must comply with stringent EIRP limits in the frequency band of operation to reduce interference. It should be noted that EIRP levels must be measured following specified measurement methods.

3.1–10.6 GHz band

The frequency range regulated for unlicensed UWB operation worldwide in the 3.1−10.6 GHz band is shown divided into the bands defined by the WiMedia Alliance [8] in Fig. 5. Only the Band Group #6 is common worldwide and without DAA requirements. UWB maximum EIRP requirements in the U.S., the EU, Japan, and Korea are summarized in Table II. UWB regulation has also been proposed in other countries such as China and Canada [106]. Fig. 6 depicts the UWB EIRP mask for indoor communications, which is the application focus of this work.

In March 2006, the Electronic Communications Committee (ECC) opened the door for the use of UWB devices in the EU with the recommendations ECC/DEC/(06)04, amended in July 2007. The recommendations ECC/DEC/(06)12 of December 2006 amended October 2008 provide supplementary regulation regarding DAA mitigation techniques [5]. The European Telecommunications Standards Institute (ETSI) Harmonised Standard includes specific new definitions, methods of measurements, limits and mitigation DAA techniques required for UWB technology in close cooperation with ECC [107].

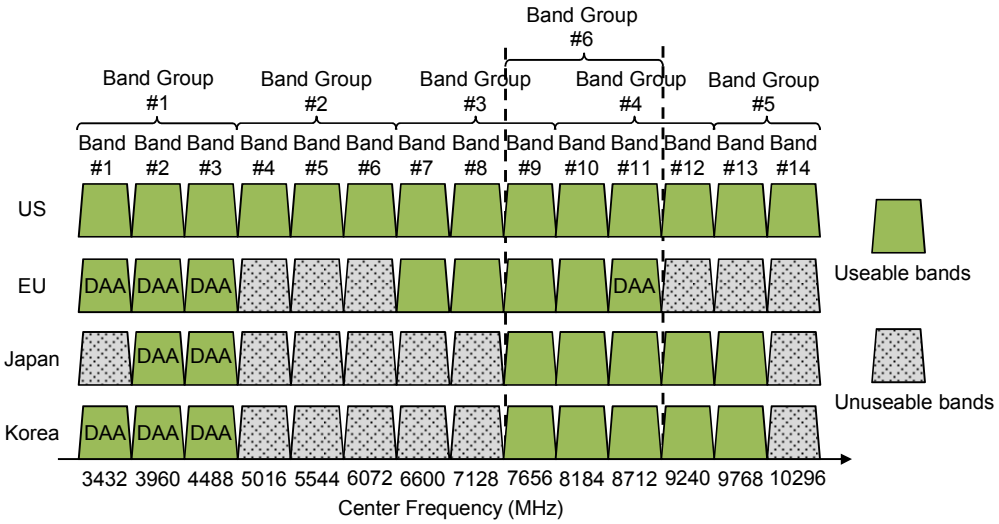

Fig. 5. UWB frequency range worldwide regulatory status in the 3.1−10.6 GHz band (as of October 2010). DAA: Band useable with protection requirements.

Table II. UWB regulation worldwide in the 3.1−10.6 GHz band

Country	Frequency Range	Maximum EIRP	Minimum Bandwidth	Ref.
U.S.	3.1−10.6 GHz	−41.3 dBm/MHz average 0 dBm/50 MHz peak	500 MHz (or 20% fractional bandwidth) at −10 dB	[1]
EU	3.1−4.8 GHz 6−9 GHz	−41.3 dBm/MHz average 0 dBm/50 MHz peak	50 MHz at −13 dB	[107]
Japan (indoor only)	3.4−4.8 GHz 7.25−10.25 GHz	−41.3 dBm/MHz average 0 dBm/50 MHz peak	450 MHz at −10 dB	[108]
Korea	3.1−4.8 GHz 7.2−10.2 GHz	−41.3 dBm/MHz average 0 dBm/50 MHz peak	450 MHz at −10 dB	[109]

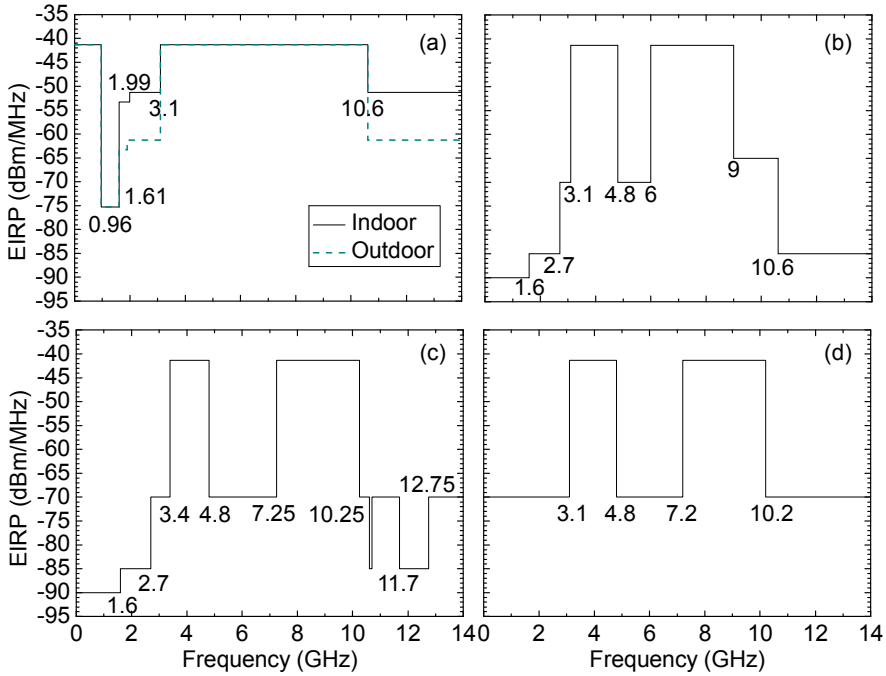

Fig. 6. UWB emission masks in the 3.1−10.6 GHz band for communications systems in: (a) the U.S.; (b) the EU; (c) Japan (indoor only); and (d) Korea.

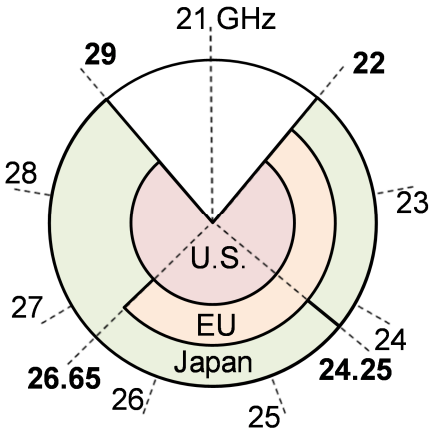

Fig. 7. UWB frequency range worldwide regulatory status in the 24 GHz band (as of October 2010).

Table III. UWB regulation worldwide in the 24 GHz band

Country	Frequency Range	Maximum EIRP	Reference
U.S.	22–29 GHz	−41.3 dBm/MHz average 0 dBm/50 MHz peak	[1]
EU	22–26.65 GHz	−41.3 dBm/MHz average 0 dBm/50 MHz peak	[109]
Japan	22–24.25 GHz 24.25–29 GHz	−41.3 dBm/MHz average 0 dBm/50 MHz peak	[111]

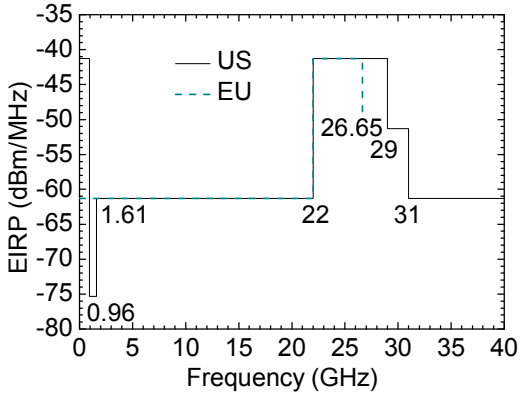

Fig. 8. UWB emission mask in the 24 GHz band for vehicular short-range radar systems in the U.S. and in the EU.

24 GHz band regulation

UWB worldwide regulation regarding frequency range in the 24 GHz band for vehicular short-range radar applications is shown in Fig. 7 and maximum EIRP requirements are summarized in Table III [2]. The UWB EIRP emission mask in the U.S., the EU, and Japan is depicted in Fig. 8. 24 GHz UWB radars have also been approved in many other countries with more constrained frequency range which is likely to be extended in the future. Note that additional limitations have been defined worldwide in the 23.6–24 GHz band shared for radio astronomy, earth

exploration satellite, and space research passive services. In the U.S., a first Report and Order FCC 02-48 (February 2002) allowed UWB vehicular short-range radar systems to operate in the frequency range from 22 GHz to 29 GHz [1]. This rulemaking mainly addresses impulse signals with a minimum bandwidth of 500 MHz. The centre frequency of the emission and the frequency at which the highest radiated emission occurs are greater than 24.075 GHz. In addition, UWB vehicular short-range radar operation has been authorized in 23.12−29 GHz employing a frequency carrier hopping or other modulation techniques with a minimum bandwidth of 10 MHz as defined in the second Report and Order FCC 04-285 (December 2004). In Europe, the ECC adopted Decision ECC/DEC/(04)10 (November 2004 amended September 2007) that regulates the temporary introduction of UWB vehicular short-range radar in the range from 21.65 GHz to 26.65 GHz. Decision ECC/DEC/(04)10 applies to the 46 CEPT countries in Europe until July 1, 2013 with a maximum of 7% market penetration. After July 2013, the 79 GHz band (not feasible today) designated in Decision ECC/DEC/(04)03 (March 2004) or alternative permitted technical solutions must be used, but vehicles equipped with 24 GHz UWB short-range radar will remain in service. The ECC decision is accompanied by the ETSI harmonized standard EN 302 288 (October 2004) defining the UWB EIRP emission mask. On January 17, 2005, the Decision 2005/50/EC was issued by the European Commission for the 25 EU countries including content parallel to the ECC Decision [109]. Decision 2005/50/EC has been recently amended (July 2011) to extend the authorisation to use the 24 GHz band for UWB short-range radar until January 1, 2018 [110]. Finally, in April 2010, Japan released regulation for UWB vehicular short-range radar in two frequency ranges from 22 GHz to 24.25 GHz, until December 31, 2016 not applying to devices already in use, and from 24.25 GHz to 29 GHz [111].

2.3.3 Major implementations

UWB regulation does not specify the type of signal and modulation scheme. There are two major UWB implementations: based on multiband OFDM technology as defined by the WiMedia Alliance [8] and adopted by the ECMA-368 standard [9] and based on impulse radio technology.

Multiband OFDM UWB

The WiMedia Alliance has defined a UWB physical layer (PHY) dividing the unlicensed 3.1−10.6 GHz band into 14 bands of 528 MHz bandwidth each and 6 Band Groups as shown in Fig. 5, where each band provides a carrier frequency for an OFDM baseband signal.

Each band is divided into 128 orthogonal subcarriers spaced 4.125 MHz apart. There are 6 null subcarriers and of the remaining 122 useful subcarriers, 100 are data carriers, 10 are guard carriers, and 12 pilot subcarriers. The duration of an OFDM Symbol including a null cyclic suffix is 312.5 ns. The Null Cyclic Suffix mitigates the effects of multi-path at the receiving end, plus provides a time window to allow sufficient time for the transmitter and receiver to switch between the different Band centre frequencies during hopping sequences. The OFDM symbols are grouped into packets and a number of OFDM symbols are inserted at the beginning of each packet to facilitate synchronization and channel estimation.

Frequency-domain spreading, time-domain spreading, modulation and FEC coding are used to vary the data rates. WiMedia specifications version 1.2 adopted by the ECMA-368 standard support data rates of 53.3, 80, 106.7, 160 and 200 Mb/s employing QPSK modulation and 320, 400 and 480 Mb/s employing DCM. More recent WiMedia specifications version 1.5 support data rates of 640, 800, 960 and 1024 Mb/s employing Modified DCM.

Multi-user support is provided by definition of hopping sequences over the bands within a Band Group, so called Time Frequency Codes (TFCs). Three types of TFCs have been defined: one where the information is interleaved over three bands of a Band Group, referred to as Time-Frequency Interleaving (TFI); one where the information is interleaved over two bands, referred to as two-band TFI or TFI2; and one where the information is transmitted all the time on a single band, referred to as Fixed Frequency Interleaving (FFI) or non-hopping. Band Groups 1–4 and Band Group 6 each supports four TFI codes (TFC 1–4), three FFI codes (TFC 5–7), and three TFI2 codes (TFC 8−10). Band Group 5 supports two FFI codes (TFC 5–6) and one TFI2 code (TFC 8). TFI and TFI2 minimize interference while FFI maximizes spectral efficiency.

A maximum permissible relative constellation root-mean-square (RMS) error is also specified. The relative constellation EVM limits are more restrictive at higher data rates and higher power levels (below −41.3 dBm/MHz in current regulation). The EVM tested as specified in the standard shall be lower than −19.5 dB at 480 Mb/s for devices transmitting at −41.3 dBm/MHz.

Multiband OFDM UWB provides high spectral efficiency and single-chip-based devices are readily available in the market, which take advantage of OFDM Tx/Rx IP-cores, providing multi-Gb/s communications when several bands from different devices are combined. Some of these devices support DAA functionalities. The multiband OFDM implementation is software configurable to meet specific spectral requirements thus allowing UWB operation in a range of regulatory and radio coexistence scenarios. Multiband OFDM permit to disable occupied subcarriers (tone nulling capability), select bands and TFCs, and control band powers in a flexible way with a simplified system design to react to narrowband interferers [12].

Impulse-radio UWB

Impulse-radio UWB employs pulses of short time duration (typically hundreds of picoseconds). Data are usually encoded on UWB pulses by modulating amplitude (OOK modulation), phase (BPSK modulation), time position (PPM), and/or shape of the pulse (PSM). The type of modulation determines the trade-off between implementation complexity and system performance. Impulse-radio UWB systems also present a trade-off between range and data rate since the energy in each pulse depends on the data rate to meet the bandwidth and the peak power specification.

The power spectral density of an impulse-radio UWB signal is critical for the design and practical deployment of an UWB system because it influences UWB performance and interference with other wireless systems. The power spectral density of an impulse-radio UWB signal is not only affected by pulse shape, pulse width, and pulse repetition frequency but also by the modulation scheme employed. Furthermore, UWB power spectral density is affected by optical fibre transmission in UWB-over-fibre systems [112].

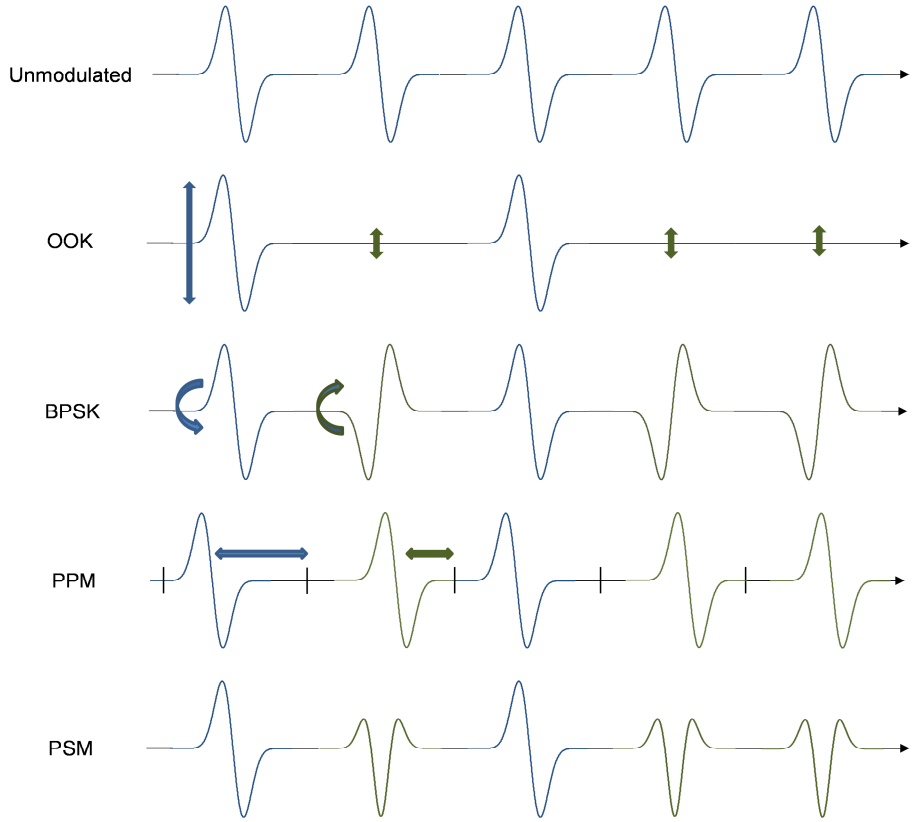

Fig. 9. Impulse-radio UWB waveforms associated with typical modulation formats. A bit sequence '10100' is illustrated.

OOK is the simplest form of pulse amplitude modulation (or amplitude shift keying (ASK) modulation), where the information bits '0' and '1' are represented by the absence or presence of a pulse, respectively, as illustrated in Fig. 9. OOK modulation is relatively simple to implement however it has significant spectral peaks which limit EIRP efficiency to meet UWB mask thus limiting performance.

BPSK is the simplest form of pulse phase modulation (or phase shift keying (PSK) modulation) where the information bits '0' and '1' are represented by a phase of 0° and 180°, respectively, as shown in Fig. 9. BPSK eliminates spectral peaks caused by non-antipodal modulation schemes [112]. BPSK requires coherent demodulation which generally provides better performance however increases receiver complexity.

In PPM, the information bits '1' and '0' are represented by two different time positions of UWB pulses within a bit period, as illustrated in Fig. 9. PPM presents nulls in the spectrum so that it can be used in combination with techniques eliminating spectral peaks to facilitate coexistence [113]. PPM is sensitive to multipath interference however distortion and noise are less important.

PSM employs two different UWB pulse shapes to represent the information bits '1' and '0', as illustrated in Fig. 9.

The same impulse-radio UWB signal can provide various stand-alone applications including high-resolution radar and high-speed communications. Furthermore, impulse-radio UWB

systems are flexible in spectrum and in data rate which is equal to the pulse repetition frequency. However, impulse-radio UWB technology may require RF circuits and ADC and DCA with large bandwidth.

2.4 60 GHz radio technology

Radios operating in the 60 GHz band have unique characteristics that make them significantly different from traditional radios operating at lower frequencies around 5 GHz. These qualities give 60 GHz radios operational advantages not found in other wireless systems, providing great potential for indoor WPAN communications. 7 GHz bandwidth has been allocated around 60 GHz for unlicensed generic use in several countries. This has led to launch various standards in the 60 GHz band to easily support multigigabit communications. 60 GHz standardization has in turn led to first consumer electronics products. The 60 GHz band is just beginning to be used for consumer applications but may be attractive for future uses such as HD video streaming because it can offer such high data rates albeit within short range.

2.4.1 Characteristics of the 60 GHz band

The wide bandwidth useable in the 60 GHz band easily supports multigigabit wireless links not necessarily requiring complex signal modulation with high spectral efficiency which may require higher cost system designs [18].

The high free-space path loss in the 60 GHz band limits coverage area as compared with links operating at lower frequencies (loss increases with frequency squared at a given wireless distance). In addition, the high atmospheric attenuation in the 60 GHz band further limits outdoor range, being also the reason that 60 GHz links cannot cover the large distances achieved by other millimetre-wave links without employing very large and very high gain antennas [86]. The frequency band is close to a peak in the oxygen absorption: the attenuation of a 60 GHz signal, according to Recommendation ITU-R P.676 is 12−16 dB per kilometre (half of the energy is absorbed for every 200 m of signal). 60 GHz signals may suffer from up to 15 dB/km additional atmospheric absorption depending on the atmospheric conditions [18]. However, the 60 GHz range limitation enables higher frequency reuse per environment, i.e. a higher number of smaller wireless cells, permitting to minimize interference and to provide secure communications.

Radios operating at 60 GHz usually employ very directional (narrow beam) and high gain antennas, unlike lower frequency radios which employ antennas more omnidirectional. Narrow beam reduce interference from other 60 GHz signals unless signals are lined up on the exact same trajectory and in the immediate locale of the targeted transmitter. Hence, directionality of 60 GHz or millimetre-wave antennas facilitates radio coexistence and reduces multipath effects. Directionality also arise “pointing” issues between transmitter and receiver, which could be addressed employing steerable beam antennas [18].

Additionally, the gain possible from an antenna of any given size increases with frequency. This means that 60 GHz systems employ antennas with gain higher than the lower frequency

bands. The higher gain of 60 GHz antennas permits higher power links, as allowed by regulation in force, to extend range and to enable 60 GHz signals to penetrate solid objects even with associated attenuation. On the other hand, the decreased ability of 60 GHz or millimetre-wave signals to penetrate objects may reduce interference. Furthermore, small 60 GHz antennas makes it possible to have very small radios with multiple antennas solutions, enabling multiple-input multiple-output (MIMO), beam forming and beam steering, which enhances the channel capacity and also supports NLOS communications.

Finally, high-performance 60 GHz transceivers are difficult to design given the phase noise and amplifier limitations at 60 GHz [18]. This is also of special importance when OFDM modulation is employed due to the sensitiveness to phase noise and high PAPR. There are further special challenges to adding 60 GHz capabilities to a chip. For instance, the higher the frequency, the more difficult the manufacturing issues and the interference issues are multiplied.

2.4.2 Worldwide regulatory status

The unlicensed frequency range regulated for 60 GHz radio worldwide is summarized in Fig. 10. Up to 9 GHz bandwidth in the frequency range from 57 GHz to 66 GHz is permitted in the EU and for indoor use in Australia. 7 GHz bandwidth has been allocated from 57 GHz to 64 GHz in the U.S. and Canada, and from 59 GHz to 66 GHz with maximum transmission bandwidths of 2.5 GHz in Japan.

Systems operating in the 60 GHz band must comply with power limits in the frequency band of operation, which are summarized in Table IV. It should be noted that power levels must be measured following specified measurement methods. Relatively high transmitter power limits employing shorter antennas allow for lower-power shorter-distance communications. The maximum EIRP for indoor-only use in the EU in Table IV agree with the recommendations ERC/REC 70-03 (October 6, 2010) which also includes the implementation status in the EU member states and EFTA countries.

2.4.3 Standardization status

A number of technologies capable of providing multigigabit wireless communications in the 60 GHz band targeting different markets have been proposed in recent years, which are summarized in Table V. First chips developed by SiBeam based on the WirelessHD specification have been integrated into consumer electronic products such as laptops, TVs, and wireless adapters at affordable cost [15]. Multigigabit file transfer and uncompressed HD video streaming has also been demonstrated employing ECMA-387-compliant CMOS single-chip prototypes [16]. 60 GHz transmitters based on such chip-based solutions could be used at remote antenna units after photodetection of digital baseband-over-fibre signals in hybrid wireless-optical systems. In addition, completion of the IEEE 802.11ad standard is targeted to December 2012. This standard is an amendment to the 802.11 standard that would enable 60 GHz wireless communications at data rates around 7 Gb/s. The WiGig specification was confirmed in May 2010 as the basis for the 802.11ad standard [118]. The 802.11ad specification is expected to seamlessly integrate 60 GHz Wi-Fi into existing 2.4 GHz and 5 GHz Wi-Fi networks to enable next-generation tri-band radios.

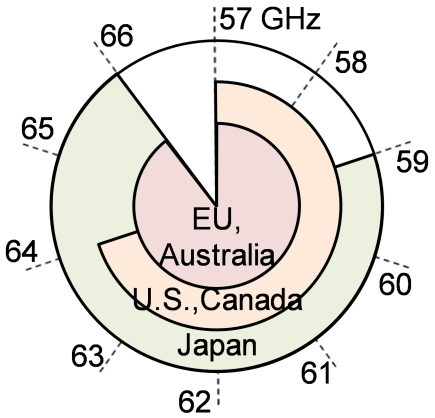

Fig. 10. Frequency range regulatory status in the 60 GHz band in major worldwide markets (as of October 2010).

Table IV. Worldwide regulation in the 60 GHz band

Country	Frequency Range	Usage	Maximum EIRP	Maximum Transmitter Power	Ref.
EU	57–66 GHz	Indoor only	13 dBm/MHz 40 dBm	Not Defined	[17]
		Indoor and Outdoor	−2 dBm/MHz 25 dBm		
Australia	57–66 GHz	Indoor only	43 dBm	13 dBm	[114]
U.S.	57–64 GHz	Not Defined	43 dBm peak (= 18 μW/cm2@ 3 m) 40 dBm average (= 9 μW/cm2@ 3 m)	27 dBm @ Bandwidth ≥100 MHz	[115]
Canada					[116]
Japan	59–66 GHz	Not Defined	57 dBm	10 dBm, antenna gain≤ 47 dBi	[117]

Table V. Wireless technologies in the 60 GHz band (as of February 2011)

Standard	Status	Maximum Data Rate (Gb/s)		Applications	Ref.
		OFDM	Single Carrier		
WirelessHD	Jan. 2008 (v1.0) May 2010 (v1.1)	7 28 (MIMO)	–	Uncompressed HD audio/video	[15]
ECMA-387	Dec. 2008	4.032	6.350 25.402 (4 bonded channels)	Bulk data transfer and HD streaming	[16]
IEEE 802.15.3c	Oct. 2009	5.775	5.28	File transfer and streaming	[119]
WiGig	Jul. 2010	7	4.6	File transfers, wireless display and docking, HD streaming	[120]

2.5 Radio-over-fibre technology

Radio-over-fibre techniques have been subject of research during the last decades and find application in optical signal processing (photonic analogue-to-digital conversion, photonic microwave filters, arbitrary waveform generation), antenna array beamforming, millimetre-wave and THz generation systems, or photonic up- and down-converting links for applications such as broadband wireless access networks, electronic warfare and radar processing, imaging and spectroscopy or radio astronomy [21], [121]. The use of optical fibre links to distribute telecommunication standards is the most successful application of radio-over-fibre technology, usually known as hybrid fibre-radio networks [122]. Hybrid fibre-radio networks have been deployed in the last decade due to the increasing demand of high data rate communication services in optical access networks. This demand is based on the steady market introduction of services requiring the transmission of massive data quantities, such as HD movie distribution, on-line gaming and rich Internet experience [123]. Hybrid fibre-radio networks enhance community antenna television (CATV) networks based on hybrid fibre-coaxial technology, in which a combination of digital and analogue channels is distributed from a central location to many users distributed geographically [124], [125]. In hybrid fibre-coaxial networks the “last mile” connection is provided through coaxial cable whereas in hybrid fibre-radio networks the last mile connection is a wireless link. This is not a minor difference, as the wireless environment is much more hostile than cable imposing restrictive radio-over-fibre link performance requirements in terms of linearity, noise and power handling capabilities, to cope with geographical dispersion of users and complex modulation formats used by current wireless standards.

The advantages of using radio-over-fibre techniques are manifold: it provides a scalable technology that allows seamless integration of the optical access network and the transmitting antenna. Radio-over-fibre allows centralising radio transmitter and frequency up-conversion in one shared location (Central office or Head-end unit) and then to use optical fibre to distribute the RF signals to the remote antenna units. In this way the remote antenna units can be simplified significantly as they only need to perform optoelectronic conversion and filtering and amplification functions. This allows important installation and operating expenses (OPEX) savings, especially in broadband wireless communication systems where a high density of remote antenna units is necessary.

A simplified schematic of a radio-over-fibre system is shown in Fig. 11. The central office and the remote antenna units perform electrooptic (E/O) and optoelectronic (O/E) conversion of RF signals. E/O conversion is achieved employing either directly modulated laser sources or laser sources modulated externally by electrooptic modulators. O/E conversion is done employing photodetectors or photoreceivers [121]. This method of transporting RF signals over fibre is called Intensity Modulation with Direct Detection (IM-DD) and is the simplest form of a radio-over-fibre system. Apart from IM-DD, other methods, which involve signal frequency up-conversion, are also employed. These methods are discussed in Section 2.5.1.

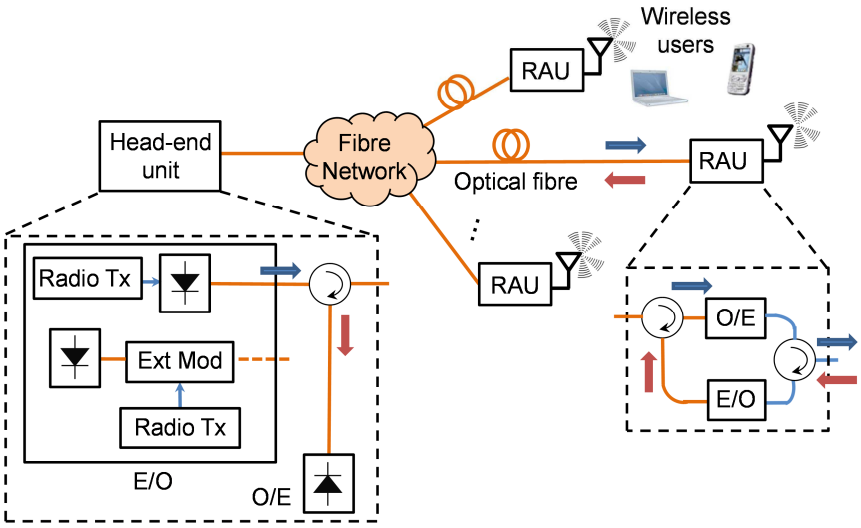

Fig. 11. Schematic diagram of a radio-over-fibre system.

As mentioned above, the most successful application of radio-over-fibre technologies has been the transmission of wireless standards over optical fibre links in centralized architectures, also known as DAS for both indoor and outdoor applications. The broad bandwidth of the optical fibre facilitates standard independent multiservice operation for cellular systems, such as GSM [126], UMTS [127], WLAN (Wi-Fi 802.11 a/b/g/n) [128]–[130], and also for emerging technologies WiMAX [131] and UWB [Llo08a], [73]. However, commercially available systems are typically limited to frequency ranges between 800−2500 MHz. Demonstrations of such DAS include their deployment to provide uniform wireless coverage in important sportive events such as the 2000 Olympic games and 2006 world cup [132], [133].

Two key factors limiting the overall transmission performance in radio-over-fibre systems are the optical source and the electrooptic modulation technique employed. Regarding the laser source, at frequencies used for major wireless standards (GSM, Wi-Fi 802.11 a/b/g, UMTS) and also WiMAX up to 5−6 GHz, directly modulated semiconductor lasers are preferred due to lower cost [134]. For higher frequencies, the required performances can be satisfied only by externally modulated transmitters. Devices with bandwidth handling capabilities in excess of 10 GHz, in particular DFB lasers offering the required bandwidth and performances, exist commercially, but normally at a high cost taking into account the number of devices required for typical applications. In addition, as external modulators have a high extinction ratio compared to direct modulated lasers, the external modulation scheme generates signal with high SNR compared to direct modulation schemes [Llo10a].

There are three main types of directly modulated lasers: (1) DFB lasers at $50−>$500 depending on the specifications; (2) Fabry-Perot lasers, which cost typically $50−$100; and (3) VCSEL at low cost ($20) as they are produced in high volume. Recently, a lot of research efforts have been devoted to the development of low-cost/high-performance VCSEL [73], [127], [128]. State-of-the-art high-speed single-mode VCSELs exhibit modulation bandwidths in excess of 23 GHz at 850 nm for short optical distances, or 17 GHz at 1550 nm for access networks [135]. Currently, single-mode/multi-mode 850 nm/1310 nm/1550 nm 10 Gb/s VCSEL are

commercially available with bandwidth up to 5−6 GHz (VERTILAS, RayCan). Regarding external electrooptic modulators, there are a large market availability of Lithium Niobate MZM with electrooptic bandwidths in excess of 40 GHz and relatively low drive voltages. MZM exhibiting 3 dB bandwidths of 70 GHz with driving voltage of 5.1 V have also been demonstrated by Noguchi *et al*. [136]. In addition, polymer-based MZM with more than 100 GHz bandwidth is commercially available [137]. Additionally, EAM based on quantum-well structures have exhibited bandwidths in excess of 40 GHz with drive voltages of less than 4 V. Travelling-wave structures can potentially lower the drive voltage required for higher bandwidths thus improving the extinction ratio. MZM have high power-handling capabilities however they are polarization sensitive whereas EAM can potentially be integrated with semiconductor lasers however they are very sensitive to wavelength and temperature changes. A travelling-wave EAM integrated with a DFB laser with a bandwidth in excess of 100 GHz has been demonstrated [138].

Regarding optoelectronic devices, high-speed waveguide-integrated PIN photodetectors exhibiting a RF bandwidth of up to 100 GHz are commercially available. Uni-travelling-carrier photodetectors exhibit higher output power and have been developed for higher frequency operation, extending beyond 300 GHz, with waveguide output connector or quasi-optic collimation with integrated antenna [139].

Signal impairments such as noise and distortion limit the SNR and the spurious free dynamic range (SFDR), respectively, of the radio-over-fibre system. The noise sources include relative intensity noise (RIN) and phase noise of continuous-wave lasers, amplitude noise and timing jitter of pulsed lasers, shot noise of photodetectors, and thermal noise of electrical amplifiers. The distortion sources include nonlinearities of electrooptic conversion.

2.5.1 Millimetre-wave systems

There are different approaches for implementing radio-over-fibre systems in the millimetre-wave band. Millimetre-wave over fibre where the millimetre-wave signal is generated in the optical domain at the central office is an attractive solution to simplify the remote antenna units thus facilitating system upgradability and reducing overall cost. On the other hand, a distributed solution based on baseband (or IF) radio over fibre and millimetre-wave up-conversion employing electrical mixers and millimetre-wave LO at each remote antenna unit. The centralised approach may find a competitor in the distributed scheme using CMOS chipset at RF front-end. The significant improvement in the frequency response of CMOS technologies has made them a potential candidate for cost-effective and low-power-consumption millimetre-wave applications. A few research groups have already demonstrated CMOS radios at 60 GHz. However, there are significant challenges such as device design and integration, making high-performance millimetre-wave communication extremely difficult.

Several techniques have been proposed for optical broadband millimetre-wave generation. The easiest way is to modulate the intensity of a laser with the millimetre-wave signal and direct detection of the millimetre-wave signal in a photodetector after fibre transmission [140]. However, the use of this technique is usually limited by the modulation bandwidth of directly modulated laser diodes (lower than 10 GHz for typical lasers) or external electrooptic

modulators (up to 40 GHz for typical modulators). Furthermore, the use of external modulation results in a double-sideband-with-carrier (DSB) modulation where the sidebands are located at the millimetre-wave frequency on either side of the optical carrier. DSB modulation scheme is extremely sensitive to RF power fading induced by fibre chromatic dispersion, which limits frequency range of operation and optical transmission distance [58]. A number of schemes have been proposed to overcome such fibre dispersion effect without employing dispersion compensation, such as schemes based on single-sideband-with-carrier (SSB) modulation by employing a dual-electrode MZM [141], or schemes employing optical frequency up-conversion which can be classified into schemes based on optical heterodyning and based on optical frequency multiplication (OFM).

In optical heterodyning schemes, the heterodyne mixing of two phase-correlated optical carriers with a frequency offset equal to the desired millimetre-wave frequency at a high-speed photodetector generates a single beat component at the millimetre-wave frequency. Two phase-correlated optical carriers can be generated based on optical carrier suppression modulation by biasing a MZM at the minimum transmission point [58], [142]–[145]. Optical carrier suppression implementation requires only half the millimetre-wave frequency to drive the MZM. Despite this simple approach, this technique requires a large RF drive power to obtain a desirable modulation depth since the modulator is biased in the nonlinear region. The attainable optical transmission distance is limited by bit-walkoff when optical carrier suppression modulation is employed [143], and by the link power budget and also by the phase decorrelation between the optical carrier and the single sideband when SSB is employed [144]. Two phase-correlated optical carriers can also be generated by using a dual-mode laser or multiwavelength laser with further optical filtering [146], [147], or by using two lasers combined with DSP-based detection [148] or injection locking and optical phase-lock loop [149]. However, these techniques require very narrow linewidth optical sources and DSP-based detection or optical phase locking to reduce the phase noise in the generated millimetre-wave signal, which increases the cost and complexity of the system.

Millimetre-wave generation based on OFM consists in generating harmonics of the local oscillator frequency. This technique is highly tolerant to dispersion-induced RF power fading and allows employing relatively-low frequency components. The main disadvantage of OFM is its power inefficiency, and therefore this technique suffers from low SNR. Hence, a chain of RF amplifiers may be required after photodetection at the remote antenna units, making OFM not cost-effective. OFM can be implemented by electrooptic phase modulation and further frequency-modulation-to-intensity-modulation (FM-IM) conversion in dispersive optical fibre links or by periodic filtering [150]. In this implementation, several harmonics are generated after photodetection, the desired harmonic being selected by filtering. This implementation has also been shown to be robust against the modal dispersion in multimode fibre. In addition, schemes based on external intensity or phase modulation with or without optical filter have also been widely used for frequency doubling, quadrupling, or higher generation [151]–[154].

Due to the advantages of radio-over-fibre techniques, much effort has been devoted to develop millimetre-wave-over-fibre systems. Systems operating within 7 GHz bandwidth in the 60 GHz band have been reported to provide capacities higher than 10 Gb/s when spectral efficient modulation formats are employed, such as 27 Gb/s for 2.5 m wireless distance

employing electrical 16QAM-OFDM [145], 21 Gb/s for 500 m SSMF and 10 m (or 2.5 m in bidirectional system) wireless transmission employing electrical 8QAM-OFDM [140], and 26.5 Gb/s for 100 km SSMF and 3 m wireless distance employing electrical adaptive-level QAM-OFDM in amplified long-reach networks [153]. Millimetre-wave-over-fibre systems in the 75−110 GHz band have also been demonstrated, such as 20 Gb/s error-free 20 cm wireless OOK data transmission [155], and 40 Gb/s 3 cm wireless 16QAM [154]. As for millimetre-wave-over-fibre links operating at higher than 110 GHz, OOK systems have been demonstrated up to 12.5 Gb/s at 300 GHz (error-free 50 cm wireless) [156].

OOK schemes occupy a larger bandwidth to provide the same data rate however they employ simple RF power detection. On the other hand, spectral efficient QAM/OFDM schemes usually employ electrical heterodyne detection with an electrical mixer and LO. The use of coherent detection after obtaining the optical baseband signal by optical single sideband filtering has also been proposed and demonstrated demodulating 16 Gb/s QPSK in the 75−110 GHz band [148].

In addition, photonic millimetre-wave links employing OOK or PSK have been demonstrated up to 10 Gb/s at 92 GHz and 120 GHz for fixed wireless access systems over the kilometre distance [157].

2.5.2 Optical fibre transmission

The cost-effective SSMF, compliant with ITU-T Recommendation G.652, is widely used in FTTH networks with distances up to about 40 km in most cases [158].

For short-distance communications networks used in-vehicle, the “last mile”, and in-building home/office/factory networks, different optical media can be employed, such as silica multimode fibre (MMF), multimode plastic optical fibre (POF) (or polymer optical fibre), and bend-insensitive fibre single-mode (BI-SMF) or multi-mode (BI-MMF).

The larger core diameter of MMF fibres (typically 50 µm or 62.5 µm) offers easier installation and simpler splicing and connectorization compared with SSMF. MMF is also easier and more efficient to couple to transceivers, leading to reduced cost. MMF is widely used for in-building fibre installations for baseband data transmission systems at higher than 10 Gb/s. Commercially-available 62.5 µm MMF fibres compliant with the OM1 recommendation support up to 1 Gb/s employing both 850 nm VCSELs and 1300 nm Fabry Perot lasers. 50 µm MMF fibres compliant with OM2/OM3/OM4 support up to 10 Gb/s at 850 nm. Performance of MMF fibres in terms of maximum distance and minimum effective modal bandwidth is summarized in Table VI. Performance is limited by modal dispersion of multimode fibre. In addition, dispersion-tolerant radio-over-fibre techniques are needed for the distribution of RF signals in MMF links. Radio-over-fibre in combination with short MMF distances can be deployed for baseband digital data transmission typically supporting wireless signals up to 2.5 GHz or beyond over passband transmission regions of the MMF link [150].

The high elasticity and ductility of polymers allows for larger POF fibre sizes compared with silica SSMF and MMF fibres. Although this together with the significantly higher loss results in

Table VI. Performance of commercially-available multimode fibre technology [159], [160]

Fibre Class	Gigabit Ethernet		10 Gigabit Ethernet
	850 nm	1300 nm	850 nm
OM1 62.5 µm	300 m 220 MHz.km	550 m 385 MHz.km	33 m 220 MHz.km
OM2 50 µm	750 m 950 MHz.km	550 m 500 MHz.km	150 m 950 MHz.km
OM3 50 µm	1000 m 2000 MHz.km	550 m 500 MHz.km	300 m 2000 MHz.km
OM4 50 µm	1100 m 4700 MHz.km	550 m 500 MHz.km	550 m 4700 MHz.km

shorter reach (typically up to 200 m), cost is significantly reduced. Further advantages of POF fibres over silica fibres are light weight, robustness, tight bend radius and better tolerance to tensile load and stress. While presenting large core diameter (970 µm) minimizing cost, conventional poly methyl methacrylate (PMMA) POF fibres exhibit low performance and are restricted to visible wavelengths (520 nm/570 nm/650 nm) [161]. Perfluorinated graded-index POF (PF-GI-POF) fibres have been developed offering lower loss a higher bandwidth for multi-Gb/s performance up to 100 m distance at 850 nm and 1300 nm [162], [163]. These POF fibres present a bandwidth exceeding 300 MHz.km at 850 nm and a core diameter of 50 µm, 62.5 µm or 120 µm. 120 µm core reduces cost while 50/62.5 µm core provides compatibility with silica MMF transceivers. Transmission of 10-GbE though 100 m of PF-GI-POF was demonstrated in [164] employing a low-cost set-up at 850 nm and electronic dispersion compensation suitable for small office/home office (SOHO) environment. In addition, data transmission of 40 Gb/s signals at 1550 nm through 100 m of POF was demonstrated in [165].

Recently-developed bend-insensitive single-mode fibres (BI-SMF) can maintain the transmission and interconnection properties of SSMF with much lower bending loss at lower bend radius and tighter dimensional specifications posing an interesting opportunity for a wide variety of applications including indoor wiring in FTTH [166]–[168]. BI-SMF facilitates fibre installation where corners, twists and staples are required, thus permitting easy installation at reduced cost. BI-SMF is also expected to reduce the size of the fibre installation and optical cabinets. Similarly, BI-MMF fibres can withstand tight bends and challenging cabling routes with significantly less signal loss than traditional MMF, reducing downtime, cost and space. Several manufacturers offer BI-SMF fibres compliant with the ITU-T Recommendation G.652.D, which are backwards compatible with all G.652 SSMF used in current optical networks while meeting or exceeding the most stringent and newest ITU-T G.657 recommendations. 50 µm BI-MMF fibres have also been developed compliant with OM2/OM3/OM4 multimode recommendations and compatible with current MMF fibres while maintaining performance. Commercially-available bend-insensitive fibres are summarized in Table VII.

Non-zero dispersion-shifted fibres (NZ-DSF) have a zero-dispersion wavelength slightly shifted from zero-dispersion dispersion-shifted fibre (DSF) to reduce the impact of the four-wave mixing (FWM) nonlinear effect while coping with chromatic dispersion limitations of SSMF in the 1550 nm wavelength window. However, NZ-DSF has some limitations to the realization of

Table VII. State-of-the-art of commercially-available bend-insensitive fibre technology

Manufacturer	Type	Model	Standard	Max. Bend loss @ bend radius, wavelength
Sumitomo Electric	BI-SMF	PureAccess-R5	G.657.B3	0.15 dB / 0.08 dB @ 5 mm / 7.5 mm, 1550 nm
Corning Incorporated	BI-SMF	ClearCurve XB	G.657.A1	0.5 dB @ 10 mm, 1550 nm
		ClearCurve LBL	G.657.A2/B2	0.4 dB @ 7.5 mm, 1550 nm
		ClearCurve ZBL	G.657.B3	0.1 dB @ 5 mm, 1550 nm
	BI-MMF	ClearCurve multimode	OM2/OM3/OM4	0.2 dB / 0.1 dB @ 7.5 mm / 15 mm, 850 nm
Draka Communications	BI-SMF	BendBright-XS	G.657.A2/B2	0.5 dB / 0.1 dB @ 7.5 mm / 10 mm, 1550 nm
		BendBright-XS 200 µm	G.657.A1/A2/B2	
		BendBright-Elite	G.657.B3	0.15 dB / 0.08 dB @ 5 mm / 7.5 mm, 1550 nm
	BI-MMF	MaxCap-BB-OMx	OM2/OM3/OM4	0.2 dB / 0.1 dB @ 7.5 mm / 15 mm, 850nm
OFS	BI-SMF	AllWave FLEX	G.657.A1	0.2 dB @ 10 mm, 1550 nm
		AllWave FLEX+ZWP	G.657.A2	0.5 dB / 0.1 dB @ 7.5 mm / 10 mm, 1550 nm
		EZ-Bend	G.657.B3	0.1 dB @ 5 mm, 1550 nm

long-haul transmission, such as trade-off of low dispersion slope and large effective area. An interesting solution can be employing dispersion management fibres comprised of SSMF plus inverse dispersion fibre (IDF) (both with approximately same length) at expense of fibre length flexibility which can be required in terrestrial systems [169]. IDF have inverse dispersion and dispersion slope and one-order larger nonlinearity compared with SSMF. Compared with dispersion compensating fibre (DCF) traditionally used as a module for dispersion compensation of SSMF, IDF has lower attenuation loss, PMD and nonlinear properties so that it is more suitable for being used as a transmission media.

2.5.3 Optical access networks

Optical fibre has been widely deployed substituting conventional copper cable in access networks (referred to as Fibre-to-the-X (FTTx)) to meet the increasing demand of high-bandwidth applications by residential and business customers. In particular, FTTH is the fastest growing global broadband technology with significant deployments occurring in Asia, Europe and North America [170]. FTTH deploys fibre all the way to individual residential dwellings.

There are two major architectures in optical access networks, namely point-to-point (P2P) and point-to-multipoint (P2MP). P2P architectures employ dedicated transceivers and a dedicated fibre from an optical line terminal (OLT) located at the central office (local exchange) to the customer premises, which can reach up to 80 km [171]. P2P networks are simple to design, provide the ultimate bandwidth and they are very flexible to upgrade services for customers individually [172]. However, they are cost prohibitive in most cases as they require significant

fibre deployment, space and powering in the OLT, and active devices at the customer premises. Alternatively, P2MP architectures include active optical networks (AON) and passive optical networks (PON) following a star (standard) topology. In AON star networks, a single fibre (distribution fibre), up to 70 km, carries all traffic to an active node close to the end users, from where individual fibres (drop fibres), up to 20 km, run to each home/building. While the fibre cost is reduced, the active nodes require powering and maintenance [172]. In PON star networks, the active node is replaced by a passive optical power splitter/combiner [172]. The distribution fibre in a PON network can be shared by up to 128 users. Commercially-available passive optical splitters have typical insertion loss of 13.5, 16.5, 20, and 23.5 dB for splitting factors of 16, 32, 64, and 128, respectively [173]. The splitting factor employed is limited by power budget in the network. Typically a PON is capable of reaching customers 20 km from the original transmitter [174]. A PON is characterized by the use of no active components (amplifiers, regenerators) in the field. PON are supported by a set of mature standards (Broadband B-PON, Ethernet E-PON, Gigabit G-PON) [172], [174], [175] and underway next-generation standards (10 Gb/s 10G-EPON, Next-generation NG-PON), and is the most widely deployed FTTH architecture. Current standard PON based on time-division multiple access (TDMA) are expected to evolve toward PON based on WDM (WDM-PON) to keep up with the requirements of future access networks [19]. In FTTH, the optical network terminal (ONT) receives the signal from the OLT and converts it into usable electronic signals for voice, video, and data at the customer premises.

2.5.4 UWB application scenarios

UWB-over-fibre extends the UWB radio range to in-home/office, in-building or even wide area applications. Optical fibre is the transmission media of choice enabling a large number of UWB users share a single fibre.

UWB-over-fibre systems are applied in two main scenarios: indoor (in-home/office or in-building) DAS and FTTH access networks. The fibre distance in DAS is relatively short (few hundred meters) and the variations among distances are relatively small. On the other hand, FTTH distances can be long (20 km or more) with relatively long variations (on the order of kilometres).

In-home/office or in-building distributed antenna systems

In the DAS application, the UWB signal is generated at the residential gateway (RG), shown in Fig. 12(a), which can be modulated with the data coming from the FTTH network. The generated UWB signal is distributed over the indoor optical fibre to the remote antenna units where the UWB signal is only photodetected, amplified, and filtered. Furthermore, the same indoor radio-over-fibre infrastructure can integrate a UWB cellular network, as shown in Fig. 12(b). The concept of UWB cellular clusters has been proposed in the European project FP7-ICT-1-216785 UCELLS to provide pervasive Gb/s communications in wider areas employing standard low-cost UWB transceivers.

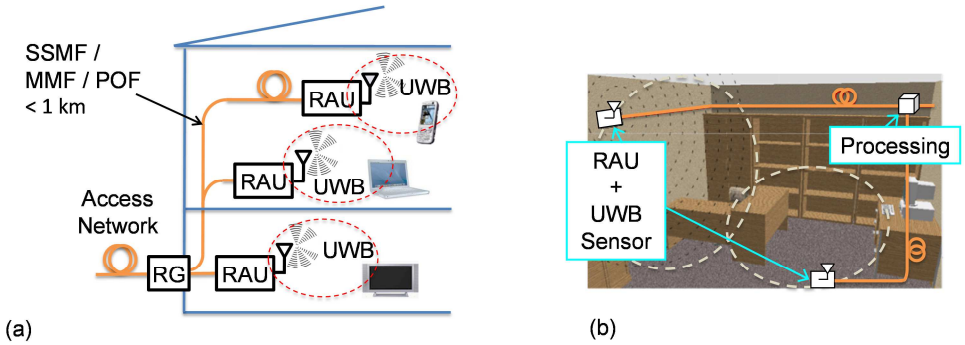

Fig. 12. (a) UWB radio-over-fibre in-home/office or in-building distributed antenna system. (b) UWB cellular network integrated in the radio-over-fibre infrastructure shown in (a).

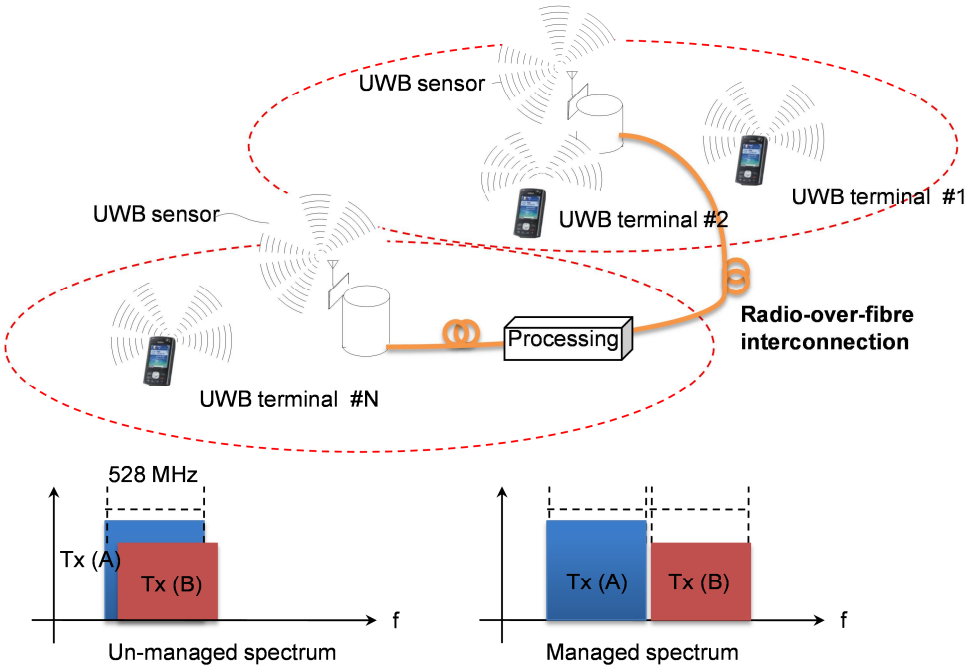

Fig. 13. Interference and spectral management in UWB cell cluster architectures. The in-home radio-over-fibre infrastructure interconnects UWB sensors.

UWB cell cluster operation requires spectral management of the UWB terminals in operation. UWB management implies the sensing of UWB transmissions by a set of UWB sensors and the proper configuration of UWB terminals to avoid interference between the different UWB terminals and to guarantee coexistence with other wireless communications systems in operation in the same area. Real-time sensing of wide-bandwidth low-power UWB signals has been proposed to be enabled by a photonic ADC employing the in-home radio-over-fibre infrastructure [Llo08b], [Bel08a], [Bel08b], [Llo09b]. The photonic ADC is based on optical time-stretched processing previous to electronic ADC [186]. The optical time-stretched process relaxes the requirements of the ADC employed in the processing.

Fig. 13 depicts the concept of UWB cell cluster together with the photonic ADC infrastructure. Fig. 13 shows a set of UWB transceivers arranged in different UWB cells which can connect to an UWB sensor. Fig. 13 also shows a simplified example of the management strategy: The UWB spectrum allocation and maximum power transmitted by each UWB terminal is centrally controlled in order to control mutual interference.

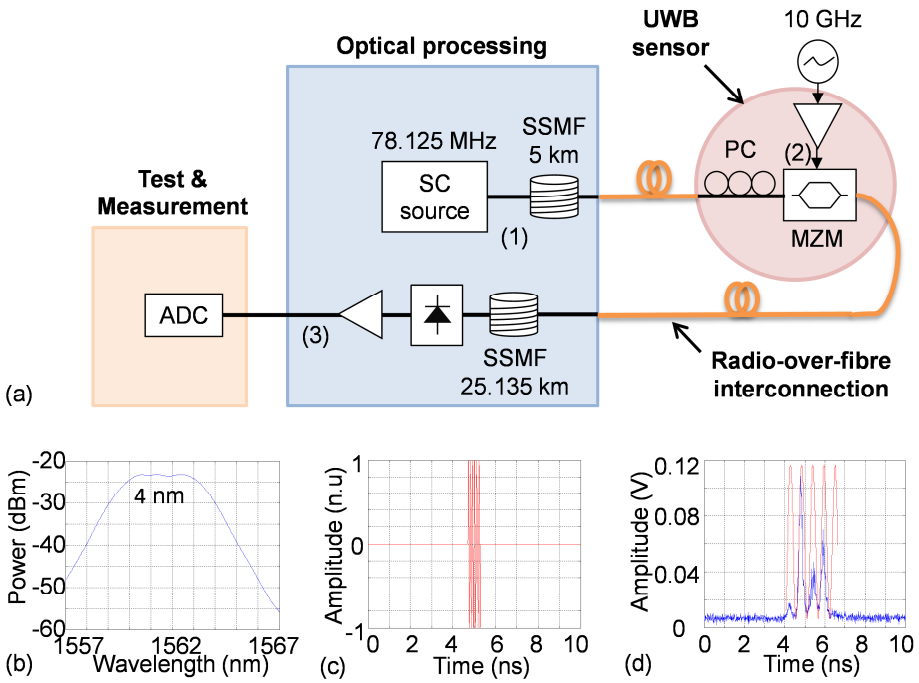

Fig. 14. (a) Experimental setup of a photonic time-stretched ADC for sensing of UWB signals according to Fig. 12(b) and Fig. 13. (b) Supercontinuum (SC) spectrum at point (1); (c) Ideal UWB signal at point (2); (d) Time-stretched UWB signal at point (3).

In this Ph.D. thesis, an optical time-stretched processor for sensing of UWB signals has been demonstrated in a proof-of-concept experiment [Llo08b], [Bel08a], [Bel08b]. Fig. 14(a) shows the experimental setup targeting to demonstrate photonic time-stretched ADC operation on UWB signals. The photonic ADC comprises two spans of fibre from the radio-over-fibre links shown in Fig. 13. Photonic ADC operation is as follows: The optical pulses from a supercontinuum (SC) source are chirped and stretched to 340 ps by propagation through 5 km SSMF. Fig. 14(b) shows the supercontinuum spectrum at point (1) in Fig. 14(a) exhibiting 4 nm bandwidth. The supercontinuum source is based on a pulsed laser at 1561.5 nm (2 ps full-width at half-maximum (FWHM), 1.2 nm of 3 dB bandwidth, 10 GHz repetition rate), a MZM driven by a bit pattern at 10 Gb/s (one '1' every 128 bits), an Erbium-doped fibre amplifier (EDFA), a span of HNLF (900 m length, 1562 nm zero-dispersion wavelength, 0.018 ps/nm^2/km dispersion slope, 10.8 $W^{-1} \cdot km^{-1}$ nonlinear coefficient), and an optical bandpass filter. The MZM is biased at the minimum transmission point and is employed to reduce the pulse repetition frequency from 10 GHz to 78.125 MHz. The UWB signal received from the antenna is modulated with the chirped optical pulses in a MZM. In the experiment, the UWB signal is a RF pulse comprising 6 cycles of 100 ps period, compatible with UWB regulation. Fig. 14(c) shows the ideal input UWB pulse under analysis. The UWB modulated signal is time stretched in 25.135 km SSMF before photodetection. Fig. 14(d) shows the time-stretched UWB signal at point (3) in Fig. 14(a) superimposed to the ideal time-stretched UWB signal. A stretch factor of 6 (= 1+25.135 km/5 km) is implemented in the experiment, which implies that the whole UWB band can be digitized for Fourier transform and analysis employing an electronic ADC with 1.8 GHz bandwidth.

UWB-over-FTTH networks

UWB-over-fibre has been indicated as an interesting solution to distribute HD multimedia content in FTTH networks [Llo08a], [Llo08c]. This approach combines UWB advantages and bandwidth capacity of FTTH networks. This is a rapid and cost-effective solution over other distribution networks, like hybrid fibre-coaxial, for several reasons:

1) No transmodulation or frequency up-conversion stages are required at the user premises, leading to lower deployment cost. Modulation and frequency up-conversion can be performed at an optical central unit thus simplifying the remote antenna units. Data is delivered to the remote antenna units already in their UWB wireless format.
2) Transparency to the specific modulation employed. This flexibility is of special interest for network operators as UWB regulation is still evolving.
3) Multistandard wireless services are supported on the same infrastructure [Llo11b].
4) UWB signals can be received by commercially-available low-cost receivers.

Fig. 15 depicts an example of the UWB-over-fibre approach integrating the SSMF-based FTTH access network and BI-SMF-based indoor optical user network. In the example, UWB radio provides raw data connectivity, HD audio/video and also connectivity to an UWB-enabled cell phone. In the UWB-over-FTTH application, the head-end unit shown in the figure is responsible of the central generation of the UWB signal. At the user premises, the optical access distribution can be extended by indoor optical distribution e.g. BI-SMF to the remote antenna units where UWB signals are photodetected, filtered, amplified, and radiated to a UWB-enabled television set [176] or computer [177]. The residential gateway (RG) provides inter-room communications and other network functionality.

BI-SMF opens up an interesting opportunity for UWB-over-fibre to be deployed at in-home environments. Compared with SSMF, BI-SMF facilitates installation under practical bending conditions such as corners and multiple staples, thus reducing cost, and also reduces the size of the associated infrastructure. Compared with conventional copper cable, BI-SMF provides high bandwidth necessary to distribute UWB signals. Furthermore, BI-SMF is backwards compatible with SSMF and can maintain the optical transmission properties of SSMF, which is particularly important at high frequencies such as around 60 GHz, compared with other types of fibres used for indoor distribution such as multimode fibres.

A major impairment of the FTTH network on the UWB signal is due to the chromatic dispersion of SSMF [24], [52], [56]. In the case of impulse-radio UWB signals, chromatic dispersion stretches pulses in time thus influencing the centre frequency and bandwidth of the UWB signal. This effect is dependent on the optical bandwidth and the chirp of the optical signal in propagation. The wider the optical bandwidth, the lower the tolerance to the chromatic dispersion. Dispersion managing techniques could be used to compensate for chromatic dispersion effects. This solution is not flexible and cost-effective, however it could enable UWB transmission over long distances (>40 km) [48].

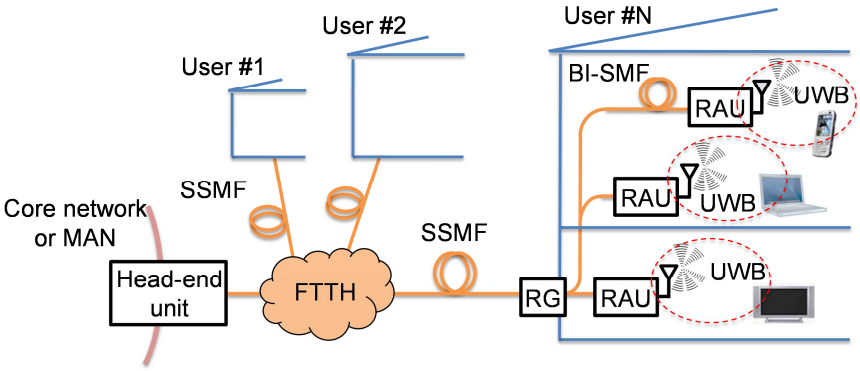

Fig. 15. Radio-over-fibre system integrating FTTH optical access distribution and indoor optical-radio transmission of multistandard multi-Gb/s UWB signals for HD contents provision.

Chromatic dispersion in the fibre may cause additional effects on the UWB signal. Fibre chromatic dispersion may have a higher impact in UWB generation techniques employing more than one wavelength due to the walk-off effect [54], [143]. Another impact of chromatic dispersion is due to mode partition noise. Fibre dispersion causes the fluctuations of the energy between the longitudinal modes of the laser to be translated into intensity fluctuations on the transmitted optical signal, thus reducing SNR [56].

3

Optical generation of impulse-radio UWB signals

3.1 Introduction

Nowadays, the multiband OFDM UWB implementation defined by WiMedia [8] is actively used in wireless USB and HD audio/video streaming applications [11]. On the other hand, impulse-radio UWB implementation has found its application for ranging and localization as radar [178]. For UWB-over-fibre applications, photonic generation of impulse-radio UWB signals have widely been investigated in recent years, with reported data rates up to 5 Gb/s [179].

Generation of impulse-radio UWB in the 60 GHz band is investigated in this Ph.D. thesis. The main advantages of OFDM UWB over impulse-radio UWB are less important in the 60 GHz band. A high-capacity system in the 60 GHz band does not necessarily require high spectral efficiency. In addition, the 60 GHz band overcomes coexistence issues in the 3.1−10.6 GHz band and directionality of the 60 GHz antennas would facilitate future radio coexistence in the 60 GHz band. Directionality of the 60 GHz antennas also reduces multipath fading effect.

The selection of the pulse shape is one of the fundamental considerations in designing an impulse-radio UWB system, because the pulse shape will determine the performance of the system. Gaussian-monocycle is the most widely used pulse shape due to its simplicity however it requires filtering to comply with the FCC-specified UWB spectrum mask in the 3.1−10.6 GHz band. Higher-frequency pulses have been proposed to comply with the FCC mask with higher power efficiency. Higher-order derivative Gaussian pulses have been proposed, as theoretically analised in [27]. Furthermore, linear combination of polarity-reversed monocycles with different pulsewidth [28] or modified doublets with different delay [29] have been proposed targeting to simplify implementation and to increase power efficiency, which look close to the 5^{th} order Gaussian derivative. In addition, the use of photonic integration is highly desirable to implement compact and cost-effective impulse-radio UWB transmitters [180].

3.2 Baseband with Gaussian-monocycle pulse shaping

3.2.1 Introduction

In this Ph.D. thesis, two photonic impulse-radio UWB generation techniques are proposed and demonstrated in two proof-of-concept experiments which are described in Sections 3.2.2 and 3.2.3. The techniques are based on combining two Gaussian pulses with opposite polarity and relative time delay to shape Gaussian-monocycles. The first technique employs optical delay and balanced photodetection whereas the second technique employs a differential photoreceiver and electrical delay. The proposed techniques are simple and permit to adapt UWB spectrum to FTTH networks with different fibre dispersion by simply adjusting delay. Such reconfiguration enables great flexibility since the techniques are implemented at the remote antenna units. This functionality is not available in other previously reported photonic impulse-radio UWB generation techniques to our knowledge. Previous techniques provide little or no reconfiguration. Nevertheless, a technique based on spectral shaping and frequency-to-time conversion has been recently proposed, which is also capable of post-compensating for variable fibre dispersion employing FBG devices and further balanced photodetection to remove the rectangular pulse superimposed to the desired waveform [52]. The corresponding application scenario is that discussed in Section 2.5.4.

The generation of baseband Gaussian-monocycles is experimentally demonstrated in this thesis. Gaussian monocycles are shaped after optical access fibre transmission of optical pulses. Optical pulses are generated by a mode-locked laser and are further modulated with data in a MZM. The installed fibre is exploited to reduce pulse shaping complexity. Baseband Gaussian monocycles could meet FCC-specified UWB spectrum mask in the 3.1−10.6 GHz band provided an adequate bandwidth is generated and further adequate filtering is performed e.g. by a commercially-available UWB antenna which acts as a band pass filter [24]. This avoids the need for up/down-conversion required when Gaussian pulses are employed [Llo08a], [Llo08c], [Mor08a]. Bandwidth is dependent on the original Gaussian pulsewidth, pulse time-stretching induced by fibre chromatic dispersion, which depends on the optical bandwidth, and the optical/electrical time delay. The wider the pulse after fibre transmission and the longer the time delay, the narrower bandwidth and the lower the peak frequency.

3.2.2 Optical delay and balanced photodetection technique

Fig. 16 shows the experimental setup of the photonic technique for impulse-radio UWB generation based on optical delay and balanced photodetection to perform Gaussian-monocycle shaping [Bel08c], [Llo09a], [Llo10a]. A 1560 nm actively mode-locked fibre laser generates optical pulses with approximately 2 ps FWHM, 1.2 nm of 3 dB bandwidth, and 10 GHz repetition rate. Optical pulses are intensity modulated with a fix pattern “1000 0000 0000 0000” (one ‘1’ every 16 bits) at a data rate of 10 Gb/s, which is equivalent to return-to-zero (RZ) data at 1.25 Gb/s with a duty cycle of approximately 1/16, in a MZM. The MZM is biased at the minimum transmission point to reject the undesired laser pulses, resulting in OOK-modulated pulse train at 1.25 GHz repetition rate.

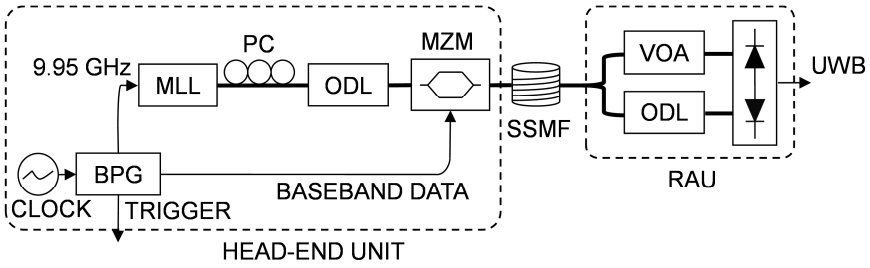

Fig. 16. Experimental setup for photonic generation of impulse-radio UWB signals based on optical delay and balanced photodetection.

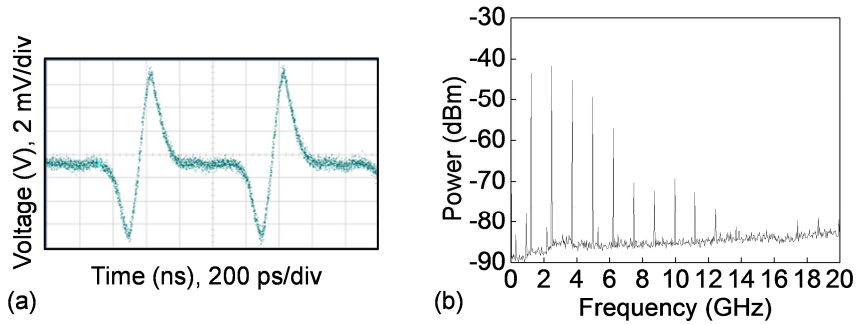

Fig. 17. Baseband Gaussian monocycles measured at the output of the system in Fig. 16 for 2 ps 1.2 nm laser pulses and 5 km SSMF. (a) Signal in time domain. (b) Electrical spectrum for RZ data all '1' at 1.25 Gb/s (resolution bandwidth: 30 kHz).

The modulated pulses are distributed over fibre to the remote antenna units where the pulses are split into two paths driving the two inputs of a balanced photodetector (u^2t Photonics, BPDV2020R). A variable optical delay line is employed in one of the paths to set the relative time delay between the positive and negative part of the Gaussian monocycles which are obtained at the output of the balanced photodetector. A variable optical attenuator is employed to compensate for the path loss difference.

In the proof-of-concept experiment, the modulated pulses are stretched in time as they are transmitted over 5 km of SSMF and a relative time delay of 150 ps is set. In this way, baseband Gaussian monocycles exhibiting 400 ps pulsewidth and 5 GHz 10 dB bandwidth are generated, as shown in Fig. 17.

3.2.3 Differential photoreception and electrical delay technique

Fig. 18 shows the experimental setup of the photonic technique for impulse-radio UWB generation based on a differential photoreceiver and electrical delay to perform Gaussian monocycle shaping [Bel09a], [Bel10a], [Llo09a], [Llo10a]. A 1560 nm actively mode-locked fibre laser generates optical pulses with approximately 2 ps FWHM, 1.2 nm of 3 dB bandwidth, and 10 GHz repetition rate. Optical pulses are intensity modulated with a fix pattern "1000 0000 0000 0000" (one '1' every 16 bits) at a data rate of 10 Gb/s, which is equivalent to RZ data at 1.25 Gb/s with a duty cycle of approximately 1/16, in a MZM. The MZM is biased at the minimum transmission point to reject the undesired laser pulses, resulting in OOK-modulated pulse train at 1.25 GHz repetition rate.

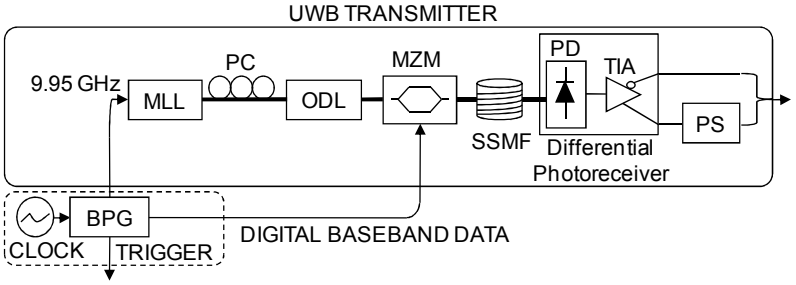

Fig. 18. Experimental setup for photonic generation of impulse-radio UWB signals based on differential photoreception and electrical delay.

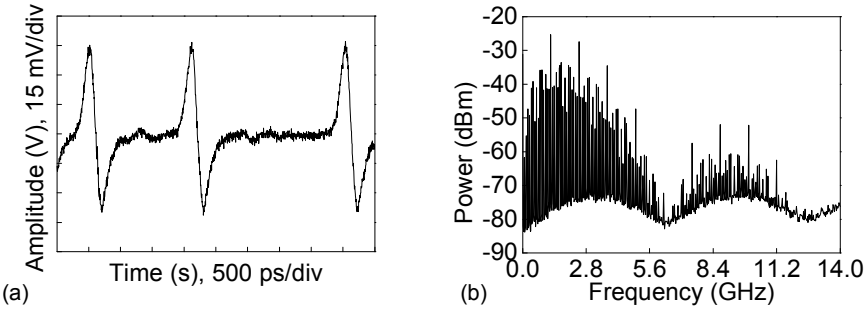

Fig. 19. Baseband Gaussian monocycles bearing fix data "1011100110100100" at 1.25 Gb/s measured in Fig. 18 for 2 ps 1.2 nm laser pulses and 10 km SSMF. (a) Part of the signal in time domain corresponding to the sequence "101001". (b) Electrical spectrum (resolution bandwidth: 300 kHz).

The modulated pulses are distributed over fibre to the remote antenna units where the pulses are photodetected by a differential photoreceiver (Teleoptix, Balanced Photoreceiver with Limiting TIA) [181]. The photoreceiver is operated in unbalanced mode and in linear regime of the transimpedance amplifier (TIA). The differential TIA provides complementary outputs which are combined after adjusting their relative time delay by a variable electrical delay line.

In the proof-of-concept experiment, the modulated pulses are stretched in time as they are transmitted over 10 km of SSMF and a relative time delay of 200 ps is set. In this way, baseband Gaussian monocycles exhibiting 600 ps pulsewidth and 3.8 GHz of 10 dB bandwidth are generated, as shown in Fig. 19. These baseband Gaussian monocycles are suitable for further frequency up-conversion in the proof-of-concept experiment of a UWB-over-fibre system in the 60 GHz band, as described in Section 3.3.4. Nevertheless, wider bandwidth can be generated, which could be further filtered and radiated to provide UWB connectivity in the 3.1–10.6 GHz band.

3.3 60 GHz radio-over-fibre for in-flight communications

An impulse-radio UWB photonic generation system targeting high user density in-flight communications with simultaneous ranging capabilities in the 60 GHz radio band is proposed and experimentally demonstrated and the implementation cost is analyzed [Bel09a], [Bel10a], [Llo10a], [Llo10b], [Par10]. Impulse-radio UWB Gaussian monocycles are employed for

signalling. Baseband Gaussian monocycles are generated based on differential photoreception and variable electrical time delay, as described in Section 3.2.3. After external modulation in a MZM, optical frequency up-conversion is performed based on optical carrier suppression in another MZM [76], [145]. In the experiment, Gaussian monocycles at a 1.25 Gb/s data rate with 3.8 GHz bandwidth are generated and up-converted to 57 GHz. The performance of the 57 GHz UWB signal after the transmission over a SSMF at in-cabin distances up to 100 m is studied. The experimental results show that good quality UWB pulses can be obtained with the proposed system. The impact of the system parameters on performance including wireless transmission and associated cost is analysed, indicating that a high number of remote antenna units can be cost-effectively supported by the proposed 60 GHz UWB-over-fibre system.

3.3.1 Introduction

The 3.1–10.6 GHz UWB band is not equally regulated worldwide due to spectral coexistence concerns. Outside the U.S., available effective bandwidth is 1.5 GHz, which only supports data rates of hundreds of megabits per second. The 60 GHz band offers a large frequency range worldwide: 57−66 GHz in Europe and Australia, 57−64 GHz in the U.S. and Canada, 59−66 GHz in Japan. The match between the allocated frequency band for UWB and the bandwidth available in the 60 GHz band makes 60 GHz UWB a very interesting approach for multi-Gb/s wireless communications. Moreover, radio attenuation in the 60 GHz band benefits coexistence when a large number of users are present and reduces the potential interference with in-flight electronics.

UWB-over-fibre DAS systems is a cost-effective solution to extend the UWB coverage taking advantage of the large bandwidth and transparency to signal formats of the optical fibre [6].

This Ph.D. thesis proposes, for the first time to our knowledge, the use of impulse-radio UWB signals in the 60 GHz radio band for in-flight communications with potential ranging and localization functionalities. The impulse-radio UWB signal in the 60 GHz band is optically generated and distributed through SSMF to a high number of distributed remote antenna units as in an in-cabin radio-over-fibre installation.

Photonic generation of the impulse-radio UWB signal is an interesting approach because it enables signal generation in the 60 GHz band and seamless optical distribution in the plane. Impulse-radio UWB exhibits several advantages, which can be summarized as follows.

1) UWB technology is capable of high data rate at relative low EIRP density minimizing interference on other wireless signals. This is a key aspect revealing UWB as a very interesting radio technology in avionics. Provision of high data rate communications is required in HD audio/video entertainment services offered in-flight.
2) The specific signalling employed in impulse-radio UWB permits simultaneously communications, localization and ranging to a sub-centimetre resolution. This is of special interest for in-flight environments, like a plane passenger's cabin, where beside communications, localization of users or group of users exhibiting potentially large radio interference is necessary. This approach is also interesting for radio tagging and passenger identification applications.

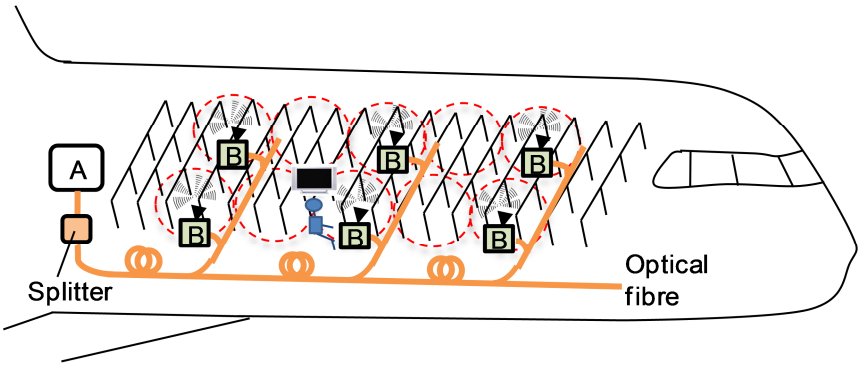

Fig. 20. Impulse-radio UWB radio-over-fibre in the 60 GHz band for in-flight communications. Block “A”: central unit for optical UWB generation. Block “B”: on-seat remote antenna units.

The experimental work herein reported demonstrates the photonic generation of impulse-radio UWB Gaussian monocycles at 57 GHz bearing data at 1.25 Gb/s and its further transmission over 100 m fibre targeting in-flight communications. The use of Gaussian monocycles permits to remove residual RF carrier easily by filtering to avoid receiver saturation. Furthermore, devices based on Gaussian monocycles available for UWB generation in the 3.1−10.6 GHz band could be reused.

The remainder of Section 3.3 is organized as follows: Section 3.3.2 describes the proposed application scenario for the 60 GHz UWB-over-fibre system. Comparison between experiment and simulation and a comprehensive analysis of the system by simulation is presented in Section 3.3.3. The experimental demonstration is presented in Section 3.3.4. Finally, a techno-economic analysis comparing the radio-over-fibre approach with a conventional baseband-over-fibre approach is performed in Section 3.3.5.

3.3.2 In-aircraft distributed antenna system

Fig. 20 depicts the proposed impulse-radio UWB radio-over-fibre technique targeting to distribute HD multimedia contents in aircrafts. This figure shows a cabin where a 100 m SSMF is transporting UWB radio-over-fibre to provide passenger connectivity. The block marked “A” in Fig. 20 is a central unit, which generates in the optical domain the impulse-radio UWB data signal to be further distributed through SSMF to the on-seat remote antenna units, which are marked as “B” in Fig. 20. In the remote antenna unit, the UWB data signal is photodetected resulting in an impulse-radio UWB signal in the 60 GHz band, which is further amplified, filtered, and radiated to be available to passengers in a given short-range coverage area (WPAN). In this way, multi-Gb/s wireless connectivity can be provided along the cabin minimizing the interference due to the intrinsic low radiation level of UWB and the radiation-immune optical fibre distribution.

The system demonstrated in this study in the 60 GHz band is the central transmission system in the plane. This radio-over-fibre technique gives the advantage that the remote antenna units would be very simple (no up/down-conversion or modulation is required). This is important if there are a large number of passengers in the plane.

3.3.3 Simulation analysis

The proposed system, shown in Fig. 33 in Section 3.3.4, has been analysed employing the commercial simulation tool VPItransmissionMaker™ (version 7.5) using the characteristics of the devices in Table VIII in Section 3.3.4. Simulation results have been compared to measurements presented in Section 3.3.4 to verify the simulation model and then the impact of the system parameters on the performance in terms of the BER has been evaluated.

In simulation, data modulated optical pulses at the output of the modulator, MZM in Fig. 33, are generated from a hyperbolic-secant pulse transmitter at 1.25 Gb/s. From these pulses, monocycles are generated as in Section 3.2.3 and are shown in Fig. 21. The noise in the monocycles has been modelled as additive Gaussian white noise at 20 nA/Hz$^{1/2}$ (noise figure: 63.9 dB). This noise figure value, although impractical, permits to set in simulation a maximum noise power spectral density according to the experimental work. Slight discrepancies between monocycles measured and simulated are mainly due to the deviation of the measured pulse shape from the ideal hyperbolic-secant shape. The filters of the digital communications analyser have been modelled as Gaussian filters.

Fig. 22 shows the simulated monocycles at point (1) in Fig. 33. The frequency response of Amp 1 and the LPF in Fig. 33 has been considered.

The relative intensity noise (RIN = −145 dB/Hz) of the CW laser in Fig. 33 and the insertion loss of the MZM 1 (13 dB) set the power level at point (2) in Fig. 33 assuming a maximum possible extinction ratio of the MZM of 25 dB. MZM 1 is biased at the quadrature point. Fig. 23 shows the simulated monocycles at point (2) in Fig. 33.

The gain of the Erbium-doped fibre amplifier (EDFA) in Fig. 33 (25 dB), and the insertion loss of the MZM2 (8 dB) set the maximum power spectral density at point (4) in Fig. 33, assuming a maximum possible extinction ratio of the MZM of 25 dB. MZM 2 is biased at the minimum transmission point. The OBPF is modelled as a Gaussian filter. A double of the LO frequency of 28.75 GHz is set limited by the simulation tool. In this way, the RF carrier frequency is 57.5 GHz so that the frequency response of the components in Fig. 33, PD, LNA, BPF 1, HPA, BPF 2, and frequency dependence of the mixer conversion loss is shifted by 0.5 GHz.

It should be noted that with the proposed frequency up-conversion technique, the baseband signal is also available after photodetection, as shown in Fig. 24. The baseband signal could be used for wired connectivity employing a low-cost receiver or for wireless connectivity in the 3.1–10.6 GHz UWB band provided wider bandwidth is generated and further adequate filtering is performed. Hence, the proposed system is capable of seamless operation in the 3.1−10.6 GHz band and in the emerging 60 GHz band. This flexibility to emerging standards is of special importance in avionics, where the upgrade of in-flight avionics is a lengthy and expensive maintenance process.

Fig. 25 shows the simulated spectrum at point (4) in Fig. 33. Note that, in the measurement in Fig. 36, the dependence on frequency of the conversion loss of the harmonic mixer of the spectrum analyser has not been considered.

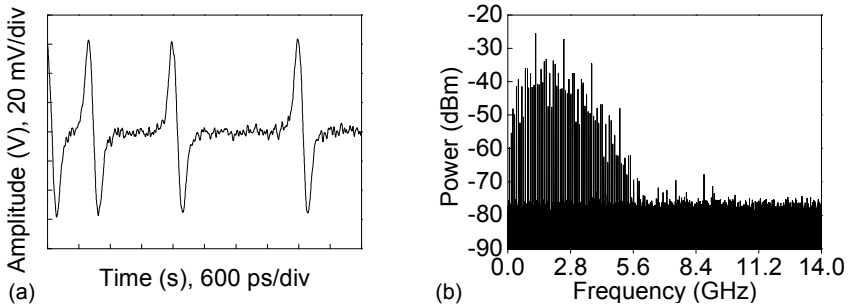

Fig. 21. Simulated Gaussian monocycles generated in Fig. 18 to be compared with Fig. 19. (a) Signal in time domain. (b) Electrical spectrum (resolution bandwidth: 600 kHz).

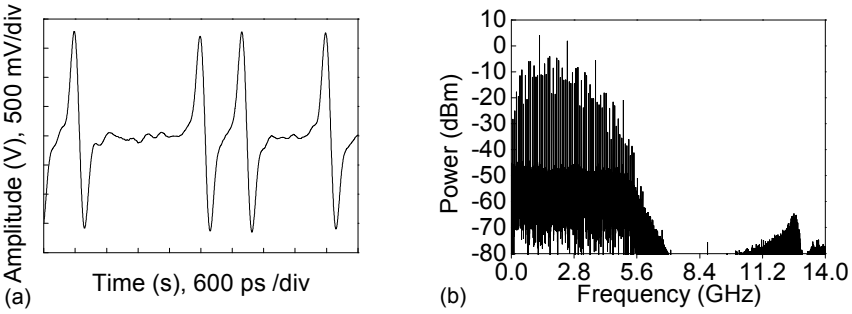

Fig. 22. Simulated monocycles at point (1) in Fig. 33 to be compared with Fig. 34. (a) Signal in time domain. (b) Electrical spectrum (resolution bandwidth: 600 kHz).

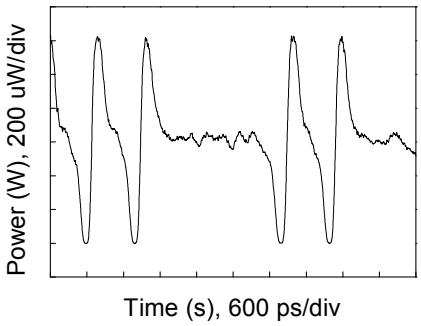

Fig. 23. Simulated optical monocycles at point (2) in Fig. 33 to be compared with Fig. 35.

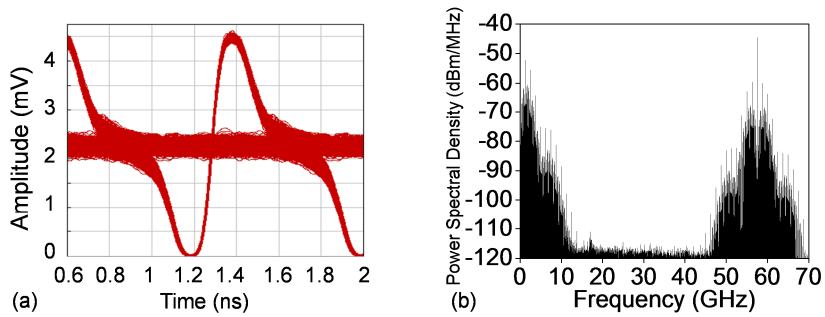

Fig. 24. Simulated signal after the photodetector in Fig. 33. (a) Signal in time domain after further low-pass filtering (Gaussian 12.4 GHz). (b) Electrical spectrum (resolution bandwidth: 600 kHz).

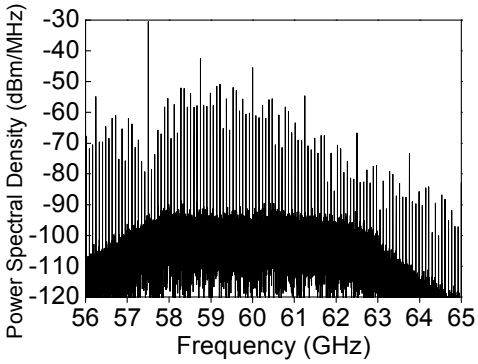

Fig. 25. Simulated spectrum of the signal at point (4) in Fig. 33 after 100 m SSMF transmission to be compared with Fig. 36 (resolution bandwidth: 600 kHz).

At the receiver, the noise figure of the HPA in Fig. 33 is assumed to be 6 dB. An LO signal at 57.5 GHz is employed for down-conversion.

The asymmetry and polarity of the eye diagram is dependent on the phase of this LO signal (adjusted by the PS in Fig. 33 in the experiment). Fig. 26 shows the simulated eye diagram and spectrum of the down-converted signal at point (5) in Fig. 33 at an LO phase of 225°. The eye diagram is symmetric at 270° (or at 90° for inverted polarity).

It is verified that the transmission over 100 m of SSMF [attenuation: 0.2 dB/km @ 1550 nm, dispersion: 16 ps/nm/km @ 1550 nm, dispersion slope: 0.08 ps/nm^2/km] does not practically impact the UWB signal in the 60 GHz band and down-converted signal.

Simulation results are in excellent agreement with experimental measurements. Slight discrepancies are mainly ascribed to the uncertainty in the edges of the frequency response of the amplifiers LNA and HPA, and filters BPF 1 and BPF 2 in Fig. 33. The data of these frequency responses have been interpolated linearly. In addition, note that the noise floor in Fig. 36 and at high frequencies in the measurements in Fig. 34 and Fig. 37(b) is limited by that of the spectrum analyser. This limitation is not present in the corresponding simulated traces.

In order to evaluate the BER performance in the UWB radio-over-fibre system, pseudorandom bit sequence data are considered. In addition, the residual RF carrier frequency at 57.5 GHz in the spectrum of the UWB signal in the 60 GHz band is suppressed considering a commercially-available band-pass filter, BPF 1 in Fig. 33, different from that employed in the experiment (referred as “BPF 1b” in Table VIII), otherwise the wireless transmission distance is limited by saturation of the power amplifier. Fig. 27 shows the simulated signal at point (4) in Fig. 33. At the receiver, down-conversion is performed employing an LO at 57.5 GHz, at 300° phase to optimize the BER. A Gaussian low-pass filter with a 3 dB bandwidth of 10 GHz is employed at mixer output to remove the unwanted frequency components. BER estimation is performed by statistical analysis employing a Chi-squared model, which provides a more accurate estimation than a Gaussian model when the SNR of the system is dominated by amplified optical noise. The sampling instant and the decision threshold for BER estimation are determined by optimum methods. BER is estimated in each case evaluating at least 2^{12} data symbols. Fig. 28 shows the down-converted signal exhibiting a BER of $7 \cdot 10^{-39}$, demonstrating that the system is error free. The filters LPF and BPF 2 in Fig. 33 are found to not significantly impact the BER.

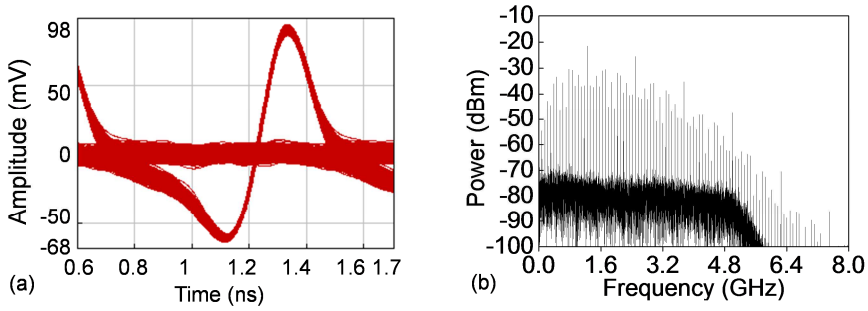

Fig. 26. Simulated signal at point (5) in Fig. 33 to be compared with Fig. 37(b) and (d). (a) Eye diagram. (b) Electrical spectrum (resolution bandwidth: 600 kHz).

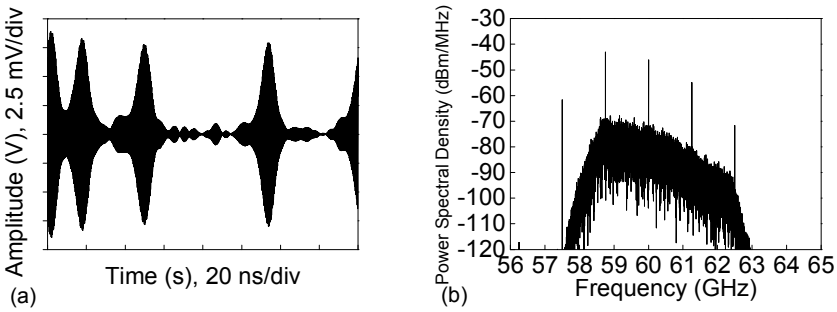

Fig. 27. Simulated signal at point (4) in Fig. 33 to evaluate BER performance. (a) Signal in time domain exhibiting Gaussian envelope. (b) Electrical spectrum (resolution bandwidth: 600 kHz).

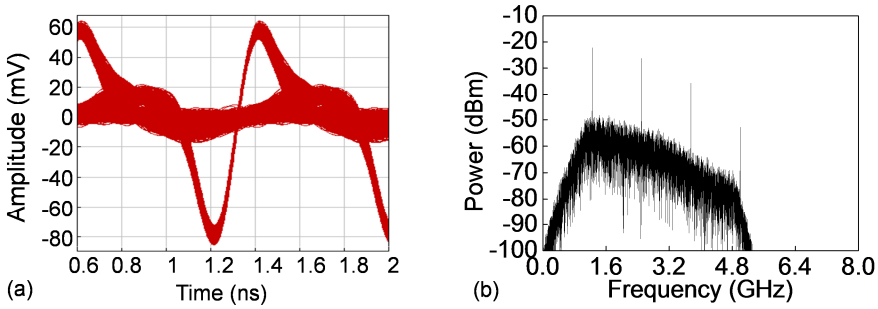

Fig. 28. Simulated signal at point (5) in Fig. 33 to evaluate BER performance. (a) Eye diagram. (b) Electrical spectrum (resolution bandwidth: 600 kHz).

The system is optimized in order to maximize the number of remote antenna units supported while meeting the criterion that the BER performance is below the typical value for error-free operation of 10^{-9} without employing FEC codes at 1.25 Gb/s. Performance analysis is performed as a function of the different contributions to overall optical noise due to the uncertainty in the experimental individual contributions. Optical noise contributions include the noise of the original monocycles converted to the optical domain, relative intensity noise from the CW laser in Fig. 33, and ASE noise from optical amplification. The ASE noise figure is considered fixed at 4 dB.

Note that in all simulated, it is ensured that the maximum photodiode input power and 1 dB compression point of the electrical amplifiers LNA and HPA in Fig. 33 is not exceeded.

Fig. 29 and Fig. 30 show the BER performance and the maximum power spectral density of the UWB signal in the 60 GHz band as a function of the modulation indices of MZM 1 and MZM 2 in Fig. 33, defined as $m_{MZM1} = V_m / V_{\pi 1}$ and $m_{MZM2} = V_{LO} / V_{\pi 2}$, where V_m and V_{LO} are the peak amplitude of the input monocycles and LO signal, respectively, and $V_{\pi 1}$ and $V_{\pi 2}$ are the half-wave voltage of the MZM 1 and MZM 2, respectively, shown in Table VIII. The BER and power spectral density are shown as a function of the relative intensity noise in Fig. 29(a) at 20 nA/Hz$^{1/2}$ noise of the input monocycles, and in Fig. 29(b) for two values of the noise of the input monocycles differing 1 dB in noise figure at RIN= −145 dB/Hz. As shown in Fig. 29 and Fig. 30, the higher the LO amplitude is, the better the BER is and the higher the power spectral density is. The power spectral density increases by approximately 7.6 dB every time the LO power increases by 4 dB. For m_{MZM2} higher than 0.5, BER degrades significantly as the LO peak-to-peak amplitude is higher than $V_{\pi 2}$, entering in another nonlinear part of the MZM 2 transfer function. In addition, for m_{MZM2} lower than approximately 0.16, BER degrades rapidly as m_{MZM2} decreases because the SNR of the generation system becomes dominated by thermal noise instead of by the amplified optical noise. In addition, there is a range of m_{MZM1} within that the BER approximately maintains at its optimum value, for higher values of m_{MZM1}, the BER degrades rapidly as the peak-to-peak amplitude of the input monocycles exceeds the linear zone of the MZM 1 transfer function appearing signal clipping, and for lower values of m_{MZM1}, the BER degrades rapidly as the SNR of the system becomes dominated by thermal noise. The minimum BER is at $m_{MZM2} = 0.48$ of approximately 10^{-42} at $m_{MZM1} = 0.35$ at RIN= −145 dB/Hz, of approximately 10^{-48} at $m_{MZM1} = 0.27$ at RIN= −155 dB/Hz, and of approximately 10^{-47} at $m_{MZM1} = 0.35$ at 18 nA/Hz$^{1/2}$.

A variable optical attenuator is inserted at the fibre input to simulate the optical splitting and distribution losses in the system. Operation as a function of the number of remote antenna units is achieved by adjusting the attenuator attenuation. The number of remote antenna units supported for a given optical link budget (maximum attenuation) depends on the optical splitting scheme. For instance, by considering an optical splitter $1 \times N$ at the output of the optical generation system, as shown in Fig. 20, N remote antenna units are supported and the same SNR is received at the input of all remote antenna units. In this configuration, N fibres would be required to distribute the generated signal to the remote antenna units. Passive optical splitters are commercially available up to 1×128 with typical insertion loss of 13.5 dB, 16.5 dB, 20 dB, and 23.5 dB for 1×16, 1×32, 1×64, and 1×128, respectively [173]. The optical link budget depends on the optical power available at the input of the optical splitter. The system performance has been evaluated for the previous optimum modulation indices of MZM 1 and MZM 2 in Fig. 33, increasing the optical power by increasing the gain of the optical amplifier by 7 dB (from 25 to 32 dB). In addition, performance has been evaluated by inserting a second optical amplifier equal to the first one before the optical splitter. In this case, the gain of the first amplifier is set to 19 dB to not exceed the maximum input optical power of 3 dBm of the second amplifier, and the gain of the second amplifier is set to the maximum of 28 dB. The system performance has been evaluated as a function of the optical link budget and wireless transmission distance.

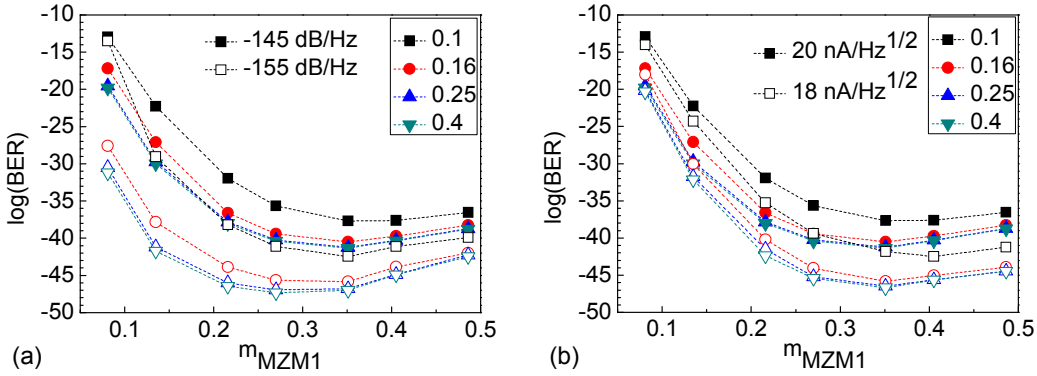

Fig. 29. Simulated BER as a function of the modulation indices of the modulators and (a) relative intensity noise; (b) noise of the input monocycles.

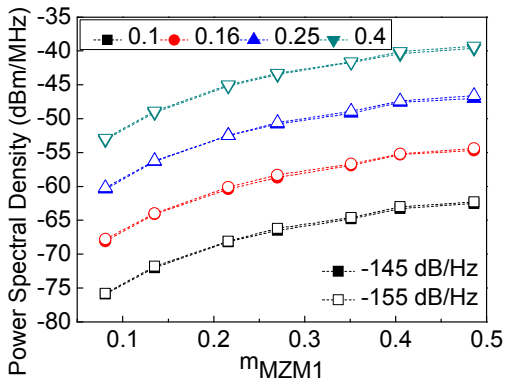

Fig. 30. Simulated maximum power spectral density at point (4) in Fig. 33 as a function of the modulation indices of the modulators and relative intensity noise.

The wireless channel is simulated only considering free-space path losses including its dependence on frequency. The antennas are simulated as a gain of 20 dB as 20 dBi is a typical gain of commercially-available horn antennas in the 50–75 GHz band (e.g. Wisewave, ARH-1520-02, 3 dB beamwidth: 12°) suitable for the target in-flight application.

Fig. 31 shows performance as a function of the attenuation and optical amplification at RIN= −145 dB/Hz and 20 nA/Hz$^{1/2}$ noise of the input monocycles for the back-to-back configuration (direct connection between point (4) in Fig. 33 and receiver). The maximum power spectral density at point (4) in Fig. 33 is also indicated in Fig. 31 for one optical amplifier at 25 dB gain. In Fig. 31, the performance is limited by thermal noise for a larger number of remote antenna units at a given optical power. Increasing the number of remote antenna units degrades the BER due to the reduction in the SNR. Moreover, error-free operation is not achieved without optical amplification. Increasing the optical power increases the number of remote antenna units supported or improves the SNR in the case limited by thermal noise resulting in improved performance. The minimum BER obtained with two amplifiers is not degraded compared to the system with one amplifier, which indicates that no signal degradation is induced by the second optical amplifier. Performance is also shown in Fig. 31 at RIN= −155 dB/Hz or 18 nA/Hz$^{1/2}$ noise of the input monocycles. At lower optical noise, the SNR becomes limited by thermal noise at lower number of remote antenna units.

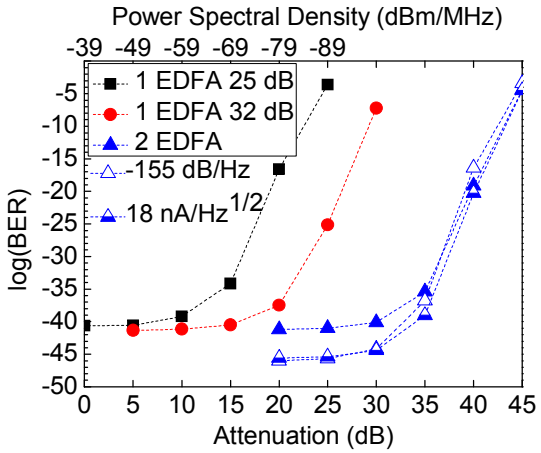

Fig. 31. Simulated BER as a function of optical losses, optical amplification, relative intensity noise, and noise of the input monocycles.

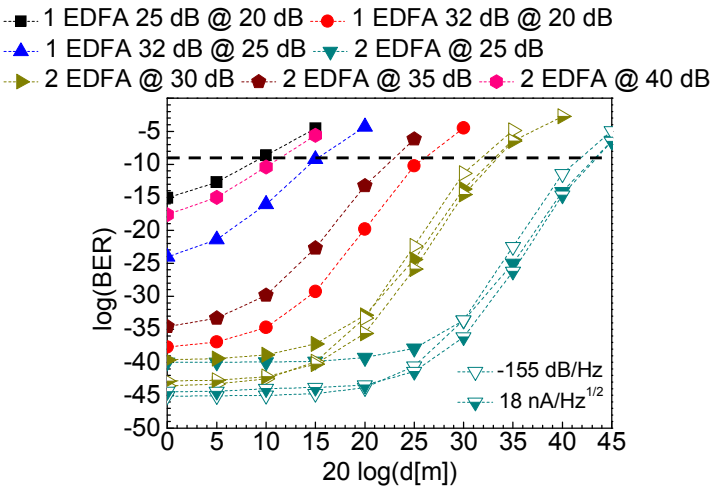

Fig. 32. Simulated BER as a function of the wireless distance *d* and optical noise comparing optical amplification and link budget. The BER limit for error-free operation is shown via a horizontal dashed line.

The maximum power spectral density decreases by 10 dB every time the optical power decreases by 5 dB, and decreases by approximately 1.6 dB at RIN= −155 dB/Hz with respect to RIN= −145 dB/Hz, or by 0.2 dB at noise of the input monocycles 18 nA/Hz$^{1/2}$ with respect to 20 nA/Hz$^{1/2}$. In case of employing two optical amplifiers, the maximum power spectral density decreases by 10 dB every time the gain decreases by 5.35 dB.

Performance as a function of the wireless transmission distance and optical noise at a given optical amplification and link budget is compared in Fig. 32. The higher the optical power is, either the longer the wireless range is for error-free operation at a given number of remote antenna units or the higher the number of remote antenna units is at a given wireless range. For instance, at 64 remote antenna units, the range increases from 3.2 m to 20 m by increasing the optical amplification from 25 dB to 32 dB or at 128 remote antenna units, the range increases from 5.6 m to 149.6 m by increasing the optical amplification from 32 dB with one amplifier to 47 dB with two amplifiers.

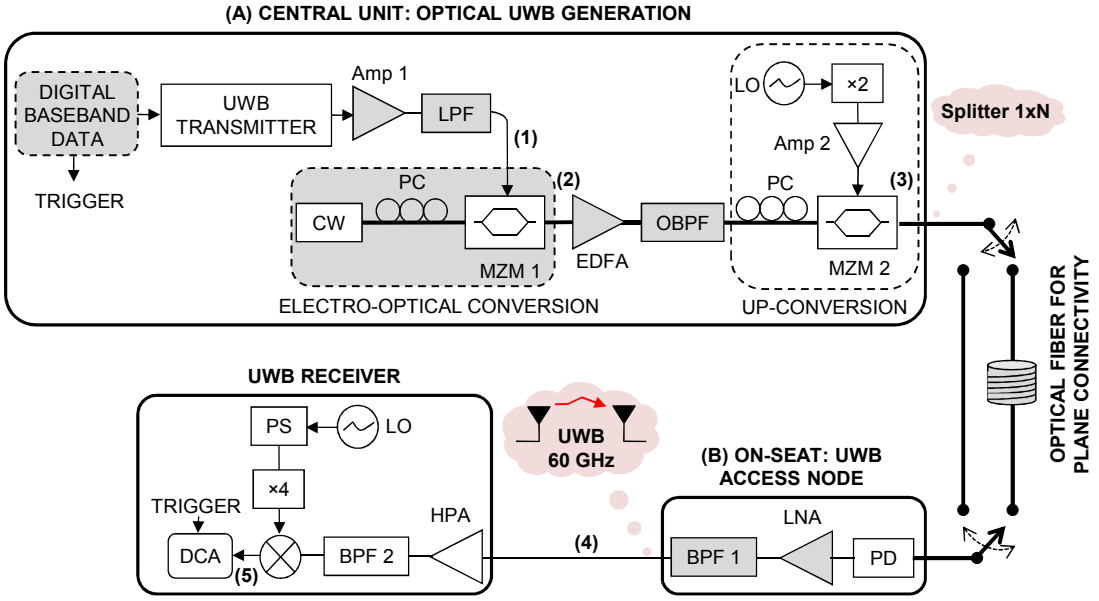

Fig. 33. Experimental setup of the 60 GHz UWB-over-fibre system according to Fig. 20. The UWB transmitter is that shown in Fig. 18.

The wireless range decreases from 149.6 m to 44.7 m, 14.1 m or 3.8 m when the link budget increases from 25 dB (128 remote antenna units) by 5 dB, 10 dB, or 15 dB when employing two optical amplifiers. Furthermore, the wireless distance is shorter by decreasing the relative intensity noise and is longer by decreasing the noise of the input monocycles. This suggests that the optical noise is limited by the noise of the input monocycles converted to the optical domain. The range decreases from 44.7 m to 39.8 m when the relative intensity noise increases from −145 dB/Hz to −155 dB/Hz or increases from 44.7 m to 47.3 m when the noise of the input monocycles decreases from 20 to 18 nA/ $Hz^{1/2}$.

The simulation results herein reported demonstrate that the proposed 60 GHz UWB radio-over-fibre system can support a high number of remote antenna units at WPAN distances lower than 10 m required for the target in-flight application.

3.3.4 Experimental demonstration

An impulse-radio UWB signal in the 60 GHz band is generated and transmitted over 100 m of SSMF. The experimental setup is shown in Fig. 33 and the system parameters are shown in Table VIII.

At the central unit, the generated Gaussian monocycles shown in Fig. 19 are amplified and converted to optical domain by external modulation in a MZM (MZM 1 in Fig. 33) biased at the quadrature point at which the operation is the most linear. A low-pass filter is employed to remove noise at expense of some distortion in the skirt of the pulses. Fig. 34 shows the Gaussian monocycles measured at point (1) in Fig. 33. Fig. 35 shows the optical Gaussian monocycles measured at point (2) in Fig. 33. Subsequently, an optical amplifier sets the emission level of the UWB signal in the 60 GHz band at point (4) in Fig. 33. A tunable optical band-pass filter is employed to suppress amplified spontaneous emission (ASE) noise.

Table VIII. System parameters

Device	Description	Characteristics
Amp 1	Picosecond Pulse Labs, Driver Amplifier 5865	Gain: 34 dB Noise figure: 6 dB
LPF	Mini-Circuits, VLP-41	3-dB bandwidth: 4.1 GHz Loss >20 dB @ 5.6 GHz
CW	Fibernet	Center wavelength: 1559.8 nm Average power: 14 dBm
MZM 1	Covega, Mach-40 005	3-dB bandwidth: 35 GHz $V\pi$: 3.7 V
EDFA	Amonics, AEDFA-30-B	Saturation power: 30 dBm Noise figure: 4 dB Input power: −6 – 3 dBm
OBPF	Tecos, FC-1570 B-2-1	3-dB bandwidth: 1 nm
MZM 2	Corning-OTI, 40 Gb/s	3-dB bandwidth: 30 GHz $V\pi$: 5 V
PD	u^2t Photonics, XPDV3120R-VF-FC	3-dB bandwidth: 75 GHz Responsivity: 0.63 A/W Dark current: 3.5 nA Thermal noise: 10 pA/√Hz Average input< 13 dBm
LNA	Terabeam-hxi, HLNAV-262	Bandwidth: 55 – 65 GHz Gain: 18.7 dB P1dB: 10.5 dBm Noise figure: 4.5 dB WR-15 connectors
BPF 1	Wisewave, PFB-15605040-01	3-dB bandwidth: 57.5 – 62.5 GHz Rejection: 40 dB @ 52 GHz, 68 GHz Passband insertion loss: 1.5 dB
HPA	Terabeam-hxi, HHPAV-222	Bandwidth: 55 – 65 GHz Gain: 28.7 dB P1dB: 14.5 dBm
BPF 2	Spacek Labs, F60-10	3-dB bandwidth: 56.26 – 62 GHz Rejection: 24 dB @ 55 GHz, 22 dB @ 63.75 GHz Passband insertion loss: 1.1 dB
×4 Active frequency multiplier	Terabeam-hxi, HAFMV4-158	Output frequency: 58.6 – 62.2 GHz Input power: 10 dBm Max output power: 15 dBm WR-15, SMA connectors
Mixer	Spacek Labs, M60-10	RF bandwidth: 55 – 65 GHz IF bandwidth: DC – 10 GHz Conversion loss: 4.6 dB LO power: 18 dBm WR-15, SMA connectors
Electrical signal analyzer	Rohde&Schwartz, FSQ40	9 kHz – 40 GHz External harmonic mixer: 40 – 60 GHz, 24 dB conversion loss
DCA	Agilent 86100C, HP83481A and HP83482A	Electrical bandwidth: 12.4 GHz Optical bandwidth: 30 GHz
BPF 1b (see Section 3.3.3)	Spacek Labs, F60-5	3 dB bandwidth: 58.125 – 61.875 GHz Rejection: 20 dB @ 57.5 GHz, 29 dB @ 62.5 GHz Passband insertion loss: 1.1 dB

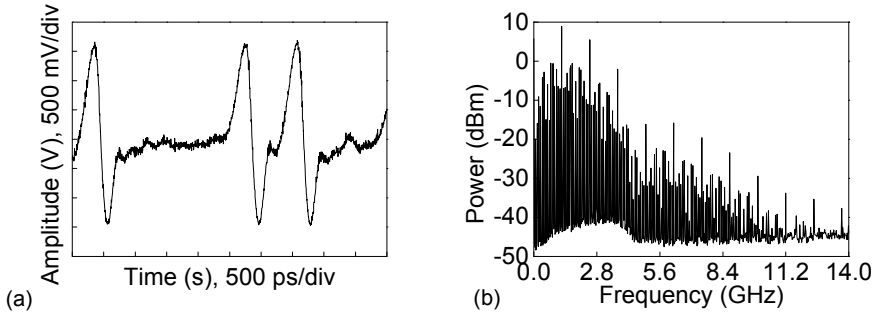

Fig. 34. Gaussian monocycles measured at point (1) in Fig. 33. (a) Signal in time domain. (b) Electrical spectrum (resolution bandwidth: 300 kHz).

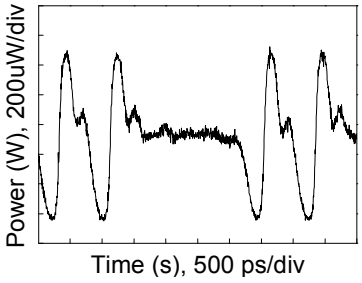

Fig. 35. Optical Gaussian monocycles measured at point (2) in Fig. 33.

Subsequently, frequency up-conversion of the optical Gaussian monocycles employing low-frequency electrooptic components is performed. A LO at 14.25 GHz is doubled in frequency and amplified to 14 dBm. The resulting 28.5 GHz signal is modulated with the optical Gaussian monocycles in a MZM (MZM 2 in Fig. 33) biased at the minimum transmission point to perform optical carrier suppression modulation. Gaussian monocycles up-converted to 57 GHz ($2 \cdot 28.5$ GHz) are obtained after photodetection at the remote antenna unit. The photodetector output is coupled to a low-noise amplifier by a WR15 adapter, and then a band-pass filter is employed to filter the 60 GHz band. Fig. 36 shows the electrical spectrum of the UWB Gaussian monocycles in the 60 GHz band to be radiated at point (4) in Fig. 33 after transmission over 100 m of SSMF. In practice, the residual RF carrier at 57 GHz has to be filtered as it may limit the dynamic range of the receiver as well as the power levels regulated in the 60 GHz band, which are summarized in Table IV.

To verify the appropriate operation, direct demodulation (with no air transmission) of the 57 GHz impulse-radio UWB signal is performed by electrical heterodyne receiver, as shown in Fig. 33. The received 57 GHz impulse-radio UWB signal is amplified by a high-power amplifier, band-pass filtered, and down-converted employing broadband electrical mixing with a LO signal at 57 GHz. The LO signal is generated by frequency quadrupling of the same LO signal employed at the transmitter. A phase shifter is employed for assuring proper phase matching for accurate down-conversion. Fig. 37 shows the down-converted signal measured at point (5) in Fig. 33 after transmission over 100 m of SSMF. In Fig. 37(c), the original data pattern can be easily recognized. The quality of the down-converted signal is evaluated from the *Q*-factor parameter measured in the eye diagram only on the positive part of the Gaussian monocycle. In this way, the scope considers the pulse as a RZ pulse and can measure *Q*-factor.

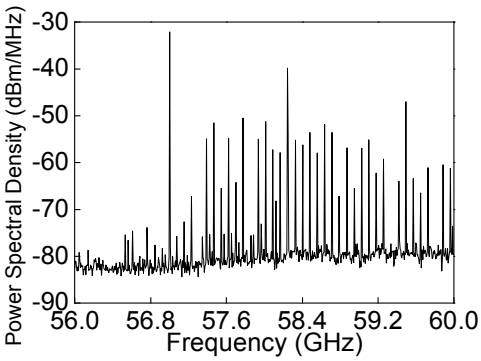

Fig. 36. Electrical spectrum of the impulse-radio UWB signal in the 60 GHz band after 100 m SSMF transmission, measured at point (4) in Fig. 33 (resolution bandwidth: 300 kHz).

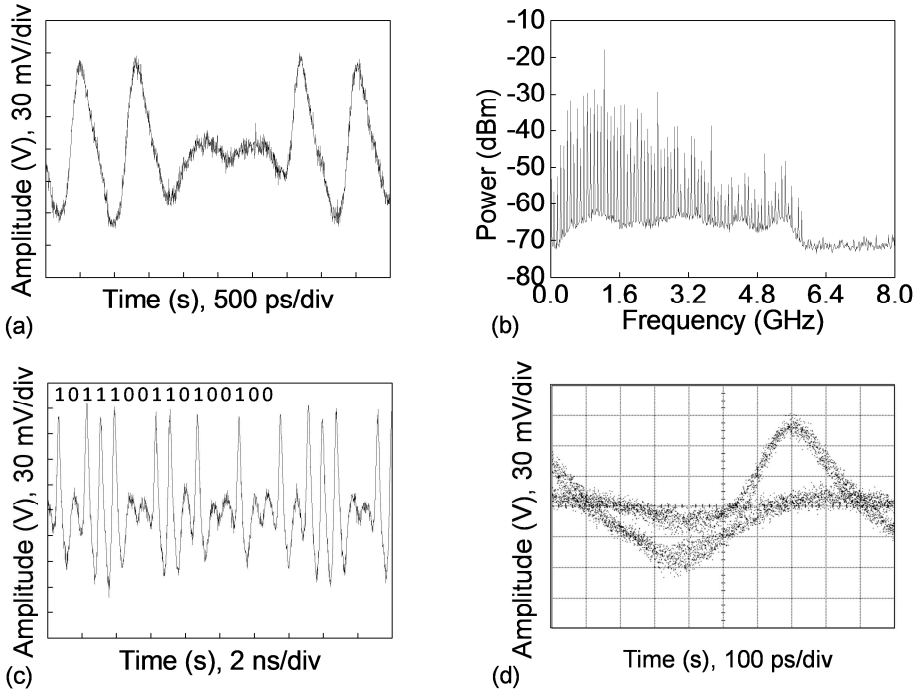

Fig. 37. Down-converted impulse-radio UWB Gaussian monocycles after 100 m SSMF transmission, measured at point (5) in Fig. 33. (a) Time-domain pulses (time span: 5 ns). (b) Electrical spectrum (resolution bandwidth: 300 kHz). (c) Time-domain pulses (time span: 20 ns) showing the original data pattern. (d) Eye diagram.

Excellent quality of the down-converted signal with a *Q*-factor of approximately 7 is obtained. This quality corresponds to a maximum EIRP density of approximately −15 dBm/MHz when a gain of 20 dBi of a typical 60 GHz antenna is considered. This EIRP level is well below 13 dBm/MHz as of current 60 GHz regulation. Note that no signal degradation is obtained after 100 m SSMF transmission compared with the optical back-to-back configuration.

3.3.5 Techno-economic analysis

The 60 GHz UWB radio-over-fibre photonic generation demonstrated in Section 3.3.4 distributes the same signal, from a single source, to all seats in the plane targeting to distribute HD multimedia contents.

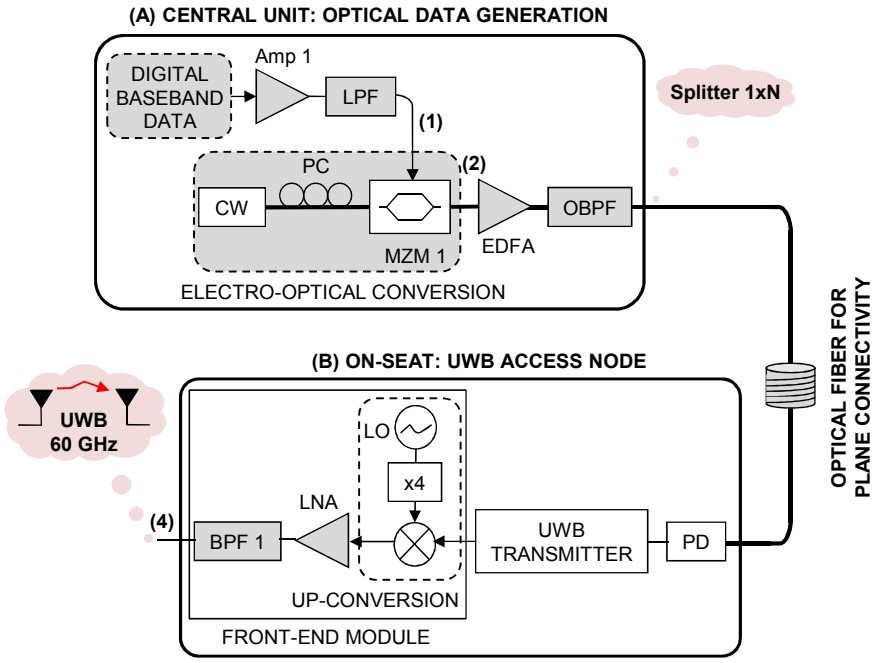

Fig. 38. Electrical approach of the 60 GHz UWB-over-fibre system according to Fig. 20 to be compared with the photonic approach in Fig. 33.

UWB is a short-range (WPAN) very high data rate technology. So the simplest receiver is of the utmost interest due to cost and reliability parameters. Centralized optical frequency up-conversion appears as an interesting low-cost solution compared to perform broadband electronic mixing with a 60 GHz LO in each remote antenna unit of the radio-over-fibre system.

In this Section, the cost of the 60 GHz UWB radio-over-fibre system demonstrated in Section 3.3.4 based on photonic generation and frequency up-conversion at the central unit, shown in Fig. 18 and Fig. 33, is compared with an all-electrical approach based on conventional transmission over fibre of digital baseband data and further UWB generation and frequency up-conversion at remote antenna units in the electrical domain, as shown in Fig. 38. The cost analysis is based on real costs of commercially available devices (as of November 2009).

The overall cost of both systems as a function of the number of remote antenna units is summarized in Table IX. The cost is also compared in Fig. 39. The electrooptic conversion, optical amplification, optical splitting, fibre interconnections and low-noise amplification are considered to be the same in both systems, shown in Fig. 33 and Fig. 38 as the grey-filled area. The cost of the low-pass filter, optical band-pass filter, and band-pass filter 1, is not considered in the analysis.

The order in which the modulations, MZM 1 and MZM 2 in Fig. 33, have been performed, permits to perform the electrooptic conversion by direct modulation of laser diodes at relative low cost and performance depends critically on the selected laser. While at higher cost, the scheme employing external MZM can generate higher modulated power resulting in higher SNR compared to direct modulation schemes. A 10 Gb/s transmitter packaging a laser diode and a MZM for cost/performance ratio better than the alternative separated components has been considered in the cost analysis.

Table IX. Total cost [USD] photonic radio-over-fibre (RoF) vs. photonic baseband and electronics (BB)

# Remote antenna units	1	10	50	100	250	500
RoF central unit	14,397	14,397	14,397	14,397	14,397	14,397
RoF remote antenna units	801.2	8,012	38,162	71,826	163,253	280,830
BB central unit	7,000	7,000	7,000	7,000	7,000	7,000
BB remote antenna units	1,049	10,400	42,085	79,829	147,073	287,250
RoF and BB Splitting+Fibre	70	935	4,320	8,500	20,595	41,140
RoF COMPLETE DEPLOYMENT	15,268	23,344	56,879	94,723	198,244	336,367
BB COMPLETE DEPLOYMENT	8,119	18,335	53,405	95,329	189,668	335,390

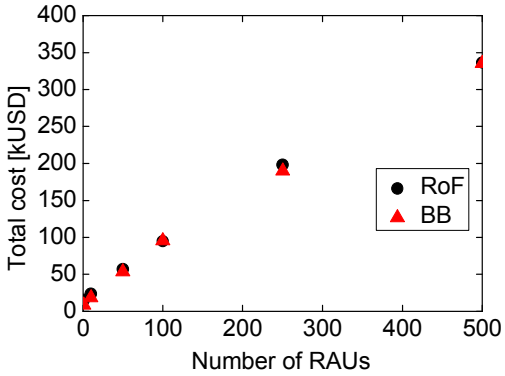

Fig. 39. Comparison of the overall cost of the photonic radio-over-fibre (RoF) vs. photonic baseband and electronics (BB) schemes as a function of the number of remote antenna units.

Planar lightwave circuit (PLC) splitter modules including optical connectors are considered for optical splitting. The price considered in the analysis corresponds to that for one passive optical splitter 1 × 16 at ten remote antenna units, one 1 × 64 at 50, one 1 × 128 at 100, one 1 × 2 and two 1 × 128 at 250, and one 1 × 4 and four 1 × 128 at 500.

100 m spools of SSMF (SMF-28e+ with 900 µm jacket at $0.70/m) are considered for fibre interconnections in the cost analysis.

Individual modules with connectors are considered for the cost evaluation of the photonic UWB transmitter. The cost (~$35 000) of the actively mode-locked fibre laser employed in the experiment at 5–11 GHz repetition rate drives the overall cost of the photonic UWB transmitter. Mode-locked laser diodes at 10 GHz are commercially available at lower cost, e.g. u^2t Photonics, TMLL1550; however, at much lower power and worse noise specifications. Mode-locked lasers at repetition rates of ~1 GHz (e.g., PriTel or Onefive) are currently custom designs at a cost exceeding $35 000. Nevertheless, pulsed sources at 10 GHz repetition rate could be used employing RZ data with adequate pulsewidth so that future higher rates could be handled with no additional cost. Generation of optical pulsed data by the pulsed laser, polarization controller, optical delay line and electrooptic modulator could be substituted by a low-cost solution consisting in a module integrating RZ pulse generator and data modulator (e.g., JDS Uniphase or Covega at ~$1280 at 10 Gb/s or higher rate), sinusoidal drive and electrical phase shifting instead of the optical delay line to adjust the time gating of the optical pulses with the data. This alternative has been considered in the cost evaluation shown in

Table IX and Fig. 39. In addition, an adequate chirped FBG is considered for pulse stretching at lower cost than by 10 km of SSMF employed in the experiment. A 10 Gb/s differential photoreceiver including one photodiode is considered at much lower cost than a 43 Gb/s photoreceiver comprising two photodiodes, as employed in the experiment.

Frequency doubling and further amplification for optical frequency up-conversion could be performed by an active frequency doubler, which is available in low-cost monolithic microwave integrated circuit (MMIC) technology. A commercial voltage-controlled oscillator MMIC chip is considered as well. The unit price of these MMIC chips is under $50 at > ten units. The packaging of a MMIC chip into a module with connectors increases the price by ~$1000.

The cost of the remote antenna units in both systems is obtained by summing up the costs of their constitutive parts, considering individual chips, which, in practice, would be integrated into a single module reducing significantly costs because of the reduced packaging costs. Nevertheless, the number of interconnects and packaging of the module critically impact the performance and overall cost of both systems.

The overall cost of the radio-over-fibre approach critically depends on the cost of the 60 GHz photodetector at the remote antenna units, which depends on the type of packaging, as well as several other factors, such as minimum specifications and the type of testing or assurances. Currently, few manufacturers produce photodetectors capable of working in the 60 GHz band in high volume. The market of these photodetectors has not matured yet. The application herein proposed would not require the ultimate specifications of the high-performance photodetector employed in the experiment. The unit price of the photodetector considered in the cost analysis corresponds to that of a chip with connector upon the end of a fibre optical cable with a guaranteed 3 dB bandwidth >50 GHz and 10 dB bandwidth >60 GHz, high maximum responsivity >0.56 A/W, and polarization dependent loss (PDL) < 0.1 dB. In addition, this photodetector features excellent pulse response and high optical power capability. As shown in Table IX, the unit price of the photodetector is significantly better for high quantities. It should be noted that a currency change of 1 €= 1.45 USD has been considered for the price of the 60 GHz photodetector.

In Table IX, the cost of a photodetector with coaxial packaging including fibre connector at 3 dB bandwidth >2.5 GHz is considered to evaluate the cost of the remote antenna units in the electrical scheme.

To the best of our knowledge, impulse-radio UWB transmitters capable of providing the multi-Gb/s wireless communication required by multimedia streaming in WPAN applications are not commercially available. A Gaussian monocycle generator consisting of an impulse generator followed by an impulse forming network is a commercially available solution [33]. This impulse generator requires a clock input to generate impulses, which can be gated by external data up to 2.5 Gb/s. Although the cost of this generator is significantly reduced for high quantities, it makes no sense to employ this generator at remote antenna units from the cost point of view. In addition, few electrical impulse-radio UWB transmitters with gigabit modulation capabilities have been demonstrated in the literature [31], [34]. The single-chip prototype demonstrated

in [31] includes reconfigurable and modulation capabilities up to 2.5 Gb/s. This transmitter has been implemented in 0.18 μm CMOS technology with potential cost advantage. However, these circuits employ complicated electronic circuitry and are not easy to manufacture. Compared to all electrical transmitters, the photonic generation of monocycles employed in the proposed system in Section 3.3.4 has technical advantages, as it is simple in operation principle, easily reconfigurable in data rate and bandwidth being capable of providing wider bandwidth and rates higher than 2.5 Gb/s suitable for future upgrade, while it is able to provide higher-quality pulses.

In Table IX, the cost of an electrical UWB transmitter based on OFDM UWB transceivers, which are commercially available, is considered. A number of standard-compliant OFDM UWB transceiver chipsets at data rates up to 480 Mb/s are commercially available. For instance, Alereon AL5100/AL5300 chipsets are produced in high volume (>10 000 units) for the top-tier PC and consumer electronics vendors. The unit price of these chipsets is under $10 at thousands of chipsets without neither nondisclosure agreement, nor volume commitment. The cost of the electrical UWB transmitter considered in Table IX has been obtained by summing up the cost of three OFDM UWB chipsets, providing an aggregated data rate of 1.44 Gb/s, and the cost of a four-port combiner module with SMA connectors at 4−8 GHz frequency range, which would be employed to combine the output of the three chipsets. A unit price of $150, $100, $50 and $30 of the OFDM UWB chipset is assumed up to 10, 100, 250 and 500 units, respectively.

60 GHz MMIC dies are considered for the local oscillators, mixers, frequency quadruplers and low-noise amplifiers at remote antenna units at very low cost under $50 at > ten units. The cost of the oscillator and low-noise amplifier is the same in both systems under comparison. Note that the 60 GHz MMIC mixer and frequency quadrupler exhibit worse performance than the corresponding prototype modules employed in the experiment. Many 60 GHz MMIC chipsets have been demonstrated [182] and there are also commercially available (e.g. Endwave or Gotmic).

From the cost comparison shown in Fig. 39, the UWB radio-over-fibre approach presents deployment cost equivalent to cost associated to a conventional baseband transmission scheme based on electronics even considering that the radio-over-fibre approach presented here operates in the 60 GHz radio band. Devices and subsystems operation at 60 GHz, mainly the 60 GHz photodetector, drive the budget in this case. It is expected that when 60 GHz technology became mature, radio-over-fibre cost will drop substantially, making the radio-over-fibre approach especially interesting for large count deployments. Furthermore, the radio-over-fibre technique is advantageous in terms of transparency to the specific wireless standard not requiring modulation at each remote antenna unit, large bandwidth, more flexibility in terms of bandwidth and data rate.

3.4 Dual-band generation by frequency shifting in remote-connectivity fibre

An impulse-radio UWB photonic generation technique based on frequency shifting in the remote connectivity fibre in optical access networks is proposed and analysed in this Ph.D. thesis [Bel10b], [Bel11d]. This technique is based on optical carrier suppression modulation combined with fibre chromatic dispersion targeting to overcome the bandwidth limitation of optical up-conversion, with the advantage of being easily reconfigurable generating simultaneously different RF bands. A comprehensive simulation analysis is performed with special focus on capabilities for dual 24 GHz/60 GHz operation paired with experimental demonstration at 1.25 Gb/s. 60 GHz wireless performance after optical generation and transmission in 12.5 km of SSMF is measured demonstrating error-free transmission at 1 m radio distance. The inclusion of remote Gaussian monocycle pulse shaping is also analysed in this paper considering dual 24 GHz/60 GHz operation. Pulse-shaped dual 24 GHz/60 GHz generation is experimentally demonstrated at 1.25 Gb/s. Transmission performance is measured at 24 GHz demonstrating error-free transmission. The simulation analysis further indicates that the technique is suitable for UWB generation at higher RF bands such as the *W*-band (75−110 GHz). Practical implementation considerations and trade-offs (e.g., in terms of cost and number of remote antenna units supported) of this system are also analysed by simulation showing that the technique is cost effective.

3.4.1 Introduction

UWB radio transmissions have been allocated in the frequency range from 3.1 to 10.6 GHz [1]. UWB can also operate in the 24 GHz band for vehicular short-range radar applications [2]. UWB operation in the 60 GHz band is an open opportunity to overcome coexistence issues with other radio technologies operating in the same frequency band, such as 3.5 GHz WiMAX and 5 GHz Wi-Fi. UWB bandwidth in current regulation (up to 7.5 GHz) can be allocated very well in the unlicensed frequency range regulated for generic 60 GHz radio worldwide: 57−66 GHz in Europe and Australia, 57−64 GHz in the U.S. and Canada, 59−66 GHz in Japan. Furthermore, UWB operation in the 60 GHz band permits to increase the mean EIRP density from −41.3 dBm/MHz as in current UWB regulation worldwide to 13 dBm/MHz as permitted in regulation in force in the band [17]. This permits extending UWB reach provided the 20 dB higher free-space path loss in the 60 GHz band is compensated. Nevertheless, the atmospheric attenuation in the 60 GHz band of up to approximately 30 dB/km further limits outdoor reach [18]. UWB radio-over-fibre transmission has been indicated as a rapid and cost-effective solution to deliver high-bandwidth services in FTTH networks [Llo08a], [Llo08c], as discussed in Section 2.5.4. 60 GHz UWB targets to provide multi-Gb/s WPAN connectivity in such home environments [Bel10c], as proposed in Section 4. 60 GHz UWB also targets environments where interference is a critical issue like aircrafts, telecommunication operators, and government premises [Bel09a], as proposed in Section 3.3.

A number of impulse-radio UWB-over-fibre systems have been demonstrated in different RF bands, as summarized in Table I. In the 3.1−10.6 GHz band, wireless distances below 1 m have been demonstrated meeting regulation in the U.S. and employing OOK modulation up to 3.125 Gb/s for optical access networks. In the 60 GHz band, up to 40 km of SSMF and 5 m wireless transmission has been demonstrated employing BPSK modulation at 1.44 Gb/s [Bel10c], as demonstrated in Section 4.1, or up to 6.5 km of SSMF and 2 m employing OOK at 3.125 Gb/s [Bel11b], as demonstrated in Section 4.2. Finally, an optical system operating in the 75−110 GHz band (*W*-band) has been demonstrated up to 1.6 m of wireless distance employing OOK modulation at 2.5 Gb/s and a dispersion-compensated link for high-density user in-building applications [59].

This Ph.D. thesis targets to provide a comprehensive simulation analysis paired with supporting experimental work in order to investigate the technical aspects and possible configurations of a multiband impulse-radio UWB optical generation tailored for UWB-over-fibre transmission in optical access networks.

The principle of operation of the proposed technique is presented in Section 3.4.3. Section 3.4.4 describes simulation work demonstrating multiband capabilities and addressing practical considerations. Dual-band operation is experimentally demonstrated in Section 3.4.5 employing two different system configurations. Enabling technologies for a simple and cost-effective practical implementation of the UWB-over-fibre system are discussed in Section 3.4.6.

3.4.2 Integrating multiband operation in the optical access network

Fig. 40 depicts the application scenario considering optical generation of impulse-radio UWB signals and radio-over-fibre transmission through the remote connectivity fibre in a FTTH network. Photonic generation of impulse-radio UWB is capable of simultaneously generate UWB signals in different RF bands, ranging from baseband to millimetre-wave. In this way, the same UWB signal can simultaneously provide a wide variety of functionalities [Bel10b]. The proposed optical generation technique can be integrated in FTTH networks to deliver 60 GHz services such as high-speed data and HD audio/video streaming, and also to provide connectivity to an UWB-enabled cell phone operating in the standard 3.1–10.6 GHz band, as depicted in Fig. 40.

In [Bel11d], we further investigate by simulation the capabilities of UWB over fibre to simultaneously generate an impulse-radio UWB signal in the 24 GHz band for vehicular radar and infrastructure-to-car communications applications served by an optical access infrastructure, as is also depicted in Fig. 40.

The proposed UWB-over-fibre generation scheme requires up-conversion at a central unit, Head-end in Fig. 40, and further frequency shifting to different RF bands. This is performed by different total dispersion in the fibre links providing remote connectivity. In addition, dual 24 GHz/60 GHz band generation is experimentally demonstrated employing a different system configuration and Gaussian-monocycle shaping at 24 GHz remote antenna units.

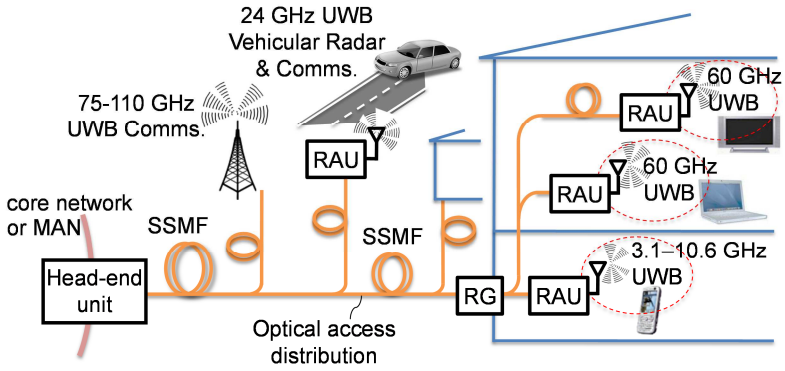

Fig. 40. Radio-over-fibre system integrating optical access network and outdoor/in-building radio transmission of multiband multi-Gb/s impulse-radio UWB for several applications.

Performing simple adjustable pulse shaping remotely is proposed to flexibly adapt the UWB spectrum to different fibre dispersion. Gaussian-monocycle shaping can provide spectrum flexibility and could permit to radiate the baseband signal, which is also available after photodetection, in the 3.1−10.6 GHz band employing commercially available antennas [24]. Note that this work is focused on dual 24 GHz/60 GHz band operation. Nevertheless, multiband operation is also addressed in this work considering higher frequency bands, in particular the 75−110 GHz band. Higher frequency bands show larger potential bandwidths available and lower atmospheric attenuation which could extend wireless reach. This approach could be alternatively implemented introducing optical UWB generation in the FTTH residential gateway, RG in Fig. 40, provided an in-home optical distribution network is in place thus reducing the potential impact of failure in the central head-end unit.

3.4.3 Principle of operation

Fig. 41 shows the technique proposed for generation of RF impulse-radio UWB signals in the optical domain. At the head-end unit, transform-limited optical pulses with pulsewidth T_o and optical bandwidth $\Delta\lambda$ are chirped and stretched in time to $T_{IN} = \Delta\lambda \cdot D_{t1}$ in a first dispersive element with total dispersion D_{t1}. The generation technique relies on the conversion of the spectral components of the pulsed laser to time domain (wavelength-to-time mapping). This is performed in the first dispersive element as long as the condition $T_0^2 << |\ddot{\phi}_0|$ is met, where $\ddot{\phi}_0$ is the first-order dispersion coefficient [183]. The spectrally-resolved pulses is the impulse-radio signal which is modulated with a LO signal with frequency f_{LO} in an intensity electrooptic modulator to perform frequency up-conversion. The modulated impulse-radio signal is dispersed in a second dispersive element with total dispersion D_{t2} for further frequency shifting. The second dispersive element stretches or compresses the impulse-radio envelope by a factor $M = 1 + D_{t2} / D_{t1}$, resulting in further frequency down-shifting or up-shifting, respectively. Time stretching is performed when D_{t1} and D_{t2} have the same sign ($M > 1$) whereas the envelope is compressed in time when D_{t1} and D_{t2} have opposite sign ($0 \le M < 1$) [184]. Time compression or stretching of a time-reversed version of the impulse-radio envelope is performed when D_{t1} and D_{t2} have opposite sign so that $-1 < M < 0$ or $M < -1$, respectively [185]. The envelope is the time-reversed version of the original envelope at $M = -1$ (nor time compression or stretching).

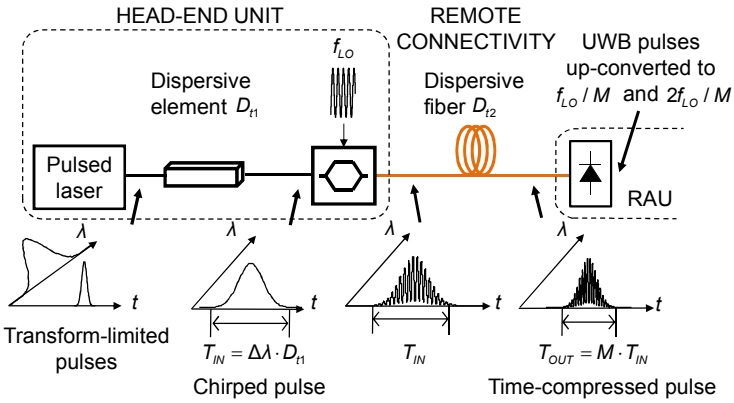

Fig. 41. Schematic diagram of the photonic technique for RF impulse-radio UWB generation based on frequency shifting by the dispersive fibre providing remote connectivity. $M = 1 + D_{t2} / D_{t1}$.

This chirped microwave amplitude modulation technique with matched dispersion has been demonstrated for several applications [184], [186]. Chirped optical pulses that are amplitude-modulated by a microwave signal have been used for frequency shifting of the microwave signal [184]. The technique has also been used to increase the sampling rate and input bandwidth of electronic analogue-to-digital converters [186]. The application of the technique for radio over fibre with multiband capabilities is proposed in this Ph.D. thesis. In this application, the same fibre employed to provide remote connectivity, e.g. SSMF in FTTH networks, is employed as second dispersive element. The use of optical carrier suppression modulation by biasing a MZM at the minimum transmission point is also proposed for this application. This reduces RF power fading induced by fibre chromatic dispersion at expense of reduced power [143]. RF power fading limits LO frequency without employing dispersion compensation [186]. Optical carrier suppression also relaxes frequency requirement of the up-conversion stage for frequency shifting to the same centre frequency in the same remote fibre. This frequency requirement is further relaxed when time compression is performed thus effectively reducing cost. Furthermore, two RF bands centred at f_{LO}/M and $2 \cdot f_{LO}/M$ are generated in the same remote fibre after photodetection when optical carrier suppression modulation is employed. This enables up-conversion to the same centre frequency in two remote fibres with different total dispersion from the same head-end unit without employing dispersion compensation. Two additional total dispersions are possible for this purpose when the corresponding time-reversed versions are generated, i.e. the same value of M with opposite sign is employed.

In order to generate at a given centre frequency simultaneously by total dispersions of remote fibre beyond the four cases discussed above, dispersion could be managed by adding remote dispersion compensation. This can be of interest in FTTH networks where different distances exist from the central head-end unit to the remote antenna units, the number of central head-end units being a trade-off for a high-number of remote antenna units. Remote dispersion compensation could be centralized in residential gateways, RG in Fig. 40, to simplify remote antenna units and reduce cost. However, the variation in the in-home fibre lengths could induce performance degradation limiting splitting ratios in FTTH to support more users. At the remote antenna units, RAU in Fig. 41, the impulse-radio UWB signals are

photodetected, amplified, filtered, and radiated to the end-user terminals. The baseband signal is also available after photodetection, which can be used either for a wired connectivity employing a low-speed receiver or for UWB wireless connectivity in the 3.1–10.6 GHz band, shown in Fig. 40, provided adequate pulse shaping is performed in the system [27].

The use of IDF for frequency shifting and remote connection poses an interesting solution for multiband generation of RF impulse-radio UWB signals performing both time compression and time stretching from the same head-end unit. Compared with DCF, IDF is more suitable for optical transmission [169].

3.4.4 Simulation analysis

A model of the photonic generation technique depicted in Fig. 41 has been developed employing the simulation tool VPItransmissionMaker™ (version 8.3). The simulation model has been employed to design the system for the experimental demonstrations reported in Section 3.4.5, taking into account the operation principle discussed in Section 3.4.3. The simulation model has been verified from experimental measurements, as shown in Section 3.4.5.

Multiband generation capabilities of the RF impulse-radio UWB generation technique have been investigated by simulation employing the experimental head-end unit in Section 3.4.5. Furthermore, the influence of UWB pulse shape has been analysed including Gaussian-monocycle shaping in the system. The operational limits employing both Gaussian and Gaussian-monocycle pulse shapes have also been investigated by simulation considering impulse-radio UWB generation in the 24 GHz, 60 GHz, and 75−110 GHz bands.

In simulation, hyperbolic-secant pulses modulated with data at 1.25 Gb/s are generated at 1550 nm by an optical pulse transmitter. The pulses have 2 ps FWHM and 1.27 nm of 3 dB bandwidth, as in the experiments in Section 3.4.5. Dispersive fibre is considered as first dispersive element. A dispersion coefficient of 17 ps/nm/km at 1550 nm is considered for remote SSMF.

Simultaneous multiband generation in different remote fibres in FTTH networks

The capability of the technique in Fig. 41 of generating impulse-radio UWB signals in different RF bands by remote fibres with different total dispersion from the same head-end unit has been investigated by simulation. The analysis is focused on the 24 GHz, 60 GHz, and 75−110 GHz bands. Multiband generation from the head-end unit configured as in the 60 GHz experiment in Section 3.4.5 is herein demonstrated. The optical band pass filter (OBPF) limiting the optical bandwidth in the experiment is modelled as a Gaussian filter with 0.8 nm of 3 dB bandwidth.

UWB bandwidth centred at $2 \cdot f_{LO} / M$ can be generated by 12.6 km of remote SSMF for 60 GHz, as shown in Fig. 42(b); and by 17 km of remote SSMF for 93.75 GHz, as shown in Fig. 42(c). Up-conversion to a centre frequency of 25 GHz can be performed by 5 km of remote IDF with a dispersion coefficient of −17 ps/nm/km at 1550 nm, as shown in Fig. 42(a). Other IDF lengths are supported provided IDF with a different dispersion coefficient is employed [169].

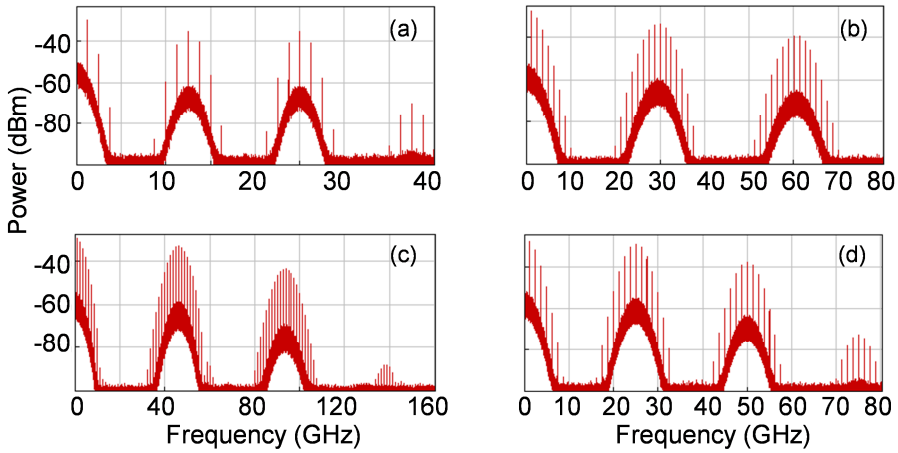

Fig. 42. Peak spectrum simulated at the output of the photodetector in Fig. 41 for 3 dB filtered bandwidth $\Delta\lambda = 0.8nm$, dispersion $D_{t1} = -425ps/nm$, $f_{LO} = 15GHz$, and (a) remote IDF with dispersion $D_{t2} = -85ps/nm$; (b) 12.6 km remote SSMF; (c) 17 km remote SSMF; (d) 10 km remote SSMF.

In addition, a centre frequency of f_{LO}/M can be generated by 10 km of remote SSMF for 25 GHz, as shown in Fig. 42(d); by 18.8 km of remote SSMF for 60 GHz; and by 21 km of remote SSMF for 93.75 GHz. The corresponding lengths of remote SSMF when time reversal is performed are 55 km and 40 km for 25 GHz, 37.4 km and 31.2 km for 60.625 GHz, and 33 km and 29 km for 93.75 GHz, respectively. This demonstrates that the technique can operate with remote SSMF with length exceeding typical FTTH distances. The number of central head-end units can be reduced by increasing the reach of the passive FTTH network. The goal is to reduce operating expenses. However, long fibre distances can induce RF power fading and also reduce splitting ratio thus reducing number of remote antenna units served by a head-end unit.

Different total dispersion of remote fibre can induce different UWB bandwidth and tolerance to variation in the total dispersion of remote fibre, as shown in Table X. The smallest UWB bandwidth limits the maximum data rate which can be provided by the head-end unit in different RF bands simultaneously. The higher the total dispersion of remote fibre, the UWB spectrum is more sensitive to the variation in the total link dispersion which can be induced by inaccuracy in the location of remote antenna units and by the thermal sensitivity of the dispersion coefficient of remote fibre. The higher the temperature variations, the lower the performance and therefore the number of users supported without employing adaptive dispersion compensation could be reduced. The maximum permissible performance degradation will determine the maximum in-home fibre distance to centralize remote fibre length compensation in residential gateways. For instance, for the configuration in Table X, performance does not vary significantly in the 60 GHz band for a variation in the remote SSMF length of 400 m. By considering the equivalent variation in the total dispersion of remote fibre, this could cover typical in-building connections to simple remote antenna units while tolerating reasonable temperature changes.

The operational limits of the proposed technique have been investigated by simulation. Table XI includes some examples of system parameters for impulse-radio UWB generation in the 24 GHz band, in the 60 GHz band as well as in the 75−110 GHz band. Note the influence of optical bandwidth on UWB bandwidth at $f_{LO} = 15GHz$ by comparing with Table X.

Table X. Multiband impulse-radio UWB generation at filtered bandwidth $\Delta\lambda = 0.8nm$, dispersion $D_{t1} = -425\,ps/nm$, and $f_{LO} = 15GHz$

Remote Total Dispersion D_{t2} (ps/nm)	Remote Fibre Length (km)	UWB 10 dB frequency range (GHz)
−30.6 – −45.9	1.8 − 2.7 [a]	26.25 − 28.75
−47.6 – −74.8	2.8 − 4.4 [a]	25 − 27.5
−76.5 – −102	4.5 − 6 [a]	23.75 − 26.25
166.6 – 173.4	9.8 − 10.2	22.5 − 27.5
175.1 – 180.2	10.3 − 10.6	22.5 − 28.75
181.9 – 183.6	10.7 − 10.8	23.75 − 28.75
213.35 – 215.9	12.55 − 12.7	57.5 − 63.75
216.75 – 218.45	12.75 − 12.85	57.5 − 65
219.3 – 220.15	12.9 − 12.95	58.75 − 65
265.2	15.6	75 − 83.75
272	16	78.75 − 87.5
280.5	16.5	82.5 − 93.75
289	17	87.5 − 98.75
297.5	17.5	93.75 − 106.25

[a] IDF with −17 ps/nm/km. The rest of fibre lengths correspond to SSMF.

Table XI. Multiband impulse-radio UWB generation at optical bandwidth $\Delta\lambda = 1.27nm$ and dispersion $D_{t1} = -425\,ps/nm$

f_{LO} (GHz)	Remote SSMF Length (km)	UWB 10 dB frequency range (GHz)
5	15, 35	23.75 – 26.25
5	20.8, 29.2	55 – 65, 25 – 33.75
5	23.65, 26.35	78.75 – 106.25
5	22.3, 27.7	83.75 – 101.25, 35 – 48.75
10	15, 35	23.75 – 26.25, 48.75 – 51.25
15	10, 40	23.75 – 26.25, 48.75 – 51.25
15	18.75, 31.25	57.5 – 63.75
15	12.5, 37.5	58.75 – 61.25, 28.75 – 31.25
15	21.25, 28.75	96.25 – 106.25
15	17.5, 32.5	97.5 – 102.5, 48.75 – 52.5

Gaussian-monocycle pulse shaping

RF impulse-radio UWB generation employing Gaussian-monocycle pulse shaping has been investigated. The Gaussian-monocycle shaping is performed at the remote antenna unit in Fig. 41 based on a differential photoreceiver whose outputs are combined after adjusting their relative time delay τ [Bel09a], as proposed in Section 3.2.3. This permits to adjust UWB bandwidth by changing the delay depending on the remote fibre dispersion. The Gaussian-monocycle shaping introduces nulls in the spectrum, as shown in Fig. 43, which are dependent on the relative time delay τ .

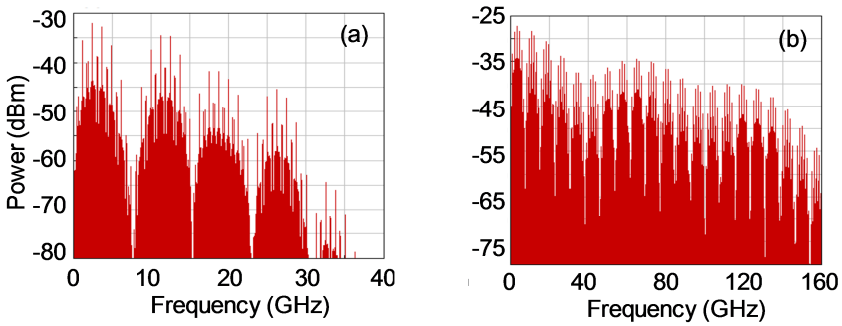

Fig. 43. Peak spectrum after Gaussian-monocycle shaping with $\tau = 130\,ps$ simulated for 3 dB filtered bandwidth $\Delta\lambda = 0.8nm$, $f_{LO} = 40GHz$, and (a) dispersion $D_{fi} = 34\,ps/nm$, 5 km remote SSMF; (b) dispersion $D_{fi} = -34\,ps/nm$, 0.67 km remote SSMF.

Table XII. Multiband impulse-radio UWB generation at optical bandwidth $\Delta\lambda = 1.27nm$, dispersion $D_{fi} = -34\,ps/nm$, and Gaussian-monocycle shaping with $\tau = 140\,ps$

f_{LO} (GHz)	Remote SSMF Length (km)	UWB 10 dB frequency range (GHz)
20	1.2, 2.8	22.5 – 26.25, 58.75 – 62.5, 80 – 85, 87.5 – 91.25, 93.75 – 98.75, 101.25 – 106.25
40	0.67, 3.3	58.75 – 62.5, 22.5 – 27.5, 80 – 83.75, 86.25 – 91.25, 93.75 – 98.75, 101.25 – 106.25
40	4.4	23.75 – 27.5, 58.75 – 63.75, 80 – 83.75

The Gaussian-monocycle pulse shaping enables the generation of multiple RF bands in the same remote fibre as the spectrum lobes can be filtered individually. For instance, the 24 GHz band, the 60 GHz band and the 75−110 GHz band, as shown in Fig. 43(b). The bandwidth of the spectrum lobes is dependent on the pulsewidth T_{OUT} in Fig. 41 and the monocycle delay τ. Furthermore, simulation results show that the spectrum of the RF Gaussian-monocycle signal is symmetric and centred at $2 \cdot f_{LO}/M$ (or f_{LO}/M) at certain equal-spaced values of the monocycle delay τ. These values are dependent on the LO frequency f_{LO} and the length of the remote SSMF performing the frequency shifting. Note that in Fig. 43, there is overlapping between the baseband and the frequency band at f_{LO}/M and between the frequency band at f_{LO}/M and $2 \cdot f_{LO}/M$.

Table XII includes examples of operational limits when Gaussian-monocycle shaping is performed, which are suitable for impulse-radio UWB generation in the 24 GHz band, in the 60 GHz band as well as in the 75−110 GHz band.

3.4.5 Experimental demonstration

The experimental setup for photonic impulse-radio UWB generation in the 24 GHz band and in the 60 GHz band is shown in Fig. 44. At the head-end unit, an actively mode-locked laser generates nearly transform-limited optical pulses with 2 ps of FWHM, 1.27 nm of 3 dB bandwidth, 9.9536 GHz repetition rate, and 1550 nm central wavelength. The pulses are OOK modulated with RZ data at 1.2442 Gb/s in a MZM biased at the minimum transmission point. The modulated pulses are chirped employing dispersive fibre and amplified by an EDFA. An OBPF is employed to remove noise.

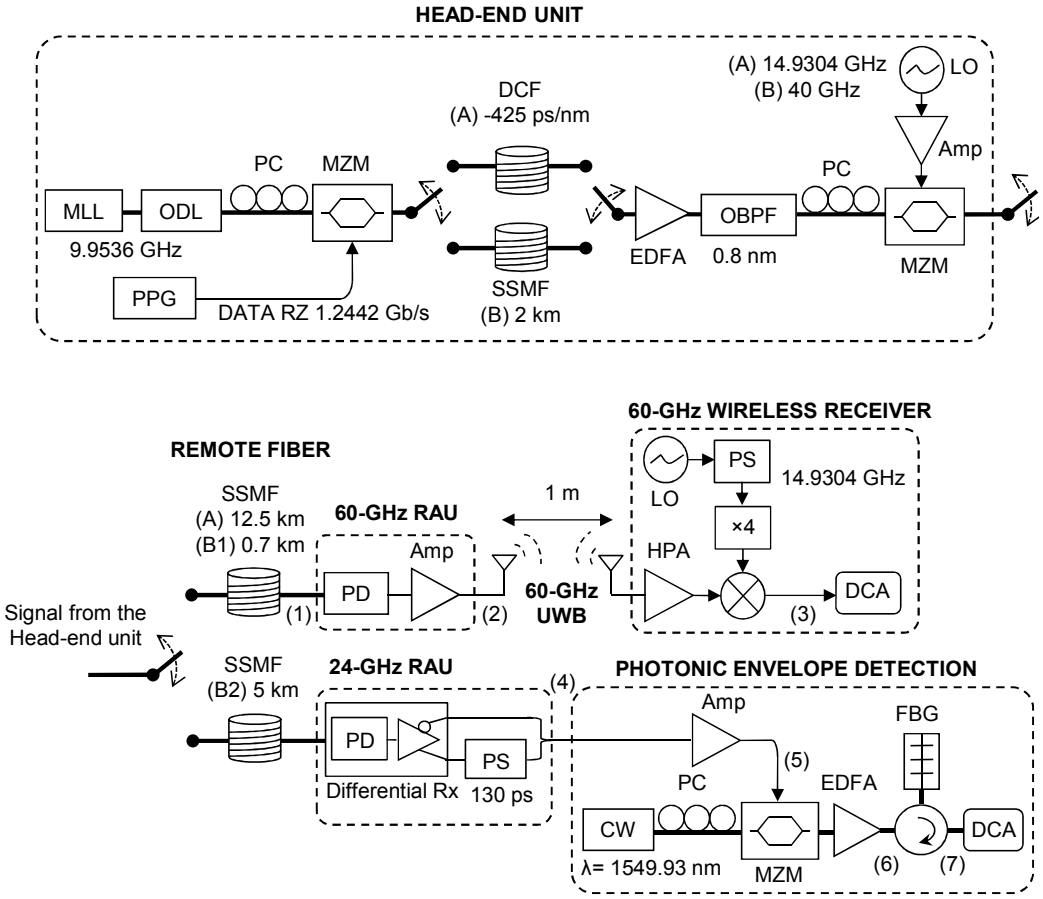

Fig. 44. Experimental setup for photonic dual impulse-radio UWB generation in the 24 GHz band and in the 60 GHz band with simultaneous multiband generation capabilities.

The bandwidth of the OBPF limits the optical 3 dB bandwidth to $\Delta\lambda = 0.8nm$. Subsequently, the chirped pulses are modulated with a LO signal in a MZM (V_π of 3.7 V, 3 dB bandwidth of 35 GHz, −0.7 chirp) to perform frequency up-conversion. The MZM is biased at the minimum transmission point to perform optical carrier suppression modulation. Further frequency up-shifting or down-shifting is performed employing the dispersion of remote-connectivity SSMF.

Generation in the 60 GHz band by frequency up-shifting

The generation of impulse-radio UWB signals in the 60 GHz band has been demonstrated in a proof-of-concept experiment [Bel10b] by employing the SSMF in a typical FTTH network, as depicted in Fig. 41. The corresponding configuration of the dispersive fibre and LO at the head-end unit and of the remote-connectivity fibre is marked as (A) in Fig. 44. Pseudo-random binary sequence data with a word length of 2^{15}–1 are generated by a pulse pattern generator (Agilent 81134A). DCF with dispersion $D_{t1} \simeq -425 ps/nm$ is employed as first dispersive element. The LO signal has a frequency of $f_{LO} = 14.9304GHz$. 12.5 km of SSMF ($D_{t2} \simeq 212.5 ps/nm$) provides FTTH connectivity while performs pulse time compression by a factor of $M \simeq 0.5$. Fig. 45(a) shows the time-compressed optical pulses measured at point (1) in Fig. 44, which exhibit ~140 ps of FWHM.

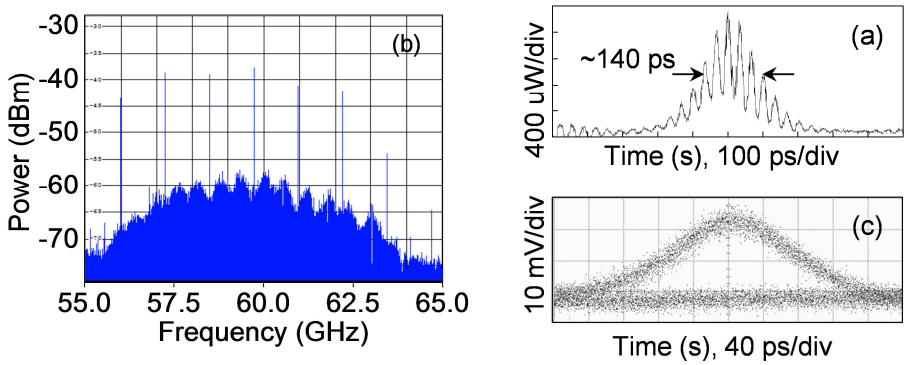

Fig. 45. Measurements for configuration (A) in Fig. 44. (a) Time-compressed signal at point (1) in Fig. 44. (b) Peak spectrum of the 60 GHz impulse-radio UWB signal at point (2) in Fig. 44 (video bandwidth: 10 MHz). (c) Eye diagram at point (3) in Fig. 44.

In order to verify the appropriate operation, the received impulse-radio UWB signal in the 60 GHz band is amplified by a high-power amplifier (28.7 dB gain) and down-converted by electrical mixing with a LO signal. The LO signal is generated by frequency quadrupling of the same LO signal employed at the head-end unit. A phase shifter is employed for assuring proper phase matching for accurate down conversion. The feasibility of the proposed generation technique is demonstrated combining fibre and radio transmission. Commercial rectangular horn antennas with a frequency range of 50−75 GHz, 20 dBi gain and 12° beamwidth are employed. Eye diagram and *Q*-factor are measured at point (3) in Fig. 44 by a digital communications analyser (Agilent DCA 86100C, 20 GHz electrical bandwidth). The eye diagram exhibits a *Q*-factor of ~11 without wireless transmission at −9.5 dBm received optical power. *Q*-factor decreases to ~9 after 70 cm of wireless transmission and to ~6.6 at 1 m. Fig. 45(c) shows the eye diagram for 1 m of wireless transmission. Hence, the generation technique is demonstrated to be error-free for 1 m of wireless distance at a maximum mean EIRP density of −29 dBm/MHz [Bel10b], which is well below 13 dBm/MHz [17]. Note that in this experiment the maximum mean EIRP density is more restrictive than the maximum mean EIRP level of 40 dBm [17] and the maximum peak EIRP level of 43 dBm [115].

Additionally, the 60 GHz experimental system in configuration (A) in Fig. 44 has been simulated to verify the model developed in Section 3.4.4. A LO frequency of $f_{LO} = 15GHz$ is set in simulation. The frequency response and noise characteristics of the photodetector, the electrical amplifiers and the mixer are included in simulation. The wireless channel is modelled as free-space path losses. The filtering of the digital communications analyser is modelled as a Gaussian filter with an electrical bandwidth of 20 GHz and an optical bandwidth of 30 GHz. Fig. 46(a) shows the time-compressed optical pulses simulated at point (1) in Fig. 44, which exhibit ~140 ps FWHM. Fig. 46(b) shows the electrical spectrum in the 60 GHz band simulated at point (2) in Fig. 44. The eye diagram demodulated employing a LO frequency of 60 GHz is shown in Fig. 46(c), simulated at point (3) in Fig. 44. The simulation results in Fig. 46 are in excellent agreement with the experimental measurements in Fig. 45.

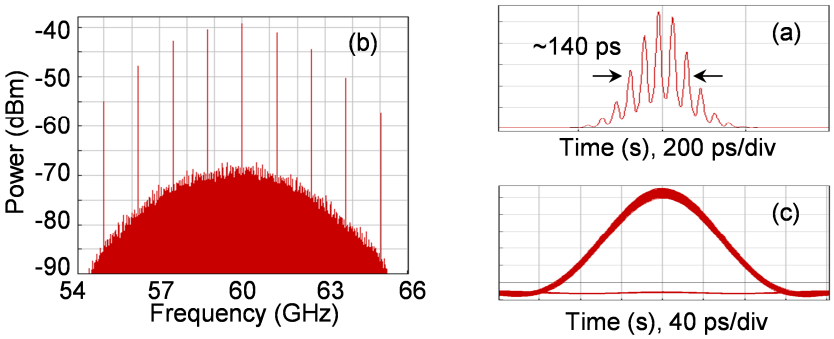

Fig. 46. Simulation results for configuration (A) in Fig. 44 to be compared with experimental measurements in Fig. 45. (a) Time-compressed signal at point (1) in Fig. 44. (b) Peak spectrum of the 60 GHz impulse-radio UWB signal at point (2) in Fig. 44. (c) Eye diagram at point (3) in Fig. 44.

Dual generation in the 24 and 60 GHz bands by frequency down-shifting

The simultaneous generation of impulse-radio UWB signals in the 24 GHz band and in the 60 GHz band has been demonstrated by frequency down-shifting in remote-connectivity SSMF. The corresponding configuration of the dispersive fibre and LO at the head-end unit is marked as (B) in Fig. 44 and the remote-connectivity fibre is marked as (B2) for the 24 GHz band and (B1) for the 60 GHz band. A fix RZ data pattern "1001000111101010" is employed. At the 24 GHz remote antenna unit, the optical pulses are photodetected by a differential photoreceiver (Teleoptix, balanced photoreceiver with limiting TIA) (3 dB bandwidth of 35 GHz) [181]. The outputs of the photoreceiver are combined after adjusting their relative time delay by an electrical delay line to generate a Gaussian-monocycle pulse shape [Bel09a], as proposed in Section 3.2.3. The photoreceiver is operated in unbalanced mode [Bel09c], which provides better performance than the balanced mode [Bel09b] in this UWB pulse shaping application. In previous proof-of-concept experiments reported in [Bel09c] and [Bel09b], optical generation of impulse-radio UWB was demonstrated in the 24 GHz band employing DSB-based up-conversion and without remote connectivity fibre.

The UWB monocycles generated in the 24 GHz band at point (4) in Fig. 44 are demodulated by photonic envelope detection without wireless transmission, as shown in Fig. 44. Photonic envelope detection is performed employing the technique proposed in [187]. Detection of 24 GHz impulse-radio UWB signals employing this technique was demonstrated in [Bel09c]. The received 24 GHz impulse-radio UWB signal is amplified, and modulated with a tunable optical carrier (0.01 nm wavelength accuracy) in a MZM (V_π of 3.7 V, 3 dB bandwidth of 35 GHz) biased at the minimum transmission point to perform half-wave rectification. A FBG filter selects one optical sideband corresponding to the envelope of the half-wave rectified optical signal. The envelope is measured by a digital communications analyser (Agilent DCA 86100C, 2.85 GHz optical bandwidth).

UWB generation in the 24 GHz band is demonstrated employing 2 km of SSMF as the first dispersive element ($D_{t1} \simeq 34\,ps/nm$), LO signal at $f_{LO} = 40GHz$, 5 km of SSMF ($D_{t2} \simeq 85\,ps/nm$) providing remote connectivity while performing pulse time stretching by a factor of $M \simeq 3.5$, and Gaussian-monocycle shaping with relative time delay $\tau = 130\,ps$. This configuration is marked as (B) and (B2) in Fig. 44.

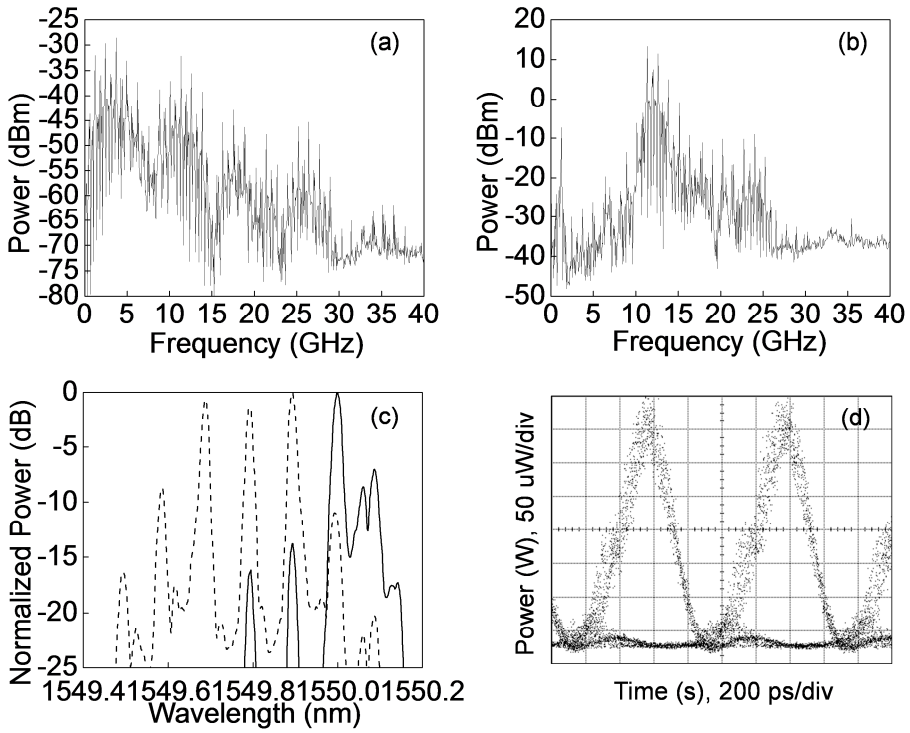

Fig. 47. Impulse-radio UWB generation in the 24 GHz band performing time stretching and Gaussian-monocycle shaping for configuration (B) and (B2) in Fig. 44. (a) Peak spectrum measured at point (4) in Fig. 44. (b) Peak spectrum measured at point (5) in Fig. 44. (c) Optical spectrum measured at point (6) (dashed line) and point (7) (solid line) in Fig. 44 (resolution bandwidth: 0.01 nm). (d) Eye diagram measured at point (7) in Fig. 44.

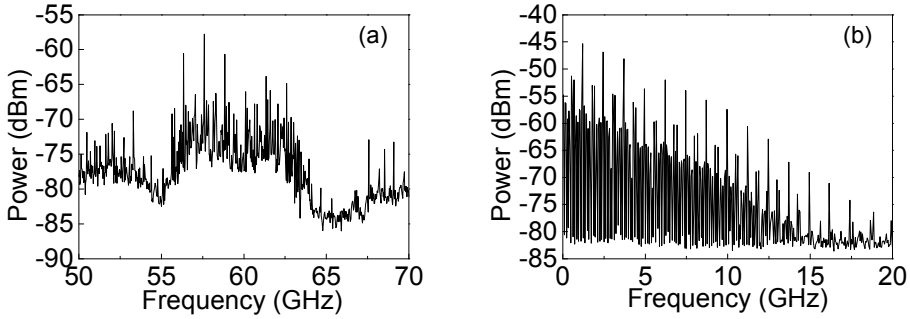

Fig. 48. Impulse-radio UWB generation in the 60 GHz band by time stretching for configuration (B) and (B1) in Fig. 44. (a) Peak spectrum measured at point (2) in Fig. 44. (b) Peak spectrum in baseband measured at the output of the 60 GHz photodetector in Fig. 44.

Fig. 47(a) shows the electrical spectrum measured at point (4) in Fig. 44, which would meet the current UWB in the 24 GHz band [2] provided adequate filtering is performed. In the experiment, the filtering is performed by the combined frequency response of the electrical amplifier and FBG at the photonic envelope detector. Fig. 47 also shows the electrical spectrum measured at point (5) in Fig. 44, the optical spectrum measured at point (6) and point (7) in Fig. 44, as well as the eye diagram measured at point (7) in Fig. 44. The eye diagram exhibits a *Q*-factor of ~11 demonstrating the feasibility of the generation technique when frequency down-shifting is employed.

Frequency down-shifting to the 60 GHz band of the Gaussian impulse-radio UWB signal is demonstrated from the same head-end unit for 0.7 km of SSMF ($D_{t2} \simeq 11.9 ps/nm$) providing remote connectivity while performing pulse time stretching by a factor of $M \simeq 1.35$. This configuration is marked as (B) and (B1) in Fig. 44. Fig. 48(a) shows the electrical spectrum measured at point (2) in Fig. 44 after high-power amplification and filtering (28.7 dB gain, 55−65 GHz). The baseband electrical spectrum is shown in Fig. 48(b), which would meet current regulation in the 3.1−10.6 GHz band provided adequate filtering is performed.

3.4.6 Practical considerations

The radio-over-fibre system providing UWB wireless connectivity remotely should be reliable, simple and cost-efficient. The use of a mode-locked laser, intensity modulators, and dispersive fibre at the head-end unit in Fig. 44, makes the system complex for real application. Mode-locked lasers can offer picosecond pulses, excellent pulse quality close to transform-limited operation, and low noise to support a high number of remote antenna units with relative low cost [52], [188]. The cost of the mode-locked laser could be reduced employing semiconductor mode-locked lasers compatible with chip integration [189] and new mode-locked fibre lasers [190]. In addition, data modulation and up-conversion could be performed by a single integrated dual-cascaded MZM device thus reducing cost and size, for instance using silicon photonics technology [191]. Compared with dispersive fibre as first dispersive element, a linearly chirped FBG made with polarization-maintaining fibre can provide compactness and the required polarization stability permitting the use of a polarization-sensitive MZM for up-conversion [51], [192].

In Section 3.4, RF impulse-radio UWB generation has been demonstrated employing OOK modulation. Nevertheless, the technique could be employed with other modulation formats, such as bi-phase modulation [Bel10c]. Envelope detection can be employed for OOK signals to avoid the need for a phase-locked LO. Photonic envelope detection provides transparency to the RF frequency and devices realized using photonic integration are available [148]. Compared with the technique employed in Section 3.4, photonic envelope detection based on full or half-wave rectification and low-speed photodetection [3], [22] would be simpler for application in the system herein proposed however it would be less tolerant to dispersion for uplink optical distribution of RF signals to a central unit. Alternatively, RF power detectors could provide simple and low power consumption detection [59].

3.5 Conclusion

Two photonic techniques for impulse-radio UWB generation in the 3.1–10.6 GHz band have been proposed and experimentally demonstrated. The techniques perform Gaussian monocycle shaping which can flexibly compensate the effect of optical access fibre. Nevertheless, the generation of Gaussian monocycles suitable for being radiated in the 3.1−10.6 GHz band without up-conversion and the dynamic range of fibre dispersion compensation is to be further investigated. The generation of Gaussian monocycles adequate to be further up-converted to the 60 GHz band has been experimentally demonstrated.

Furthermore, the proposed Gaussian monocycle shaping has been demonstrated to enable simultaneous multiband generation in the same fibre in an also proposed photonic impulse-radio UWB generation system based on frequency shifting in remote-connectivity fibre.

An impulse-radio UWB radio-over-fibre system at 57 GHz has been demonstrated at 1.25 Gb/s in a proof-of-concept experiment. The system is suitable for in-flight multi-Gb/s communications and radar. Transmission over SSMF at 100 m in-cabin distance has also been successfully demonstrated. The proposed system can compete in cost and also has advantages in terms of transparency and high bandwidth compared with a conventional solution based on digital baseband data over fibre and further electrical UWB modulation and frequency up-conversion at distributed remote antenna units. Nevertheless, significant progress has recently been made for 60 GHz CMOS technology, that may lead to different conclusion. The system is suitable for the provision of UWB signals in the 3.1–10.6 GHz and 60 GHz bands simultaneously employing low-frequency electrooptic devices. The system operation has been verified by simulation and the impact of the system parameters including optical noise on performance has been evaluated, demonstrating that the system can serve the high number of remote antenna units at WPAN distances required for the proposed in-flight application. Performance is limited by thermal noise for a higher number of remote antenna units. Simulation results show that using an optical amplifier to compensate for splitting and distribution losses can help to improve performance.

Flexible photonic generation of RF impulse-radio UWB signals based on frequency shifting in optical access fibre has been proposed. Fibre dispersion can effectively reduce broadband up-conversion cost. The technique can cover numerous applications simultaneously in different RF bands providing good cost and performance trade-off. The feasibility of the technique in FTTH networks delivering 1.25 Gb/s services has been experimentally demonstrated when operating in the 60 GHz band. Practical multiband capabilities and the limitations of this system have been addressed by simulation. Simulation analysis also indicates that Gaussian-monocycle shaping enables simultaneous multiband generation in the same fibre and can greatly increase flexibility when implemented remotely. Dual 24 GHz/60 GHz operation has been experimentally demonstrated when 24 GHz Gaussian-monocycle shaping is performed. The approach could operate in high RF bands such as 75−110 GHz as indicated by the simulation analysis. Some of the required components could be compatible with photonic integration to simplify the architecture.

4

Generation and optical-wireless transmission of UWB signals in the 60 GHz band

This Ph.D. thesis proposes the operation of UWB in the 60 GHz band and evaluates the combined optical and wireless transmission performance when relative low cost VCSELs are employed with two functionalities:

1) Electrooptic conversion with further up-conversion in a MZM for FTTH networks, as demonstrated in Section 4.1.
2) Optical frequency up-conversion with application both in FTTH networks and indoor DAS, as demonstrated in Section 4.2. The same VCSEL employed for up-conversion could be directly modulated by a signal if desired, but this dual functionality is out of the scope of this study.

4.1 DCM OFDM and BPSK impulse radio employing VCSEL direct modulation

The performance of radio-over-fibre optical transmission employing VCSELs, and further wireless transmission, of the two major UWB implementations is reported when operating in the 60 GHz radio band [Bel10c], [Bel11a], [Llo11a], [Llo11b], [FIVER D2.6]. Performance is evaluated at 1.44 Gb/s data rate. The two UWB implementations considered employ DCM OFDM and BPSK impulse radio modulation respectively. Optical transmission distances up to 40 km in SSMF and up to 500 m in BI-SMF with wireless transmission up to 5 m in both cases is demonstrated with no penalty. A simulation analysis has been also performed in order to investigate the operational limits. The analysis results are in excellent agreement with the experimental work and indicate good tolerance to chromatic dispersion due to the chirp characteristics of electrooptic conversion when a directly-modulated VCSEL is employed.

The performance comparison indicates that BPSK impulse-radio UWB exhibits better tolerance to optical transmission impairments requiring lower received optical power than its DCM-OFDM UWB counterpart when operating in the 60 GHz band.

4.1.1 Introduction

UWB operation in the 60 GHz band permits to overcome coexistence issues limiting UWB operation in the 3.1−10.6 GHz band. Regarding the application scenario, UWB in the 60 GHz band has been indicated as a viable approach to provide multi-Gb/s WPAN connectivity in scenarios where interference is a critical issue like aircrafts [Bel09a], [Bel10a], as discussed in Section 3.3. In addition, UWB-over-fibre has been indicated as an interesting solution for FTTH access networks delivering HD audio/video [Llo08a], [Llo08c]. This application is discussed in Section 2.5.4. This Ph.D. thesis proposes the operation of UWB in the 60 GHz band and evaluates the performance in FTTH networks for the first time to our knowledge.

The UWB-over-FTTH approach is transparent to the UWB modulation employed. Two major UWB technologies are currently used: impulse-radio UWB and multi-band OFDM as specified in the ECMA-368 standard [9]. OFDM provides high spectral efficiency and efficient software to facilitate coexistence. Furthermore, there is large market availability of low-cost OFDM-UWB-based solutions. On the other hand, impulse-radio UWB is not constrained in terms of bandwidth and data rate and it is capable of providing simultaneous communications and high-resolution radar. The 60 GHz band facilitates coexistence to impulse-radio UWB technology and allows it to provide multi-Gb/s capacity in spite of its relative low spectral efficiency.

The study herein presented compares the experimental performance after radio-over-fibre and further wireless transmission in the 60 GHz radio band of two major UWB implementations at 1.44 Gb/s: Standard OFDM based on DCM and impulse radio based on BPSK modulation. This study targets to give light on the best implementation for future UWB systems in the 60 GHz band. Different fibre types are evaluated including SSMF and BI-SMF. Direct modulation of a low-cost free-running uncooled VCSEL is employed for electrooptic conversion of the UWB signals. Optical frequency up-conversion is performed at the head-end unit based on optical carrier suppression modulation in a MZM [76], [145]. Simulation analysis is performed to verify the experimental measurements. The system proposed could operate in a dual 3.1–10.6 GHz/60 GHz configuration if desired, but dual operation is out of the scope of this analysis. 60 GHz band operation would re-use and extend UWB technology in terms of range and flexibility, and is the focus of this work.

4.1.2 Experimental setup

The experimental setup of the UWB radio-over-fibre system in the 60 GHz band employing a directly-modulated VCSEL is shown in Fig. 49.

At the head-end unit, a 1550 nm 10 Gb/s VCSEL (VERTILAS, 1550-10G-P2-P4-Diff-Flex) is directly modulated by the UWB signal [193]. Frequency up-conversion to the 60 GHz band is performed by driving a MZM (V_π of 3.7 V, 3 dB bandwidth of 35 GHz, chirp of –0.7) by a LO signal after frequency doubling. The MZM is biased at the minimum transmission point to perform optical carrier suppression. The peak-to-peak amplitude of the signal driving the MZM is 3.5 V. Subsequently, the optical signal is distributed over optical fibre to the remote antenna units where the UWB signal is up-converted to the 60 GHz band after photodetection (u^2t Photonics, XPDV3120R).

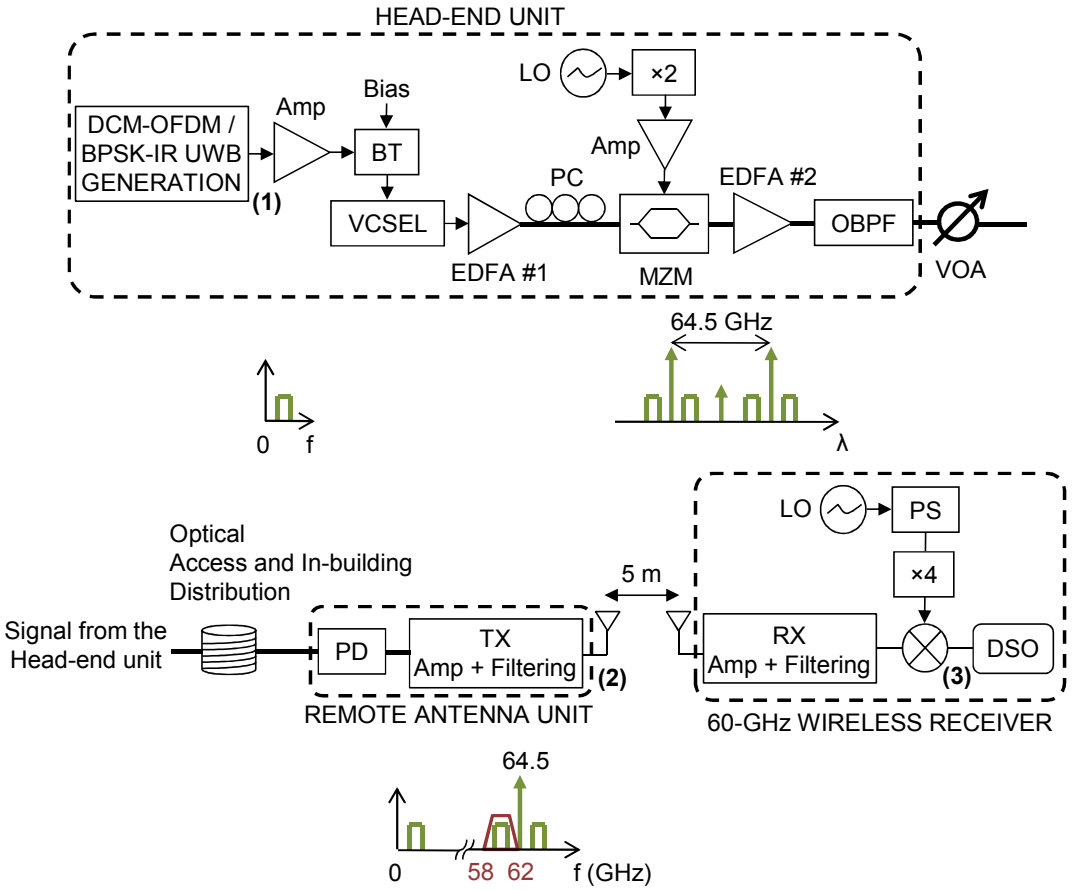

Fig. 49. Experimental setup and principle of operation of a UWB radio-over-fibre system in the 60 GHz band employing direct modulation of a VCSEL.

FTTH distribution over 25 km and 40 km of SSMF and integrated FTTH and in-building distribution over 25 km of SSMF extended by 500 m of BI-SMF is considered. Optical transmission performance of BI-SMF is evaluated employing a spool of commercially-available BI-SMF (OFS EZ-bend) without bending the fibre. The UWB signal in the 60 GHz band is amplified and filtered before being applied to an antenna for 5 m of wireless transmission. The antennas are rectangular horn antennas with a frequency range of 50–75 GHz, 20 dBi gain and a 3 dB beamwidth of 12°. The optical amplifier EDFA #1 in Fig. 49 (average output power of 15 dBm) is used to compensate for the insertion loss of the MZM. The second EDFA, EDFA #2 in Fig. 49, sets a maximum average power at the photodetector input (henceforth referred to as received optical power) of 10 dBm. A variable optical attenuator decreases this power level to analyse the performance as a function of the received optical power. An optical band-pass filter (3 dB bandwidth of 0.8 nm) is used to suppress ASE noise.

At the receiver, the received UWB signal in the 60 GHz band is amplified and filtered, and down-converted by electrical mixing (RF bandwidth of 55–65 GHz, IF bandwidth of DC–10 GHz, conversion loss of 4.6 dB). The same LO signal used to drive the MZM at the transmitter is employed for frequency down-conversion after frequency quadrupling (output frequency of 58.6–62.2 GHz). A phase shifter is employed for assuring proper phase matching for accurate down-conversion. The down-converted signal is captured by a real-time DSO (13 GHz bandwidth, 40 GS/s sampling rate) and analysed by DSP.

VCSEL driving, i.e. bias current and UWB peak-to-peak voltage, LO frequency, and amplification and filtering stages in the 60 GHz band (TX and RX Amp+Filtering in Fig. 49) are configured differently for DCM-OFDM UWB and BPSK impulse-radio UWB. The different configurations employed give the best performance in the optical back-to-back configuration at the maximum received optical power of 10 dBm.

4.1.3 DCM-OFDM UWB performance

The DCM-OFDM UWB signal at point (1) in Fig. 49, shown in Fig. 50, is generated by combining the outputs of three standard UWB transmitter modules (Wisair, WSR601). The modules support the UWB Band Group #1 [9]. The time-frequency codes TFC5, TFC6 and TFC7 are selected for each module respectively. In this way, each module transmit in the Band #1 (3.168–3.696 GHz, 3.432 GHz central frequency), Band #2 (3.696–4.224 GHz, 3.96 GHz central frequency), and Band #3 (4.224–4.752 GHz, 4.488 GHz central frequency) of the UWB Band Group #1, respectively. The time-frequency codes employed perform fixed frequency interleaving (FFI), i.e. the information is transmitted in each band all the time. The FFI configuration maximizes bitrate compared with the time frequency interleaving (or frequency hopping) configuration which minimizes interference. The maximum bitrate of 480 Mb/s is configured for each band, which is achieved employing DCM data modulation, providing an aggregated bitrate of 1.44 Gb/s and a spectral efficiency of 0.91 b/s/Hz.

The bias current and UWB peak-to-peak voltage applied to the VCSEL are set to 750 mVpp and 9.8 mA, respectively. The LO frequency is set to 16.125 GHz so that the DCM-OFDM UWB signal is up-converted to 64.5 GHz. The configuration of the RF amplification and filtering block at the remote antenna units is a band-pass filter (58.125–61.875 GHz) and two low-noise amplifiers with 18.7 dB and 16.2 dB gain, respectively. The configuration at the receiver is a high-power amplifier with 28.7 dB gain and a band-pass filter (57.5–62.5 GHz).

The performance of the demodulated DCM-OFDM UWB signal at point (3) in Fig. 49 is evaluated by the EVM parameter. The EVM is measured on the constellation diagram for each frequency band, Band #1, Band #2 and Band #3 in Fig. 50, employing commercially-available software (Agilent, 89600-Series Vector Signal Analyser). The EVM is evaluated over 72 OFDM symbols (10,800 bits) in all configurations. The EVM of the DCM-OFDM UWB signal in the 60 GHz band combining optical and 5 m wireless transmission is shown in Fig. 51 as a function of the received optical power. Six optical transmission cases are shown: 500 m BI-SMF, 25 km SSMF, 40 km SSMF, 25 km SSMF compensated by 25 km of IDF, 40 km SSMF readjusting the VCSEL bias current from 9.8 mA to 13.85 mA, and 40 km SSMF compensated by DCF equivalent to compensation of 40 km SSMF. The EVM in Fig. 51 is limited by electrical noise at low received optical power. Decreasing the received optical power further increases the EVM due to the reduction in SNR. In addition, the EVM improves at low received optical power with respect to the optical back-to-back configuration after optical transmission over 25 km of SSMF, as shown in Fig. 51(a), (c) and (e), and 40 km of SSMF, as shown in Fig. 51(b), (d) and (f). This is ascribed to gain in the fibre transfer function induced by the interaction of the chirp of the directly-modulated VCSEL with fibre chromatic dispersion [194], as verified in Section 4.1.5. The gain is dependent on the fibre length.

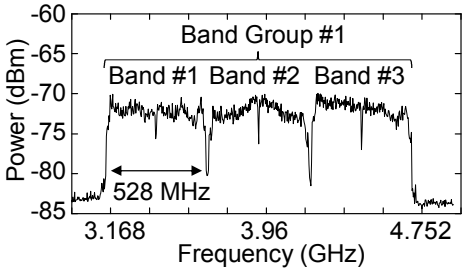

Fig. 50. RMS average spectrum of the generated DCM-OFDM UWB signal at point (1) in Fig. 49 (resolution bandwidth: 1 MHz).

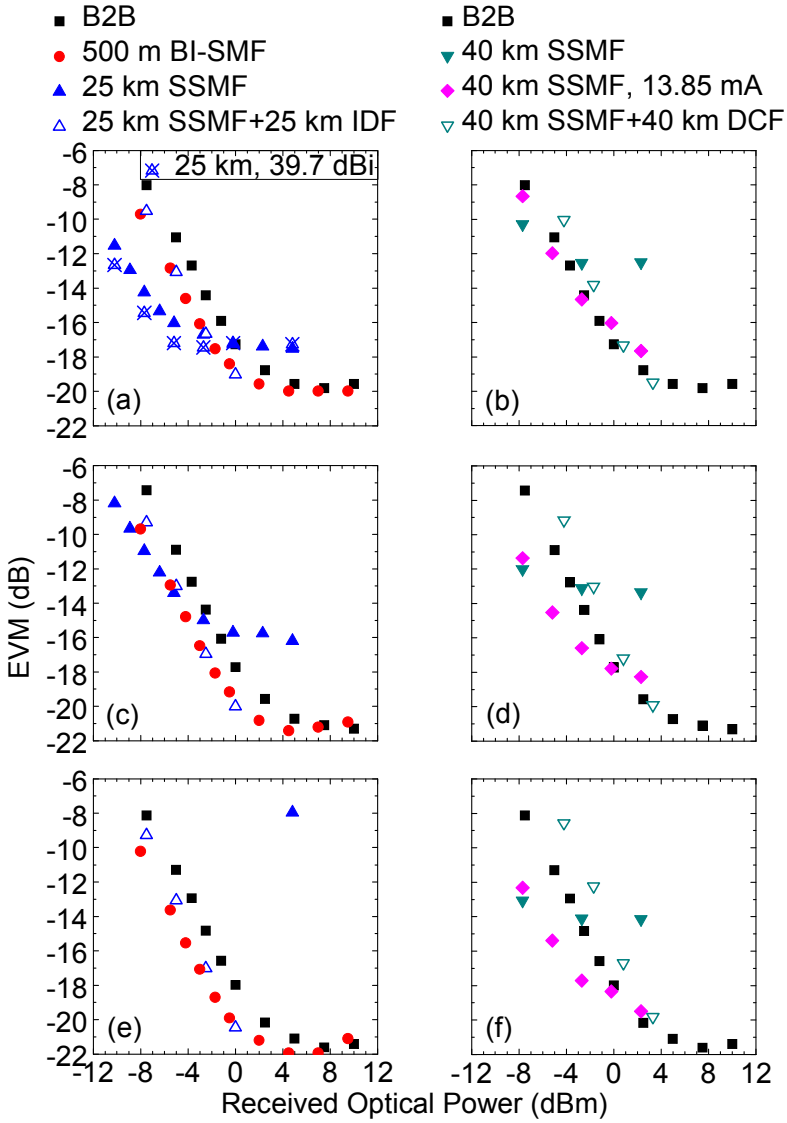

Fig. 51. Performance measured at point (3) in Fig. 49 of the DCM-OFDM UWB radio-over-fibre system in the 60 GHz band combining optical and 5 m wireless transmission. (a), (b) UWB Band #1 in Fig. 50. (c), (d) UWB Band #2 in Fig. 50. (e), (f) UWB Band #3 in Fig. 50.

The increase of power level after 25 km and 40 km SSMF transmission with respect to back-to-back as well as its dependence on fibre length can be verified in Fig. 52(a), (c) and (d).

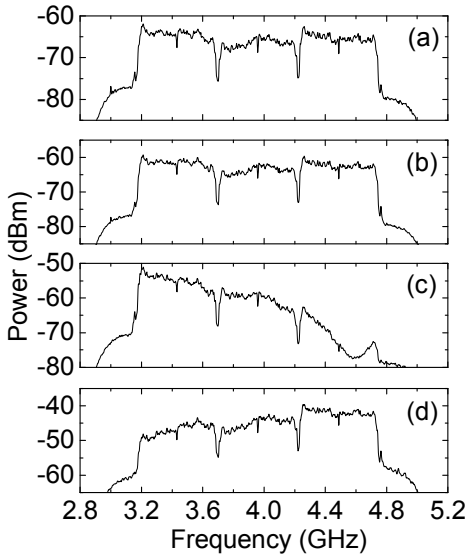

Fig. 52. RMS average spectrum of the demodulated DCM-OFDM UWB signal at point (3) in Fig. 49 combining optical and 5 m wireless transmission (resolution bandwidth: 5 MHz). (a) B2B at −2.5 dBm received optical power. (b) 500 m BI-SMF at −3 dBm. (c) 25 km SSMF at −2.7 dBm. (d) 40 km SSMF at 2.3 dBm.

The minimum EVM obtained at high received optical power is degraded after 25 km and 40 km SSMF transmission with respect to the optical back-to-back configuration. This is due to signal distortion by the fibre transfer function induced by chromatic dispersion and further modified by VCSEL chirp [194]. Signal distortion and its dependence on frequency and fibre length can be observed in Fig. 52(c), (d).

Signal distortion prevents recovering the complete DCM-OFDM UWB signal in the 60 GHz band after 25 km of SSMF, as shown in Fig. 51(e), and also after 25 km of SSMF extended by 500 m of BI-SMF, not shown in Fig. 51 for simplicity. Successful recovery of the complete DCM-OFDM UWB signal in the 60 GHz band is achieved employing dispersion management by matched IDF, as shown in Fig. 51(a), (c) and (e). The 25 km SSMF link is compensated by 25 km of IDF. Compared with DCF, IDF is more suitable for being used as transmission fibre, thus extending the FTTH network reach [169]. Similar EVM performance is obtained in the three DCM-OFDM UWB bands. The EVM improves by approximately 2 dB depending on the received optical power with respect to the optical back-to-back configuration. Equivalently, the optical receiver sensitivity improves by 1.5 dB depending on the EVM threshold. The optical receiver sensitivity at EVM below −17 dB [9] is −2.1 dBm. The EVM improvement with respect to the optical back-to-back configuration is ascribed to gain in the fibre transfer function induced by the interaction of the VCSEL chirp with a residual fibre chromatic dispersion, as a similar EVM improvement is obtained after transmission over 500 m of BI-SMF, as also shown in Fig. 51(a), (c) and (e). The power level increases after 500 m BI-SMF transmission with respect to the optical back-to-back configuration, as can be verified in Fig. 52(a) and (b). The DCM-OFDM UWB signal in the 60 GHz band is successfully distributed over 500 m of BI-SMF, which is sufficient for most in-building networks, with an optical receiver sensitivity of −2.1 dBm at EVM< –17 dB. The signal is not distorted as the minimum EVM obtained at high received

optical power is not degraded with respect to the optical back-to-back configuration. This can also be verified in Fig. 52(a) and (b).

The three DCM-OFDM UWB bands are recovered after 40 km SSMF transmission, as shown in Fig. 51(b), (d) and (f), however with not clear constellation. The EVM after 40 km SSMF transmission at high received optical power can be improved by readjusting the VCSEL driving with respect to the optical back-to-back configuration. The EVM is improved due to the readjustment of the VCSEL chirp, without employing dispersion compensation or management of the VCSEL chirp [195]−[197]. This is shown in Fig. 51(b), (d) and (f) for readjustment of the bias current applied to the VCSEL from 9.8 mA to 13.85 mA. Considering an EVM threshold of −17 dB, the optical receiver sensitivity for successful recovering of the three DCM-OFDM UWB bands is 1 dBm, limited by the signal distortion in the UWB Band #1. This corresponds to a power penalty of 1.3 dB with respect to the optical back-to-back configuration.

The expected performance employing dispersion compensation by DCF is also investigated. The 40 km SSMF link is compensated by 6.5 km of DCF which has dispersion equivalent to compensation of 40 km SSMF. The EVM in the three DCM-OFDM UWB bands improves at high received optical power and is degraded at low received optical power with respect to the uncompensated 40 km link, as shown in Fig. 51(b), (d) and (f). The optical receiver sensitivity at EVM< –17 dB is 1 dBm limited by the UWB Band #3, corresponding to a power penalty of 1.6 dB with respect to the optical back-to-back configuration. It should be noted that the successful transmission after dispersion compensation by IDF or DCF with EVM< −17 dB is achieved increasing the amplification EDFA #2 in Fig. 49 by 5 dB to compensate for the increased loss of the combined fibre link.

The impact of the gain of the receiving antenna on performance is also studied. Fig. 51(a) shows the EVM of the DCM-OFDM UWB Band #1 after 25 km SSMF transmission when a Cassegrain antenna with 39.7 dBi gain is employed at receiver instead of the 20 dBi antenna. The optical receiver sensitivity improves by 1.3 dB at low received optical power whereas the minimum EVM is maintained at high received optical power.

Fig. 53 shows examples of DCM-OFDM UWB spectra in the 60 GHz band measured at point (2) in Fig. 49. The power level decreases by approximately 2 dB every time the received optical power decreases by 1 dB. The signal spectrum meets current regulation in the 60 GHz band [115] in all configurations. However, spectra of noise and distortion are observed due to imperfect filtering. These spectra could cause interference to other radio signals in the current 60 GHz band (57−66 GHz) or to future frequencies outside 57−66 GHz, particularly around 52 GHz. The undesired spectra could be reduced by adequate filtering in practice or by system design. Nevertheless, undesired spectra do not impact on the measured performance as this is evaluated only over the bandwidth of each DCM-OFDM UWB band.

Fig. 54 shows examples of DCM constellation diagrams at point (3) in Fig. 49. Signal degradation translates into more disperse constellation points thus degrading the EVM. The constellation diagrams in Fig. 54 confirm the good performance with EVM< –17 dB of the radio-over-fibre system for generation with combined fibre and wireless transmission of high-quality DCM-OFDM UWB signals in the 60 GHz band.

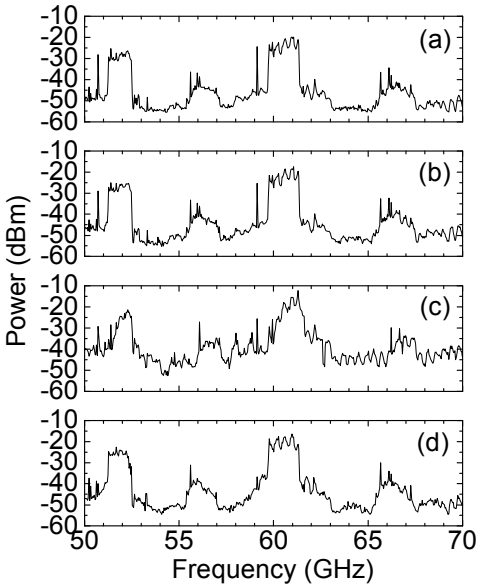

Fig. 53. Peak spectrum of the DCM-OFDM UWB signal in the 60 GHz band at point (2) in Fig. 49 (video bandwidth: 10 MHz). RF carrier frequency: 64.5 GHz. (a) B2B at 5 dBm received optical power. (b) 500 m BI-SMF at 4.5 dBm. (c) 25 km SSMF at 4.8 dBm. (d) 40 km SSMF at 2.3 dBm.

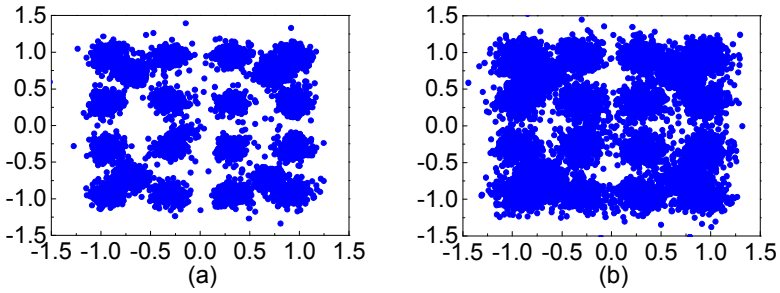

Fig. 54. Constellation diagrams of the demodulated DCM-OFDM UWB Band #1 at point (3) in Fig. 49 combining fibre and 5 m wireless transmission. (a) B2B, EVM= −19.5 dB at 5 dBm received optical power. (b) 500 m BI-SMF, EVM= −16.1 dB at −3 dBm.

4.1.4 BPSK impulse-radio UWB performance

The BPSK impulse-radio UWB signal at point (1) in Fig. 49 is generated by an arbitrary waveform generator (Tektronix AWG, 7122B) at 23.04 GS/s. A pseudo random bit sequence of 2^{11}–1 word length at 1.44 Gb/s is employed. The BPSK impulse-radio UWB pulse is a fifth-order derivative Gaussian shape with a standard deviation of 0.068 ns so as to be in good compliance with the UWB emission mask [1] with the highest spectral efficiency of 0.28 b/s/Hz [27]. In this way, the system could operate in dual band 3.1–10.6 GHz/60 GHz as the baseband signal, which is also available after photodetection, could be radiated meeting the current UWB regulation [Jen10]. The BPSK impulse-radio UWB signal, shown in Fig. 55, comprises a single band (3.26–8.45 GHz at 10 dB, 5.58 GHz peak frequency). BPSK data modulation is employed in order to avoid spectral peaks at multiples of the data rate, which limit UWB reach [Jen10], as verified in Fig. 55(b).

The bias current and UWB peak-to-peak voltage applied to the VCSEL are set to 820 mVpp and 13 mA, respectively. The LO frequency is set to 16.165 GHz so that the BPSK impulse-radio UWB signal is up-converted to 64.66 GHz.

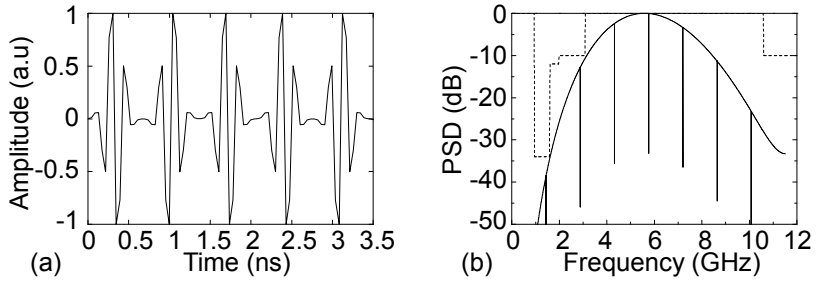

Fig. 55. Programmed BPSK impulse-radio UWB signal applied to the AWG. (a) Part of the signal in the time domain corresponding to the bit sequence "10110". (b) Normalized power spectral density of the signal (solid line) and UWB EIRP spectral density indoor mask [1] (dashed line).

The configuration of the RF amplification and filtering block at the remote antenna units is a low-noise amplifier with 18.7 dB gain, a band-pass filter (58.125–61.875 GHz) and a high-power amplifier with 28.7 dB gain. The configuration at the receiver is a high-power amplifier with 28.7 dB gain, a low-noise amplifier with 16.2 dB gain and a band-pass filter (57.5–62.5 GHz).

The performance of the demodulated BPSK impulse-radio UWB signal at point (3) in Fig. 49 is evaluated by the BER parameter. BER is measured on the eye diagrams employing off-line custom DSP. The DSP software consists of re-sampling by a factor of 1.008, low-pass filtering at a cut-off frequency optimum for each configuration (5.1 GHz for back-to-back, 6.5 GHz for 25 km SSMF and 25 km SSMF extended by 500 m BI-SMF, and 5 GHz for 40 km SSMF), matched filtering with the original UWB pulse shape, bit synchronization and calculation of the optimum decision threshold. The BER is calculated by bit-by-bit comparison with the original pseudorandom bit sequence over 120,000 bits in all configurations. BER performance of the BPSK impulse-radio UWB signal in the 60 GHz band combining optical and 5 m wireless transmission is shown in Fig. 56 as a function of the received optical power. Three optical transmission cases are considered: 25 km SSMF, 25 km SSMF extended by 500 m BI-SMF, and 40 km SSMF. Successful recovery of the BPSK impulse-radio UWB signal with BER below the FEC limit of $2.2 \cdot 10^{-3}$ is achieved in all fibre configurations. After considering the 7% FEC overhead, the effective data rate is 1.34 Gb/s. Very low optical receiver sensitivities of −12.5 dBm and −15.6 dBm after 25 km and 40 km of SSMF, respectively, and −14.3 dBm after 25 km of SSMF extended by 500 m of BI-SMF are obtained. This corresponds to an improvement of 0.1 dB, 3.2 dB and 1.9 dB, respectively, compared with optical back-to-back. The BER is limited by electrical noise in Fig. 56. Decreasing the received optical power further increases the BER due to reduction in SNR. In addition, the improvement in optical receiver sensitivity after fibre transmission is ascribed to gain in the fibre transfer function induced by the interaction of the chirp of the directly-modulated VCSEL with the fibre chromatic dispersion [194], as verified in Section 4.1.5.

Note that the same VCSEL driving adjusted initially in the optical back-to-back configuration has been employed in all fibre configurations. Nevertheless, optimization of the VCSEL driving in a given fibre configuration could lead to different performance, as has been shown in Section 4.1.3 for DCM-OFDM UWB.

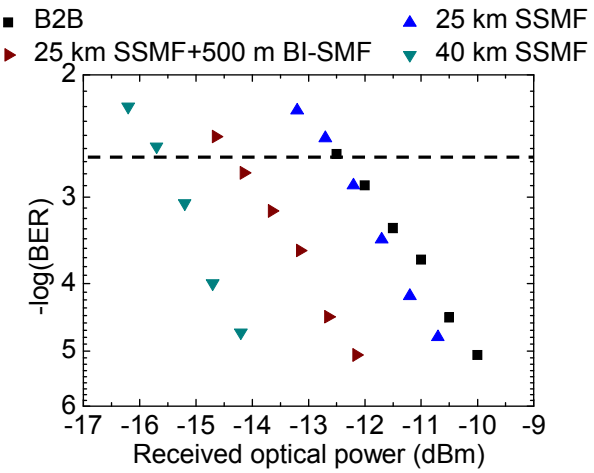

Fig. 56. Performance measured at point (3) in Fig. 49 of the BPSK impulse-radio UWB radio-over-fibre system in the 60 GHz band combining optical and 5 m wireless transmission. The FEC limit of $2.2 \cdot 10^{-3}$ is shown via a dashed line.

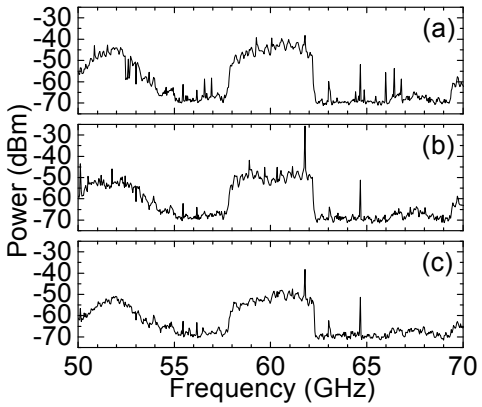

Fig. 57. Peak spectrum of the BPSK impulse-radio UWB signal in the 60 GHz band at point (2) in Fig. 49 (video bandwidth: 10 MHz). RF carrier frequency: 64.66 GHz. (a) B2B at −9.8 dBm received optical power. (b) 25 km SSMF at −15 dBm. (c) 40 km SSMF at −17.5 dBm.

Fig. 57 shows examples of BPSK impulse-radio UWB spectra in the 60 GHz band at point (2) in Fig. 49. Residual spectral lines at frequencies multiple of the bitrate are caused by asymmetry of the BPSK pulses. This is due to the nonlinear transfer function of the VCSEL and distortion from fibre dispersion. The power level decreases by approximately 2 dB every time the received optical power decreases by 1 dB. The increase of power level after fibre transmission with respect to the optical back-to-back configuration as well as its dependence on fibre length can be verified in Fig. 57(a) and (c). The signal spectrum meets current regulation in the 60 GHz band [115] in all configurations. However, residual RF carrier at 64.66 GHz and noise spectrum around 52 GHz are observed due to imperfect filtering. These spectra could cause interference to other radio signals in the current 60 GHz band (57−66 GHz) or to future frequencies around 52 GHz. The undesired spectra could be reduced by adequate filtering in practice or by system design. The undesired spectra do not impact on performance because frequency down-conversion is done with the same RF carrier, and DSP low-pass filtering is done at the receiver.

BPSK eye diagrams at point (3) in Fig. 49 are shown in Fig. 58. The open eye diagrams in Fig. 58, especially after 40 km of SSMF, confirm the excellent performance shown in Fig. 56.

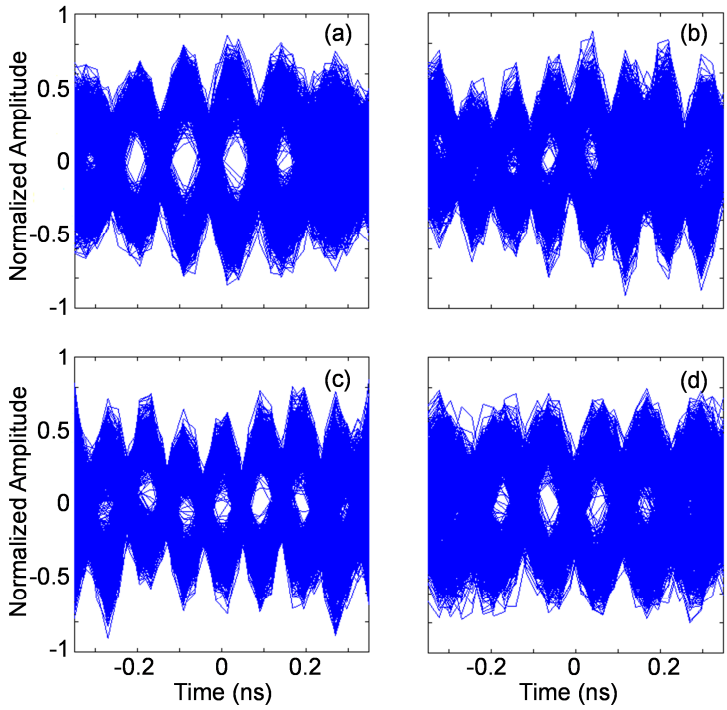

Fig. 58. Eye diagrams of the demodulated BPSK impulse-radio UWB signal at point (3) in Fig. 49 combining optical and 5 m wireless transmission. (a) B2B, BER= $8.57 \cdot 10^{-6}$ at −10 dBm received optical power. (b) 25 km SSMF, BER= $3.4 \cdot 10^{-3}$ at −12.7 dBm. (c) 25 km SSMF extended by 500 m BI-SMF, BER= $3.43 \cdot 10^{-5}$ at −12.7 dBm. (d) 40 km SSMF, BER= $1.01 \cdot 10^{-4}$ at −14.7 dBm.

Signal degradation closes the eye diagram resulting in increased BER. At −12.7 dBm received optical power, the gain in the fibre transfer function after transmission over 25 km SSMF+500 m BI-SMF enables recovering the BPSK impulse-radio UWB signal at BER< $2.2 \cdot 10^{-3}$ at received optical power lower than in the back-to-back configuration for the same performance, unlike the 25 km SSMF configuration, as shown the eye diagrams in Fig. 58(b) and (c). In addition, the gain in the fibre transfer function after 40 km SSMF transmission does not compensate for the received optical power reduction at −14.7 dBm with respect to the optical back-to-back configuration at −10 dBm, as shown the eye diagrams in Fig. 58(a) and (d). Furthermore, Fig. 58(c) and (d) exhibit similar maximum eye opening resulting in similar BER performance.

4.1.5 Simulation analysis

Performance improvement after dispersive fibre transmission compared with the optical back-to-back configuration has been achieved in the experiments for both DCM-OFDM and BPSK impulse-radio UWB signals. This is likely assisted by the chirp characteristics of the directly-modulated VCSEL [194], as has been pointed out in Section 4.1.3 and 4.1.4. Similarly, performance improvement after 20 km SSMF transmission of OOK baseband signals is observed in [197]. Chirp management of a directly-modulated DFB laser is performed by a tunable optical filter in [197]. In order to verify the experimental measurements, a simulation model for the UWB radio-over-fibre system in the 60 GHz band has been developed employing the commercial simulation tool VPItransmissionMaker™ (version 8.3).

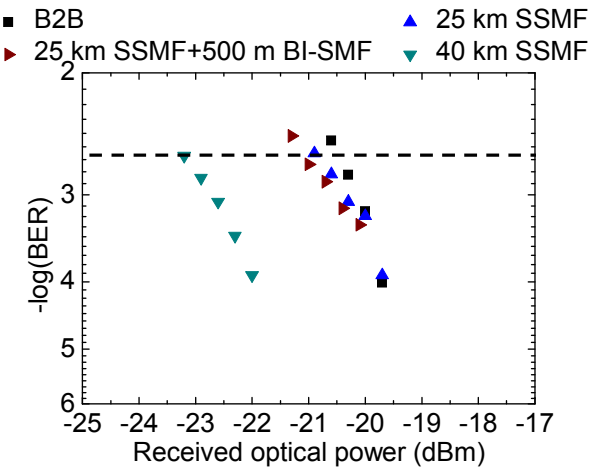

Fig. 59. Performance simulated at point (3) in Fig. 49 of the BPSK impulse-radio UWB radio-over-fibre system in the 60 GHz band combining optical and 5 m wireless transmission, to be compared with Fig. 56. The FEC limit of $2.2 \cdot 10^{-3}$ is shown via a dashed line.

A single-mode rate-equation model of a VCSEL is employed. The measured power- and voltage-bias current curves and thermal frequency shift of the VCSEL are included in the model. Furthermore, we previously verified that the model for the VCSEL can reproduce the behaviour of the real VCSEL by measuring the output of the VCSEL in the time and frequency domains under modulation with a NRZ pseudorandom bit sequence of 2^7–1 word length at 7.5 Gb/s. 7.5 Gb/s was chosen in order to have similar spectral width in the simulations and the experiments. Due to the fifth derivative Gaussian pulse shape, the spectral properties, and therefore also the chirp- and dispersion-related characteristics are more similar to 7.5 Gb/s OOK leading to more accurate results. Parameters of the VCSEL model giving a simulated output of the VCSEL very similar to that measured are found by multi-parameter sweep at a given drive voltage and bias current. Simulation results are obtained at approximately the same drive voltage and bias current as in the experiment and setting the corresponding VCSEL parameters obtained from the sweep.

Simulated BER performance of the BPSK impulse-radio UWB signal in the 60 GHz band is shown in Fig. 59 combining optical and 5 m wireless transmission which is modelled as free-space path loss. The same optical transmission cases as in Fig. 56 are considered: 25 km SSMF, 25 km SSMF extended by 500 m BI-SMF, and 40 km SSMF. Simulated BER exhibits the same behaviour as experimental BER shown in Fig. 56. Furthermore, it is verified that no performance improvement is obtained after fibre transmission with respect to optical back-to-back when the chirp of the VCSEL is disabled in simulation.

4.2 OOK impulse radio employing VCSEL and ECL up-conversion

Optical generation of impulse-radio UWB signals in the 60 GHz band is proposed and experimentally demonstrated [Bel11b]. ECL and VCSEL are employed for frequency up-conversion by heterodyne mixing with a UWB optical signal for comparison purposes. Real-time BER performance of generated signals at 3.125 Gb/s is evaluated combining fibre and 2 m wireless transmission. Different optical fibre types including 1 km BI-SMF and 20 km NZ-DSF is

evaluated. BER < 10^{-9} for the ECL and BER < $2.2 \cdot 10^{-3}$ for the VCSEL requiring higher received optical power than the ECL is demonstrated employing electrical power detection.

4.2.1 Introduction

UWB operation in the 60 GHz band permits to overcome coexistence issues limiting UWB operation in the 3.1 to 10.6 GHz band. In this Ph.D. thesis, we propose and analyse 60 GHz UWB photonic generation and integrated optical-radio transmission employing VCSEL and ECL. 60 GHz photonic generation and integrated transmission is an interesting approach for multi-Gb/s access in FTTH networks [Bel10c], [Bel11a], in WPAN supporting audio/video streaming, as discussed in Section 4.1, and in interference-sensitive scenarios like on-board plane equipment [Bel09a], [Bel10a], as discussed in Section 3.3. Previous works, summarized in Table I, demonstrate wireless distances below 1 m employing OOK modulation up to 3.125 Gb/s in the 3.1−10.6 GHz band [24], [25], [48], [67]. In the 60 GHz band, optical transmission up to 40 km SSMF and 5 m wireless distance has been demonstrated employing BPSK modulation at 1.44 Gb/s [Bel10c], [Bel11a]. Finally, wireless transmission up to 1.6 m employing OOK modulation at 2.5 Gb/s has been demonstrated in the 75–110 GHz band for 250 m SSMF and 50 m of DCF [59].

The analysis herein presented addresses the photonic generation, optical transmission up to 20 km and wireless transmission up to 2 m of impulse-radio UWB signals in the 60 GHz band. OOK modulation at 3.125 Gb/s is employed. OOK permits envelope detection avoiding down-conversion at the receiver and phase locking. The photonic generation technique employed is based on frequency up-conversion by heterodyne photodetection of an impulse-radio UWB signal and a semiconductor diode laser at a wavelength 60 GHz apart. This technique permits dual operation in the 3.1−10.6 GHz and in the 60 GHz band. Optical transmission performance is evaluated experimentally considering 1 km of BI-SMF without bending (1.1 dB loss) and 20 km of NZ-DSF (4.7 dB loss). The BI-SMF is employed for indoor distribution due to its low bend loss and suitability for indoor installation. The NZ-DSF is employed for FTTH distribution due to the improved dispersion performance compared to SSMF. The total dispersion of the 20 km of NZ-DSF employed is equivalent to that of 6.5 km of SSMF.

4.2.2 Experimental setup

Fig. 60 shows the experimental setup. At the head-end unit (HEU), an impulse-radio UWB signal at 3.125 Gb/s is optically generated based on the incoherent optical field summation resulting from cross-gain modulation of an uncooled DFB laser at ~1552.4 nm with an ECL (ECL1 in Fig. 60) at ~1553.5 nm [48]. The ECL1 is modulated at 3.125 Gb/s by a RZ pseudo-random binary sequence signal with a duty cycle of 0.25. A programmed 2^7-1 pseudorandom bit sequence from the pulse pattern generator is employed, “1000” and “0000” corresponding to 1 and 0 UWB bits, respectively. The signal at point (1) in Fig. 60 is shown in Fig. 61(a). The pulse shape is in excellent compliance with the UWB EIRP density regulated in the U.S. provided an antenna with an adequate frequency response is used for operation in the 3.1−10.6 GHz band [48]. Fig. 61(b) shows the signal in the 3.1–10.6 GHz band, which is available at point (3) in Fig. 60 simultaneously to the 60 GHz signal.

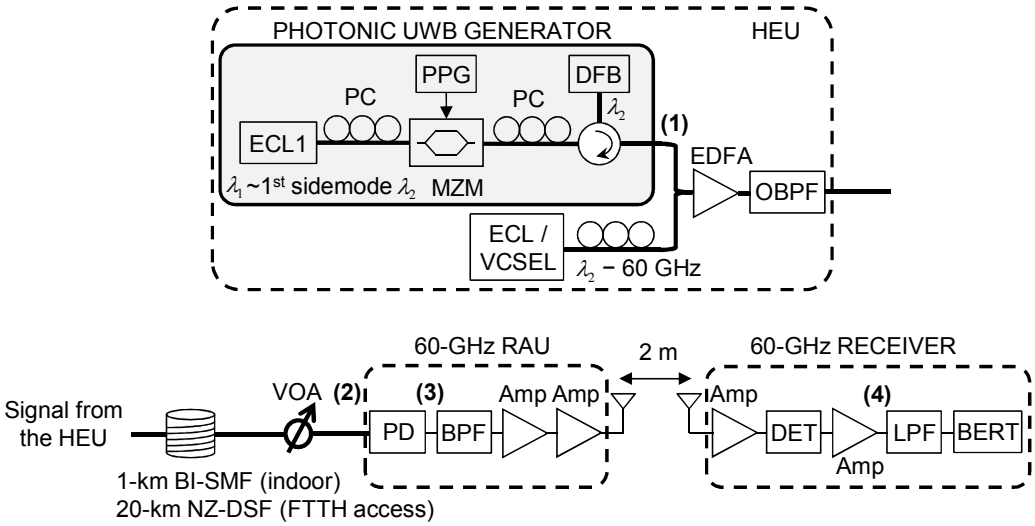

Fig. 60. Experimental setup for optical impulse-radio UWB generation in the 60 GHz band with combined fibre and wireless transmission.

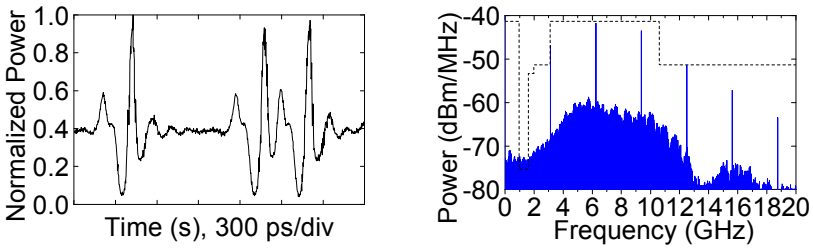

Fig. 61. (a) Impulse-radio UWB signal at point (1) in Fig. 60. (b) RMS spectrum of the signal in the 3.1−10.6 GHz band at point (3) in Fig. 60 for optical B2B, which is similar for ECL and VCSEL (resolution bandwidth: 1 MHz). The UWB EIRP regulated in the U.S. is shown via a dashed line.

The impulse-radio UWB signal is combined with a laser, ECL (HP/Agilent 8168C) or uncooled unmodulated 10 Gb/s VCSEL (VERTILAS, 1550-10G-P2-P4-Diff-Flex) [193]. The laser is tuned at a wavelength of 60 GHz lower than the DFB wavelength. In this way, frequency up-conversion of the impulse-radio UWB signal to the 60 GHz band is achieved after 75 GHz photodetection at the remote antenna unit. The combined optical signal is amplified by an EDFA, 5 nm filtered, and distributed over fibre. A variable optical attenuator is employed to vary the received optical power. At the remote antenna unit, the photodetected signal is band-pass filtered (56.26−62 GHz) and amplified by a low-noise amplifier (18.7 dB gain) and a high-power amplifier (28.7 dB gain) before being fed to an antenna for 2 m of wireless transmission. Rectangular horn antennas with 50−75 GHz frequency range, 20 dBi gain, and 12° beamwidth are employed. At the receiver, the 60 GHz impulse-radio UWB signal is amplified by a high-power amplifier (28.7 dB gain) and demodulated by a power detector (50–75 GHz). The detected envelope is amplified to accommodate its level to the BERT and 7.5 GHz low-pass filtered. Eye diagrams are measured at point (4) in Fig. 60.

The signals at point (1) in Fig. 60 and from the ECL or VCSEL are optimized for the best possible minimum BER in each case of ECL or VCSEL and back-to-back or optical transmission. The optimum DFB bias is approximately the same in all cases. The output power of the ECL and VCSEL should be high. The maximum output power of 2 dBm is employed in both cases.

4.2.3 Performance analysis

BER as a function of the received optical power of the 60 GHz optical and 2 m radio link is compared for ECL and VCSEL. ECL is suitable for heterodyning due to the relative narrow-linewidth [198]. In recent years, VCSEL have gained a lot of interest due to the relative low cost. VCSEL placed at a remote site is also investigated to compare different scenarios.

For ECL, the spectrum at point (2) in Fig. 60 is shown in Fig. 62(a). Fig. 63 shows BER performance which is limited by electrical noise. Decreasing the received optical power further increases the BER due to reduction in SNR. BER $< 10^{-9}$ is achieved at an optical receiver sensitivity of −10.1 dBm, −9.8 dBm, and −7.6 dBm for optical back-to-back, 1 km BI-SMF, and 20 km NZ-DSF, respectively. The power budget apart from fibre loss is 12.3 dB, 11.1 dB, and 4.2 dB, respectively. Hence, fibre dispersion introduces a power budget penalty of 1.2 dB, and 8.1 dB, respectively.

For VCSEL, Fig. 62(b) shows the spectrum at point (2) in Fig. 60. There is a small difference in DFB bias between ECL and VCSEL due to the lower wavelength accuracy of the VCSEL. This causes different DFB chirp so that the DFB bandwidth in Fig. 62(b) is wider than that in Fig. 62(a). Fig. 64 shows BER performance. BER floor is limited by the optical SNR. The optical SNR for back-to-back is degraded compared with ECL due to the VCSEL noise. Simulation results suggest that the VCSEL linewidth (20 MHz min. vs. 100 kHz of the ECL, as of datasheets) dominates over the VCSEL relative intensity noise, as discussed in Section 4.2.4. A maximum relative intensity noise of −135 dB/Hz is considered for both VCSEL and ECL. In addition, the influence of the VCSEL chirp on the fibre RF transfer function mitigates dispersion-induced RF power fading compared with ECL. BI-SMF dispersion does not degrade BER floor like in Fig. 63. Hence, BI-SMF penalty in Fig. 63 is not due to pulse time stretching but to 60 GHz signal distortion induced by RF power fading. BER floor degradation by NZ-DSF dispersion in Fig. 64 is lower than that in Fig. 63. Hence, RF power fading contributes to NZ-DSF penalty in Fig. 63. Furthermore, BER floor degradation by NZ-DSF in Fig. 64 does not induce penalty in optical receiver sensitivity. This excellent transmission property is the result of gain in the fibre RF transfer function further induced by VCSEL chirp [194]. This gain improves SNR at low received optical power. This effect is also the cause of the improvement in optical receiver sensitivity for BI-SMF with respect to back-to-back in Fig. 65. Additionally, assuming that the BER floor degradation by NZ-DSF in Fig. 64 is only caused by pulse time stretching, time stretching (which is dependent on DFB bandwidth) induces a maximum penalty of 1 dB. BER is below the FEC limit of $2.2 \cdot 10^{-3}$ at optical receiver sensitivity approximately the same of −4 dBm for optical back-to-back, 1 km BI-SMF, and 20 km NZ-DSF. The power budget apart from fibre loss is 8 dB, 7.1 dB, and 3.1 dB, respectively. The power budget penalty with respect to ECL at BER $< 2.2 \cdot 10^{-3}$ is 7 dB, 6.9 dB, and 4.2 dB, respectively. After considering the 7% FEC overhead, the effective data rate is 2.91 Gb/s.

Fig. 65 shows BER when the VCSEL, polarization controller and 3 dB coupler are moved to point (2) in Fig. 60. The optical spectrum at point (2) in Fig. 60 at 0.9 dBm maximum received optical power is like that in Fig. 62(b) with a power level reduced by 7.7 dB and 0.4 dB for VCSEL and DFB, respectively, and increased by 1.1 dB for ECL1. BER floor is limited by the optical SNR.

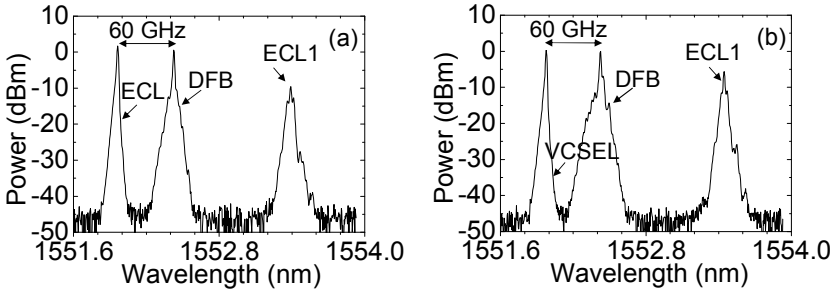

Fig. 62. Optical spectrum measured at point (2) in Fig. 60 for optical B2B. (a) ECL at 2.2 dBm maximum received optical power. (b) VCSEL at 4 dBm maximum received optical power. (Resolution bandwidth: 0.02 nm).

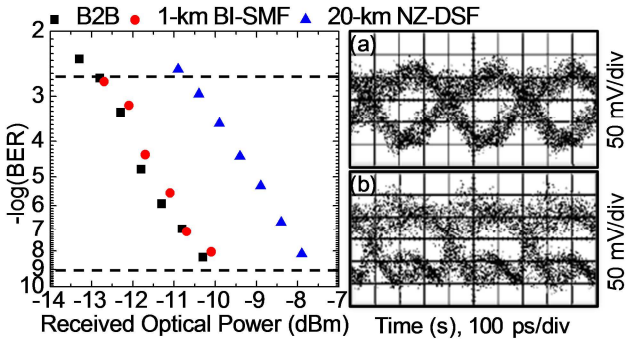

Fig. 63. BER for ECL. (a) 1 km BI-SMF at −7.7 dBm received optical power, BER < 10^{-9}. (b) 20 km NZ-DSF at −7.9 dBm, BER = $7 \cdot 10^{-9}$.

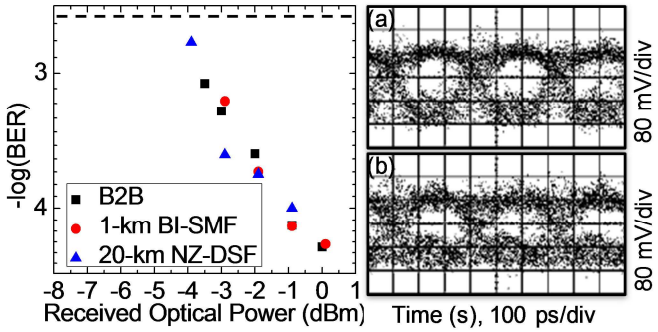

Fig. 64. BER for VCSEL at the head-end unit. (a) 1 km BI-SMF at 0.1 dBm received optical power, BER < $4.8 \cdot 10^{-5}$. (b) 20 km NZ-DSF at −0.9 dBm, BER = $1 \cdot 10^{-4}$.

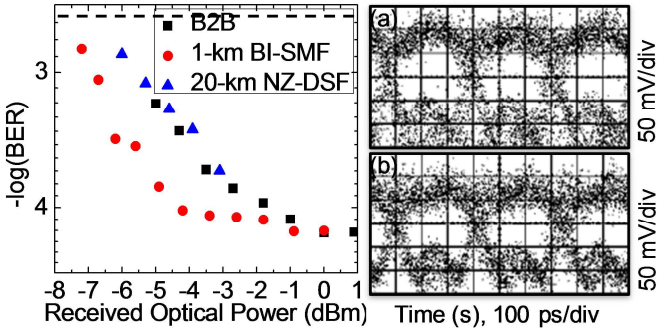

Fig. 65. BER for remote VCSEL. (a) 1 km BI-SMF at 0 dBm received optical power, BER < $6.3 \cdot 10^{-5}$. (b) 20 km NZ-DSF at −3.1 dBm, BER = $2 \cdot 10^{-4}$.

The noise at the coupler output is dominated by the noise at the EDFA output for back-to-back at high received optical power. The lower power used for up-conversion and the different optical noise result in optical SNR for back-to-back degraded compared with Fig. 63 and Fig. 64. BER $< 2.2 \cdot 10^{-3}$ is achieved at an optical receiver sensitivity of −7 dBm, −7.7 dBm, and −6.7 dBm for back-to-back, 1 km BI-SMF, and 20 km NZ-DSF, respectively. The power budget apart from fibre loss is 7.9 dB, 7.7 dB, and 3.6 dB, respectively. These results demonstrate that VCSEL used for remote direct modulation could also be used for heterodyning. Furthermore, remote VCSEL potentially eliminates RF power fading.

Note that the wavelength of the VCSEL was adjusted to track the temperature drift (0.1 nm/°C typ.). In practice, temperature control could improve stability.

4.2.4 Simulation analysis

The BER floor in Fig. 64 is limited by the optical SNR. The signal at point (1) in Fig. 60 is more or less the same for ECL and VCSEL and the output power of the ECL and VCSEL is the same. Hence, the optical SNR for back-to-back may be significantly degraded compared with ECL due to the VCSEL noise.

The experimental setup has been simulated employing VPItransmissionMaker™ (version 8.5) to study the influence on BER floor for back-to-back of linewidth and relative intensity noise (RIN) of the laser employed for heterodyning. We have considered the linewidth of the ECL employed in the experiment (100 kHz) and the minimum linewidth specified by VERTILAS for the VCSEL (20 MHz). Two values of RIN, −135 dB/Hz and −145 dB/Hz, are considered for both ECL and VCSEL. Note that RIN< −135 dB/Hz is a typical maximum RIN for VCSEL at the bias current employed in the experiment. Simulation results are shown in Fig. 66 without considering wavelength drift with temperature (deltaT= 0 in the legend).

BER degradation with linewidth is verified at the same RIN for ECL and VCSEL. In addition, reducing RIN slightly improves BER for VCSEL whereas BER significantly improves for ECL. Hence, VCSEL noise is dominated by linewidth but of course RIN and other impairments affect performance.

The influence of wavelength drift with temperature has also been investigated. The typical temperature coefficient specified by VERTILAS for the VCSEL (12.5 GHz/ºC) is considered and 2.5 GHz/ºC is assumed for ECL. Fig. 66 shows simulation results for a wavelength drift of 1.25 GHz for both ECL and VCSEL. Wavelength drift causes similar BER floor degradation at both RIN values for ECL whereas degradation is different for VCSEL due to the linewidth limitation.

BER floor is degraded for VCSEL compared with ECL even when VCSEL has higher relative intensity noise. Hence, VCSEL performance is limited by linewidth and wavelength drift with temperature.

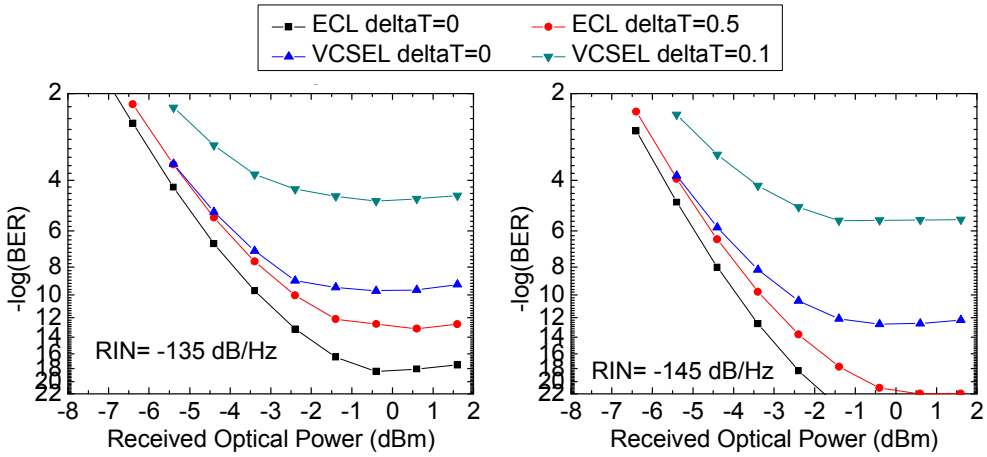

Fig. 66. Simulation of the influence of relative intensity noise, linewidth and wavelength drift with temperature of the laser employed for up-conversion.

4.3 Conclusion

UWB radio-over-fibre in the 60 GHz band for providing multi-Gb/s integrated FTTH and WPAN connectivity has been proposed and experimentally demonstrated. Radio-over-fibre transmission over 40 km SSMF without any dispersion compensation and further 5 m wireless transmission has been demonstrated for both DCM-OFDM and BPSK impulse-radio UWB signals at 1.44 Gb/s in the 60 GHz band. The BPSK impulse-radio UWB implementation is more tolerant to fibre impairments requiring lower received optical power than the DCM-OFDM UWB counterpart, although other UWB generation and DSP detection techniques could lead to different results. The use of the same AWG for both OFDM and impulse-radio UWB generation will provide a thorough conclusion. Experimental results verified by simulation show that the UWB radio-over-fibre system in the 60 GHz band can benefit from the chirp of low-cost directly-modulated VCSELs to increase optical receiver sensitivity.

We believe that these results underpin the flexibility of UWB signalling not only in the 3.1−10.6 GHz band, but also in the 60 GHz band.

Simple optical generation of OOK 60 GHz impulse-radio UWB signals at 3.125 Gb/s has been experimentally demonstrated. Cost-effective VCSEL is proposed for optical heterodyning. VCSEL is demonstrated to be suitable for integrated FTTH or optical indoor and WPAN transmission in two scenarios including centralized VCSEL and remote VCSEL. Compared with ECL, VCSEL could be directly modulated and VCSEL chirp improves dispersion tolerance. However, BER is degraded for VCSEL. Reduced VCSEL linewidth for centralized VCSEL and high VCSEL output power for remote VCSEL could reduce the BER degradation.

5

Reconfigurable multiwavelength source based on electrooptic phase modulation of a pulsed laser

A reconfigurable multiwavelength source based on time-domain electrooptic phase modulation of a pulsed laser is proposed and experimentally demonstrated [Bel11c], [Llo12]. The technique permits great reconfiguration in wavelength separation –by multiplying the number of wavelengths within the optical bandwidth, as well as in the spectrum allocation. A tunable 5 GHz and 2.5 GHz frequency spacing from a 10 GHz mode-locked laser is experimentally demonstrated. A 5 GHz frequency shift is also demonstrated.

5.1 Introduction

Multiwavelength light sources are fundamental components in a variety of photonic applications including optical communications, signal processing, and spectroscopy [199]. Several approaches for multiwavelength light generation have been reported [200]–[207]. For instance, multifrequency operation of an Erbium-doped fibre laser can be achieved by adding a frequency shifter in the ring cavity [201]. A different approach is based on stimulated Brillouin scattering. In this technique, mode spacing adjustment is possible by changing the free spectral range of an intracavity birefringent loop mirror filter [202]. On the other hand, mode-locked lasers [200] are ideally well suited for multifrequency generation as they provide a regularly spaced series of stable and sharp spectral components and have low noise qualities. However, these multimode pulsed lasers usually present limited reconfiguration capabilities in terms of, e.g., wavelength spacing. Optical frequency combs based on electrooptic modulators driven by large-amplitude sinusoidal signals permit arbitrary wavelength spacing by adjusting the frequency of the sinusoidal signals, and wavelength can be shifted employing a tunable continuous-wave laser. For instance, comb generation based on a phase modulator [203], a dual-drive MZM [204], or cascaded phase and intensity modulators [205]. Although this technique can provide a relatively flat optical comb, it can be limited by the insertion loss of the modulator together with the modulation efficiency. Gain-switched pulsed lasers can also be employed for simple and cost efficient multiwavelength generation with tunable wavelength spacing [206]. However, these comb sources usually present limited bandwidth and flatness

capabilities. To further broaden the comb, nonlinear fibre processes [204], [206], recirculating schemes [205], and phase modulation processes [207] have been demonstrated.

A multiwavelength source with reconfiguration capabilities based on a mode-locked laser and an electrooptic phase modulator is proposed and experimentally demonstrated in this Ph.D. thesis. The phase modulation process enables discrete tuning in wavelength spacing or offset of a pulsed laser without influencing bandwidth. Furthermore, the reconfiguration does not influence the pulse train in intensity. The technique has potential application for "elastic" WDM systems, such as OFDM systems with reconfigurable subcarrier spacing (optical OFDM) or subband spacing (multiband electrical OFDM) [205 and references therein], as illustrated in Fig. 4, and optical code division multiple access (OCDMA) systems [199].

5.2 Principle of operation

Fig. 67 shows a schematic diagram of the proposed technique for generation of a reconfigurable multiwavelength source from a pulsed laser. A periodic input pulse train with period T_{rep} is considered which corresponds, in frequency domain, to an optical frequency comb with frequency spacing equal to the pulse repetition rate, i.e., $f_{rep} = 1/T_{rep}$. This optical spectrum constitutes the original multiwavelength source. By applying an adequate time-domain periodic multistep phase modulation on the input train, a change in the frequency spacing of the multiwavelength source is achieved. The periodic phase sequence is obtained from the expression [Car11]

$$\varphi_n = \pm\frac{s}{r}\pi n^2, \qquad (1)$$

where s and r are mutually prime integer numbers and φ_n is the phase shift applied on the pulse n in the sequence. This phase shift can be assumed to be applied on a time slot equal to the pulse repetition rate T_{rep}. If these phase shifts are reduced into a 2π range, a periodic sequence of phase steps is obtained. Under these specific temporal modulation conditions, the frequency spacing of the multiwavelength source is reduced by the integer factor r. In addition, a frequency shifting effect is observed in the spectral lines under other particular modulation conditions. All these features can be interpreted as the spectral analogue of the so-called temporal self-imaging effect [Car11], [208], [209]. Fig. 67 schematically shows the case of the temporal periodic modulation with the sequence {0, $\pi/2$, 0, $\pi/2$, …} derived from (1) with $s = 1$ and $r = 2$ leading to a reduction of the frequency spacing by a factor of 2. In this Ph.D. thesis, we demonstrate the feasibility of the approach proposed in [Car11] employing electrooptic phase modulation.

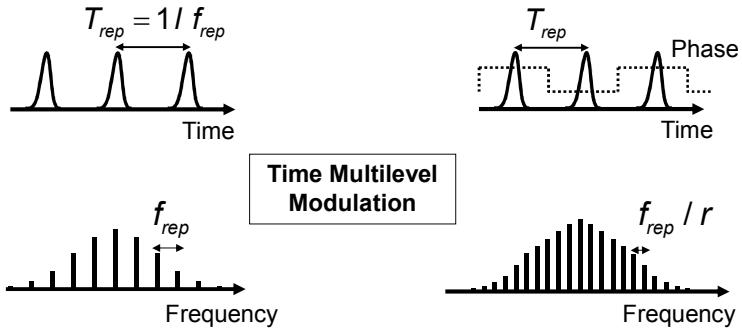

Fig. 67. Principle of operation of a reconfigurable multiwavelength source by time-domain phase modulation of a pulsed laser.

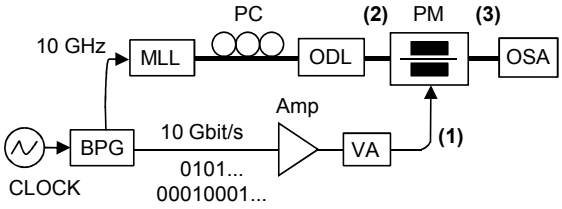

Fig. 68. Experimental setup of a reconfigurable multiwavelength source.

5.3 Experimental setup

Fig. 68 shows the experimental setup. The original multiwavelength source is an active mode-locked laser (Calmar Laser, PSL-10-2T), MLL block in Fig. 68. The laser generates pulses with 2 ps of FWHM at a repetition rate of 10 GHz. This pulse train is temporally modulated with a bit pattern in an electrooptic phase modulator (Covega, LN53S) ($V_\pi = 3.5V$). An optical delay line is used to synchronize the modulation pattern with the pulse train. The modulation depth is tuned by using a variable electrical attenuator. Fig. 69(a) shows the original 10 GHz pulse train measured at point (2) in Fig. 68. Fig. 70(a) shows the original multiwavelength spectrum.

5.4 Functional demonstration

Three experimental cases are considered to demonstrate a reconfigurable multiwavelength source. Two different bit patterns with different amplitude are employed to decrease the wavelength separation of the mode-locked laser in Fig. 68 by two different factors. By adjusting either the bit pattern or the amplitude of the bit sequence, the centre wavelength is shifted alternatively to decrease the wavelength separation.

5.4.1 Reduction of the frequency spacing by a factor of 2

First, we experimentally demonstrate reduction of the frequency spacing of the mode-locked laser by a factor of 2, as introduced in Section 5.2. A bit pattern 0101… at 10 Gb/s is employed to drive the electrooptic modulator. Fig. 69(b) shows the bit pattern measured at point (1) in Fig. 68. The modulation depth of the electrooptic modulator is carefully tuned until a $\pi/2$ phase shift is achieved.

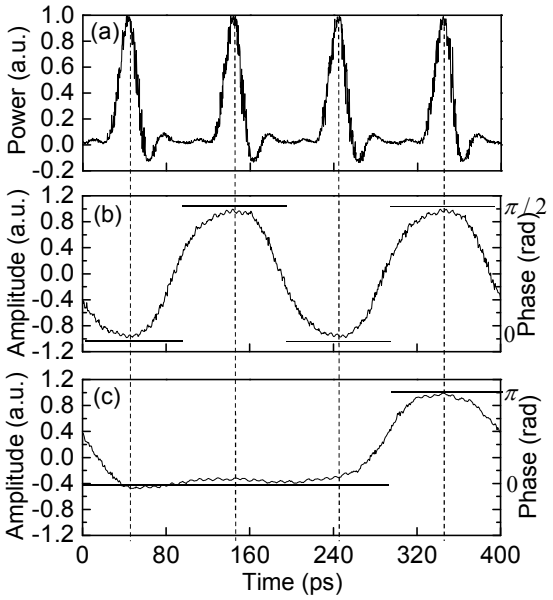

Fig. 69. (a) Input 10 GHz optical pulse train measured at point (2) in Fig. 68 (Analyzer optical bandwidth: 30 GHz). (b) and (c) Modulating signal at point (1) in Fig. 68 for twofold and fourfold decrease in the frequency spacing of the pulsed laser, respectively.

Note that the driving signal guarantees that the same phase shift is applied along the whole optical pulse duration. Fig. 70(b) shows the reconfigured multiwavelength spectrum measured at point (3) in Fig. 68. The spectrum exhibits a frequency spacing of 5 GHz in agreement with the theory introduced in Section 5.2.

5.4.2 Reduction of the frequency spacing by a factor of 4

In a second experimental demonstration, the frequency spacing of the mode-locked laser is reduced by a factor of 4 by driving the phase modulator with a sequence 00010001… at 10 Gb/s and setting a π phase shift. The modulating sequence is shown in Fig. 69(c). The resultant periodic sequence in this case is {0, 0, 0, π, 0, 0, 0, π, …} which, although not derived from (1), also provides a fourfold reduction in the frequency spacing [208]. Fig. 70(c) shows the reconfigured multiwavelength spectrum measured at point (3) in Fig. 68. The spectrum exhibits a frequency spacing of 2.5 GHz as expected. Note that the correspondence to the original spectrum in Fig. 70(a) is not perfect due to the resolution of the trace (375 points in 1.5 nm).

5.4.3 Wavelength shift by half frequency spacing

The proposed technique also permits to shift the wavelength of the original multiwavelength spectrum. The spectrum is shifted by half of the original frequency spacing when an alternate π phase shift is set. The sequence in this case {0, π, 0, π, …} is derived from (1) with $s=1$ and $r=1$. Fig. 70(d) shows the reconfigured multiwavelength spectrum measured at point (3) in Fig. 68. The spectrum exhibits a frequency shift of 5 GHz with respect to the input spectrum.

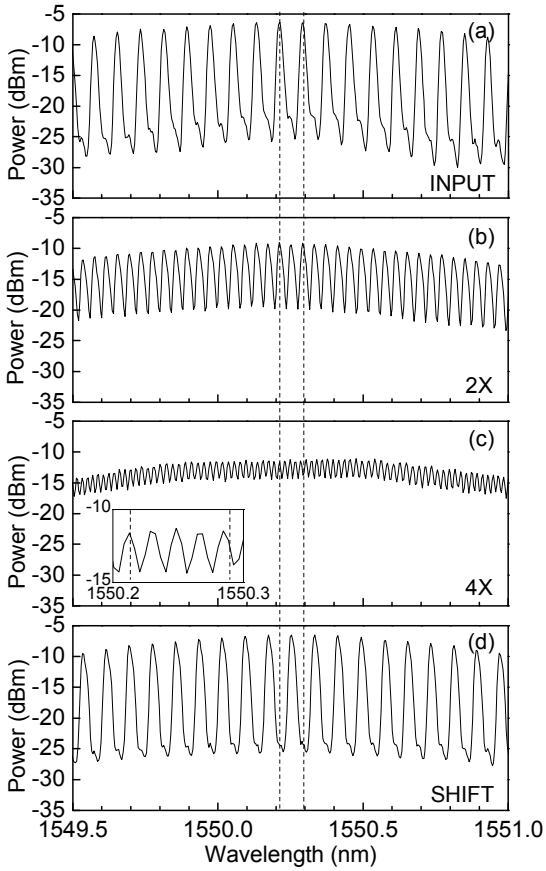

Fig. 70. (a) Input 10 GHz multiwavelength laser spectrum measured at point (2) in Fig. 68. (b) and (c) Decrease by an integer factor of 2 and 4 in the frequency spacing, respectively. (d) Frequency shifting by half of the original frequency spacing. (Resolution bandwidth: 0.01 nm).

It should be noted that the experimental examples reported here only use two phase levels, while in general multilevel phase sequences are required. For instance, the periodic sequence {0, $\pi/4$, π, $\pi/4$, …} derived from (1) with $s=1$ and $r=4$ also leads to a fourfold decrease in the frequency spacing of the pulsed laser. However, the implementation of such a case may require a more complex multilevel modulation approach [97], [98].

5.5 Chirp and noise impact analysis

The influence of chirp, timing jitter and amplitude noise of the original source on the proposed technique has been analysed by numerical simulations. A sequence of Gaussian pulses with 5 ps FWHM and repetition rate $f_{rep}=10\,GHz$ is considered. The phase modulation process does not influence the pulse train in intensity in the presence of chirp and noise.

The spectrum of the linearly-chirped Gaussian pulses is broader than that of the unchirped pulses. Fig. 71 shows simulation results of the reconfigurable multiwavelength source for linearly-chirped Gaussian pulses. Chirp does not influence the proposed reconfiguration technique neither for frequency spacing reduction nor for frequency shifting.

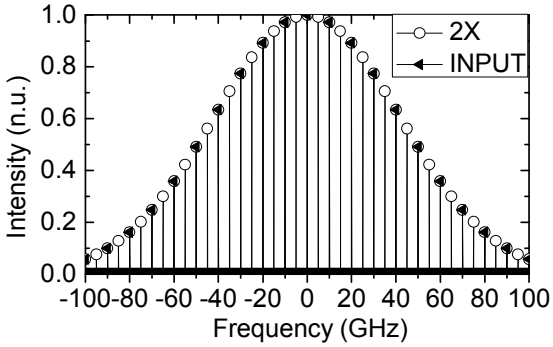

Fig. 71. Multiwavelength spectrum reconfigured for twofold decrease in the frequency spacing compared with the input spectrum when chirp is considered in simulation.

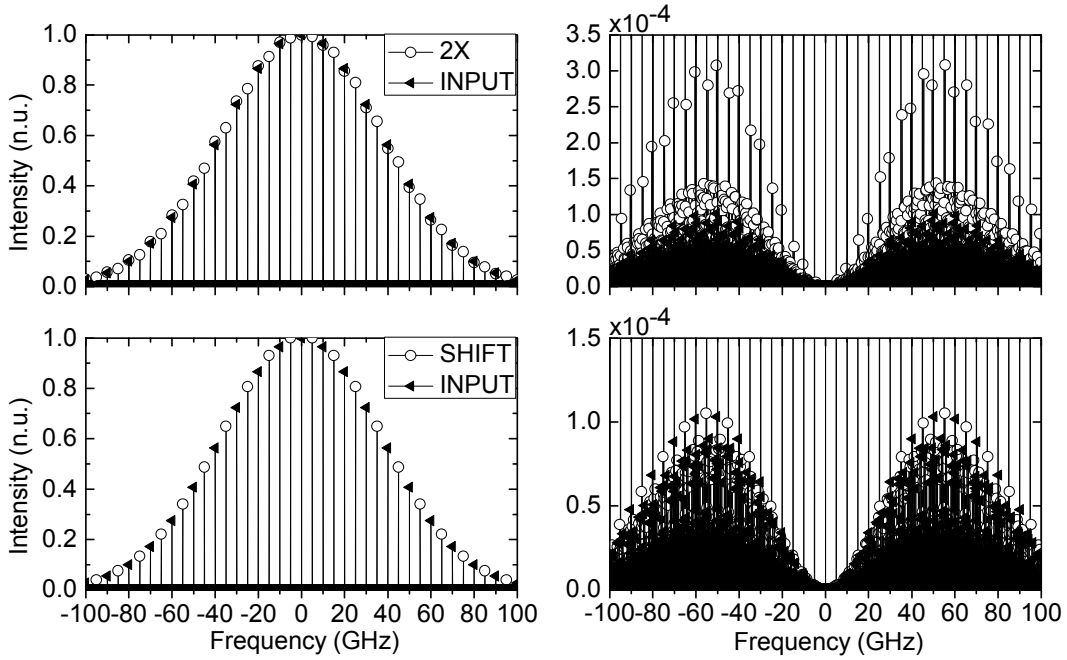

Fig. 72. Multiwavelength spectrum reconfigured for twofold decrease in the frequency spacing and for frequency shifting by half frequency spacing compared with the input spectrum when timing jitter is considered in simulation.

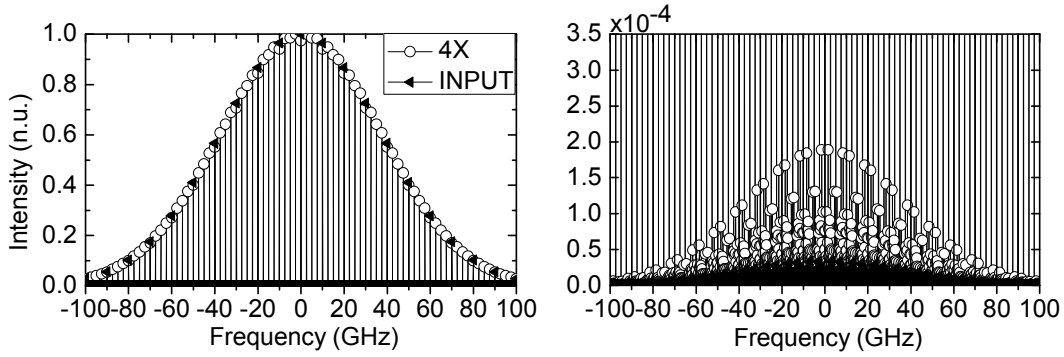

Fig. 73. Multiwavelength spectrum reconfigured for fourfold decrease in the frequency spacing compared with the input spectrum when amplitude noise is considered in simulation.

The spectrum of the Gaussian pulses with timing jitter is narrower than that of the pulses without jitter and presents noise between spectral lines. Fig. 72 shows simulation results of the reconfigurable multiwavelength source when a pulse-to-pulse random time shift with Gaussian distribution at 1 ps mean and 0.3 ps standard deviation is considered. The phase modulation process in the presence of timing jitter induces nonuniformity in the spectral envelope and increases the noise between spectral lines for frequency spacing reduction. The higher the frequency spacing reduction factor the higher the noise increment. For frequency shifting, phase modulation shifts the noise between spectral lines.

Finally, amplitude noise influences the reconfigured spectrum similarly to timing jitter. The spectrum of the Gaussian pulses with amplitude noise presents noise between spectral lines. Fig. 73 shows simulation results of the reconfigurable multiwavelength source when a pulse-to-pulse random amplitude variation with Gaussian distribution at 0.1 mean and 0.03 standard deviation is considered. The phase modulation process in the presence of amplitude noise induces nonuniformity in the spectral envelope and increases the noise between spectral lines for frequency spacing reduction. The higher the frequency spacing reduction factor the higher the noise increment. For frequency shifting, phase modulation shifts the noise between spectral lines.

5.6 Conclusion

Multilevel electrooptic phase modulation is suitable for adding flexibility in both wavelength spacing and centre wavelength to pulsed lasers. The theory reported in [Car11] has been verified experimentally. Twofold and fourfold reduction of wavelength spacing by doubling and quadrupling the number of wavelengths and wavelength shift by half wavelength spacing has been demonstrated employing a simple electrooptic phase modulator driven by a binary signal. The technique is insensitive to chirp, and increases the spectral noise after wavelength spacing reconfiguration.

The technique has been demonstrated to reconfigure a 10 GHz mode-locked laser. Alternatively, the technique could be applied to optical combs based on electrooptic modulators provided they are configured to operate as pulsed lasers as well as to gain-switched lasers. These pulsed lasers may offer lower cost solutions however they usually exhibit worse performance which could translate into higher overall cost in radio-over-fibre architectures supporting a large number of remote antenna units.

Silicon-based optical modulators have been demonstrated which can alternatively be used for phase modulation targeting to reduce cost [191]. Although these silicon modulators offer several advantages, the technology is still in development and device performance need to be improved. In addition, phase modulation can be implemented by nonlinear optical processes, as suggested in [Car11].

6

Conclusion and further work

6.1 Conclusion

The study on different techniques allowing the development, implementation and maintenance of optical access networks providing high capacity wireless connectivity in a flexible and cost-effective way is required for next-generation access networks and has been subject of study in this Ph.D. thesis. The feasibility of new UWB radio-over-fibre techniques to provide multigigabit wireless communications in FTTH networks has been demonstrated. The techniques studied are transferable to real product systems and actual optical networks.

Two techniques have been proposed and experimentally demonstrated for UWB generation integrating optical access transmission. Optical pulses are remotely shaped to UWB Gaussian monocycles based on optical delay and balanced photodetection or based on differential photoreceiver and electrical delay. Simple optical schemes for UWB generation, which are scalable to high-frequency waveforms, reconfigurable and employ off-the-shelf components, are yet to be proposed. Such methods may significantly enhance UWB radio-over-fibre integration.

UWB in the 60 GHz band has also been presented as a very interesting approach for next-generation radio systems which would benefit from the unlicensed nature of this band together with the intrinsic coexistence characteristics of UWB technology. Application of UWB-over-fibre systems in the 60 GHz band to interference-sensitive locations such as in-aircraft communications and to integrated optical access and indoor radio networks has been proposed and experimentally demonstrated. Commercially available technology has been employed and the use of other evolving technologies has been discussed, which could lead to simpler and lower overall cost implementations.

There are several challenges limiting practical application of 60 GHz wireless systems for high-speed WPAN. First, LOS transmission is required for high-speed operation. Several solutions have been proposed to support NLOS communications, such as MIMO, beam forming, and beam steering. Their implementation in practical commercial compact and cost-effective CMOS transceivers as required for WPAN has been demonstrated however it is still in

development. In addition, in practical applications, it is often desired to combine mobility and high-speed capability of the LOS directional links. Hence, solutions are required to provide wide coverage without increasing complexity significantly.

60 GHz downlink radio-over-fibre transmission suitable for HDTV delivering has been investigated in this thesis. Enabling technologies for full-duplex systems keeping the remote antenna units simple should be further investigated. These systems could involve the uplink transmission of 60 GHz wireless and wired services. The 60 GHz signal could be down-converted at the remote antenna units for baseband uplink optical transmission over extended distances. The use of 60 GHz CMOS transceivers may provide a cost-effective solution.

In addition, varying fibre dispersion in optical access networks covering different distances can be exploited to cover a wide range of applications in different RF bands simultaneously, including 60 GHz FTTH, 24 GHz infrastructure-to-car radar and communications, and 75−110 GHz outdoor communications. 60 GHz generation has been experimentally demonstrated employing 15 GHz up-conversion devices and 12.5 km of SSMF in FTTH networks at 1.25 Gb/s. Wireless transmission at 1 m has also been demonstrated.

Integration of 60 GHz UWB-over-fibre in FTTH networks is proposed and demonstrated for >1 m wireless distance up to 3.125 Gb/s. 60 GHz operation reuses UWB technology to overcome UWB coexistence issues and to extend UWB range. VCSEL enables cost-effective electrooptic conversion and optical frequency up-conversion. Combined 40 km SSMF and 5 m wireless transmission has been experimentally demonstrated for the two mainstream UWB implementations -OFDM and impulse-radio- at 1.44 Gb/s. The results permit, from an application point-of-view, to select a given UWB implementation depending on network reach and system complexity desired. The use of a direct-modulated VCSEL in combination with optical carrier suppression in a MZM has been proposed. VCSEL chirp has been shown to improve optical receiver sensitivity.

VCSEL has also been proposed for frequency up-conversion and compared with conventional ECL. Combined 6.5 km SSMF and 2 m wireless transmission has been experimentally demonstrated at 3.125 Gb/s. The results permit, from an application point-of-view, to select a given laser technology depending on network reach and system complexity desired.

The application of the theory developed in [Car11] to multiwavelength sources has been proposed and experimentally demonstrated in this thesis. Multiwavelength sources with easily reconfigurable wavelength spacing or centre wavelength are proposed based on electrooptic multi-phase modulation of a pulsed laser. Twofold and fourfold multiplication of comb lines and wavelength shift by half of the wavelength spacing of a mode-locked laser has been experimentally demonstrated employing a simple phase modulator driven by a binary signal. Since the pulse train is unaltered in intensity, the proposed reconfigurable source can be used simultaneously for time-domain applications such as optical time division multiplexing (OTDM) systems.

Finally, since impulse-radio UWB is nowadays mostly used for radar/positioning application, we believe that a combination of multi-Gb/s communications and accurate positioning is very attractive as a research topic.

6.2 Ongoing and further work

There are two ongoing research lines related with this Ph.D. thesis, in the context of hybrid millimetre-wave optical networks and reconfigurable multiwavelength sources:

First, a collaboration has been done proposing and experimentally demonstrating the combined optical access and wireless transmission of compressed HD video in the 60 GHz band [Leb11a], [Leb11b]. The study demonstrates that performance in terms of wireless distance or optical power budget can be improved employing advanced video coding, performance degradation induced by video compression being a trade-off. The system is based on DFB direct modulation, frequency up-conversion by optical carrier suppression in a MZM, and RF power detection. Employing this system, in addition, reuse of widely deployed in-building MMF as extension of optical access networks has been proposed and experimentally demonstrated for in-building gigabit wireless access in the 60 GHz band [Pha11]. Distribution of 2 Gb/s data in combined 10 km SSMF/1 km MMF and further 6.5 m wireless distance has been demonstrated.

Second, in the line of spectral reconfiguration of multiwavelength sources, there is ongoing work targeting to investigate the flexibility of the phase modulation technique proposed in this thesis by employing multilevel electrooptic modulation. Of particular interest, the possibility of achieving high multiplication factors without increasing complexity significantly. Several applications are also being investigated, where the use of this technique may be relevant. For instance, in photonic millimetre-wave wireless systems based on multiband OFDM signals. The use of a reconfigurable optical comb in this application is an attractive approach to provide flexible seamless slicing of the wide RF bandwidth. The optical comb generates the multiple optical wavelengths supporting the different OFDM bands to serve different users in the system. Optical SNR reduction due to reconfiguration may limit the number of comb lines supported in the system. The multiband OFDM technique can also reduce the power and bandwidth requirements of DAC/ADC equipment for energy-efficient and cost-effective systems. Joint experiments have started to investigate photonic millimetre-wave wireless systems in the 75–110 GHz band based on electrical OFDM and optical comb generation [Den11], [Bel12].

A

Original contributions

Peer-reviewed journals

[Bel11d] **M. Beltrán** and R. Llorente, "Dual photonic generation ultrawideband impulse-radio by frequency shifting in remote-connectivity fiber," *J. Lightw. Technol.*, vol. 29, no. 24, pp. 3645–3653, Dec. 2011.

[Bel11c] **M. Beltrán**, J. Caraquitena, R. Llorente, and J. Martí, "Reconfigurable multiwavelength source based on electrooptic phase modulation of a pulsed laser," *IEEE Photon. Technol. Lett.*, vol. 23, no. 16, pp. 1175–1177, Aug. 2011.

[Bel11b] **M. Beltrán**, J. B. Jensen, R. Llorente, and I. Tafur Monroy, "Experimental analysis of 60-GHz VCSEL and ECL photonic generation and transmission of impulse-radio ultra-wideband signals," *IEEE Photon. Technol. Lett.*, vol. 23, no. 15, pp. 1055–1057, Aug. 2011.

[Bel11a] **M. Beltrán**, J. B. Jensen, X. Yu, R. Llorente, R. Rodes, M. Ortsiefer, C. Neumeyr, and I. Tafur Monroy, "Performance of a 60-GHz DCM-OFDM and BPSK-impulse ultra-wideband system with radio-over-fiber and wireless transmission employing a directly-modulated VCSEL," *IEEE J. Sel. Area Comm., Special Issue on "Distributed Broadband Wireless Communications,"* vol. 29, no. 6, pp. 1295–1303, Jun. 2011.

[Bel10a] **M. Beltrán** and R. Llorente, "60-GHz ultra-wideband radio-over-fiber system using a novel photonic monocycle generation," *IEEE Trans. Microw. Theory Tech.*, vol. 58, no. 6, pp. 1609–1620, Jun. 2010.

[Den11] L. Deng, **M. Beltrán**, X. Pang, X. Zhang, V. Arlunno, Y. Zhao, A. Caballero, A. Dogadaev, X. Yu, R. Llorente, D. Liu, and I. Tafur Monroy, "Fiber wireless transmission of 8.3 Gb/s/ch QPSK-OFDM signals in 75-110 GHz band," *IEEE Photon. Technol. Lett.*, vol. 24, no. 5, pp. 383–385, Mar. 2012.

[Leb11b] A. Lebedev, T. T. Pham, **M. Beltrán**, X. Yu, A. Ukhanova, R. Llorente, I. Tafur Monroy, and S. Forchhammer, "Optimization of high-definition video coding and hybrid fiber-wireless transmission in the 60 GHz band," *Opt. Express*, vol. 19, no. 26, pp. B895-B904, Dec. 2011.

[Car11] J. Caraquitena, **M. Beltrán**, R. Llorente, J. Martí, and M. A. Muriel, "Spectral self-imaging effect by time-domain multilevel phase modulation of a periodic pulse train," *Opt. Lett.*, vol. 36, no. 6, pp. 858–860, Mar. 2011.

[Par10] M. C. Parker, S. D. Walker, R. Llorente, M. Morant, **M. Beltrán**, I. Möllers, D. Jäger, C. Vázquez, D. Montero, I. Librán, S. Mikroulis, S. Karabetsos, and A. Bogris, "Radio-over-fibre technologies arising from the building the future optical network in Europe (BONE) project," *IET Optoelectron.*, S*pecial Issue on "Next Generation of Optical Access,"* vol. 4, no. 6, pp. 247−259, Dec. 2010.

[Llo08c] R. Llorente, T. Alves, M. Morant, **M. Beltrán**, J. Pérez, A. Cartaxo, and J. Marti, "Ultra-wideband radio signals distribution in FTTH networks," *IEEE Photon. Technol. Lett.*, vol. 20, no. 11, pp. 945–947, Jun. 2008.

Book chapters

[Llo11a] R. Llorente, **M. Beltrán**, and M. Morant (2011). UWB-over-Fibre in Next-generation Access Networks, Ultra Wideband Communications: Novel Trends - System, Architecture and Implementation, Mohammad Matin (Ed.), ISBN: 978-953-307-461-0, InTech, Available from: http://www.intechopen.com/articles/show/title/uwb-over-fibre-technology-performance-and-next-generation-applications

[Llo10a] R. Llorente and **M. Beltrán** (2010). Radio-over-Fibre Techniques and Performance, Frontiers in Guided Wave Optics and Optoelectronics, Bishnu Pal (Ed.), ISBN: 978-953-7619-82-4, InTech, Available from: http://sciyo.com/articles/show/title/radio-over-fibre-techniques-and-performance

Conferences

[Llo12] R. Llorente, **M. Beltrán**, M. Morant, and E. Pellicer, "Cost and Energy Efficient Multi-standard OFDM Integrated Optical Access and In-building Network Architecture," in *International Conference on Transparent Optical Networks (ICTON)*, Coventry, England, Jul. 2012. **Invited paper.**

[Bel12] **M. Beltrán**, L. Deng, X. Pang, X. Zhang, V. Arlunno, Y. Zhao, X. Yu, R. Llorente, D. Liu, and I. Tafur Monroy, "38.2-Gb/s Optical-wireless transmission in 75-110 GHz based on electrical OFDM with optical comb expansion," in *Optical Fiber Communication Conference and Exposition (OFC)*, Los Angeles, USA, Mar. 2012, paper OM2B.2.

[Llo11b] R. Llorente, S. Walker, I. Tafur Monroy, **M. Beltrán**, M. Morant, T. Quinlan, and J. B. Jensen, "Triple-play and 60-GHz radio-over-fibre techniques for next-generation optical access networks," in *European Conference on Networks and Optical Communications (NOC)*, Newcastle upon Tyne, United Kingdom, Jul. 2011, pp. 16–19. **Invited paper.**

[Bel10c] **M. Beltrán**, J. B. Jensen, X. Yu, R. Llorente, and I. Tafur Monroy, "Experimental performance comparison of 60 GHz DCM OFDM and impulse BPSK ultra-wideband with combined optical fibre and wireless transmission," in *European Conference and Exhibition on Optical Communication (ECOC)*, Torino, Italy, Sept. 2010, paper Th.9.B.3.

[Llo10b] R. Llorente, M. Morant, and **M. Beltrán**, “Optical technologies for multi-Gbit/s ultra-wideband radio: From the access to the pico-cell,” in *International Conference on Transparent Optical Networks (ICTON)*, Munich, Germany, Jun. 2010, paper We.A3.3. **Invited paper.**

[Bel10b] **M. Beltrán** and R. Llorente, "Optical generation with FTTH transmission of 60 GHz impulse-radio ultra-wideband signals," in *Access Networks and In-house Communications (ANIC)*, Karlsruhe, Germany, Jun. 2010, paper AWC7.

[Bel09c] **M. Beltrán**, R. Sambaraju, A. La Porta, R. Llorente, and J. Perez, "Photonic generation and envelope detection of millimeter-wave ultrawideband impulse-radio employing Mach-Zehnder modulators," in *IEEE International Conference on Ultra-Wideband (ICUWB)*, Vancouver, Canada, Sept. 2009, pp. 428–432.

[Llo09a] R. Llorente, M. Morant, and **M. Beltrán**, “Ultra-wideband radio-over-fibre in transparent optical networks,” in *International Conference on Transparent Optical Networks (ICTON)*, Azores, Portugal, Jun. 2009, paper Tu.A5.1. **Invited paper.**

[Bel09b] **M. Beltrán**, R. Llorente, R. Sambaraju, and J. Marti, “24 GHz UWB-over-fiber system for simultaneous vehicular radar and communications,” in *Proc. ICT-MobileSummit*, Santander, Spain, Jun. 2009.

[Bel09a] **M. Beltrán**, R. Llorente, R. Sambaraju, and J. Marti, “60 GHz UWB-over-fiber system for in-flight communications,” in *IEEE MTT-S International Microwave Symposium (IMS)*, Boston, USA, Jun. 2009, pp. 5–8. **Finalist in the best student paper competition**.

[Bel08c] **M. Beltrán**, M. Morant, J. Perez, R. Llorente and J. Marti, “Photonic generation and frequency up-conversion of impulse-radio UWB signals,” in *IEEE Lasers and Electro-Optics Society Annual Meeting (LEOS)*, Newport Beach, USA, Nov. 2008, pp. 498–499.

[Leb11a] A. Lebedev, T. T. Pham, **M. Beltrán**, X. Yu, A. Ukhanova, L. Deng, N. Guerrero Gonzalez, R. Llorente, I. Tafur Monroy, and S. Forchhammer, “Optimization of high-definition video coding and hybrid fiber-wireless transmission in the 60 GHz band,” in *European Conference and Exhibition on Optical Communication (ECOC)*, Geneva, Switzerland, Sept. 2011, paper We.10.P1.97.

[Pha11] T. T. Pham, A. Lebedev, **M. Beltrán**, X. Yu, R. Llorente, and I. Tafur Monroy, “SMF/MMF based in-building Gigabit wireless access systems using simplified 60-GHz transceivers,” in *European Conference and Exhibition on Optical Communication (ECOC)*, Geneva, Switzerland, Sept. 2011, paper We.10.P1.111.

[Jen10] J. B. Jensen, R. Rodes, **M. Beltrán**, I. Tafur Monroy, “Shared medium 2 Gbps baseband & 2 Gbps UWB in-building converged optical/wireless network with multimode fiber and wireless transmission,” in *European Conference and Exhibition on Optical Communication (ECOC)*, Torino, Italy, Sept. 2010, paper We.7.B.4.

[Mor09] M. Morant, J. Perez, **M. Beltrán**, and R. Llorente, “Performance evaluation of in-building radio-over-fiber distribution of multi-band OFDM UWB signals,” in *IEEE International Topical Meeting on Microwave Photonics (MWP)*, Valencia, Spain, Oct. 2009, paper Th4.13.

[Per09d] J. Perez, M. Morant, **M. Beltrán**, and R. Llorente, “Performance of MB-OFDM UWB and WiMAX IEEE 802.16e converged radio-over-fiber in PON,” in *IEEE International Topical Meeting on Microwave Photonics (MWP)*, Valencia, Spain, Oct. 2009, paper Th4.41.

[Llo09b] R. Llorente, M. Morant, and **M. Beltrán**, “Photonics-aided sensing for context awareness in complex radio environments,” presented at *European Commission workshop on localization and context awareness*, Brussels, Belgium, Sept. 2009.

[Bel09d] **M. Beltrán**, M. Morant, J. Perez, and R. Llorente, "Performance evaluation of OFDM and impulse-radio ultra-wideband over fiber distribution for in building networks," in *IEEE International Conference on Ultra-Wideband (ICUWB)*, Vancouver, Canada, Sept. 2009, pp. 348–352.

[Per09c] J. Perez, **M. Beltrán**, M. Morant, L. Cavallin, and R. Llorente, “Protection margins for joint operation of WiMAX 802.16e and WiMedia-defined UWB radio in personal area networks,” in *IEEE International Conference on Ultra-Wideband (ICUWB)*, Vancouver, Canada, Sept. 2009, pp. 723–727.

[Per09b] J. Perez, M. Morant, L. Cavallin, **M. Beltrán**, R. Gaudino, and R. Llorente, “Experimental analysis of WiMedia-defined UWB and WiMAX 802.16e coexistence in personal area networks,” in *Proc. ICT-MobileSummit*, Santander, Spain, Jun. 2009.

[Per09a] J. Perez, **M. Beltrán**, M. Morant, R. Llorente, A. Rahim Biswas, R. Piesiewicz, M. Cotton, D. Führer, B. Selva, I. Bucaille, and S. Zeisberg, “Experimental analysis of 3.5 GHz WiMAX 802.16e interference in WiMedia-defined UWB radio transmissions,” in *IEEE Vehicular Technology Conference (VTC-Spring)*, Barcelona, Spain, Apr. 2009, pp. 1–5 .

[Mor08c] M. Morant, J. Perez, **M. Beltrán**, R. Llorente and J. Marti, “Integrated performance analysis of UWB wireless optical transmission in FTTH networks,” in *IEEE Lasers and Electro-Optics Society Annual Meeting (LEOS)*, Newport Beach, USA, Nov. 2008, pp. 87–88.

[Mor08b] M. Morant, R. Llorente, J. Perez, **M. Beltrán**, and Javier Marti, “Impact of pilot tone-assisted equalization in Wimedia-defined OFDM-UWB signals transmission in FTTH networks,” in *IEEE International Topical Meeting on Microwave Photonics (MWP)*, Gold Coast, Australia, Oct. 2008, pp. 217–220.

[Bel08b] **M. Beltrán**, R. Llorente, and J. Marti, “Photonic ADC technology for spectrum measurement and wireless coexistence in UCELLS project,” presented at *Walter UWB Workshop*, Ispra, Italy, Jul. 2008.

[Mor08a] M. Morant, **M. Beltrán**, J. Perez, and R. Llorente, “Impulse-radio ultra wide-band signals distribution in FTTH networks,” presented at *ISIS Network of Excellence* W*orkshop on FTTH, Wireless Communications, and their interaction*, Stockholm, Sweden, Jun. 2008.

[Llo08b] R. Llorente, J. Pérez, **M. Beltrán**, M. Morant, and J. Martí, "UWB picocell clusters: Real-time interference monitoring," in *Proc. ICT-MobileSummit*, Stockholm, Sweden, Jun. 2008.

[Bel08a] **M. Beltrán**, M. Morant, J. Perez, and R. Llorente, "UWB wireless coexistence by fibre-based photonic ADC interference monitoring," presented at *ISIS Network of Excellence* W*orkshop on FTTH, Wireless Communications, and their interaction*, Stockholm, Sweden, Jun. 2008.

[Llo08a] R. Llorente, T. Alves, M. Morant, **M. Beltrán**, J. Perez, A. Cartaxo, and J. Marti, "Optical distribution of OFDM and impulse-radio UWB in FTTH networks," in *Optical Fiber Communication Conference and Exposition (OFC)*, San Diego, USA, Feb. 2008, paper JWA109.

[Llo07] R. Llorente, J. Perez, **M. Beltrán**, and J. Marti, "Convertidores analógico-digital fotónicos: tecnología y aplicaciones en telecomunicación," in *Proc. Telecom I+D*, Valencia, Spain, Oct. 2007.

[Per07] J. Perez, **M. Beltrán**, R. Llorente, and J. Marti, "Performance evaluation of the parallel Mach-Zehnder differential linearization architecture," presented at *E-PhotonONe+ / COST 291 Summer School on Advanced optical communications systems: From short range to long haul networks*, Brest, France, Jul. 2007.

[Llo06] R. Llorente, **M. Beltrán**, J. Perez, N. Uehara, Md. Saad Khan, and J. Marti, "Long-term and short-term spectral stability characterization of supercontinuum laser sources," in *IEEE Lasers and Electro-Optics Society Annual Meeting (LEOS)*, Montreal, Canada, Nov. 2006, pp. 685–686.

Technical reports

[EURO-FOS D8.3] C. Kouloumentas, A. Maziotis, P. Bakopoulos, M. Spyropoulou, H. Avramopoulos, B. Schrenk, F. Bonada, E. Tommy, V. Polo, J. Prat, J. A. Lazaro, P. Ossieur, X. Z. Qiu, J. Bauwelinck, X. Yin, J. Seoane, D. Zibar, P. Perez, **M. Beltrán**, E. Tangdiongga, D. Erasme, C. Ware, "3rd Activity report on CE4: Next Generation Optical Access Subsystems and on related Research Topics," *ICT EURO-FOS Project Deliverable D8.3*, Apr. 2011.

[FIVER D2.6] M. Morant, T. Quinlan, R. Llorente, S. Walker, N. Medina, **M. Beltrán**, C. Rodrigues, A. Gamelas, V. Mirones, J. M. Silva, I. Freitas Oliveira, A. Ng'Oma, "CWDD integrated network architecture specification," *ICT FIVER Project Deliverable D2.6*, Dec. 2010.

[FIVER D3.4] Ł. Cywioski, A. Schmidt, R. Llorente, M. Morant, F. Martínez, J. Matres, **M. Beltrán**, J. Sánchez, M. Maestro, J. A. P. Morgado, D. D. Fonseca, A. Cartaxo, "Report on baseband and radio-over-fibre OFDM transmission impairment compensation algorithms and expected performance," *ICT FIVER Project Deliverable D3.4*, Dec. 2010.

[FIVER D3.2] A. Schmidt, D. Burggraf, T. Bartzsch, M. Morant, **M. Beltrán**, R. Llorente, T. Quinlan, M. Parker, S. Walker, P. Cluzeaud, F. Carvalho, A. Cartaxo, "Report on radio transmission coexistence requirements," *ICT FIVER Project Deliverable D3.2*, Sept. 2010.

[UCELLS D4.2] R. Llorente, **M. Beltrán**, M. Morant, J. Pérez, J. Martí, D. Meshulam, A. Cartaxo, J. Romme, H. Porte, J. Puche, J. Duplicy, T. van Waterschoot, V. Le Nir, N. Amiot, "Intermediate report on the RF, photonic subsystems, multichannel ADC and enhanced UWB terminals," *ICT UCELLS Project Deliverable D4.2*, Dec. 2009.

[UCELLS D5.1] R. Llorente, M. Morant, J. Perez, **M. Beltrán**, J. Puche, J. Romme, T. Alves, A. Cartaxo, J. Hauden, J. Duplicy, R. Bañales, V. Le Nir, B. Uguen, Y. Lostanlen, Y. Kolkovich, "Intermediate reported on the cellular-UWB laboratory platform," *ICT UCELLS Project Deliverable D5.1*, Dec. 2009.

[UCELLS D7.2] R. Llorente, J. Perez, **M. Beltrán**, M. Morant, J. Duplicy, D. Meshulam, "First report on the UWB technology evolution," *ICT UCELLS Project Deliverable D7.2*, Dec. 2009.

[UCELLS D4.1] R. Llorente, M. Morant, **M. Beltrán**, J. Perez, J. Marti, Y. Otiker, T. Danon, S. Mantel, D. Schmertz, R. Korman, T. Alves, A. Cartaxo, J. Romme, J. Hauden, H. Porte, "RF and photonic subsystem specification," *ICT UCELLS Project Deliverable D4.1*, Oct. 2008.

[UCELLS D2.1] R. Llorente, M. Morant, J. Perez, **M. Beltrán**, T. Danon, S. Mantel, D. Schmertz, Y. Otiker, J. Duplicy, J. Puche, T. van Waterschoot, V. Le Nir, T. Alves, A. Cartaxo, J. Romme, N. Amiot, B. Uguen, Y. Lostanlen, R. Bañales, "Report on cellular-UWB functionalities, real-time UWB spectrum monitoring functionalities. Photonic-ADC and radio-over-fibre architecture, suitable scenarios and technology state-of the-art," *ICT UCELLS Project Deliverable D2.1*, Oct. 2008.

[FREDIT D2.1] A. Zafra, J. Puche, V. Perales, C. Vernich, J. Pérez, **M. Beltrán**, J. L. Torralba, "Arquitectura y especificaciones del ADC fotónico," *FREDIT Project Deliverable D2.1*, Jun. 2007.

[FREDIT D2.2] **M. Beltrán**, J. Puche, "Especificaciones de la fuente láser supercontinuum," *FREDIT Project Deliverable D2.2*, Jun. 2007.

Bibliography

[1] “Revision of part 15 of the Commission’s rules regarding ultra-wideband transmission systems,” FCC, Rep. FCC 02-48, Apr. 2002.

[2] M. Kunert, G. Rollmann, H.-L. Bloecher, and J. Schuermann, “24 GHz ultra-wideband vehicular short range radar systems. Technology and regulatory aspects overview,” in International Wroclaw Symposium and Exhibition on Electromagnetic Compatibility (EMC), Jun. 2006. [Online]. Available: http://www.sara-group.org

[3] T. Kuri, Y. Omiya, T. Kawanishi, S. Hara, and K. Kitayama, “Optical transmitter and receiver of 24-GHz ultra-wideband signal by direct photonic conversion techniques,” in *IEEE International Topical Meeting on Microwave Photonics (MWP)*, pp. 1–4, Oct. 2006.

[4] A. Paier, J. Karedal, N. Czink, H. Hofstetter, C. Dumard, T. Zemen, F. Tufvesson, C. F. Mecklenbrauker, and A. F. Molisch, "First results from car-to-car and car-to-infrastructure radio channel measurements at 5.2GHZ," *IEEE International Symposium on Personal, Indoor and Mobile Radio Communications (PIMRC)*, pp. 1–5, Sept. 2007.

[5] “ECC Decision of 1 December 2006 amended 31 October 2008 on supplementary regulatory provisions to Decision ECC/DEC/(06)04 for UWB devices using mitigation techniques,” ECC, Amended ECC/DEC/(06)12, Oct. 2008.

[6] Y. Le Guennec, A. Pizzinat, S. Meyer, B. Charbonnier, P. Lombard, M. Lourdiane, B. Cabon, C. Algani, A.-L. Billabert, M. Terré, C. Rumelhard, J.-L. Polleux, H. Jacquinot, S. Bories, and C. Sillans, “Low-cost transparent radio-over-fiber system for in-building distribution of UWB signals,” *J. Lightw. Technol.*, vol. 27, no. 14, pp. 2649–2657, Jul. 2009.

[7] L. Hutcheson, “FTTx: Current status and the future”, *IEEE Commun. Mag.*, vol. 46, no. 7, pp. 90–95, Jul. 2008.

[8] WiMedia Alliance. [Online]. Available: http://www.wimedia.org

[9] “High rate ultra wideband PHY and MAC standard,” ECMA, ECMA-368, Dec. 2008.

[10] Alereon, Inc., AL5301 Chipset. [Online]. Available: http://www.alereon.com/products/chipsets/al5100al5301-chipset

[11] Wisair, Wireless USB single chip. [Online]. Available: http://www.wisair.com/products/wireless-usb-single-chip/

[12] J. Lansford, “The WiMedia UWB radio: Is it the ideal cognitive radio processor?” in *IEEE International Conference on Ultra-Wideband (ICUWB)*, pp. 173–176, Sep. 2008.

[13] D. Dardari, A. Conti, U. Ferner, A. Giorgetti, and M. Z. Win, “Ranging with ultrawide bandwidth signals in multipath environments,” *Proc. IEEE*, vol. 97, no. 2, pp. 404–426, Feb. 2009.

[14] C. Snow, “Ultra wideband communications past, present and future,” in *UBC-IEEE Workshop on Future Communication Systems*, Mar. 2007.

[15] WirelessHD, LLC. [Online]. Available: http://www.wirelesshd.org

[16] “ECMA publishes 60 GHz standard," Press release, Dec. 2008. [Online]. Available: http://www.ecma-international.org/news/PressReleases/PREcma%20publishes%2060%20GHz%20Standard.htm

[17] “Broadband Radio Access Networks (BRAN); 60 GHz Multiple-Gigabit WAS/RLAN Systems; Harmonized EN covering the essential requirements of article 3.2 of the R&TTE Directive,” ETSI, EN 302 567 v1.1.1, Mar. 2009.

[18] R. C. Daniels and R. W. Heath, “60 GHz wireless communications: Emerging requirements and design recommendations,” *IEEE Veh. Technol. Mag.*, vol. 2, no. 3, pp. 41–50, Sep. 2007.

[19] K. Grobe and J. P. Elbers, “PON in adolescence: From TDMA to WDM-PON,” *IEEE Commun. Mag.*, vol. 46, no. 1, pp. 26–34, Jan. 2008.

[20] K. Prince, J. B. Jensen, A. Caballero, X. Yu, T. B. Gibbon, D. Zibar, N. Guerrero, A. V. Osadchiy, and I. T. Monroy, “Converged wireline and wireless access over a 78-km deployed fiber long-reach WDM PON,” *IEEE Photon. Technol. Lett.*, vol. 21, no. 17, pp. 1274–1276, Sep. 2009.

[21] J. Capmany and D. Novak, “Microwave Photonics combines two worlds,” *Nature Photon.*, vol. 1, no. 6, pp. 319–330, 2007.

[22] M. Abtahi, M. Mirshafiei, S. LaRochelle, and L. A. Rusch, “All-Optical 500 Mb/s UWB Transceiver: An Experimental Demonstration,” *J. Lightwave Technol.*, vol. 26, no. 15, pp. 2795–2802, Aug. 2008.

[23] X. Chen and S. Kiaei, "Monocycle shapes for ultra wideband system," *IEEE International Symposium on Circuits and Systems (ISCAS)*, vol. 1, pp. I-597− I-600, Aug. 2002.

[24] S. Pan and J. Yao, “Photonic generation of chirp-free UWB signals for UWB over fiber applications,” in *IEEE International Topical Meeting on Microwave Photonics (MWP)*, pp. 1–4, Oct. 2009.

[25] M. Hanawa, K. Mori, K. Nakamura, A. Matsui, Y. Kanda, and K. Nonaka, ”Dispersion tolerant UWB-IR-over-fiber transmission under FCC indoor spectrum mask,” in *Optical Fiber Communication Conference and Exposition (OFC)*, Paper OTuJ, Mar. 2009.

[26] X. Yu, X. Yin, T. B. Gibbon, and I. T. Monroy, "Simultaneous transmission of 256-QAM WIMAX at 5.7GHz and optically generated impulse radio UWB over fiber for indoor wireless multi-services," in *Optical Fiber Communication Conference (OFC),* Paper JThA36, Mar. 2010.

[27] H. Sheng, P. Orlik, A. M. Haimovich, L. J. Cimini, and Jr. J. Zhang, “On the spectral and power requirements for ultra-wideband transmission,” in *IEEE International Conference on Communications (ICC)*, pp. 738–742, May 2003.

[28] S. T. Abraha, C. Okonkwo, H. Yang, D. Visani, Y. Shi, H.-D. Jung, E. Tangdiongga, and T. Koonen, “Performance evaluation of IR-UWB in short-range fiber communication using linear combination of monocycles,” *J. Lightwave Technol.*, vol. 29, no. 8, pp. 1143–1151, Apr. 2011.

[29] S. T. Abraha, C. M. Okonkwo, E. Tangdiongga, and A. M. J. Koonen, “Power-efficient impulse radio ultrawideband pulse generator based on the linear sum of modified doublet pulses,” *Opt. Lett.*, vol. 36, no. 12, pp. 2363–2365, Jun. 2011.

[30] M. Jazayerifar, B. Cabon, and J. A. Salehi, “Transmission of multi-band OFDM and impulse radio ultra-wideband signals over single mode fiber,” *J. Lightwave Technol.*, vol. 26, no. 15, pp. 2594–2603, Aug. 2008.

[31] Y. Zhu, J. E. Zuegel, J. R. Marciante, and H. Wu, “Distributed waveform generator: A new circuit technique for ultra-wideband pulse generation, shaping and modulation,” *IEEE J. Solid-State Circuits*, vol. 44, no. 3, pp. 808–823, Mar. 2009.

[32] P. Protiva, J. Mrkvica, and J. Macháč, “Ultra-wideband pulse waveform generation based on combining subnanosecond Gaussian pulses,“ *Microw. Opt. Technol. Lett.*, vol. 52, no. 11, pp. 2401–2405, Nov. 2010.

[33] B. McLaughlin, “A guide to using Picosecond Pulse Labs generators in UWB applications,” Picosecond Pulse Labs, Mar. 2004. [Online]. Available: http://www.picosecond.com

[34] T. Kikkawa, P. K. Saha, N. Sasaki, and K. Kimoto, “Gaussian monocycle pulse transmitter using 0.18 µm CMOS technology with on-chip integrated antennas for inter-chip UWB communication,” *IEEE J. Solid-State Circuits*, vol. 43, no. 5, pp. 1303–1312, May 2008.

[35] J. P. Yao, F. Zeng, and Q. Wang, “Photonic generation of ultra-wideband signals,” *J. Lightw. Technol.*, vol. 25, no. 11, pp. 3219–3235, Nov. 2007.

[36] V. T. Company, K. Prince, and I. T. Monroy, “Fiber transmission and generation of ultrawideband pulses by direct current modulation of semiconductor lasers and chirp-to-intensity conversion,” *Opt. Lett.*, vol. 33, no. 3, pp. 222–224, Feb. 2008.

[37] F. Zeng and J. Yao, “Ultrawideband impulse radio signal generation using a high-speed electrooptic phase modulator and a fiber-Bragg-grating-based frequency discriminator,” *IEEE Photon. Technol. Lett.*, vol. 18, no. 19, pp. 2062–2064, Oct. 2006.

[38] F. Zeng, Q. Wang, and J. P. Yao, “All-optical UWB impulse generation based on cross-phase modulation and frequency discrimination,” *Electron. Lett.*, vol. 43, no. 2, pp. 121–122, Jan. 2007.

[39] Q. Wang and J. P. Yao, “An electrically switchable optical ultra-wideband pulse generator,” *J. Lightw. Technol.*, vol. 25, no. 11, pp. 3626–3633, Nov. 2007.

[40] Q. Chang, Y. Tian, T. Ye, J. Gao, and Y. Su, “A 24-GHz ultrawideband over fiber system using photonic generation and frequency up-conversion,” *IEEE Photon. Technol. Lett.*, vol. 20, no. 19, pp. 1651–1653, Oct. 2008.

[41] Q. Wang and J. P. Yao, “Optically switchable UWB monocycle and doublet generation using a reconfigurable photonic microwave delay-line filter,” *Opt. Express*, vol. 15, no. 22, pp. 14667–14672, Oct. 2007.

[42] H. Chen, M. Chen, T. Wang, M. Li, and S. Xie, “Methods for ultra-wideband pulse generation based on optical cross-polarization modulation,” *J. Lightw. Technol.*, vol. 26, no. 15, pp. 2492–2499, Aug. 2008.

[43] M. Bolea, J. Mora, B. Ortega, and J. Capmany, “Optical UWB pulse generator using an N tap microwave photonic filter and phase inversion adaptable to different pulse modulation formats,” *Opt. Express*, vol. 17, no. 7, pp. 5023–5032, Mar. 2009.

[44] F. Zhang, S. Fu, J. Wu, N. Q. Ngo, K. Xu, Y. Li, X. Hong, P. Shum, and J. Lin, “UWB impulse radio transmitter using an electrooptic phase modulator together with a delay interferometer,” *IEEE Photon. Technol. Lett.*, vol. 22, no. 20, pp. 1479–1481, Oct. 2010.

[45] J. Dong, X. Zhang, J. Xu, and D. Huang, “All-optical ultrawideband monocycle generation utilizing gain saturation of a dark return-to-zero signal in a semiconductor optical amplifier,” *Opt. Lett.*, vol. 32, no. 15, pp. 2158–2160, Aug. 2007.

[46] V. T. Company, K. Prince, and I. T. Monroy, “Ultrawideband pulse generation based on overshooting effect in gain-switched semiconductor laser,” *IEEE Photon. Technol. Lett.*, vol. 20, no. 15, pp. 1299–1301, Aug. 2008.

[47] X. Yu, T. B. Gibbon, M. Pawlik, S. Blaaberg, and I. T. Monroy, “A photonic ultra-wideband pulse generator based on relaxation oscillations of a semiconductor laser,” *Opt. Express*, vol. 17, no. 12, pp. 9680–9687, Jun. 2009.

[48] T. B. Gibbon, X. Yu; R. Gamatham, N. Guerrero Gonzalez, R. Rodes, J. B. Jensen, A. Caballero, I. T. Monroy, “3.125 Gb/s impulse radio ultra-wideband photonic generation and distribution over a 50 km fiber with wireless transmission,” *IEEE Microw. Wireless Compon. Lett.*, vol. 20, no. 2, pp. 127–129, Feb. 2010.

[49] X. Yu, T. B. Gibbon, and I. T. Monroy, I. T. “Experimental demonstration of all-optical 781.25-Mb/s binary phase-coded UWB signal generation and transmission,” *IEEE Photon. Technol. Lett.*, vol. 21, no. 17, pp. 1235–1237, Sep. 2009.

[50] J. D. McKinney, I. S. Lin, and A. M. Weiner, “Shaping the power spectrum of ultra-wideband radio-frequency signals,” *IEEE Trans. Microw. Theory Tech.*, vol. 54, no. 12, pp. 4247–4255, Dec. 2006.

[51] C. Wang and J. P. Yao, “Simultaneous optical spectral shaping and wavelength-to-time mapping for photonic microwave arbitrary waveform generation,” *IEEE Photon. Technol. Lett.*, vol. 21, no. 12, pp. 793–795, Jun. 2009.

[52] M. Abtahi and L. A. Rusch, “RoF delivery over PONs of optically shaped UWB signals for gigabit/s wireless distribution in the home,” *IEEE J. Sel. Areas Comm., Special Issue on “Distributed Broadband Wireless Communications,”* vol. 29, no. 6, pp. 1304–1310, Jun. 2011.

[53] A. Zadok, X. Wu, J. Sendowski, A. Yariv, and A. E. Willner, “Reconfigurable generation of high-order ultra-wideband waveforms using edge detection,” *J. Lightw. Technol.*, vol. 28, no. 16, pp. 2207–2212, Aug. 2010.

[54] E. Zhou, X. Xu, K. Lui, and K. K. Wong, "High-speed photonic power-efficient ultra-wideband transceiver based on multiple PM-IM conversions," *IEEE Trans. Microw. Theory Tech.*, vol. 58, no. 11, pp. 3344–3351, Nov. 2010.

[55] H. Shams, A. Kaszubowska-Anandarajah, P. Perry, L. P. Barry, "Optical generation, fiber distribution and air transmission for ultra wide band over fiber system," in *Optical Fiber Communication Conference and Exposition (OFC)*, Paper OWR, Mar. 2009.

[56] H. Shams, A. Kaszubowska-Anandarajah, P. Perry, P. Anandarajah, and L. P. Barry, "Electro-optical generation and distribution of ultrawideband signals based on the gain switching technique," *J. Opt. Commun. Netw.*, vol. 2, no. 3, pp. 122–130, Mar. 2010.

[57] S. Pan and J. Yao, "UWB-over-fiber communications: Modulation and transmission," *J. Lightw. Technol.*, vol. 28, no. 16, pp. 2445–2455, Aug. 2010.

[58] H. Schmuck, "Comparison of optically millimeter-wave system concepts with regard to chromatic dispersion," *Electron. Lett.*, vol. 31, no. 21, pp. 1848–1849, 1995.

[59] C. W. Chow, F. M. Kuo, J. W. Shi, C. H. Yeh, Y. F. Wu, C. H. Wang, Y. T. Li, and C. L. Pan, "100 GHz ultra-wideband (UWB) fiber-to-the-antenna (FTTA) system for in-building and in-home networks," *Opt. Express*, vol. 18, no. 2, pp. 473–478, Jan. 2010.

[60] Y. Le Guennec and R. Gary, "Optical frequency conversion for millimeter-wave ultra-wideband-over-fiber systems," *IEEE Photon. Technol. Lett.*, vol. 19, no. 13, pp. 996–998, Jul.2007.

[61] S. Fu, W. Zhong, Y. J.Wen, and P. Shum, "Photonic monocycle pulse frequency up-conversion for ultrawideband-over-fiber applications," *IEEE Photon. Technol. Lett.*, vol. 20, no. 12, pp. 1006–1008, Jun. 2008.

[62] J. Li, Y. Liang, and K. Kin-Yip Wong, "Millimeter-wave UWB signal generation via frequency up-conversion using fiber optical parametric amplifier," *IEEE Photon. Technol. Lett.*, vol. 21, no. 17, pp. 1172–1174, Sep. 2009.

[63] H. C. Chien, A. Chowdhury, Z. Jia, Y. T. Hsueh, and G. K. Chang, "60 GHz millimeter-wave gigabit wireless services over long-reach passive optical network using remote signal regeneration and upconversion," *Opt. Express*, vol. 17, no. 5, pp. 3036–3041, Mar. 2009.

[64] F. Zhang, J. Wu, S. Fu, K. Xu, Y. Li, X. Hong, P. Shum, and J. Lin, "Simultaneous multi-channel CMW-band and MMW-band UWB monocycle pulse generation using FWM effect in a highly nonlinear photonic crystal fiber," *Opt. Express*, vol. 18, no. 15, pp. 15870–15875, Jul. 2010.

[65] K. Nakamura, M. Hanawa, and K. Nonaka, "24GHz-band UWB-IR pulse generation using optical signal processing," in *OptoElectronics and Communications Conference (OECC)*, Paper ThD2, Jul. 2009.

[66] N. Deparis, A. Siligarisy, P. Vincenty, and N. Rolland, "A 2 pJ/bit pulsed ILO UWB transmitter at 60 GHz in 65-nm CMOS-SOI," in *IEEE International Conference on Ultra-Wideband (ICUWB)*, pp. 113–117, Sep. 2009.

[67] Y. M. Chang, J. Lee, D. Koh, H. Chung, and J. H. Lee, "Ultrawideband doublet pulse generation based on a semiconductor electroabsorption modulator and its distribution over a fiber/wireless link," *J. Opt. Commun. Netw.*, vol. 2, no. 8, pp. 600–608, Aug. 2010.

[68] T. B. Gibbon, X. Yu, and I. T. Monroy, "Photonic ultra-wideband 781.25-Mb/s signal generation and transmission incorporating digital signal processing detection," *IEEE Photon. Technol. Lett.*, vol. 21, no. 15, pp. 1060–1062, Aug. 2009.

[69] T. Mizuochi. Forward Error Correction, High Spectral Density Optical Communication Technologies, Optical and Fiber Communications Reports, vol. 6, Part 3, pp. 303-333, 2010, M. Nakazawa *et al.* (Eds.), ISBN: 978-3-642-10419-0, Springer Berlin Heidelberg, Available from: http://dx.doi.org/10.1007/978-3-642-10419-0_17

[70] R. A. Shafik, S. Rahman, and A. H. M. Razibul Islam, "On the extended relationships among EVM, BER and SNR as performance metrics," in *International Conference on Computer and Electrical Engineering (ICCEE)*, pp. 408–411, Dec. 2006.

[71] M. Morant, J. Pérez, R. Llorente, and J. Marti, "Combined analysis of OFDM-UWB transmission in hybrid wireless-optical access networks," *IEEE Photon. Technol. Lett.*, vol. 21, no. 19, pp. 1378–1380, Oct. 2009.

[72] M. N. Sakib, B. Hraimel, X. Zhang, M. Mohamed, W. Jiang, K. Wu, and D. Shen, "Impact of optical transmission on multiband OFDM ultra-wideband wireless system with fibre distribution," *J. Lightw. Technol.*, vol. 27, no. 18, pp. 4112–4123, Sep. 2009.

[73] M. P. Thakur, T. J. Quinlan, C. Bock, S. D. Walker, M. Toycan, S. E. M. Dudley, D. W. Smith, A. Borghesani, D. Moodie, M. Ran, and Y. Ben-Ezra, "480-Mbps, bi-directional, ultra-wideband radio-over-fiber transmission using a 1308/1564-nm reflective electro-absorption transducer and commercially available VCSELs," *J. Lightw. Technol.*, vol. 27, no. 3, pp. 266–272, Feb. 2009.

[74] C. Lethien, C. Loyez, J. P. Vilcot, R. Kassi, N. Rolland, C. Sion, and P. A. Rolland, "Review of glass and polymer multimode fibers used in a Wimedia ultrawide band MB-OFDM radio over fiber system," *J. Lightw. Technol.*, vol. 27, no. 10, pp. 1320–1331, May 2009.

[75] M. Mohamed, X. Zhang, B. Hraimel, and K. Wu, "Optical generation of millimeter-wave multiband OFDM ultra-wideband wireless signal and distribution over fiber," *IEEE Photon. Technol. Lett.*, vol. 22, no. 15, pp. 1180–1182, Aug. 2010.

[76] G. H. Nguyen, B. Cabon, and Y. Le Guennec, "Generation of 60-GHz MB-OFDM signal-over-fiber by up-conversion using cascaded external modulators," *J. Lightw. Technol.*, vol. 27, no. 11, pp. 1496–1502, Jun. 2009.

[77] J. Perez, M. Morant, R. Llorente, and J. Martí, "Joint distribution of polarization-multiplexed UWB and WiMAX radio in PON," *J. Lightw. Technol.,* vol. 27, no. 12, pp. 1912–1919, Jun. 2009.

[78] M. Morant, T. Quinlan, R. Llorente, and S. Walker, "Full standard triple-play bi-directional and full-duplex CWDM transmission in passive optical networks," in *Optical Fiber Communication Conference and Exposition (OFC)*, Paper OWB3, Mar. 2011.

[79] M. Morant, T. Quinlan, S. Walker, and R. Llorente, ""Real world" FTTH optical-to-radio interface performance for bidirectional multi-format OFDM wireless signal transmission," in *Optical Fiber Communication Conference and Exposition (OFC)*, Paper NTuB6, Mar. 2011.

[80] M. Morant, T. Quinlan, A. Ng'oma, S. Dudley, S. Walker, and R. Llorente, "Specialty fiber evaluation for in-building distribution of multiple-format OFDM radio signals," in *Optical Fiber Communication Conference and Exposition (OFC)*, Paper JWA16, Mar. 2011.

[81] Y. Shi, D. Visani, C. M. Okonkwo, H. P. A. van den Boom, G. Tartarini, E. Tangdiongga, and A. M. J. Koonen, "Simultaneous transmission of wired and wireless services over large core POF for in-home networks," in *European Conference and Exhibition on Optical Communication (ECOC)*, Paper Tu.3.C.5, Sep. 2011.

[82] Z. Bouhamri, Y. Le Guennec, J.–M. Duchamp, G. Maury, A. Schimpf, V. Dobremez, L. Bidaux, and B. Cabon, "Multistandard transmission over plastic optical fiber," *IEEE Trans. Microw. Theory Tech.*, vol. 58, no. 11, pp. 3109–3116, Nov. 2010.

[83] R. Freund, M. Nölle, C. Schmidt-Langhorst, R. Ludwig, C. Schubert, G. Bosco, A. Carena, P. Poggiolini, L. Oxenløwe, M. Galili, H. C. Hansen Mulvad, M. Winter, D. Hillerkuss, R. Schmogrow, W. Freude, J. Leuthold, A. D. Ellis, F. C. Garcia Gunning, J. Zhao, P. Frascella, S. K. Ibrahim, and N. Mac Suibhne, "Single- and multi-carrier techniques to build up Tb/s per channel transmission systems," in *International Conference on Transparent Optical Networks (ICTON)*, Paper Tu.D1.4, Jul. 2010.

[84] S. Sarkar, S. Dixit, and B. Mukherjee, "Hybrid wireless-optical broadband-access network (WOBAN): A review of relevant challenges," *J. Lightw. Technol.*, vol. 25, no. 11, pp. 3329–3340, Nov. 2007.

[85] A. Stöhr, "10 Gbit/s wireless transmission using millimeter-wave over optical fiber systems," in *Optical Fiber Communication Conference and Exposition (OFC)*, Paper OTuO3, Mar. 2011.

[86] J. Wells, "Faster than fiber: The future of multi-Gb/s wireless," *IEEE Microw. Mag.*, vol. 10, no. 3, pp.104–112, May 2009.

[87] AOptix Technologies, Inc., Wireless Communications. [Online]. Available: http://www.aoptix.com

[88] K.-D. Langer and J. Vučić, "Optical wireless indoor networks: recent implementation efforts," in *European Conference and Exhibition on Optical Communication (ECOC)*, Paper We.6.B.1, Sep. 2010.

[89] H. Elgala, R. Mesleh, and H. Haas, "Indoor optical wireless communication: potential and state-of-the-art," *IEEE Commun. Mag.*, pp. 56–62, Sep. 2011.

[90] K. Wang, A. Nirmalathas, C. Lim, and E. Skafidas, "Experimental demonstration of a full-duplex indoor optical wireless communication system," *IEEE Photon. Technol. Lett.*, vol. 24, no. 3, pp. 188–190, Feb. 2012.

[91] J. Vučić, C. Kottke, K. Habel, and K.-D. Langer, "803 Mbit/s visible light WDM link based on DMT modulation of a single RGB LED luminary," in *Optical Fiber Communication Conference and Exposition (OFC)*, Paper OWB6, Mar. 2011.

[92] T. Lunttila, S. Iraji, and H. Berg, "Advanced coding schemes for a multiband OFDM ultrawideband system towards 1 Gbps," in *IEEE Consumer Communications and Networking Conference (CCNC)*, pp. 553–557, Jan. 2006.

[93] V. Dyadyuk, J. D. Bunton, J. Pathikulangara, R. Kendall, O. Sevimli, L. Stokes, and D. A. Abbott, "A multigigabit millimeter-wave communication system with improved spectral efficiency," *IEEE Trans. Microw. Theory Tech.*, vol. 55, no. 12, pp. 2813–2821, Dec. 2007.

[94] T. Nagatsuma, T. Takada , H. –J. Song , K. Ajito , N. Kukutsu , and Y. Kado, "Millimeter- and THz-wave photonics towards 100-Gbit/s wireless transmission," in *IEEE Photonics Society Annual Meeting*, pp. 385–386, Nov. 2010.

[95] A. Hirata, R. Yamaguchi, T. Kosugi, H. Takahashi, K. Murata, T. Nagatsuma, N. Kukutsu, Y. Kado, N. Iai, S. Okabe, H. Ikegawa, H. Nishikawa, T. Nakayama, and T. Inada, "10-Gbit/s wireless link using InP HEMT MMICs for generating 120-GHz-Band millimeter-wave signal," *IEEE Trans. Microw. Theory Tech.*, vol. 57, no. 5, pp. 1102–1109, May 2009.

[96] J. Armstrong, "OFDM for optical communications," *J. Lightw. Technol.*, vol. 27, no. 3, pp. 189–204, Feb. 2009.

[97] M. Serbay, C. Wree, and W. Rosenkranz, "Experimental investigation of RZ-8DPSK at 3×10.7 Gb/s," in *IEEE Lasers and Electro-Optics Society Annual Meeting (LEOS)*, pp. 483–484, Oct. 2005.

[98] P. J. Winzer and R. J. Essiambre, "Advanced modulation formats for high-capacity optical transport networks," *J. Lightw. Technol.*, vol. 24, no. 12, pp. 4711–4728, Dec. 2006.

[99] IMEC Research Center, Belgium. Ultra-low-power radio. [Online]. Available: http://www.imec.be/ScientificReport/SR2007/html/1384152.html

[100] Pulse~LINK Inc., Wireless HDMI Reference Design (PL3304 RDK) [Online]. Available: http://www.pulselink.net/

[101] R. Giuliano and F. Mazzenga, "On the coexistence of power-controlled ultrawide-band systems with UMTS, GPS, DCS1800, and fixed wireless systems," *IEEE Trans. Veh. Technol.*, vol. 54, no. 1, pp. 62–81, Jan. 2005.

[102] D. R. McKinstry and R. M. Buehrer, "Issues in the performance and covertness of UWB communications systems," in *IEEE International Midwest Symposium on Circuits and Systems (MWSCAS)*, vol. 3, pp. 601–604, Aug. 2002.

[103] M. Z. Win and R. A. Scholtz, "On the robustness of ultra-wide bandwidth signals in dense multipath environments," *IEEE Commun. Lett.*, vol. 2, no. 2, pp. 51–53, Feb. 1998.

[104] A. F. Molisch, “Ultrawideband propagation channels-theory, measurement, and modeling,” *IEEE Trans. Veh. Technol.*, vol. 54, no. 5, pp. 1528–1545, Sept. 2005.

[105] H. Gelke, “Wireless 480 Mbit/s UWB link for embedded systems,” Aug. 2009. [Online]. Available: http://www.ines.zhaw.ch/uwbmac

[106] S. Hanna, "Ultra-wideband rules in Canada and worldwide," Keynote speech at the *IEEE International Conference on Ultra-Wideband (ICUWB)*, Sep. 2009. [Online]. Available: http://www.icuwb2009.org/UWB-Rules.pdf

[107] “Electromagnetic compatibility and Radio spectrum Matters (ERM); Short Range Devices (SRD) using Ultra Wide Band technology (UWB) for communications purposes; Harmonized EN covering the essential requirements of article 3.2 of the R&TTE Directive,” ETSI, EN 302 065 v1.2.1, Oct. 2010.

[108] “UWB (Ultra-WideBand) Radio System,” ARIB, STD-T91 v1.1, Sept. 2008.

[109] “Commission Decision of 17 January 2005 on the harmonisation of the 24 GHz range radio spectrum band for the time-limited use by automotive short-range radar equipment in the Community,” EC, 2005/50/EC, Jan. 2005.

[110] “Commission Decision 2011/485/EU amending Decision 2005/50/EC of 17 January 2005 on the harmonisation of the 24 GHz range radio spectrum band for the time-limited use by automotive short-range radar equipment in the Community,” ECC, 2011/485/EU, Jul. 2011.

[111] “Development of ultra wideband radio system for short-range applications,” Furukawa Review No. 37, 2010.

[112] S. Pan and J. Yao, “Performance evaluation of UWB signal transmission over optical fiber,” *IEEE J. Sel. Areas Comm.*, vol. 28, no. 6, pp. 889–900, Aug. 2010.

[113] Y. P. Nakache and A. F. Molisch, “Spectral shape of UWB signals - influence of modulation format, multiple access scheme and pulse shape,” *IEEE Vehicular Technology Conference (VTC-Spring)*, vol. 4, pp. 2510–2514, Apr. 2003.

[114] “Radiocommunications (Low Interference Potential Devices) Class Licence 2000,” ComLaw F2009C00545, Jul. 2009.

[115] “Operation within the band 57–64 GHz,” FCC, Rep. FCC 15.255, Oct. 2002.

[116] “Low-power Licence-exempt Radiocommunication Devices (All Frequency Bands): Category I Equipment,” IC RSS-210, Jun. 2007.

[117] “Millimeter-Wave Data Transmission Equipment for Specified Low Power Radio Station (Ultra High Speed Wireless LAN System),” ARIB, STD-T74 v1.1, Nov. 2005.

[118] D. Murph, “Wi-Fi Alliance and WiGig sync up for 60GHz WiFi,” May 2010. [Online]. Available: http://www.engadget.com/2010/05/10/wi-fi-alliance-and-wigig-sync-up-for-60ghz-wifi/

[119] “802.15.3c-2009, IEEE Standard for Information technology - Telecommunications and information exchange between systems - Local and metropolitan area networks - Specific requirements. Part 15.3: Wireless Medium Access Control (MAC) and Physical Layer (PHY) Specifications for High Rate Wireless Personal Area Networks (WPANs) Amendment 2: Millimeter-wave-based Alternative Physical Layer Extension,” Oct. 2009.

[122] Wireless Gigabit Alliance. [Online]. Available: http://wirelessgigabitalliance.org

[121] A. J. Seeds and K. J. Williams, “Microwave photonics,” *J. Lightw. Technol.*, vol. 24, no. 12, pp. 4628–4641, Dec. 2006.

[122] D. Jager, and A. Stohr, “Microwave Photonics,” in *European Microwave Conference (EuMC)*, pp. 1–4, Sep. 2001.

[123] Meryll Lynch, “Telecom services-wireless/cellular,” 2007. [Online]. Available: http://www.scribd.com/doc/7656725/ML-Data-Growth

[124] T. E. Darcie and G. E. Bodeep, “Lightwave subcarrier CATV transmission systems,” *IEEE Trans. Microw. Theory Tech.*, vol. 38, no. 5, pp. 524–533, May 1990.

[125] B. Wilson, Z. Ghassemlooy, and I. Darwazeh, Analogue Optical Fibre Communications, Institution of Engineering and Technology, Aug. 1995, ISBN 978-0852968321.

[126] H. Ogawa, D. Polifko, and S. Banba, ”Millimetre-wave fibre optic systems for personal radio communication,” *IEEE Trans. Microw. Theory Tech.*, vol. 40, no. 12, pp. 2285–2293, Dec. 1992.

[127] K.-A. Persson, C. Carlsson, A. Alping, A. Haglund, J. S. Gustavsson, P. Modh, and A. Larsson, “WCDMA radio-over-fibre transmission experiment using singlemode VCSEL and multimode fibre,” *Electron. Lett.*, vol. 42, no. 6, pp. 372–374, Mar. 2006.

[128] M. Y. W. Chia, B. Luo, M. L. Yee, and E. J. Z. Hao, “Radio over multimode fibre transmission for wireless LAN using VCSELs,” *Electron. Lett.*, vol. 39, no. 15, pp. 1143–1144, Jul. 2003.

[129] T. Niiho, M. Nakaso, K. Masuda, H. Sasai, K. Utsumi, and M. Fuse, “Multi-channel wireless LAN distributed antenna system based on radio-over-fibre techniques,” in *IEEE Lasers and Electro-Optics Society Annual Meeting (LEOS)*, pp. 57–58, Nov. 2004.

[130] A. Nkansah, A. Das, C. Lethien, J.-P. Vilcot, N. J. Gomes, I. J. Garcia, J. C. Batchelor, and D. Wake, “Simultaneous dual band transmission over multimode fibre-fed indoor wireless network,” *IEEE Microw. Wireless Comp. Lett.*, vol. 16, no. 11, pp. 627–629, Nov. 2006.

[131] H. Pfrommer, M. A. Piqueras, V. Polo, J. Herrera, A. Martinez, and J. Marti, “Radio-over-fibre architecture for simultaneous feeding of 5.5 and 41 GHz WiFi or 4G access networks,” in *IEEE MTT-S International Microwave Symposium (IMS)*, pp. 301–303, Jun. 2006.

[132] I. Rivas, and L. B. Lopes, “A microcellular DCA scheme using variable channel exclusion zones,” in *IEEE Vehicular Technology Conference (VTC)*, pp. 1395–1399, May 1998.

[133] A. Cassini and P. Faccin, “Wavelength division multiplation technologies for UMTS radio coverage extension by using the radio over fibre technique,” in *IEEE International Topical Meeting on Microwave Photonics (MWP)*, pp. 123–128, Sep. 2003.

[134] X. Qian, P. Hartmann, J. D. Ingham, R. V. Penty, and I. H, White, “Directly-modulated photonic devices for microwave applications,” in *IEEE MTT-S International Microwave Symposium (IMS)*, pp. 4, Jun. 2005.

[135] M. Müller, W. Hofmann, T. Gründl, M. Horn, P. Wolf, R. D. Nagel, E. Rönneberg, G. Böhm, D. Bimberg, and M. –C. Amann, “1550-nm high-speed short-cavity VCSELs,” *IEEE J. Sel. Top. Quantum Electron.*, vol. 17, no. 5, pp. 1158–1166, Sep./Oct. 2011.

[136] K. Noguchi, O. Mitomi, and H. Miyazawa, “Millimeter-wave Ti: LiNbO3 optical modulators,” *J. Lightw. Technol.*, vol. 16, no. 4, pp. 615–619, Apr. 1998.

[137] J. Mallari, C. Wei, D. Jin, G. Yu, A. Barklund, E. Miller, P. O’Mathuna, R. Dinu, A. Motafakker-Fard, and B. Jalali, “100Gbps EO polymer modulator product and its characterization using a real-time digitizer,” in *Optical Fiber Communication Conference (OFC)*, Paper OThU2, Mar. 2010.

[138] M. Chacinski, U. Westergren, L. Thylén, R. Schatz, Jie Li, A. Djupsjöbacka, B. Stoltz, "Modulation and chirp evaluation of 100 GHz DFB-TWEAM," in *European Conference and Exhibition on Optical Communication (ECOC)*, Paper Mo.1.F.2, Sep. 2010.

[139] T. Nagatsuma and H. Ito, High-Power RF Uni-Traveling-Carrier Photodiodes (UTC-PDs) and Their Applications, Advances in Photodiodes, Gian Franco Dalla Betta (Ed.), ISBN: 978-953-307-163-3, InTech, Available from: http://www.intechopen.com/articles/show/title/high-power-rf-uni-traveling-carrier-photodiodes-utc-pds-and-their-applications

[140] P.-T. Shih, A. Ng’oma, C. –T. Lin, F. Annunziata , J. Chen , J. George , M. Sauer, and S. Chi, “2×21 Gbps symmetrical full-duplex transmission of OFDM wireless signals over a bidirectional IMDD radio-over-fiber system at 60 GHz,” in *European Conference and Exhibition on Optical Communication (ECOC)*, Paper Th.9.B.4, Sep. 2010.

[141] G. H. Smith, D. Novak, and Z. Ahmed, “Overcoming chromatic-dispersion effects in fiber-wireless systems incorporating external modulators,” *IEEE Trans. Microw. Theory Tech.*, vol. 45, no. 8, pp. 1410–1415, Aug. 1997.

[142] J. M. Fuster, J. Marti, J. L. Corral, V. Polo, and F. Ramos, “Generalized study of dispersion-induced power penalty mitigation techniques in millimeter-wave fiber-optic links,” *J. Lightw. Technol.*, vol. 18, no. 7, pp. 933–940, Jul. 2000.

[143] J. Ma, J. Yu, C. Yu, X. Xin, J. Zeng, and L. Chen, “Fiber dispersion influence on transmission of the optical millimeter-waves generated using LN-MZM intensity modulation,” *J. Lightw. Technol.*, vol. 25, no. 11, pp. 3244–3256, Nov. 2007.

[144] C. Lim, K. Lee, A. Nirmalathas, D. Novak, and R.Waterhouse, “Impact of chromatic dispersion on 60 GHz radio-over-fiber transmission,” in *IEEE Lasers and Electro-Optics Society Annual Meeting (LEOS)*, pp. 89–90, Nov. 2008.

[145] M. Weiss, A. Stöhr, F. Lecoche, and B. Charbonnier, “27 Gbit/s photonic wireless 60 GHz transmission system using 16-QAM OFDM“, *IEEE International Topical Meeting on Microwave Photonics (MWP)*, post-deadline paper, Oct. 2009.

[146] R. A. Griffin, P. M. Lane, and J. J. O’Reilly, “Dispersion-tolerant subcarrier data modulation of optical millimetre-wave signals,” *Electron. Lett.*, vol. 32, no. 24, pp. 2258–2260, 1996.

[147] H. Shams, P. M. Anandarajah, P. Perry, and L. P. Barry, “Optical generation of modulated millimeter waves based on a gain-switched laser,” *IEEE Trans. Microw. Theory Tech.*, vol. 58, no. 11, pp. 3372–3380, Nov. 2010.

[148] R. Sambaraju, D. Zibar, A. Caballero, I. Tafur Monroy, R. Alemany, and J. Herrera, “100-GHz wireless-over-fiber links with up to 16-Gb/s QPSK modulation using optical heterodyne generation and digital coherent detection,” *IEEE Photon. Technol. Lett.*, vol. 22, no. 22, pp. 1650–1652, Nov. 2010.

[149] L. A. Johansson and A. J. Seeds, “36-GHz 140-Mb/s radio-over-fiber transmission using an optical injection phase-lock loop source,” *IEEE Photon. Technol. Lett.*, vol. 13, no. 8, pp. 893–895, Aug. 2001.

[150] A. M. J. Koonen, and M. Garcia Larrode, “Radio-over-MMF techniques Part II: Microwave to millimeter-wave systems,” *J. Lightw. Technol.*, vol. 26, no. 15, pp. 2396–2408, Aug. 2008.

[151] J. Yu, G. –K. Chang, Z. Jia, A. Chowdhury, M. –F. Huang, H. –C. Chien, Y.-T. Hsueh, W. Jian, C. Liu, and Z. Dong, “Cost-effective optical millimeter technologies and field demonstrations for very high throughput wireless-over-fiber access systems,” *J. Lightw. Technol.*, vol. 28, no. 16, pp. 2376–2397, Aug. 2010.

[152] C. T. Lin, J. Chen, P.-T. Shih, W.-Jr Jiang, and S. Chi, “Ultra-high data-rate 60 GHz radio-over-fiber systems employing optical frequency multiplication and OFDM formats,” *J. Lightw. Technol.*, vol. 28, no. 16, pp. 2296–2306, Aug. 2010.

[153] C. Wei, C. Lin, M. Chao, W. Jiang, and C. Ho, "Long-reach 26.54-Gbps OFDM RoF system at 60 GHz over 100-km fiber and 3-m wireless transmission employing phase noise compensation and bit-loading algorithms," in *European Conference and Exhibition on Optical Communication (ECOC)*, Paper We.7.C.5, Sep. 2011.

[154] A. Kanno, K. Inagaki, I. Morohashi, T. Sakamoto, T. Kuri, I. Hosako, T. Kawanishi, Y. Yoshida, and K. Kitayama, “40 Gb/s W-band (75-110 GHz) 16-QAM radio-over-fiber signal generation and its wireless transmission,” *Opt. Express*, vol. 19, no. 26, pp. B56–B63, Nov. 2011.

[155] F.-M. Kuo, C.-B. Huang, J.-W. Shi, N.-W. Chen, H.-P. Chuang, J. Bowers, and C.-L. Pan, “Remotely up-converted 20-Gbit/s error-free wireless on–off-keying data transmission at W-band using an ultra-wideband photonic transmitter-mixer,” *IEEE Photon. J.*, vol. 3, no. 2, pp. 209–219, Apr. 2011.

[156] H.-J. Song, K. Ajito, A. Wakatsuki, Y. Muramoto, N. Kukutsu, Y. Kado, and T. Nagatsuma, “Terahertz wireless communication link at 300 GHz,” *IEEE International Topical Meeting on Microwave Photonics (MWP)*, Paper WE3-2, Oct. 2010.

[157] R.-W. Ridgway, D.-W. Nippa, and S. Yen, “Data transmission using differential phase-shift keying on a 92 GHz carrier,” *IEEE Trans. Microw. Theory Tech.*, vol. 58, no. 11, pp. 3117–3126, Nov. 2010.

[158] R. Hülsermann, D. Breuer, and C. Lange, “Impact of network reliability on network costs in next generation access networks,” in *International Conference on Transparent Optical Networks (ICTON)*, Paper Tu.A3.1, Jun. 2010.

[159] Draka Communications, Optical Fiber - Multimode Fibers. [Online]. Available: http://communications.draka.com/sites/eu/Pages/Optical-Fiber-Multimode-Fibers.aspx

[160] Corning Incorporated, Corning InfiniCor optical fibers. [Online]. Available: http://www.corning.com/opticalfiber/products/infinicor_fibers.aspx

[161] R. Gaudino, “High Speed Optical Transmission over Plastic Optical Fibers,” in *European Conference and Exhibition on Optical Communication (ECOC)*, Paper 3.5.3, Sept. 2009.

[162] Chromis Fiberoptics, Inc., Chromis GigaPOF™ perfluorinated plastic optical fibers. [Online]. Available: http://www.chromisfiber.com/products.htm

[163] Asahi Glass Co., Ltd., Plastic Optical Fiber FONTEX. [Online]. Available: http://www.lucina.jp/eg_fontex/

[164] C. Lethien, C. Loyez, J.–P. Vilcot, N. Rolland, and P. A. Rolland, "Potential of the polymer optical fibers deployed in a 10Gbps small office/home office network," *Opt. Express*, vol. 16, no. 15, pp. 11266–11274, Jul. 2008.

[165] S. R. Nuccio, L. Christen, X. Wu, S. Khaleghi, O. Yilmaz, A. E. Willner, and Y. Koike, “Transmission of 40 Gb/s DPSK and OOK at 1.55 µm through 100 m of plastic optical fiber,” in *European Conference and Exhibition on Optical Communication (ECOC)*, pp. 83–84, Sep. 2008.

[166] M.-J. Li, P. Tandon, D. C. Bookbinder, S. R. Bickham, M. A. McDermott, R. B. Desorcie, D. A. Nolan, J. J Johnson, K. A. Lewis, and J. J. Englebert, “Ultra-low bending loss single-mode fiber for FTTH,” in *Optical Fiber Communication Conference and Exposition (OFC)*, Paper PDP10, Feb. 2008.

[167] D. Boivin, L.-A. de Montmorillon, L. Provost, and P. Sillard, "All-solid single-trench-assisted bend-insensitive fibers: Performances and deployment aspects," in *Optical Fiber Communication Conference and Exposition (OFC)*, Paper NThB3, Mar. 2010.

[168] J. M. Fini, P. I. Borel, P. A. Weimann, M. F. Yan, S. Ramachandran, A. D. Yablon, P. W. Wisk, D. Trevor, D. J. DiGiovanni, J. Bjerregaard, P. Kristensen, K. Carlson, C. J. Martin, and A. McCurdy, "Bend insensitive fiber for FTTX applications," in *Optical Fiber Communication Conference and Exposition (OFC)*, Paper OTuL4, Mar. 2009.

[169] K. Mukasa, K. Imamura, I. Shimotakahara, T. Yagi, and K. Kokura, “Dispersion compensating fiber used as a transmission fiber: inverse/reverse dispersion fiber,” *J. Opt. Fiber. Commun. Rep.*, vol. 3, pp. 292–339, 2006.

[170] M. Kunigonis, “FTTH Explained: Delivering efficient customer bandwidth and enhanced services,” Corning Cable Systems, 2009.

[171] P. Chanclou, S. Gosselin, J. F. Palacios, V. L. Alvarez, and E. Zouganeli, “Overview of the optical broadband access evolution: a joint article by operators in the IST network of excellence e-Photon/One,” *IEEE Commun. Mag.*, vol. 44, no. 8, pp. 29–35, Aug. 2006.

[172] T. Koonen, “Fiber to the home/fiber to the premises: what, where, and when?,” *Proc. IEEE*, vol. 94, no. 5, pp. 911–934, May 2006.

[173] PLC Splitters, SQS Vláknová optika, Nová Paka, Czech Republic. [Online]. Available: http://www.sqs-fiber.cz

[174] JDS Uniphase Corporation, “Triple-Play Service Deployment,” 2007.

[175] Next-Generation FTTH Passive Optical Networks, Josep Prat (Ed.), ISBN 978-1-4020-8469-0, Springer, 2008.

[176] Hitachi Ltd., “Ultra Thin LCD TV – The UT Series.” [Online]. Available: http://www.hitachi.com/New/cnews/071023.html

[177] Lenovo, “ThinkPad T Series.” [Online]. Available: www.lenovo.com

[178] Novelda Nanoscale Impulse Radar. [Online]. Available: http://www.novelda.no

[179] X. Yu and I. Tafur Monroy, “Distribution of photonically generated 5 Gbits/s impulse radio ultrawideband signals over fiber,” *Opt. Lett.*, vol. 36, no. 6, pp. 810–812, Mar. 2011.

[180] D. Marpaung, L. Chevalier, M. Burla, and C. Roeloffzen, “Impulse radio ultrawideband pulse shaper based on a programmable photonic chip frequency discriminator,” *Opt. Express*, vol. 19, no. 25, pp. 24838–24848, Nov. 2011.

[181] Balanced Photoreceiver with Limiting TIA, Teleoptix, Optical Division of Linkra srl, Cornate d’Adda, Italy. [Online]. Available: http://www.linkra.it

[182] S. E. Gunnarsson, C. Karnfelt, H. Zirath, R. Kozhuharov, D. Kuylenstierna, C. Fager, M. Ferndahl, B. Hansson, A. Alping, A., and P. Hallbjorner, “60 GHz single-chip front-end MMICs and systems for multi-Gb/s wireless communication,” *IEEE J. Solid-State Circuits*, vol. 42, no. 5, pp. 1143–1157, May 2007.

[183] J. Azaña and M. A. Muriel, “Real-time optical spectrum analysis based on the time-space duality in chirped fiber gratings,” *IEEE J. Quantum Electron.*, vol. 36, no. 5, pp. 517–526, May 2000.

[184] J. U. Kang, M. Y. Frankel, and R. D. Esman, “Demonstration of microwave frequency shifting by use of a highly chirped mode-locked fiber laser,” *Opt. Lett.*, vol. 23, no. 15, pp. 1188–1190, Aug. 1998.

[185] F. Coppinger, A. S. Bhushan, and B. Jalali, “Time reversal of broadband microwave signals," *Electron. Lett.*, vol. 35, no. 15, pp. 1230–1232, Jul. 1999.

[186] Y. Han and B. Jalali, “Photonic time-stretched analog-to-digital converter: Fundamental concepts and practical considerations,” *J. Lightw. Technol.*, vol. 21, no. 12, pp. 3085–3103, Dec. 2003.

[187] R. Sambaraju, J. Palaci, V. Polo, and J. L. Corral, "Photonic envelope detector for broadband wireless signals using a single Mach-Zehnder modulator and a fibre Bragg grating," in *European Conference and Exhibition on Optical Communication (ECOC)*, pp. 213–214, Sep. 2008.

[188] L. A. Jiang, E. P. Ippen, and H. Yokoyama, “Semiconductor mode locked lasers as pulse sources for high bit rate data transmission,” *J. Opt. Fiber. Commun. Rep.*, vol. 2, pp. 1–31, 2005.

[189] Pico Second Laser Source with monolithic mode locked semiconductor laser chip (PSLS10), u2t Photonics, Berlin, Germany. [Online]. Available: http://u2t.de

[190] A. Martinez and S. Yamashita, “Multi-gigahertz repetition rate passivelymodelocked fiber lasers using carbon nanotubes,” *Opt. Express*, vol. 19, no. 7, pp. 6155–6163, Mar. 2011.

[191] A. Liu, L. Liao, D. Rubin, J. Basak, Y. Chetrit, H. Nguyen, R. Cohen, N. Izhaky, and M. Paniccia, “Recent development in a high-speed silicon optical modulator based on reverse-biased pn diode in a silicon waveguide,” *Semicond. Sci. Technol.*, vol. 23, pp. 1–7, 2008.

[192] X. Yi, C. Lu, X. Yang, W. Zhong, F. Wei, L. Ding, and Y. Wang, “Continuously tunable microwave-photonic filter design using high birefringence linear chirped grating,” *IEEE Photon. Technol. Lett.*, vol. 15, no. 5, pp. 754–756, May 2003.

[193] R. Shau, M. Ortsiefer, J. Rosskopf, G. Böhm, C. Lauer, M. Maute, and M.-C. Amann, “Long-wavelength InP-based VCSELs with buried tunnel junction: Properties and applications,” Vertical-Cavity Surface-Emitting Lasers VIII, *Proc. SPIE*, vol. 5364, pp. 1–15, 2004.

[194] B. Wedding, “Analysis of fibre transfer function and determination of receiver frequency response for dispersion supported transmission,” *Electron. Lett.*, vol. 30, no. 1, pp. 58–59, Jan.1994.

[195] B. Zhang, X. Zhao, L. Christen, D. Parekh, W. Hofmann, M. C. Wu, M.-C. Amann, C. J. Chang-Hasnain, and A. E. Willner, “Adjustable chirp injection-locked 1.55-µm VCSELs for enhanced chromatic dispersion compensation at 10-Gb/s”, in *Optical Fiber Communication Conference and Exposition (OFC)*, Paper OWT7, Mar. 2008.

[196] B. Boffi, A. Boletti, A. Gatto, and M. Martinelli, “VCSEL to VCSEL injection locking for uncompensated 40-km transmission at 10 Gb/s”, in *Optical Fiber Communication Conference and Exposition (OFC)*, Paper JThA32, Mar. 2008.

[197] J. Yu, P. N. Ji, Z. Jia, T. Wang, X. Zheng, Y. Matsui, D. Mahgerefteh, K. McCallion, Z. F. Fan, and P. Tayebati, “42.8 Gbit/s chirp-managed signal transmission over 20km standard SMF at 1550nm without DCF,” *Electron. Lett.*, vol. 43, no. 23, Nov. 2007.

[198] I. González Insua, D. Plettemeier, and C. G. Schäffer, “Simple remote heterodyne radio-over-fiber system for gigabit per second wireless access,” *J. Lightw. Technol.*, vol. 28, no. 16, pp. 2289–2295, Aug. 2010.

[199] P. J. Delfyett, S. Gee, M. –T. Choi, H. Izadpanah, W. Lee, S. Ozharar, F. Quinlan, and T. Yilmaz, “Optical frequency combs from semiconductor lasers and applications in ultrawideband signal processing and communications,” *J. Lightw. Technol.*, vol. 24, no. 7, pp. 2701–2719, Jul. 2006.

[200] H. Sanjoh, H. Yasaka, Y. Sakai, K. Sato, H. Ishii, and Y. Yoshikuni, "Multiwavelength light source with precise frequency spacing using a mode-locked semiconductor laser and an arrayed waveguide grating filter," *IEEE Photon. Technol. Lett.*, vol. 9, no. 6, pp. 818–820, Jun. 1997.

[201] A. Bellemare, M. Karasek, M. Rochette, S. LaRochelle, and M. Tetu, "Room temperature multifrequency erbium-doped fiber lasers anchored on the ITU frequency grid," *J. Lightw. Technol.*, vol. 18, no. 6, pp. 825–831, Jun. 2000.

[202] M. P. Fok and C. Shu, "Spacing-adjustable multi-wavelength source from a stimulated Brillouin scattering assisted erbium-doped fiber laser," *Opt. Express*, vol. 14, no. 7, pp. 2618–2624, Apr. 2006.

[203] Z. Jiang, D. E. Leaird, and A. M. Weiner, “Optical processing based on spectral line-by-line pulse shaping on a phase-modulated CW laser,” *IEEE J. Quantum Electron.*, vol. 42, no. 7, pp. 657–666, Jul. 2006.

[204] I. Morohashi, T. Sakamoto, H. Sotobayashi, T. Kawanishi, and I. Hosako, “Broadband wavelength-tunable ultrashort pulse source using a Mach–Zehnder modulator and dispersion-flattened dispersion-decreasing fiber,” *Opt. Lett.*, vol. 34, no. 15, pp. 2297–2299, Aug. 2009.

[205] J. Yu, Z. Dong, and N. Chi “Generation, transmission and coherent detection of 11.2 Tb/s (112x100Gb/s) single source optical OFDM superchannel,” in *Optical Fiber Communication Conference and Exposition (OFC)*, Paper PDPA6, Mar. 2011.

[206] P. M. Anandarajah, R. Maher, Y. Q. Xu, S. Latkowski, J. O'Carroll, S. G. Murdoch, R. Phelan, J. O'Gorman, and L. P. Barry, "Generation of coherent multicarrier signals by gain switching of discrete mode lasers," *IEEE Photon. J.*, vol. 3, no. 1, pp. 112–122, Feb. 2011.

[207] R. Zhou, S. Latkowski, J. O'Carroll, R. Phelan, L. P. Barry, and P. Anandarajah, "40nm wavelength tunable gain-switched optical comb source," in *European Conference and Exhibition on Optical Communication (ECOC)*, Paper Tu.5.LeSaleve.3, Sept. 2011.

[208] C.–B. Huang and Y. Lai, "Loss-less pulse intensity repetition-rate multiplication using optical all-pass filtering," *IEEE Photon. Technol. Lett.*, vol. 12, no. 2, pp. 167–169, Feb. 2000.

[209] J. Caraquitena, Z. Jiang, D. E. Leaird, and A. M. Weiner, “Tunable pulse repetition-rate multiplication using phase-only line-by-line pulse shaping,” *Opt. Lett.*, vol. 32, no. 6, pp. 716–718, Jun. 2007.